Fabrication of an autonomous surface stress sensor with the polymer SU-8

Keller, Stephan Sylvest; Boisen, Anja

Publication date:
2008

Document Version
Publisher's PDF, also known as Version of record

Fabrication of an autonomous surface stress sensor with the polymer SU-8

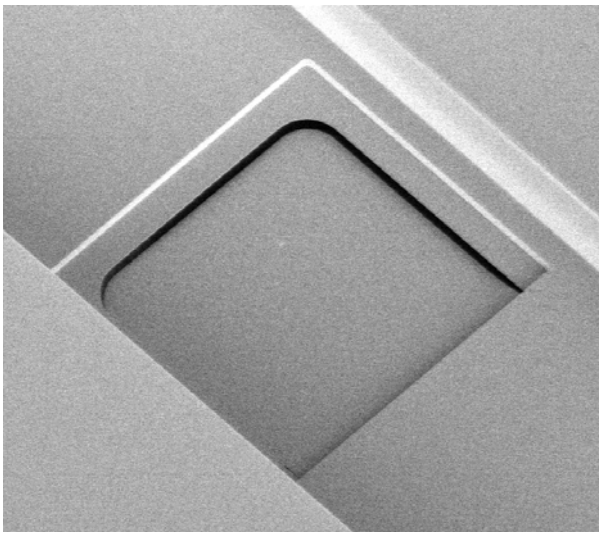

Stephan Keller PhD-Thesis April 2008

DTU Nanotech
Department of Micro- and Nanotechnology

Preface

This thesis has been written as a part of the requirements for obtaining the PhD degree at the Technical University of Denmark (DTU). The PhD project was carried out at the Department of Micro- and Nanotechnology at DTU during the period of the 1st of May 2005 to the 1st of May 2008. The project was part of the Nanoprobes group and was supervised by:

- Professor Anja Boisen, main supervisor
- PhD Daniel Häfliger, co-supervisor, presently employed at Harting AG, Selzach, Switzerland

The project was funded by the Danish Research Council for Technology and Production (FTP).

In spring 2005 I decided to leave Switzerland and to head northwards. Here, in spring 2008, I can look back and say that there was not a single moment in these three years where I have regretted my decision.

First of all I would like to thank Anja Boisen for giving me the opportunity to do a PhD project in her group. For me, Anja incorporates the perfect group-leader. Her scientific and social competence creates a very stimulating work environment and I am very grateful that she allowed my mind to drift a bit to the right and to the left in the course of my thesis. I would also like to thank all the other past and present members of the Nanoprobes group. It was great fun to work with you guys, keep up the spirit! Some persons have played a particular role during my time in the group. Daniel Häfliger, the god-father of the actual idea behind the project, was scientifically and socially a great help during my first days in Denmark. Gabriela Blagoi has during all the time showed patience to answer hundreds of my naïve questions about chemistry and biotechnology. Thanks for your support and your friendship! Finally I would like to thank my buddies of the first days Michael Lillemose and Jan Hales for the introduction to Danish culture, no integration consultant could have done a better job than you guys.

The scientific work has been supported by a number of persons at DTU Nanotech. During the three years, several interesting sideprojects on magnetic actuation were carried out in collaboration with assistant professor Mikkel Fougt Hansen. The design of the microfluidic system used for the characterization of the fabricated chip was designed and fabricated by assistant professor Oliver Geschke and his student Marco Grünefeld. Further, I would like to acknowledge the cleaonroom staff at DTU Danchip, in particular the lab-technicians. They were able to create a friendly and human atmosphere in an otherwise very unnatural environment.

It is also time to thank my friends and family in Switzerland. In particular my parents Catherine and Christoph, my brothers Bernhard and Roland and my sister Evelyn have made me to what I am and I am infinitely thankful for that.

Lyngby, 30.04.2008

Stephan Keller
Department of Micro- and Nanotechnology
Technical University of Denmark
2800 Kgs. Lyngby, Denmark

Abstract

The aim of this thesis was the demonstration of a new sensor concept for the measurement of surface stress changes due to biomolecular interactions. The novelty of the sensor is that the read-out is autonomous, which means that no external energy source is required. The core part of this device is a container filled with a coloured marker solution and closed by a thin polymer flapper. The surface of the device is functionalized with receptor molecules. Specific binding of analyte to the receptors results in a change of surface stress. As a consequence, the flapper bends mechanically and the marker solution is released. This colour change is detected by the naked eye or with an optical microscope.

The focus of this thesis was on the design and fabrication of the autonomous sensor. A high actuation of the flapper is required to release the coloured marker. This is challenging because biomolecular interactions result in very small changes of surface stress. The fabrication was done with the negative epoxy photoresist SU-8. The advantage of this polymer compared to traditional silicon-based materials is that its Young's modulus is about 50 times lower. This allows for high actuation due to changes in surface stress if the thickness of the flapper is minimized.

In a first part of the thesis, the fabrication of thin SU-8 cantilevers was redesigned. These devices were used as a model system for process optimization. A new release method for thin SU-8 cantilevers was introduced using a fluorocarbon coating as release layer. The processing of thin SU-8 films was redesigned to obtain high structural stability and low residual stress in the polymer. Further process optimization was required to minimize the initial out-of-plane bending of the cantilevers and to achieve high fabrication yield. With the optimized process, the fabrication of arrays of 2-µm-thick SU-8 cantilevers with a length of 500 µm an initial bending of less than 20 µm was demonstrated. Stability of the devices upon storage for several months was investigated and minimal influence was observed for devices fabricated with the optimized process.

First, the optimized processes were used for the fabrication of SU-8 cantilever chips for the measurement of surface stress with optical read-out. There, new approaches for process-integrated metal coating, surface functionalization and passivation of cantilever-based sensors were introduced. The fabricated sensors were used for the measurement of surface stress that is generated by DNA-hybridization. The design and characerization of these chips should allow for conclusions on the expected actuation of the flapper due to biomolecular interactions.

Finally, the flapperchip was designed and fabricated. The fabrication and release of flappers with an area of 400x400 μm^2 and a thickness of only 2 µm was demonstrated. The thin SU-8 flapper had to be integrated in a microfluidic system that allows testing of the sensor. For this purpose, a Pyrex cover was thermally bonded to the SU-8 structures. The wafer-scale release of the flapperchips bonded to the Pyrex was possible. Finally, methods for coating of the flappers with a biopolymer were evaluated. Degradation of the biopolymer coating through hydrolysis or enzymes is expected to result in a high actuation of the flappers.

In conclusion, the main achievement of this thesis was the optimization of existing and new processes for the fabrication of thin cantilever-based surface stress sensors with the polymer SU-8. The efforts were directed towards the fabrication of sensor for autonomous read-out of a change in surface stress but the discussed processes might be used for the fabrication of other sensors.

Contents

1 Introduction

1.1 Cantilever-based sensors

The use of cantilevers in microtechnology became popular with the invention of the Atomic Force Microscope in 1986 [1]. A cantilever is a beam that is clamped at one end and freestanding at the other (*Figure 1.1-1*). The length L and the width w define the cantilever plane and typically the thickness t is at least an order magnitude lower than the other dimensions. In the AFM, a sharp tip is added at the freestanding extremity and the surface of the sample is scanned while measuring the deflection of the cantilever (*Figure 1.1-2*). The low spring constant of the cantilever allows a high out-of-plane deflection of the cantilever upon small changes of the topography.

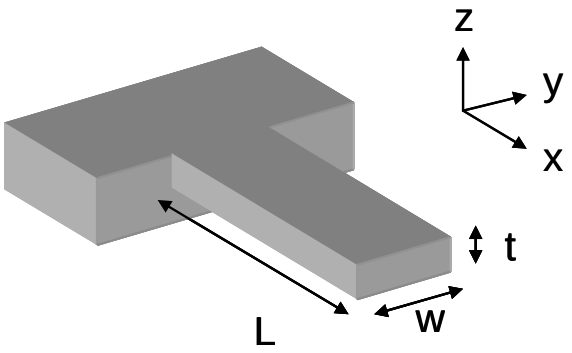

Figure 1.1-1: Schematic of a cantilever

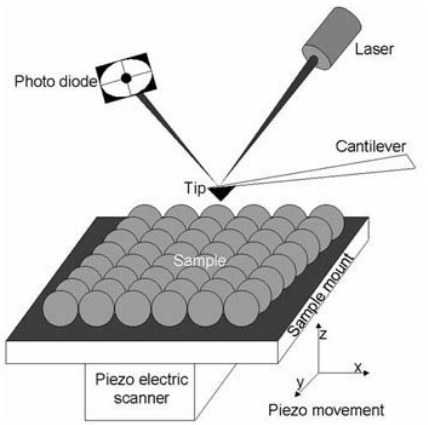

Figure 1.1-2: Principle of the AFM [2]

In the 90's, a large variety of sensor technologies based on microcantilevers were introduced. In microcalorimetry, cantilevers consisting of two layers of materials with different coefficient of thermal expansion serve as temperature sensors [3, 4]. Resonating cantilevers can be used for mass detection because added mass results in a change of the resonance frequency of the beam [5, 6]. Another sensor principle is based on changes of surface stress resulting in static bending of the cantilever [7-9]. This measurement method will be discussed in detail in the following section. Further, Colton and co-workers used magnetic forces to induce cantilever deflection upon binding of superparamagnetic particles to the sensor surface [10].
For all cantilever-based sensors, optical read-out is most commonly used for the measurement of the cantilever deflection (*Figure 1.1-2*) [3-5, 7-9, 11]. There, a laser beam is focused onto the apex of the cantilever and the reflection is monitored using a position sensitive diode (PSD). Alternatively, the use of piezoresistive [12, 13], piezoelectric [14, 15], capacitive [16-18] or MOSFET-based [19] read-out methods has been demonstrated. The selection of the read-out method depends on the specific application. For example, compared to optical read-out, the integration of piezoresistors has the advantage that the signal is not influenced by the optical properties of the surrounding medium. On the other hand, fabrication of the cantilever devices for piezoresistive read-out is more time-consuming.

1.2 Surface stress measurements

Intermolecular forces arising from absorption of molecules on a solid induce surface stress. A thin beam or plate can be used to measure changes in the differential surface stress between the two sides of the cantilever. A uniform surface stress tends either to increase or to decrease the surface area. This results in mechanical bending of the cantilever if the effect is not compensated by an equal stress on the opposite side of the cantilever *(Figure 1.2-1)*.

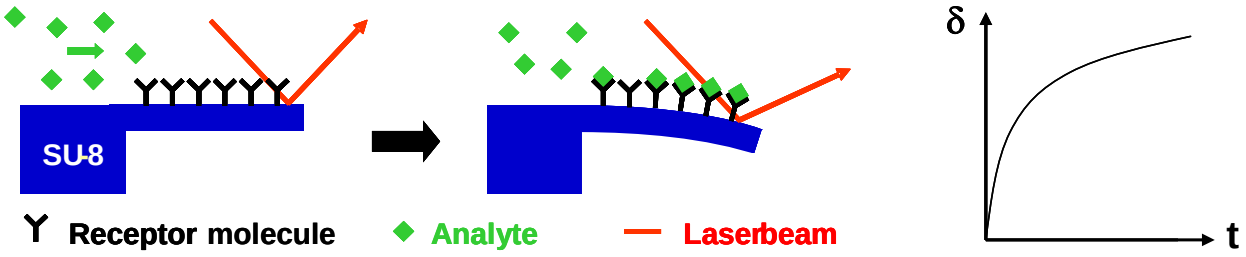

Figure 1.2-1: Cantilever-based sensor with optical read-out: Binding of the analyte to the receptor induces surface stress and leads to deflection δ of the cantilever with time t

For a rectangular beam, it is possible to write an approximate relation between differential surface stress change and the resulting change in deflection at its free end [20]:

$$\Delta\delta = \frac{3(1-\nu)}{E}\left(\frac{L}{t}\right)^2 \Delta\sigma \qquad (1.1\text{-}1)$$

σ = surface stress [N/m] E = Young's modulus [Pa] ν = Poisson's ratio
δ = deflection [m] t = cantilever thickness [m] L = cantilever length [L]

Equation 1.1-1 shows that thin cantilevers with low thickness and a low Young's modulus have a high sensitivity towards surface stress. These parameters are influenced by design and fabrication of the devices. Several other issues have to be solved to obtain high sensitivity and high selectivity for sensors based on surface stress [21]:

- Functionalization of one cantilever surface with a receptor layer is required for specific recognition of the target molecules
- Intermolecular forces have to be high. This involves issues such as surface density of receptor molecules and affinity to the target
- Passivation of the other cantilever surface allows for a high differential surface stress
- Changes in temperature, pH or ion concentration in the environment influence the bending of the cantilevers particularly for devices coated with a metal layer. These artefacts can be cancelled out by measuring the differential signal between an inert reference cantilever and the functionalized sensing cantilever [22]

Several research-groups demonstrated applications of chemical sensing based on surface stress on microcantilevers. Cantilevers coated with palladium or platinum were used for the detection of hydrogen adsorbed on the metal film [11, 16, 17]. The group of Prof. Güntherodt at the University

of Basel (Switzerland) used polymer-coated cantilevers for the detection of various volatile organic compounds (VOCs) such as vapours from different alcohols and perfumes [23, 24]. The absorption of the molecules resulted in swelling of the polymer and as a consequence in bending of the cantilevers.
In 1996, Berger et al. introduced self-assembled monolayers (SAMs) as model molecular systems [25]. The surface stress generated during the formation of monolayers of Alkanethiols was monitored using gold-coated microcantilevers.
Another area of interest is the use of cantilevers as biosensors in liquid environment [26, 27]. There, a major advantage of cantilever sensors compared to other detection methods is that no labelling of the target molecules with fluorescent or radioactive tags is required. The first real applications of cantilevers in biosensing included the measurement of biotin-streptavidin interactions (*Figure 1.2-2*) [26] and antibody-antigen binding [27, 28]. There, the devices were functionalized with antigens and binding to the specific antibody resulted in surface stress changes. Further, cantilevers were used for the monitoring of DNA hybridization [29-31]. Single-stranded DNA was immobilized on the gold-covered cantilever surface and hybridization with the complementary oligonucleotides resulted in bending of the cantilevers (*Figure 1.2-3*). Some authors even proposed to sense mechanical responses of living cells, cultured directly onto the cantilever surface, to external chemical stimuli [32]. The understanding of surface stress due to specific biomolecular interactions is still very limited as the situation is more complex than for chemical sensors. Electrostatic interactions between neighbouring molecules, changes in surface hydrophobicity, and conformational changes have to be considered. Wu et al. demonstrated that cantilever motion during DNA-detection is a result of the interplay between changes in configurational entropy and intermolecular energetics [30].
In summary, cantilever sensors based on changes of surface stress allow for the label-free detection of biomolecules. Small size, low reagent consumption, fast response time and relatively high sensitivity for various applications have been demonstrated. The use of arrays of cantilevers allows for parallel detection of multiple target molecules in real-time.

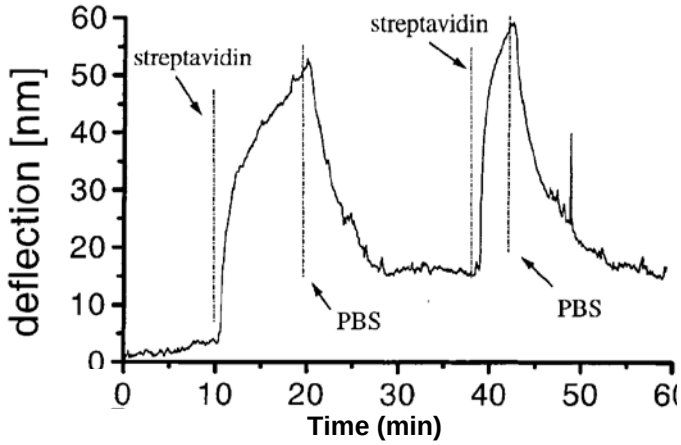

Figure 1.2-2: Deflection response of a biotinylated cantilever to the addition of 0.1 µM streptavidin. After each cycle the cantilever was rinsed with phosphate buffer saline (PBS) [26]

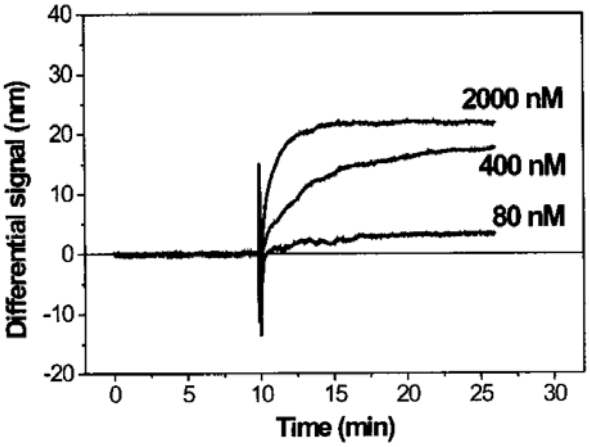

Figure 1.2-3: DNA-hybridization experiment with different 12mer oligonucleotide concentrations using a cantilever array [29]

1.3 Polymer microcantilevers

Initially, cantilever sensors were fabricated using bulk micromachining processes that were well-established for micro-electro-mechanical systems (MEMS). Classical cantilever materials were silicon, silicon-oxide or silicon-nitride. In 1994, Pechmann and co-workers fabricated the first polymer microcantilevers with a standard Novolak-based photoresist as cantilever material [33]. In 1999, Genolet used the negative epoxy photo-resist SU-8 to define AFM-cantilevers [34]. In the following years, polymers such as polyimide [35, 36], polystyrene [37, 38], polypropylene [39], polyethylene therephtalate (PET) [40] or fluoropolymer [41] were introduced as new cantilever materials. Compared to silicon-based devices, surface micromachining processes are used for the fabrication of chips with polymer cantilevers [42]. There, SU-8 and polyimide were particularly interesting because they can be patterned with standard UV-lithography [34-36, 43-45]. Other fabrication methods include injection molding [46], microstereolithography [47], micro-cutting [37], multi-photon-absorption polymerization [48] and laser ablation [40].

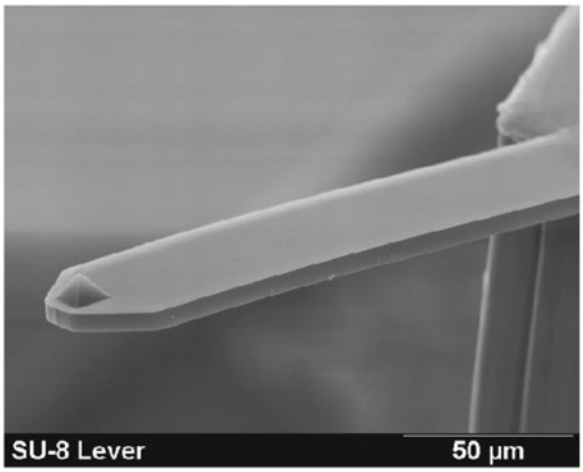

Figure 1.3-1: SU-8 cantilever for AFM [34]

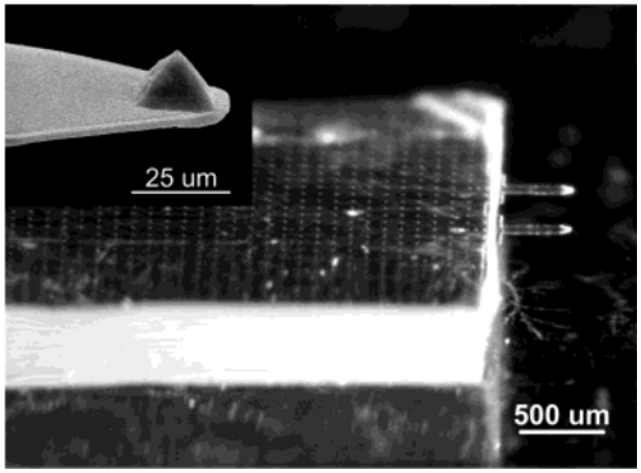

Figure 1.3-2: Hybrid scanning probe with polyimide cantilever and elastomeric tip (PDMS)[35]

The main motivation for replacing traditional cantilever materials with polymers is that the Young's modulus of polymers is typically reduced by about two orders of magnitude. Therefore, the stiffness of the cantilevers is lower and the sensitivity for most sensing applications improves. *Equation 1.1-1* shows that the cantilever bending due to surface stress is directly proportional to the Young's modulus E of the cantilever material. Other advantages using polymers are the lower costs of the raw materials and of the equipment for microfabrication and the possibilities of mass production with e.g. injection molding [46]. On the other hand, fabrication of microcantilevers with polymers is a rather recent technology with a lot of unsolved challenges.
The focus of most of the published work on polymer cantilevers lies on the technological aspects. On the other hand, some authors recently reported the use of polymer based devices for the measurement of surface stress induced by the binding of biomolecules [40, 44, 49, 50]. This demonstrates the potential of polymer microcantilevers as biosensor platforms.

1.4 Cantilever-based biochemical sensing in the Nanoprobes group

The starting point for the research on biochemical sensors at DTU Nanotech was the development of AFM cantilevers with integrated piezoresistive read-out [51, 52]. In 2000, the first application of piezoresistive AFM probes as a cantilever-based sensor operated in liquid was demonstrated [53]. There, the cantilevers were coated with a polymer and the surface stress induced by the absorption of alcohol in aqueous environment was measured. In the following years, several generations of cantilever chips with integrated piezoresistive read-out were fabricated in the Nanoprobes group of Prof. Boisen. The research focus was on design and fabrication of cantilever based sensors for the detection of chemical compounds and biomolecules. Initially, silicon-based devices for the measurement of surface stress were developed which resulted in the foundation of the company Cantion A/S in 2001. Since then, the research efforts on surface stress sensors were directed towards the design and fabrication of devices fabricated with the polymer SU-8. In 2002, Jakob Thaysen presented the first generation of SU-8 cantilevers with piezoresistive read-out [54]. Alicia Johansson redesigned cantilevers, microfluidic system and packaging of the chips [55]. In parallel, SU-8 cantilevers for optical read-out by laser beams were developed [43]. Maria Nordström fabricated cantilever devices with integrated optical read-out using the cantilever as optical waveguide [56]. The large number of publications during the past years demonstrates that the Nanoprobes group has been front-runner in the design and fabrication of cantilever sensors with SU-8. Both, silicon- and polymer-based sensors were applied for the detection of surface stress induced by immobilization of thiols on gold [57], antibody-antigen interactions [55] and DNA hybridization [21].

1.5 A new autonomous sensor – "the flapperchip"

The read-out methods presented in *Section 1.1* allow the measurement of cantilever deflections in the sub-nm range. This allows the quantitative analysis of very small changes in surface stress and the responsible molecular interactions. The measurement setup is in most cases still quite bulky and contains expensive optical or electronic components. These need to be operated in a very controlled environment to achieve the high resolution. External energy sources are required which is a further disadvantage for the design of portable devices for point-of-care analysis. For some applications such as the measurement of water- or food-quality, fast analysis in the field or in the grocery store would be an advantage. Recently, the trend is the development of more compact devices with integrated sample handling and read-out [58].
On the other hand, a sensor giving a qualitative "yes-or-no" answer often would be sufficient at a first stage and quantitative measurements could be done in the laboratory in a later stage if necessary. In 2004, Daniel Häfliger introduced a new sensor concept that could satisfy the need of a fast analysis without advanced equipment for the read-out. The sensor principle is illustrated on *Figure 1.5-1*. A coloured marker solution is loaded in a small container closed by a flexible flapper. The flapper is functionalized with receptor molecules specific to the molecules under investigation. The binding of target molecules causes the flapper to deflect, the marker solution is released and the resulting colour change can be detected by visual inspection. Another method to obtain a deflection of the flapper is the removal of a material from the surface. In both cases, a change in surface stress as described in *Section 1.2* for cantilever-based sensors is responsible for the actuation of the flapper.

Other researchers have speculated about the possibility of using functionalized nanomechanical membranes as lid for a container that could open to release substances very locally but, to our knowledge, the ideas were not pursued [24]. The sensor concept was for the first time demonstrated by Daniel Häfliger [59]. He used the etching of a thin metal layer that was previously deposited on the top of an 8-µm-thick SU-8 flapper to actuate the device. *Figure 1.5-2* shows the subsequent colour change upon the removal of aluminium with NaOH. The sensor response is quite fast and the colour change can be detected by the naked eye.

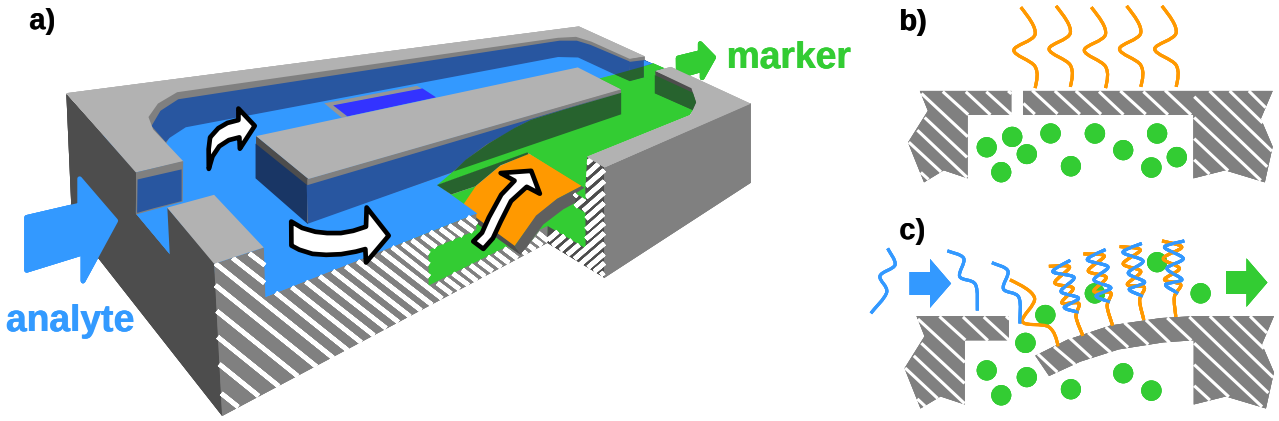

Figure 1.5-1: (a) Illustration of the new sensor concept: (b) The marker container is closed by the functionalized flapper (orange) (c) Analyte molecules (blue) bind to the surface, the flapper is deflected due to a change in surface stress and the marker solution (green) is released [59]

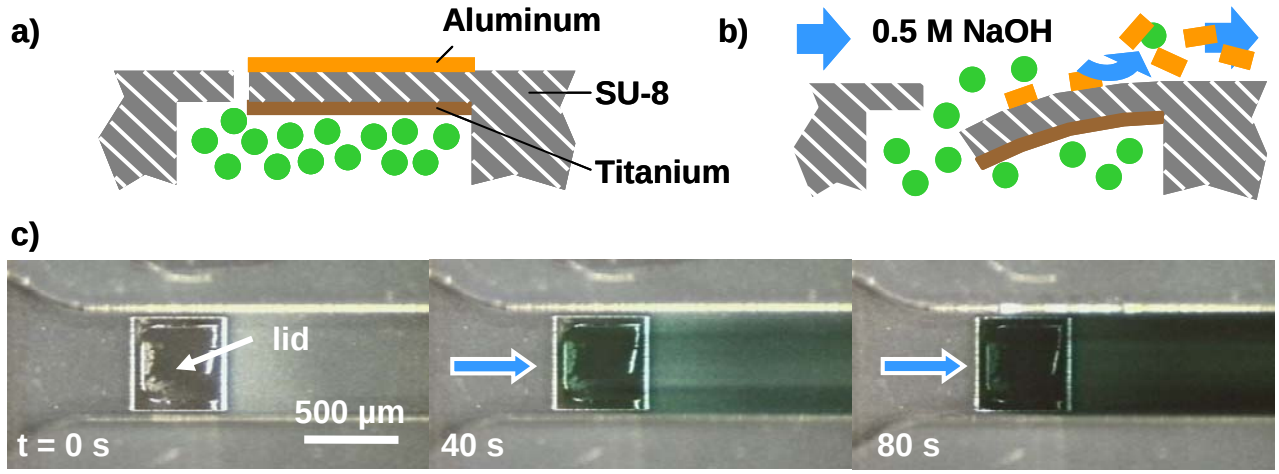

Figure 1.5-2: Proof-of-principle: A thin layer of aluminum is etched away from the top surface of the flapper; the structure starts to deflect and a green marker is released into the channel [59]

The advantage of this sensor, further called flapperchip, is that it is operating autonomously, meaning that no external power supply is necessary for its operation. The energy for the read-out should be provided by bio-chemical reaction only. The presented concept could for example be used in food diagnostics where there is a great need for cheap, disposable sensors. Similar to the metal film, removal of organic material could be done by bacterial activity and the sensor could be used for the monitoring of the presence of bacteria in food. Integration of a simple colour marker in food packaging could allow for the identification of infected products. A more visionary application is in the field of drug delivery. The coloured marker solution could be replaced by a medical drug.

The filled container could be swallowed and the drug is released upon reaction of target molecules with the receptors on the surface of the flapper.

1.6 Motivation

In the proof-of-concept shown in *Figure 1.5-2* a deflection of more than 40 µm was achieved during the release of the colour from the underlying container [59]. *Table 1.6-1* is a summary of some typical values of cantilever bending measured for different biomolecular receptor-analyte systems. With the knowledge of cantilever dimensions and material properties the corresponding surface stress can be estimated with *Equation 1.2-1*. It is easily seen that the reported values of cantilever bending are two orders of magnitude lower than for the inorganic example of the removal of the aluminum film. For the application as biosensor, optimization of the design, fabrication and actuation of the autonomous system based on the presented concept is required. This was the goal of the PhD-project. *Figure 1.6-1* presents the main focus areas of the project and the related tasks are briefly discussed in the following.

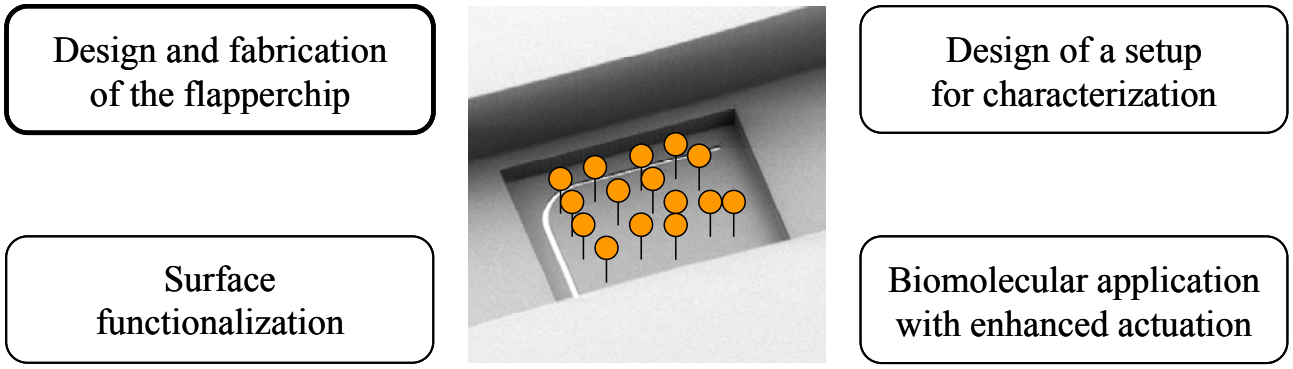

Figure 1.6-1: Major focus areas of the PhD-project

The main focus of the thesis is on the fabrication of the actual chip. With the arguments presented in *Section 1.3* and based on the experience in the Nanoprobes group it was decided to use the negative epoxy-photoresist SU-8 for this purpose. The particular goals for the design and fabrication of the flapperchip are:

- High actuation: *Equation 1.2-1* identifies the parameters that have to be considered to achieve a high actuation of the lid. The thickness t of the flapper is minimized and the length L is increased
- No leakage: The flapper shows no initial bending, no cracking and the width of the gap is small to avoid that the colour marker is released before the actual actuation
- Microfluidic system: The integration of the flapper in a microchannel system allows for the fast testing of different biomolecular applications
- Batch processing: Microfabrication results in functional chips on wafer-scale with a high reproducibility. Processes such as single chip metallization or bonding are avoided

- Long shelf-life: The SU-8 chips can be stored for some months without an effect on their functionality

The process of the immobilization of receptor molecules on the surface of a biosensor is called surface functionalization. The goals related to this task are:

- Specificity: The receptor molecules provide specificity towards the target molecules

- Modularity: The developed functionalization scheme can be used for the testing of various receptor-analyte systems

- Batch processing: Functionalization of the chips is done on wafer-scale and if possible as an integral part of the chip fabrication

The proof-of-concept of the flapper actuated by biomolecules involves further challenges:

- Measurement setup: Microfluidic interconnections allow the introduction of colour marker and analyte solution. Optionally, the measurement of the deflection of the flapper and a quantification of the colour change is integrated

- Bioactuation: A receptor-analyte system providing high surface stress is selected. Methods to enhance the actuation are evaluated

Table 1.6-1: Measured cantilever deflections δ and calculated surface stress σ for different biomolecular interactions reported in literature; dimensions = length x width x thickness

Interaction	Materials	Dimensions [µm]	δ[nm]	σ[mN/m]	Ref
DNA-hybridization (2mM)	Si/Au	500 x 100 x 1	**25**	6	[29]
DNA-hybridization (500nM)	Si/Au	180 x 40 x 1	**8**	15	[31]
Biotin-neutravidin (25µg/ml)	SiN/Au	200 x 20 x 0.5	**20**	10	[30]
Antigen-antibody (60µg/ml)	SiN/Au	200 x 40 x 0.5	**130**	70	[28]
Antigen-antibody (25µg/ml)	SiN/Au	190 x 20 x 0.6	**130**	100	[27]
Alkanethiol immobilization	SiN/Au	180 x 18 x 0.6	**200**	170	[25]
Antigen-antibody (5µg/ml)	SU-8	200 x 20 x 4.5	**11**	13	[50]
Biotin-streptavidin (5µg/ml)	SU-8	200 x 20 x 4.5	**560**	680	[50]
Alkanethiol immobilization	SU-8/Au	215 x 280 x 3.5	**580**	240	[60]

1.7 Process flow of the PhD-thesis

The main goal of the project is the fabrication of the autonomous sensor. The tasks described in *Section 1.6* are also valid for the fabrication of cantilever-based sensors for the measurement of surface stress. Therefore, a substantial part of the process optimization described in this thesis was done for the fabrication of SU-8 cantilevers. There are several motivations for this procedure:

- The fabrication of cantilevers should allow for conclusions on the optimal design and fabrication of the autonomous sensor. The flapper is in principle a large cantilever that is integrated in a microfluidic system. The fabrication of the two devices follows the same

scheme and most challenges are identical. However, evaluation of results during process optimization is more straightforward using cantilevers. The cantilever chips are easier to handle and more devices can be patterned on one 4-inch-wafer.

- The fabrication of cantilevers has been demonstrated earlier in literature and in the Nanoprobes group. This allows for comparison of the results obtained with other fabrication processes

- Quantitative surface stress measurements on cantilever chips should allow the selection of a suitable receptor-analyte system for the flapper. Systems for the characterization of chips with arrays of cantilevers are already available in the Nanoprobes group. At the point where functionalization schemes are successfully implemented for cantilevers and high actuation is demonstrated, the transfer of the protocols for a proof-of-concept of the autonomous sensor is possible

The outline of the thesis is equal to the process flow for the fabrication of SU-8 cantilevers for surface stress measurements:

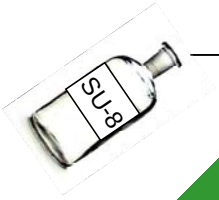

2 Processing and properties of the negative epoxy-photoresist SU-8 are presented in detail

3 A new method using fluorocarbon coatings is optimized for the dry release of SU-8 cantilevers

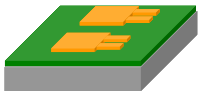

4 The influence of different processing parameters on residual film stress, structural stability, cross-linking density and lithographic resolution of SU-8 films with thicknesses below 5 µm is investigated

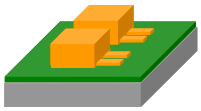

5 An additional step of SU-8 processing is added for the fabrication of cantilever chips. Cantilever bending, release yield and ageing of the devices are evaluated. An optimized fabrication process for SU-8 cantilever chips is defined

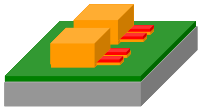

6 The optimized process is used for the fabrication of cantilever chips for surface stress measurements with optical read-out. Methods for process integrated metal coating and surface functionalization were evaluated

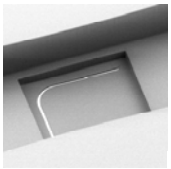

7 The flapperchip is designed and fabricated with a focus on the integration with the microfluidic systems

8 Conclusion and outlook on further research on the subject

2 Negative epoxy-photoresist SU-8

2.1 Introduction

The epoxy-based photoresist SU-8 is a result of the research on chemically amplified photoresists in the late 1980s. It was patented in 1989 by IBM at the Watson Research Center in Yorktown Heights [61]. In 1996, it has been transferred to MEMS applications in collaboration between the Institute of Microsystems at the Ecole Polytechnique Fédérale de Lausanne (EPFL, Switzerland) and IBM Zurich (Switzerland) [62, 63]. Initially, SU-8 was introduced as a thick film resist for the patterning of molds for electroplating in the LIGA-process [64, 65] but very fast it became a popular material in other areas of microfabrication such as microfluidics [66, 67] or optics [68, 69]. *Figure 2.1-1* shows structures fabricated with SU-8. The main advantage of the resist is the low absorption coefficient at wavelengths above 300 nm, which allows for the patterning of films with thicknesses in the millimeter-range at aspect-ratios of up to 20 in a single step of photolithography [70]. High chemical resistance, biocompatibility and structural stability are other factors that made SU-8 a widely employed polymer in microfabrication [71].
In the last years, a growing number of research groups discovered SU-8 as a thin film photoresist. SU-8 films with thickness in the micrometer-range can be used as cladding layer in micro-optics, as dielectric material for microelectronic circuits or as etch mask in microfabrication. Freestanding mechanical structures such as cantilevers or membranes with thickness below 10 µm have been fabricated [34, 43, 44, 72].
This chapter is an introduction to the negative photoresist SU-8 as it is the material used for the fabrication of the autonomous sensor. In *Section 2.2*, the chemical composition of the resist and the polymerization mechanism are presented. The processing of SU-8 is outlined in *Section 2.3* and the influences of the different processing steps on the properties of the polymer are briefly discussed in *Section 2.4* and *Section 2.5*. Finally, the process conventionally used for the fabrication of thin SU-8 cantilevers is presented.

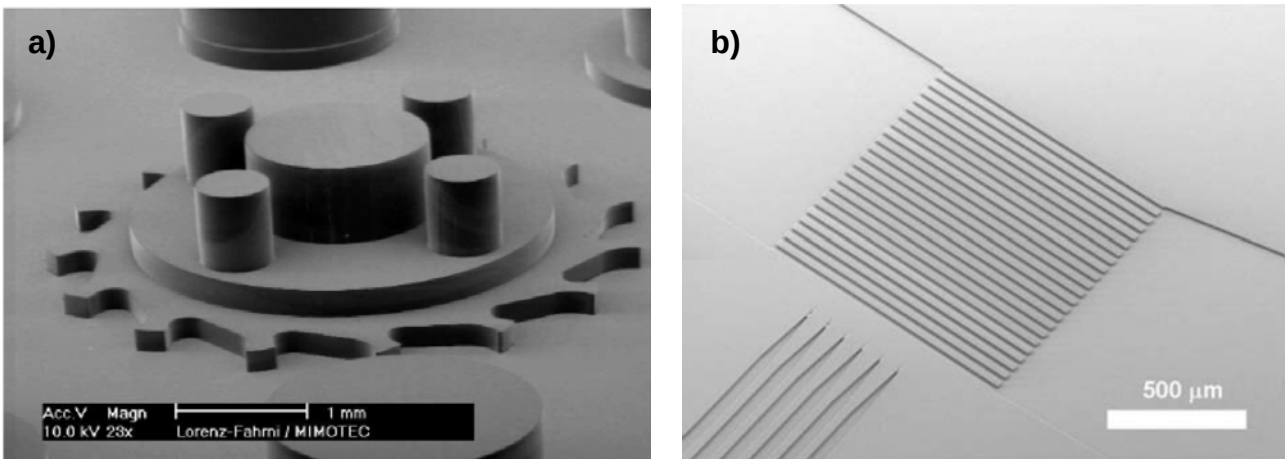

Figure 2.1-1: Structures fabricated with SU-8: (a) Mold for electroplating of micromechanical parts [73] (b) Microfluidic dye laser (center) and waveguide structures (lower left) [69]

2.2 Polymerization of SU-8

2.2.1 Negative photoresists and chemical amplification

The principal components of a photoresist are a polymer, a sensitizer and a casting solvent [74]. The polymer forms the base resin and it changes the structure when exposed to radiation. The solvent allows formation of thin layers by resist spinning. The sensitizer controls the photochemical reaction in the polymeric phase.
In case of a negative photoresist the exposure to radiation strengthens the polymer by random cross-linking and it becomes less soluble compared to the unexposed regions on the wafer. The change of solubility is achieved through increase in molecular weight or through photochemical transformation to form new insoluble products.
The sensitivity of the resist is of particular importance to produce thick 3D-polymer-structures within one photolithographic step and with a high resolution. Therefore, photoresists are chemically amplified. In such a resist, a single photon initiates a cascade of chemical reaction. This chemical amplification is based on the generation of a catalytic photoproduct that accelerates the cross-linking of the resin. An increased cross-linking rate implies shorter exposure times and improved contrast. The process of photolithography with a chemically amplified photoresist is illustrated in *Figure 2.2-1*.

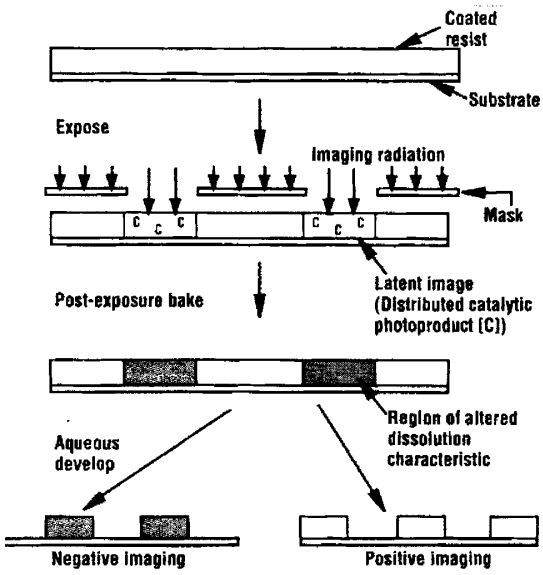

Figure 2.2-1: Chemically amplified resist process [74]

2.2.2 Chemical composition of SU-8

An epoxy resin consists of monomers having one or more epoxy-groups. The number of epoxy-groups per molecule is called the functionality of the resin. Higher functionality of a resist results in higher cross-linking density for comparable process conditions. This results in a better performance of the material in terms of resolution, aspect ratio, sidewall profile, chemical resistance and thermal stability [64].
SU-8 photoresist is based on a multifunctional glycidyl ether derivative of Bisphenol-A Novolac also known as EPON® resin SU-8 from Shell Chemical. The SU-8 monomer is composed of four Bisphenol-A-Bisepoxyether-groups. As the name of the resist suggests, the SU-8 contains on average eight epoxy-groups per monomer, which is at present the highest functionality that is commercially available. The chemical structure of an SU-8 monomer is represented on *Figure 2.2-2* and *Figure 2.2-3* shows a structural model of the same molecule.
The EPON® SU-8 resin is photosensitized with a commercially available mixture of Triarylsulfonium Hexafluoroantimonium salts (CYRACURE® UVI, Union Carbide). It is composed of Bis-Triarylsulfonium-Hexafluoroantimonium and Thio-Triarylsulfonium-Hexafluoroantimonium. The two components are represented on *Figure 2.2-4*.

Triarylsulfonium-salts are commonly used and are very efficient photoinitiators in chemically amplified resists [75]. A particular advantage compared to other compounds is the high thermal stability of these salts.
An organic solvent is added to be able to spin-coat the resist. The quantity of solvent determines the viscosity of the resist and defines the available range of resist thickness. At present SU-8 products with the solvents γ-butyro-lactone (GBL) and cyclo-pentanone (CP) are commercially available at MicroChem [76] and Gersteltec [77]. MicroChem replaced GBL by CP in their series of SU-8 2000 as the result of an experimental study [78]. This should improve the wetting of the substrate and accelerate the processing due to the lower surface tension and the higher volatility of this solvent.
As a further component, MicroChem lists Propylene Carbonate (1-5 %), which serves as solvent for the photoinitiator. Small amounts of other additives are present as e.g. Baysilicon 3739 and F47 fluorocarbon [79].

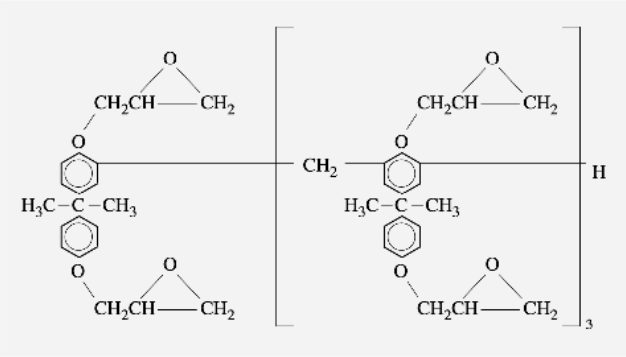

Formula VI

Glycidyl ether of bisphenol A—SU-8.

Figure 2.2-2: Chemical structure of the EPON® SU-8 monomer with eight epoxy-groups [80]

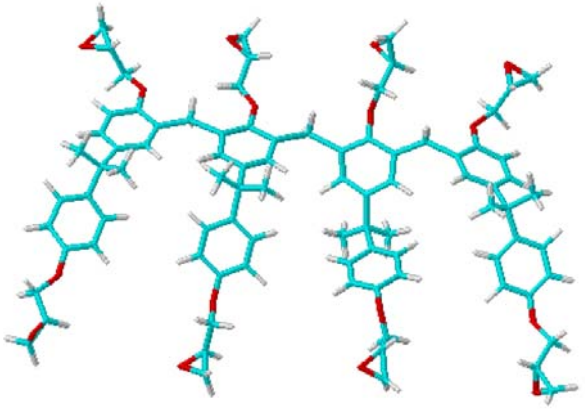

Figure 2.2-3: Structural model of the SU-8 monomer; O = red, C = blue, H = white [81]

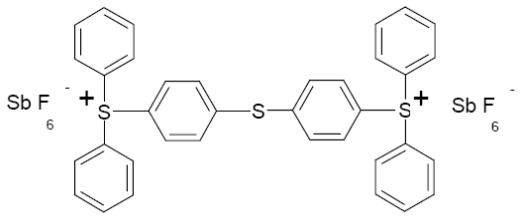

Bis-Triarylsulfoniumhexafluoroantimonat

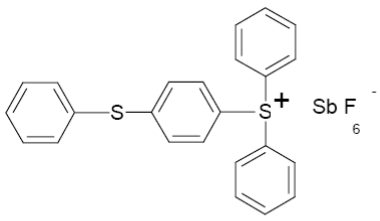

Thio-Triarylsulfoniumhexafluoroantimonat

Figure 2.2-4: Components of the onium-salt used as photoinitiator in the SU-8 photoresist [81]

2.2.3 Photopolymerization of SU-8

A chemically amplified epoxy resin like SU-8 polymerizes by cationic polymerization. The actual mechanism of polymerization using an onium salt as photoinitiator is quite complex [75]. Here, the main steps are briefly presented. A more detailed discussion is placed in *Appendix A*.

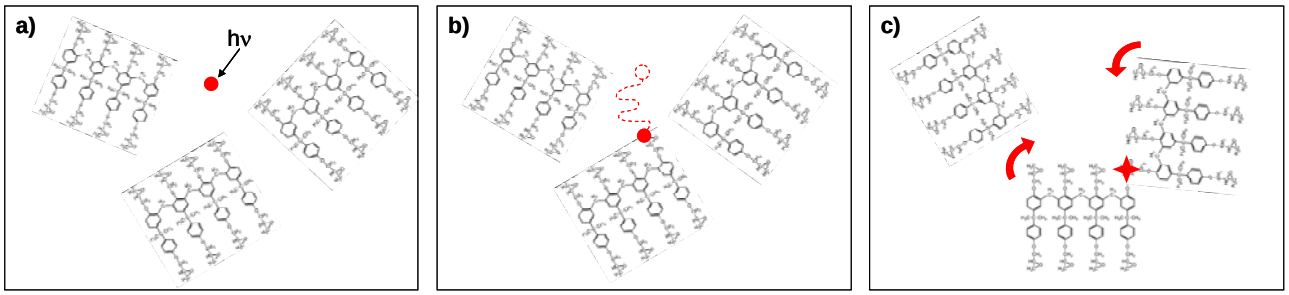

Figure 2.2-5: Schematic illustration of the polymerization of SU-8: (a) Activation of the photo-initiator by exposure to UV-light; (b) Eventual diffusion of the photo-acid to the epoxy-group of the SU-8 monomer; (c) Cross-linking between two monomers

During the step of photo-initiation, the onium-salt is decomposed by exposure to near-UV-radiation and a strong acid is formed (*Figure 2.2-5(a)*). Therefore, this process is also called photoacid-generation. The generated catalytic protons have an affinity to the oxygen of the epoxy-groups on the SU-8 monomer, which are partially negatively charged due to the free electron pairs (*Figure 2.2-5(b)*). The epoxy-ring is opened and a positive charge is formed on the carbon atom [82]:

initiation of polymerization

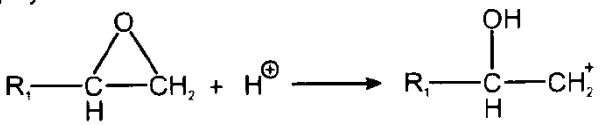

(2.2-1)

The opened epoxy-group is place for covalent binding to another epoxy-group (*Figure 2.2-5(c)*) and an ether-bond is formed [82]:

chain propagation

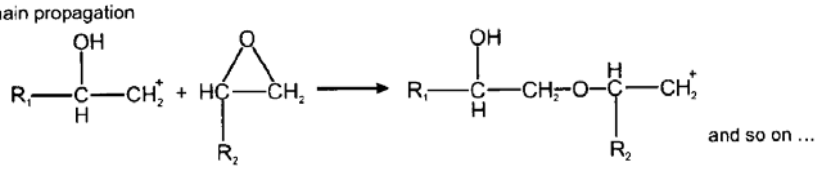

(2.2-2)

The cross-linking is continued and leads to the formation of polymer clusters and finally to a gel state. Termination of the propagating chains can occur by reaction with anions, solvent molecules or other species present in the reaction system [83].

The following mechanisms determine the polymerization of chemically amplified negative resists such as SU-8 [84]:

- Photo-acid concentration: The availability of photo-acid depends on the initial concentration of photo-initiator in the SU-8 and on the absorbed radiation energy
- Photo-acid diffusion: The generated photo-acid diffuses to the epoxy-groups of the monomers (*Figure 2.2-5(b)*). The propagation of the catalytic protons in the polymer melt is described by the diffusion rate R_d
- Monomer diffusion: Cross-linking is achieved by diffusion and rearrangement of the monomers or polymer clusters (*Figure 2.2-5(c)*)
- Polymerization reaction: The epoxy-rings are opened and formation of a cross-link takes place if another epoxy-group is available. The rate of cross-link formation among polymer chains or polymer clusters is described by the reaction rate R_p
- Cage effect: Above a certain degree of cross-linking the further polymerization is slowed down and comes finally to a complete stop. The reason is reduced mobility of the SU-8 molecules and limited diffusion of the photo-acid

If $R_d > R_p$, the polymerization of the resist is reaction-limited. In this case, the photo-acid diffusion is fast, which results in bad replication of the original lithographic pattern. If $R_d < R_p$, the diffusion of the photo-acid is the rate-determining step. The cross-linking reactions are fast, the polymer clusters are formed and further diffusion is prevented due to the cage effect.
Different authors tried to model the cross-linking of negative chemically amplified photoresists [85, 86]. Patsis and coworkers conclude on a diffusion-controlled polymerization in their study on Epoxy Cresol Novolak (ECR) resist [84, 85]. This resist had the same photo-initiator as SU-8 and structure and reaction mechanisms are comparable. Therefore, it is assumed that the photo-acid diffusion is the rate-determining step for the polymerization of SU-8 [81]. The diffusion rate R_d of the photo-acid in the SU-8 depends on the temperature and on the mobility of the photo-acid in the polymer matrix.
The high reaction rate R_p results in a fast opening of the epoxy-rings and a fast solidification of the polymer. The fast increase of the cage effect limits photo-acid diffusion and ensures the high resolution of the SU-8 structures [87]. The reaction rate R_p increases with temperature. On the other hand polymerization slows down due to a decrease in the concentration of the un-reacted epoxy groups and decreased mobility of the monomers as a consequence of the increasing cage effect.
The nature of the reaction medium plays a significant role in cationic polymerization. Large changes in rate and degree of polymerization are usually observed when the solvating power of the reaction medium is changed [83, 88].

2.3 Processing of SU-8

Figure 2.3-1 is an overview of the different steps involved in the processing of SU-8. In this section the main process parameters for each step are presented in detail.

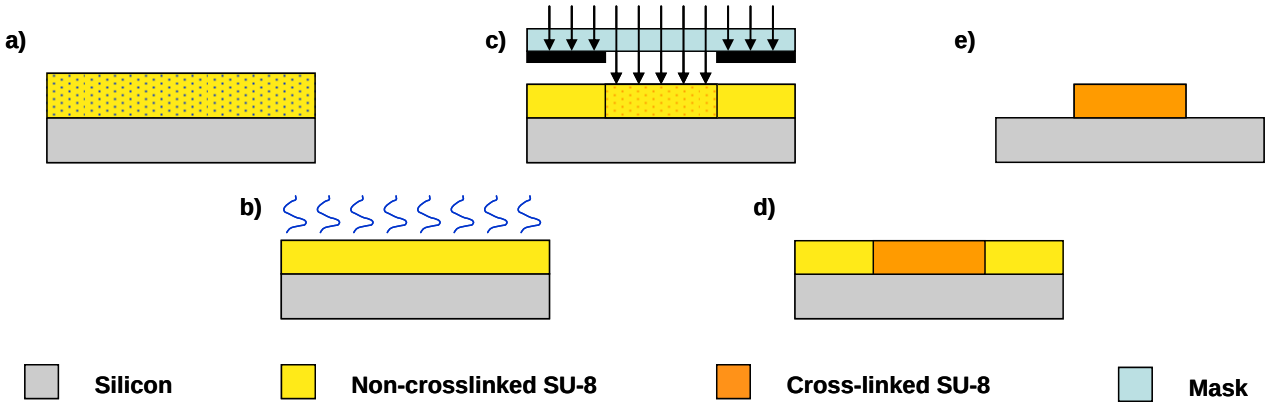

Figure 2.3-1: SU-8 processing steps: (a) spin-coating, (b) soft-bake, (c) exposure, (d) post-exposure-bake and (e) development

2.3.1 Spin-coating

A spin-coating system is used to deposit a film of photoresist on the substrate. Commonly, a first spin-coat cycle is used to spread the SU-8 on the wafer (spread cycle). This step is followed by the actual spin coating cycle (thickness definition cycle) at the final spin speed. For SU-8 layers with thicknesses t > 100 µm the use of this two-step spin-coating procedure is recommended. Furthermore, for the spin-coating of these films a rotative cover (Gyrset) can be used to improve the uniformity of the film. Solvent loss during spin-coating of thick films is minimal whereas it is considerably higher for thin films [78]. Therefore, for the spin-coating of thin SU-8 films (t < 10 µm) the spread cycle can be omitted to improve the uniformity of the films. The thickness of deposited layers ranges from 100 nm – 700 µm in one single step [63]. For thicker layers multilayer coating and baking can be applied.

Table 2.3-1: Main processing parameters for spin-coating of SU-8

Processing parameter		Range	Unit
Final spin speed	ω	0-7000/0-3000 (without/with Gyrset)	rpm
Spin speed acceleration	a_{sc}	0-5000	rpm/s
Spin coating time	t_{sc}	0-60	s
Viscosity of SU-8	η	Depends on product	Ns/m^2

Table 2.3-1 presents the main parameters for the spin-coating process. The spin-speed and the acceleration determine the final thickness and the uniformity of the resist film. The use of spin-speeds in the range of 1000-4000 rpm is optimal to achieve high uniformity.

2.3.2 Soft-bake

The goal of the soft-bake (SB) is to reduce the amount of solvent in the photoresist layer. The application of heat leads to diffusion of the solvent to the surface of the resist and to evaporation of the solvent molecules. Diffusion is the rate-determining step in this process step [78]. During the SB the viscosity and the density of the film increase. Conventionally, the SB is done on a hotplate. Soft-bakes consisting of one or of two temperature steps are frequently used. An alternative solution to evaporate the solvent is the use of an oven or an infrared-oven.

Table 2.3-2: Main processing parameters for the soft-bake of SU-8

Processing parameter		Range	Unit
Soft-bake temperature	T_{SB}	20-110	ºC
Soft-bake temperature ramping	a_{SB}	1-10	ºC/min
Soft-bake time	t_{SB}	Depends on film thickness	min

The main processing parameters for the soft-bake are presented in *Table 2.3-2*. Higher temperature and longer time result in more solvent evaporation and therefore in a lower residual solvent concentration. For T_{SB} = 130-135˚C the thermal activation of the photo-initiator will lead to a complete cross-linking of the photoresist [89]. For thick films (t > 100µm) the SU-8 is capable reflow and to self-planarize during the SB particularly at long t_{SB} (4-12 h) and high T_{SB} (90-120ºC) [90]. Therefore, it is important that the hotplate is perfectly leveled.

2.3.3 Exposure

The exposure step is responsible for the photo-initiation (*Figure 2.2-5(a)*). The processing parameters are shown in *Table 2.3-3*. Usually the exposure is done with UV-radiation at a wavelength λ = 365 nm, which corresponds to the i-line of the mercury lamp installed in conventional mask aligners. The exposure dose, determines the concentration of photo-acid that is released and that contributes to the polymerization.
Different optical phenomena must be considered to obtain good replication of the mask features. These include diffraction of incident UV light at the edge of the dark field lines of the mask, refraction of light at the air/polymer interface and reflection from the underlying substrate. First attempts of modeling the resulting UV light intensity at a specific point in the SU-8 film were published by Zhang et al. [91].
If the duration of the UV-exposure becomes long, heating at the interface with the mask can cause formation of hard skin at the surface of the SU-8 (T-topping). If the dose exceeds 250-300 mJ/cm^2 it is recommended to do the exposure of thick resist films in multiple steps. Between the exposure steps a waiting time is introduced to allow cool down of the SU-8.

Table 2.3-3: Processing parameters for SU-8 exposure

Processing parameter		Range	Unit
Exposure dose	D	Depends on film thickness	mJ/cm^2
Exposure mode		Hard, soft or proximity contact	

2.3.4 Post-exposure bake

After exposure the SU-8 is polymerized according to the cross-linking mechanism described in *Section 2.2.3*. The polymerization can in principle take place at room temperature, but a post-exposure-bake is introduced to increase the reaction rate. *Table 2.3-4* presents the processing parameters for the PEB. The PEB is usually done immediately after exposure to limit photoinitiator diffusion into non-exposed areas.

Table 2.3-4: Processing parameters for the post-exposure-bake

Processing parameter		Range	Unit
PEB temperature	T_{PEB}	0-120	ºC
PEB temperature ramping	a_{PEB}	1-10	ºC/min
PEB time	t_{PEB}	Depends on film thickness	min

2.3.5 Development

For development of the SU-8 patterns, the substrate is immersed in Propylene glycol methyl ether acetate (PGMEA). The development time is dependent on the layer thickness. After the development, the substrate is rinsed with isopropyl alcohol (IPA). White traces during rinsing indicate incomplete development of the SU-8. Finally, the wafer is dried in air or nitrogen.

2.3.6 Hardbake

Optionally a hard-bake of the SU-8 can be done on a hotplate or in an oven at temperatures of 100-200ºC. The goal is to increases the degree of cross-linking. Lin et al. introduced a second exposure followed by a hard-bake at 200ºC for 10 min after development of 1.5-mm-thick SU-8 films [90].

2.4 Influence of processing steps on the properties of SU-8

The different processing steps and the related parameters influence the processing results and the properties of the polymerized SU-8. As a result of the high interest in SU-8 for microfabrication, a large amount of work on process optimization has been published. The reports include optimization of soft-bake [92], exposure dose [91, 93] and post-exposure-bake [70] for UV-lithography but also for DUV-, X-ray, and e-beam-lithography [81, 89]. Typically, these process optimizations have been carried out for resist films with thicknesses of 50 µm up to several hundreds of micrometers and the main issues were structural stability, lithographic resolution, straight sidewall profiles and stress in the SU-8.
In this section, the relation between the processing parameters presented in *Section 2.3* and the polymerization mechanism described in *Section 2.2* is demonstrated. The discussion is a review on the influence of the processing steps on the properties of the SU-8. It is based on reported results and personal processing experience. The focus is on polymer properties that are relevant in the context of this thesis such as lithographic, mechanical and thermal properties.

2.4.1 Cross-linking density

There are different possibilities to express the degree of polymerization of a polymer. In the case of SU-8, polymerization implies opening of the epoxy-groups of the monomers as described by *Equation 2.2-2*. There, the degree of conversion is defined as the number of epoxy-groups participating in cross-linking divided by the initial number of epoxy-groups. Another closely related parameter is the cross-linking density Θ, which is the number of cross-links per volume. The cross-linking density is inversely proportional to the molecular weight between two cross-linking points M_c. In the cross-link density model Fedynyshyn defines a critical cross-linking density Θ_c to predict polymerization of negative photoresist [86]. For $\Theta > \Theta_c$ the resist becomes insoluble and image formation occurs.
In most cases, the measurement of the cross-linking is done indirectly because the mechanical and thermal properties of SU-8 are related to the degree of polymerization. Zhang et al. reported direct measurements of the degree of conversion as a function of exposure dose for a 110-µm-thick SU-8 layer (SU-8 100, MicroChem, USA). They used Fourier-Transform infrared (FT-IR) spectroscopy to determine the amount of epoxy-groups in the SU-8 resist after processing [91]. For the same samples, they measured M_c with dynamical mechanical analysis (DMA). The results of their study are represented in *Figure 2.4-1*. In the low exposure range on *Figure 2.4-1(b)* ($t < 50$ s), M_c is still very high as only long polymer chains and loosely cross-linked domains are formed. A dramatical decrease of M_c is observed for an increase of exposure time. Comparison with *Figure 2.4-1(b)* shows that the critical point corresponds to an epoxy conversion of 40%. There, enough epoxy-groups contribute to covalent bonds between the polymer chains and a highly cross-linked polymer network is formed. In summary, the processing steps have the following influence on the cross-linking density:

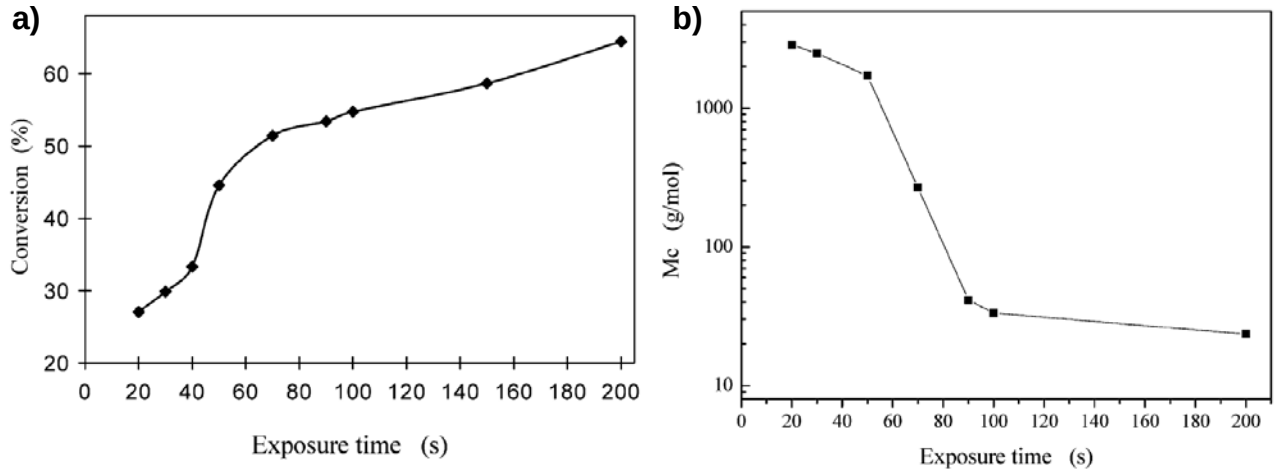

Figure 2.4-1: Measurement of epoxy-conversion (a) and molecular weight between cross-links M_c (b) as a function of exposure time with UV-lamp intensity of 10 mW/cm^2 [91]

Soft-bake:

- Small amount of solvent remaining in thick SU-8 films seems to decrease cracking. Increased residual concentration of solvent might improve cross-linking due to enhanced diffusion of the photo-acid and higher mobility of the monomers [89, 94]
- A higher solvent content might facilitate the photo-acid generation due to enhanced reaction with the anions formed during decomposition of the photoinitiator [75]

Exposure:

- The cross-linking density Θ increases for higher exposure dose D due to an increased photo-acid concentration [91, 95]

Post-exposure-bake:

- Higher T_{PEB} results in higher degree of cross-linking as a consequence of an increased rate of photo-acid diffusion R_d and a higher mobility of the SU-8 monomers
- Higher T_{PEB} increases the reaction rate R_p and therefore the cross-linking density
- Longer t_{PEB} results in higher Θ but the cross-linking rate decreases with time due to the cage effect and the decrease of the concentration of epoxy-groups

In general, the goal is to achieve a high cross-linking density during processing to ensure mechanical, chemical and thermal stability of the material. In principle, polymerization of the SU-8 continues as long as there are epoxy-groups available. This can result in a change of properties of the polymer after completed processing which is not suitable for most applications. A high initial cross-linking density should minimize polymerization after completed SU-8 processing. In this case, a reduced change of the mechanical and thermal properties with time is expected.

2.4.2 Lithographic properties

The most important lithographic properties of a photoresist are the contrast γ and the critical dose D_o. For a specific photoresist a characteristic curve can be determined and typically three domains can be identified (*Figure 2.4-2*) [74]:

- At high exposure doses the film is polymerized over the whole nominal thickness t_{nom} and nothing is dissolved after development
- Below the critical dose D_o the resist is completely dissolved during development
- A linear part in-between where the thickness evolves following $t = t_{nom}\,\gamma \ln(D/D_o)$, where the slope γ is called the contrast of the photo-resist

The contrast determines processing characteristics such as lithographic resolution and sidewall angle of the structures. Higher resist contrast results in straighter sidewalls and in improved resolution. The determination of a characteristic curve is not straightforward as it depends on the processing and on the thickness of the SU-8 [96].
Further, the absorption coefficient at the specific wavelength is important for the resist performance. The low absorption coefficient of the SU-8 at the wavelength of 365 nm (*Figure 2.4-3*) allows polymerization of thick resist films [65]. In combination with a high resist contrast this allows for the fabrication of structures with high aspect-ratio in one single step of exposure [63].

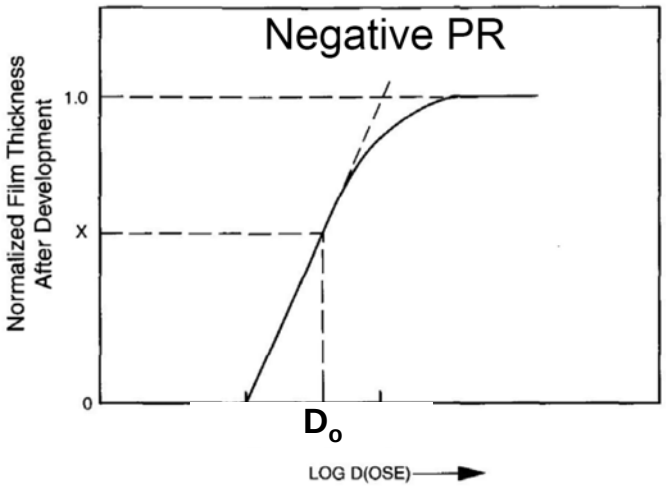

Figure 2.4-2: Sensitivity curve of a negative photoresist D_o is the critical dose where a solid is formed [74]

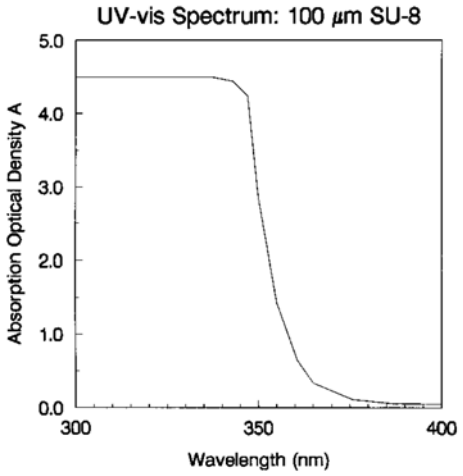

Figure 2.4-3: Absorption spectrum for a 100-µm-thick SU-8 film [65]

Most reported process optimizations are concerned with the direct consequences of the lithographic properties on the fabrication of SU-8 structures. Some conclusions are summarized in the following:

Soft-bake:

- The residual concentration of solvent after the soft-bake has a considerable influence on lithographic performance [89, 94, 97]

Exposure:

- Due to light absorption require films with a higher thickness a higher exposure dose to achieve polymerization
- Higher exposure dose has a negative impact on the resolution and leads to less vertical sidewalls [91, 93, 98, 99]
- Zhang et al. reported that the SU-8 gels wherever the exposure energy equals or exceeds the gelation energy of 30 mJ/cm^2 [91]

Post-exposure-bake:

- Thermal activation of the photo-initiator might decrease the contrast for processing at high T_{PEB} [94]

2.4.3 Mechanical properties

As mentioned in *Section 2.4.1*, the mechanical properties are closely related to the cross-linking density of the SU-8. Feng et al. have investigated the influence of the different processing parameters on the tensile properties of 130-µm-thick SU-8 films [100]. One conclusion is that the polymer undergoes a transition from ductile to fragile during the PEB. The Young's modulus E and the strength-at-break increase for higher D, longer t_{PEB} and higher T_{PEB}. Compared to the discussion in *Section 2.4.1*, this behavior can be explained with a higher cross-linking density of the SU-8.

Some published values of the mechanical properties of SU-8 are summarized in *Table 2.4-1*. The reported values for the Young's modulus E vary between 2-5 GPa. This demonstrates that the mechanical properties of the polymer film strongly depend on the processing parameters and on the film thickness.

Table 2.4-1: Mechanical properties of SU-8 reported in literature

Property	**Value**	**Ref.**
Young's modulus E	4.0 GPa (T_{PEB} = 95°C, GBL, 100 µm)	[62]
	0.7-2.7 GPa (T_{PEB} = 95°C, GBL, 130 µm)	[100]
	2.6 GPa (T_{PEB} = 96°C, GBL, 500 µm)	[101]
	1.9-2.7 GPa (T_{PEB} = 90°C, GBL, 5 µm)	[102]
Poisson's ratio ν	0.26	[103]
Strength	37.2-52.6 MPa (T_{PEB} = 95°C, GBL, 130 µm)	[100]
Elongation	3.9-5.2 % (T_{PEB} = 95°C, GBL, 130 µm)	[100]
Friction coefficient µ	0.19 (T_{PEB} = 95°C)	[62]
Surface roughness	0.4 ± 0.2 nm (fully crosslinked)	[56]

2.4.4 Thermal properties

The most relevant thermal properties are the glass transition temperature T_g and the coefficient of thermal expansion (CTE) α_{th}. Similar to the mechanical properties, the thermal properties are closely related to the cross-linking density [104]. This has been shown experimentally by Zhang and co-workers [91]. Their observations on T_g (*Figure 2.4-4*) are related to the ones on cross-linking density and epoxy-conversion (*Figure 2.4-1*). The glass transition temperature T_g increases with higher degree of cross-linking. Feng et al. studied the evolution of T_g during the PEB and identified T_{PEB} as main parameter determining T_g of the cross-linked resist [100]. There, T_g gradually increased until it reached T_{PEB} where it levels off. For T_{PEB} < 220˚C, the final T_g was about 5-10˚C higher than T_{PEB} . This can be explained by polymer physics:

$T_{PEB} > T_g$: The polymer is in the rubbery state. Cross-linking of the polymer is fast due to high mobility of the molecules and T_g increases

$T_g > T_{PEB}$: The polymer changes to the glassy state and the mobility of the SU-8 monomers is restricted. Further cross-linking becomes difficult and T_g stabilizes

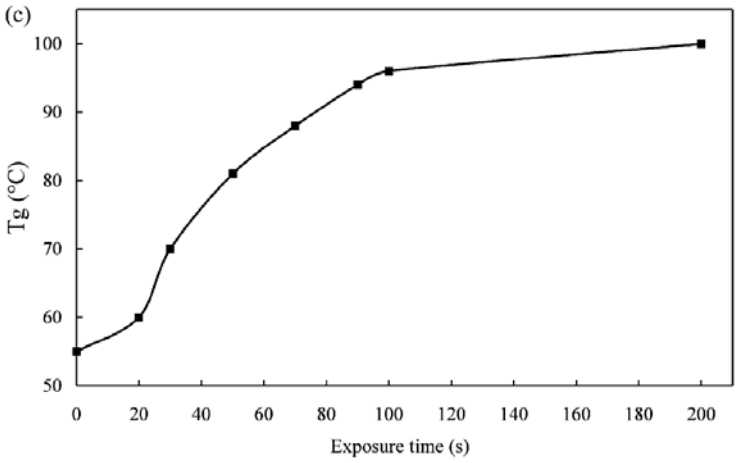

Figure 2.4-4:
T_g as a function of exposure time; film thickness = 110 µm; T_{PEB} = 95˚C [91]

It is important to remember, that the polymer reaches a kind of meta-stable state. Further increase of temperature would lead to a further increase of T_g. For fully cross-linked SU-8, T_g is reported to be higher than 200˚C [64]. The CTE is expected to decrease with an increase in cross-linking density. *Table 2.4-2* summarizes reported values for the thermal properties of SU-8.

Table 2.4-2: Thermal properties of SU-8 reported in literature

Property	Value	Ref.
Glass transition temperature T_g	~50°C (unexposed)	[64, 100]
	> 200°C (fully cross-linked)	[64, 100]
Degradation temperature T_d	~380°C (fully crosslinked)	[64]
Coefficient of thermal expansion α_{th}	52.0±5.1 ppm/K (T_{PEB} = 95°C, 20 µm)	[105]
	102 ppm/K (T_{PEB} = 200°C, 130 µm)	[100]

2.5 Stress induced in SU-8 films during processing

A critical issue in processing of polymers is the stress resulting from the different processing steps. In general, in-plane stress leads to delamination or cracking for non-released films and in out-of-plane bending for released structures such as cantilevers.
The residual stress in the SU-8 film after processing on a silicon substrate is a combination of intrinsic and extrinsic stress. Extrinsic stress involves an externally applied force or a change in ambient conditions. There, thermal stress is the important component in case of the SU-8 processing. For thin films ($t_{SU8} << t_{Si}$) processed on a silicon substrate, the residual stress can be calculated by Stoney's formula [106]:

$$\sigma_{SU8} = \frac{E_{Si}}{6(1-\nu_{Si})}\frac{t_{Si}^2}{t_{SU8}}\frac{1}{R} \quad [Pa] \qquad (2.5\text{-}1)$$

σ_{SU8} = stress in the resist E_{Si} = Young's modulus substrate t_{Si} = substrate thickness
R = curvature radius ν_{Si} = Poisson's ratio substrate t_{SU8} = film thickness

The curvature radius R can be measured by a profilometer. For thicker films calculation of the stress becomes difficult and new models have to be developed.

2.5.1 Intrinsic stress

Intrinsic stress is mostly generated during cross-linking due to the confinement of the monomers in the rigid polymer matrix. The main sources of intrinsic stress are:

- Densification due to polymerization
- Loss of mass due to solvent evaporation or swelling due to solvent absorption
- Change of stiffness due to polymerization (E increases, α_{SU8} decreases)

The shrinkage due to polymerization and solvent evaporation results in tensile stress. Only the shrinkage after solidification of the resin is able to contribute to the formation of intrinsic stress.

Before solidification the resist is considered fluid enough to allow the intrinsic stress to relax completely [107]. Stress due to solvent absorption is expected to be compressive.

2.5.2 Thermal stress

Thermal stress arises during the temperature cycling involved in SU-8 processing. It results from the mismatch of the coefficients of thermal expansion (CTE) of silicon substrate and SU-8. The thermal stress σ_{th} can be estimated by the following equation [108]:

$$\sigma_{th} = \left(\alpha_{SU8} - \alpha_{Si}\right)\frac{E_{SU8}}{\left(1-\nu_{SU8}\right)}\left(T_{PEB} - T_o\right) \qquad (2.5\text{-}2)$$

α_{Si} = CTE of substrate α_{SU8} = CTE of resist E_{SU8} = Young's modulus of resist
T_o = ambient temperature ν_{SU8} = Poisson's ratio of resist

Theoretically thermal stress has first to be considered upon the onset of polymerization of the SU-8 because the Young's modulus for non-cross-linked SU-8 is not defined. In *Section 2.4* it was discussed that E_{SU8} and α_{SU8} are dependent on the cross-linking density of the polymer. Therefore, both values are varying during the PEB of the SU-8 and estimations of the thermal stress might be difficult. The thermal stress is tensile because the polymer layer contracts more than the silicon substrate during cool-down after the PEB. The replacement of the silicon with a material with a similar CTE as SU-8 is an approach to minimize thermal stress.

2.5.3 Influence of the processing steps on stress in the SU-8

In *Section 2.3* the different processing steps and the corresponding parameters were presented. In literature, there is an on-going discussion on the influence of the process steps on the residual stress in SU-8 devices. In the following, some of the reported conclusions are summarized:

Soft-bake:

- The stress induced in the SU-8 layer during soft-bake is small due to relaxation of the non-polymerized structure [105]

Exposure:

- The exposure-step itself induces minimal stress changes in the resist [105]
- Long exposure times may heat the SU-8 and initiate the cross-linking of the top-layer. This leads to a non-uniform resist film and intrinsic stress gradients
- Increased exposure dose leads to more delamination and higher residual stress. Higher exposure dose results in improved cross-linking and probably in increased shrinkage during polymerization [81, 109]

Post-exposure-bake at T_{PEB}:

- Particularly during the first minutes of the PEB the cross-linking of epoxy resists results in densification and the formation of intrinsic stress [107]
- If the mobility of the monomers is restricted bonds with high intrinsic stress are formed which results in micro-cracks. Therefore, intrinsic stress is reduced for higher T_{PEB} [81, 105]
- Longer t_{PEB} allows relaxation of intrinsic stress [105]

Cool-down to room-temperature:

- The increase of thermal stress during cool-down is considerable and explained by the thermal mismatch between substrate and SU-8 (*Equation 2.5-2*) [105]
- Higher T_{PEB} results in more delamination after cool-down of the SU-8 probably due to thermal stress [109].
- Slower cooling allows higher stress relaxation [70]

Development:

- The crack density is increased with increasing development time. This might be caused by stress release upon removal of loosely cross-linked polymer clusters or by an increase of intrinsic stress due to developer absorption

Some authors claim that relaxation times between the different processing steps decrease the residual film stress [110].

2.5.4 Change of stress after processing

There are several sources for a change in intrinsic stress after completed processing:

- Polymerization: Cross-linking continues and the intrinsic stress increases. This can be minimized by a high initial degree of polymerization (*Section 2.4)*
- Solvent effects: Evaporation of solvent residues or absorption of compounds from the environment results in a change of intrinsic stress (*Section 2.5.2*)
- Physical ageing: At temperatures below T_g relaxation of intrinsic stress occurs

Several authors demonstrated that annealing of an epoxy resin at temperatures below T_g results in stress relaxation, even if it is considered in the fully cured state [111]. This process is called physical ageing [112]. As a thermoset is cooled through its T_g it passes into the glassy state. Particularly if the cool-down is fast, the polymer is frozen in a structural non-equilibrium. Annealing allows for stress relaxation and the approach of the equilibrium state. The ageing process results in significant changes of the properties of the resist. Further, the volume of the polymer decreases.
The amount of physical ageing is dependent on the anneal time and temperature. The closer the annealing temperature to T_g, the faster is the physical ageing [113]. Further, the rate of relaxation decreases as the polymer approaches the structural equilibrium. For other polymers it was demonstrated that physical ageing is strongly dependent on the cross-linking density [114]. Ageing takes place more rapidly for coatings with a low degree of polymerization.

The described ageing effects, and the stress history of the polymer in general, are completely reversible by heating the epoxy above its T_g [111]. This is for example the case for a hard-bake of the SU-8.

2.5.5 Stress reduction through mask design

During the design of the photomask for the UV-exposure some measures can be taken to reduce the issues related to film stress during fabrication of SU-8 structures. In general, the higher the percentage of exposed area on the wafer, the higher the resulting stress [115-117]. Large continuous surfaces should be avoided to reduce cracking and collapse of deep trenches [90]. A possible solution is the introduction of holes for stress release for example the use polygon structures [118]. Concave corners with angles below 120° should be avoided because they are sources for cracks during processing due to local stress concentration. Round corners are in general a good alternative.

2.6 Fabrication of SU-8 cantilevers

The traditional surface micromachining process for the fabrication of SU-8 cantilevers is illustrated in *Figure 2.6-1*. A Silicon substrate is used as a carrier wafer. A sacrificial layer is deposited to allow the release of the devices after the completed fabrication (*Figure 2.6-1(a)*). In a first step of SU-8 photolithography the thin cantilevers are defined *(Figure 2.6-1(b))*. Then a second step of photolithography with SU-8 is added to define the chip body (*Figure 2.6-1(c)*). The purpose of this structure is to allow the handling of the chip but even the integration of a complete microfluidic system is possible. Finally, the chip is released from the substrate by etching of the sacrificial layer (*Figure 2.6-1(d)*). In the Nanoprobes group, this approach was used for the microfabrication of a wide variety of cantilever-based sensors [43, 54-56].
Here, the fabrication parameters and the equipment conventionally used for the SU-8 processing are defined. The complete process sequence is summarized in *Appendix B*. If not stated otherwise in the course of this thesis, the described methods have been used. The release method will be discussed separately in *Chapter 3*.

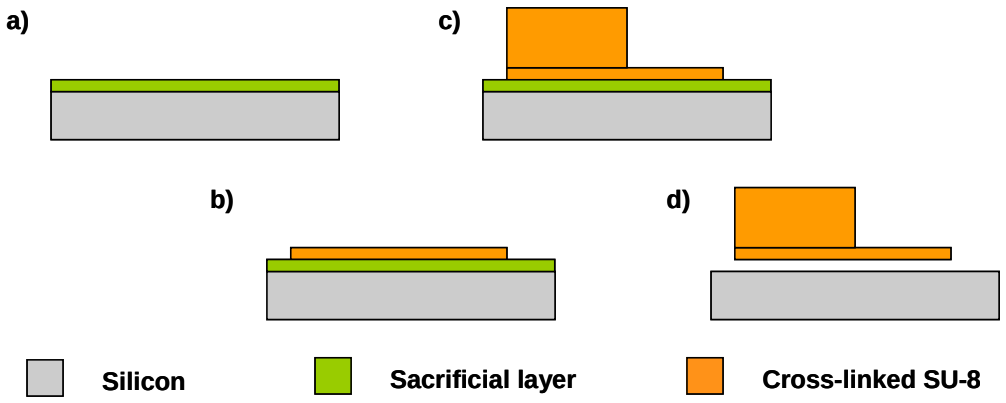

Figure 2.6-1: Cantilever fabrication process: (a) Deposition of sacrificial layer; (b) Patterning of cantilevers; (c) Patterning of chip body; (d) Release by etching of sacrificial layer

2.6.1 The cantilevers - Processing of thin SU-8 films

Thin SU-8 films in the context of this thesis are films that are processed using SU-8 2002 or SU-8 2005 (MicroChem, USA) and that have a thickness t < 10 µm. The fabrication of cantilevers and flappers with these thicknesses allows a high sensitivity of the devices towards changes in surface stress (see *Section 1.2*).
Table 2.6-1 is an overview of the parameters used for the spin-coating of the SU-8 and the measured thickness of the film. The spin-coating is done on a standard spin-coater (RC8, Karl-Süss, France). Approximately 3 ml of the resist are manually dispensed onto the substrate. Soft-bake and PEB are done on a programmable hotplate (Harry Gestigkeit GmbH, Germany). The exposure is done on an UV-aligner (MA6/BA6, Karl-Süss, Germany) using a mercury lamp. The aligner was equipped with an i-line filter (365 nm, 20 nm FWHM) because the increased SU-8 absorption at shorter wavelengths would jeopardize the resolution. The development of the SU-8 was done by immersion in two consecutive baths of PGMEA in a wet bench designated only for this purpose.
For the parameters of soft-bake, exposure and PEB most users follow the recommendations of the producer [76]. *Table 2.6-2* describes such a process that was typically used in the Nanoprobes group. This conventional processing of thin SU-8 films is defined as *Process A* in the context of this thesis. The characteristics of this approach are a soft-bake at relatively high temperature to remove most of the solvent and a PEB at the same temperature to accelerate the cross-linking. The selected temperatures are above the glass transition temperature of the non-crosslinked resist but below the temperature for thermal activation of the photoinitiator.

Table 2.6-1: Spin-coating parameters and nominal thicknesses for thin SU-8 films

Product	Spin-speed [rpm]	Acceleration [rpm/s]	Time [s]	Thickness t [µm]
SU-8 2002	5000	5000	30	1,0
	2000	5000	30	1,7
	1500	5000	30	2,0
	1000	5000	30	2,7
SU-8 2005	4000	5000	30	3,7
	2000	5000	30	5,6

Table 2.6-2: Process A - Conventional processing of thin SU-8 films

Process step	Equipment	Parameters
Spin-coating	KS Spinner	see *Table 2.6-1*
Soft-bake	Hotplate	10 min, 60ºC; 10 min, 90ºC; ramping 10ºC/min
Exposure	KS Aligner	500 mJ/cm^2; soft-contact
Post-exposure bake	Hotplate	10 min, 60ºC; 10 min, 90ºC; ramping 10ºC/min
Development	PGMEA	2 min FIRST, 2 min FINAL
Rinse	Isopropanol	30 s

2.6.2 The chip body - Processing of thick SU-8 films

Thick SU-8 films for the fabrication of the chip body or the microfluidic system are processed using SU-8 2075 (MicroChem, USA) and typically have thicknesses t > 150 µm. The processing of the thick SU-8 films is done on the same equipment as described in the previous section. For the dispensing of the viscous resist a pneumatic syringe pump is used. Further, the spin-coating is done

in two steps and the Gyrset is mounted. During the exposure, a non-contact mode is used to avoid stiction of the mask to the photoresist.
Table 2.6-3 describes a thick-film-process typically used in the Nanoprobes group and defined as Process A*. The concept of this conventional processing approach is the same as for *Process A* described previously.

Table 2.6-3: Process A - Conventional processing of 150-µm-thick SU-8 films*

Process step	Equipment	Parameters
Spin-coating	KS Spinner	100 rpm/s, 500 rpm; 15 s; 200 rpm/s, 1000 rpm; 30 s
Soft-bake	Hotplate	30 min, 60ºC; 60 min, 90ºC; ramping 10ºC/min
Exposure	KS Aligner	4x270 mJ/cm^2; proximity contact
Post-exposure bake	Hotplate	30 min, 60ºC; 60 min, 90ºC; ramping 10 ºC/min
Development	PGMEA	15 min FIRST, 15 min FINAL
Rinse	Isopropanol	30 s

2.7 Conclusion

The negative epoxy-photoresist SU-8 shows excellent properties for microfabrication. Particularly the availability of a large range of film thicknesses that can be patterned using the same equipment is an advantage for fabrication of complete microsystems. On the other hand, the processing of SU-8 involves a various parameters. The fabrication with SU-8 has to be optimized based on the properties required for a specific application. A review of reported process optimizations demonstrated the influence of the processing parameters on the properties of the polymer and on the stress in the resist. The large variety of reported results shows that exact monitoring of the process parameters is crucial. In comparison to traditional materials in microfabrication, processing of SU-8 has to include a careful control of the time between the different processing steps. The SU-8 has always to be considered in a kind of meta-stable state. The properties of the polymer can change with time due to further cross-linking and relaxation processes after the end of processing. The mechanical-, thermal- and time-stability of the polymer is increased if a high cross-linking density is achieved during the fabrication.

3 Dry release of polymer cantilevers

3.1 Goal of the process optimization

The release of micromechanical devices from supporting substrates is a critical fabrication step, due to the increased importance of adhesive surface forces at micrometer dimensions. Traditionally, etching of sacrificial layers was used for the release of polymer cantilevers after completed device fabrication as shown on *Figure 2.6-1*. Wet release methods have been used but stiction of the cantilevers upon drying is an inherent problem and the release-etch is very time consuming for large chips [55, 82, 116]. Dry release methods such as sacrificial etch of poly-silicon [118] or polyimide [119] solved some of these problems but the processes show very low etch rates and are done above room temperature which induces stress in the polymers [120].
Therefore, various attempts were made to develop dry release methods using antistiction coatings [121, 122]. The reduced adhesion between substrate and chip allows a mechanical release of the fabricated devices. Recently, a simple dry release method for thin polymer structures using a deep reactive ion etching reactor was published by Daniel Häfliger from the Nanoprobes group (DRIE) [123]. *Figure 3.1-1* illustrates the concept. The C_4F_8 precursor gas of the passivation plasma during deep anisotropic etching is applied to deposit a thin fluorocarbon layer on the substrate (*Figure 3.1-1(a)*). After completed polymer processing on this nonadhesive substrate, the polymer devices can be mechanically released by the use of razor blades or tweezers (*Figure 3.1-1(e)*). The advantages of this method are the fast release of large polymer chips and the reduced risk of stiction due to the low surface free energy of the deposited fluoropolymer.

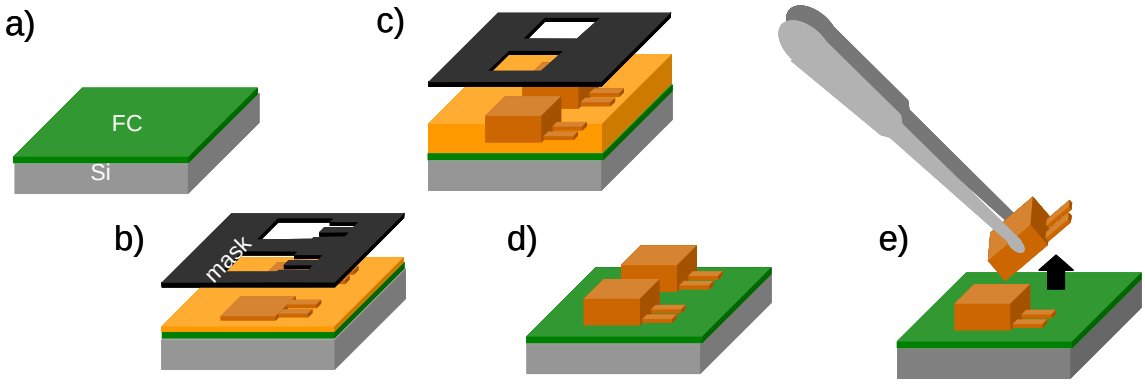

Figure 3.1-1: Dry release of polymer cantilevers: a) Coating of substrate with fluorocarbon release layer; b)-c) spin-on and lithography of SU-8; d) resist development; e) device release by mechanical tweezers [123]

As mentioned in *Chapter 1,* it is of interest to reduce the thickness of the flappers to increase the sensitivity towards changes in surface stress. This implies the compatibility of the release method for thin SU-8 films as the structures need to be removed from the handling substrate after completing fabrication. Furthermore, the processing of thin polymer films requires spin-coating of resists of low viscosity. For thin SU-8 layers encountered problems were encountered with the release method presented previously. The fluorocarbon coating was too hydrophobic to allow sufficient wetting by the low viscosity SU-8 during the spin-coating procedure. Therefore, the fabrication of structures with thicknesses below 5 µm was difficult. This demonstrates that the

release of thin SU-8 films requires a very precise control of the surface properties of the fluoropolymer.
Some research groups have published studies on film composition, deposition rate, and wetting behavior of fluorocarbon layers deposited in a DRIE but their focus has been on the use of this film as the passivation layer for deep anisotropic etching [124, 125]. Moreover, Zhuang and Menon have performed a study on the wetting properties and thermal stability of the deposited films to evaluate the use as antistiction coatings for nanoimprint lithography [126]. The latter reported no variation of the surface free energy as a function of the deposition parameters.
The goal of the following experimental study was to modify the surface properties of the release layer by varying the deposition parameters in the DRIE equipment. In *Section 3.2* the influence of the processing parameters on deposition rate and surface properties is investigated. The optimized fluorocarbon coating should allow spin-coating of arbitrary thin SU-8 films. At the same time, the dry release of thin SU-8 devices such as cantilevers or membranes should easily be possible. The results of these experiments are presented in *Section 3.3*. Finally, the influence of the release-method on the surface properties of the polymer films is demonstrated in *Section 3.4*.

3.2 Fluorocarbon deposition

3.2.1 Materials and method

The fluorocarbon coatings were deposited using the passivation cycle of a DRIE reactor (standard rate ASE, STS-Surface Technology Systems, UK). Silicon wafers without any precleaning were introduced in the plasma chamber. An O_2-plasma (coil power = 800 W, platen power = 20 W, gas flow = 45 sccm, chamber pressure = 45 mTorr, time = 5 min) was used for chamber conditioning and for removal of residuals on the substrate and the chamber walls. This step was followed by the actual fluorocarbon deposition using C_4F_8. The influence of various parameters on deposition rate and surface properties of the fluorocarbon was investigated. The design of experiments (DoE) for the initial screening experiments was made using the software MODDE 6.0 (Umetrics AB, Sweden). *Table 3.2-1* summarizes the parameter range explored by a total number of 50 experiments. According to literature, the deposition time t_{dep} has only a minor influence on the surface composition [124, 125]. Therefore, only one experimental series with variable time was performed and for the other depositions the time was fixed at 1 min. Before unloading the wafer, a short Ar-plasma was applied for declamping (400 W, 0 W, 50 sccm, 50 mTorr, 10 s). This plasma step has to be considered as an integral part of the deposition procedure. Shimmura et al. reported that extended ion irradiation of fluorocarbon films in Ar-plasma leads to defluorination and cross-linking of the surface layer [127]. During all the experiments the substrate temperature was kept constant at 20 ºC by backside-cooling with helium.

Table 3.2-1: Explored parameter range for deposition of fluorocarbon coatings

Parameter	Variable	Minimum	Maximum
Chamber pressure [mTorr]	p_c	0.3	90
Gas flow [sccm]	f	10	300
Coil power [W]	W_c	300	1000
Platen power [W]	W_p	0	20

Surface properties were determined by means of static contact angle measurements on a contact angle meter (DSA10, Krüss GmbH, Germany) equipped with automatic dispensing system and drop shape analysis software. Test liquids were de-ionized water, di-iodomethane (Aldrich 99%), and ethylene glycol (Aldrich 99,8%). For each liquid, five sessile droplets with a volume of 2 µl were deposited on the fluorocarbon surface and at least ten automated drop shape analyses were performed on each droplet. The use of three liquids with different surface tensions and variable ratios of dispersive-to-polar components allowed the calculation of the surface free energy γ_s of the deposited coating by the Owens-Wendt-Rabel-Kaelble method [128-130].
Thickness measurements were performed by a profilometer (Dektak 8, Veeco, France) on trenches in the fluorocarbon film. The trenches were made by a scalpel that was unable to penetrate the silicon substrate. The topographical resolution limit of this method is about 5 nm. Roughness measurements on the fluorocarbon surface performed with an atomic force microscope (AFM) in tapping mode were not successful. The problem was bad resolution due to the sliding of the AFM-tip on the slippery surface. Initial tests with secondary ion mass spectroscopy (SIMS) for the investigation of the film composition did not allow any conclusions. The resolution of the available equipment was not sufficient to evaluate the fluorine-to-carbon (F:C)-ratio for the different coatings.

3.2.2 Contact angles and surface free energy

For all the deposited coatings, the surface was hydrophobic with water contact angles $\theta_{H2O} > 90º$. Moreover, the contact angles for all the test liquids varied about 10º in the chosen parameter range, as defined in *Table 3.2-1*. The chamber pressure p_c was identified as the most important parameter determining the surface free energy γ_s of the fluorocarbon coatings. It was very difficult to show systematic influences of the other experimental parameters such as gas flow, coil power, and platen power.
Figure 3.2-1 shows the static water contact angle and the surface free energy as a function of chamber pressure for W_c = 300 W, W_p = 0 W, f = 120 sccm and t_{dep} = 60 s. It is possible to identify two different regimes. In the low-pressure regime $p_c < 40$ mTorr the contact angle decreased from 110.9º at 5 mTorr to 105.0º at 40 mTorr. The behaviour for the other test liquids was similar, which means that the surface energy increases from 13.8 to 17.2 mJ/m^2 in that interval. In general, an increase in surface free energy is attributed to a lower F:C-ratio in the deposited film [126, 131]. The results between 10 and 40 mTorr correspond well to those reported by Labelle et al. who observed a decrease of the F:C-ratio with increasing pressure [125]. At pressures $p_c > 40$ mTorr, water contact angle and surface free energy saturate and remain more or less constant. For this pressure regime, no data has been published by other groups.
The comparison of the values measured directly after deposition with the ones measured five days later shows a similar behaviour of contact angle and surface free energy. This suggests that some days of storage should not affect further processing.

3.2.3 Deposition rate

In accordance with results reported by other authors [124-126], the observed deposition rate was mainly governed by the coil power. It varied from 0 to 132 nm/min in the explored parameter range. Higher coil power resulted in higher deposition rates, which can be explained by the higher density of reactive components in the plasma. Furthermore, the chamber pressure had a significant

influence on the deposition rate (*Figure 3.2-2)*. In the low-pressure regime (p_c < 40 mTorr), the deposition rate decreased almost linearly. At higher pressures, no significant film thickness could be measured with the profilometer. There, the deposited film must be thinner than 5 nm. A higher chamber pressure implies a higher plasma density and in principle more species available for deposition. However, increasing the pressure also increases the significance of physical and chemical etching reactions that counteract film deposition. This could finally rather result in a surface activation of the silicon substrate by fluorocarbon species than in an actual polymer deposition. Nevertheless, the surface properties were modified (*Figure 3.2-1*). The silicon substrate was rendered considerably hydrophobic due to reactions in the fluorocarbon plasma. In the context of this thesis, the term fluorocarbon coating is used for all the investigated surfaces, well aware of the fact that it might be wrong to talk about a deposit in the high-pressure regime.

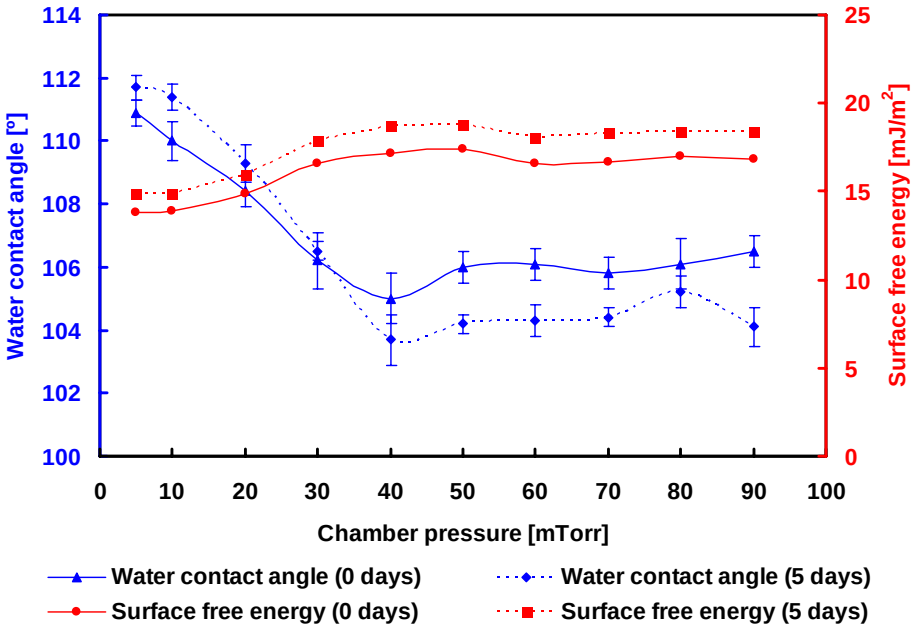

Figure 3.2-1: Water contact angle and surface free energy of fluorocarbon coatings deposited at variable p_c directly after deposition and after 5 days of storage; W_c = 300 W; W_p = 0 W; f = 120 sccm; t_{dep} = 60 s

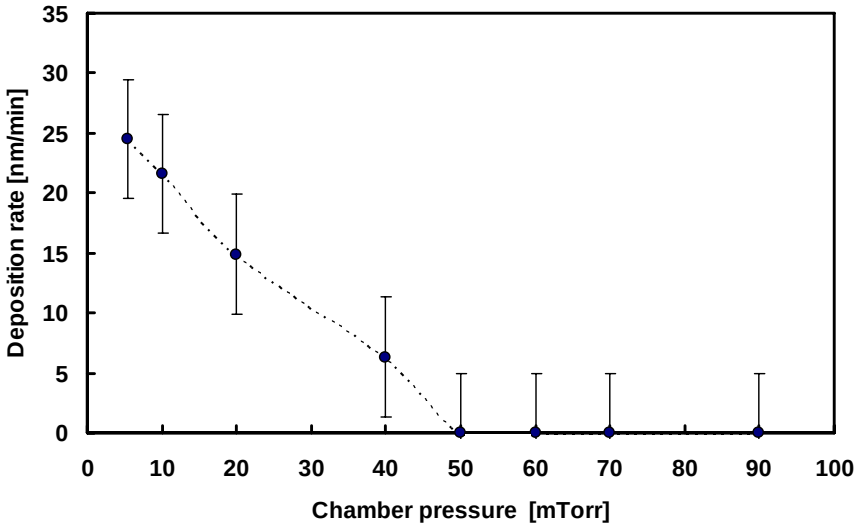

Figure 3.2-2: Fluorocarbon deposition rate at different chamber pressures; other parameters as Figure 3.2-1

3.2.4 Influence of deposition time

The influence of deposition time t_{dep} on the deposition rate and surface properties of the fluorocarbon coating was not investigated in detail. *Figure 3.2-3* shows no effect on the water contact angle if the duration of the process was longer than t_{dep} = 1 min used in most of the experiments. The thickness of deposited films seems to increase linearly with time, which compares well to results published by others [124, 125].

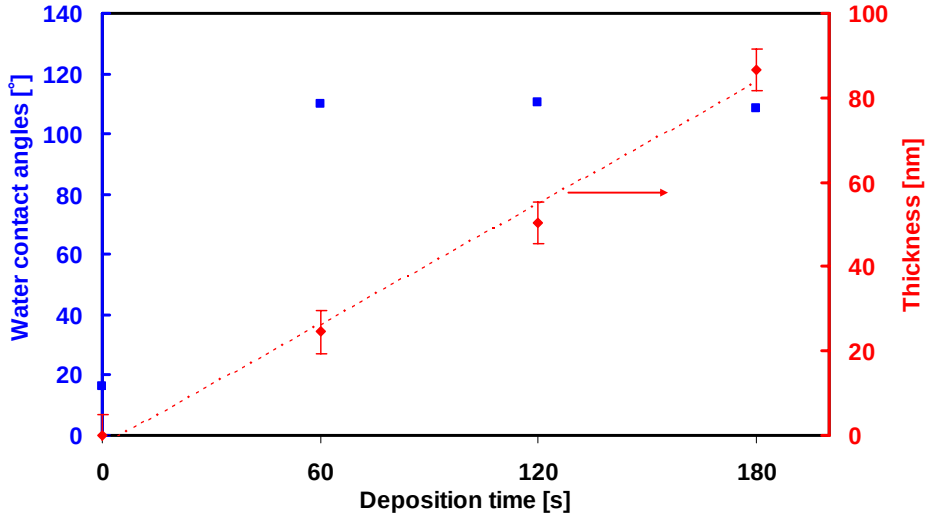

Figure 3.2-3: Water contact angle and thickness for variable t_{dep}; W_c = 300 W; W_p = 0 W; f = 120 sccm; p_c = 5 mTorr

3.2.5 Addition of O_2-gas:

Some experiments were performed to evaluate if the addition of a small amount of oxygen gas to the plasma results in more polar groups on the surface to even improve the wettability. In contradiction to the expected effect, the surface becomes more hydrophobic with increasing O_2:C_4F_8-ratio. *Figure 3.4-2* shows that the deposition rate decreases considerably with an increase in O_2:C_4F_8-ratio which indicates that etching effects might become important with an increase of the amount of oxygen in the plasma.

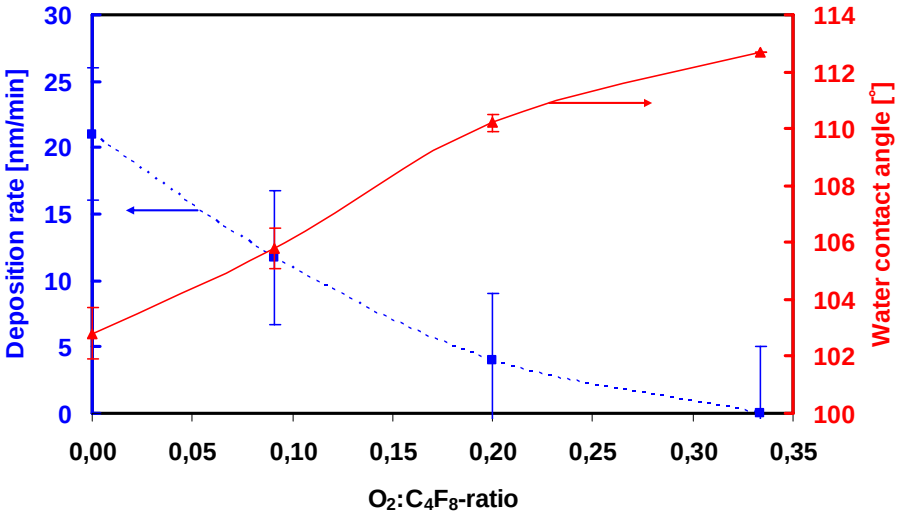

Figure 3.2-4: Deposition rate and water contact angle for variable O_2:C_4F_8-ratio at constant total gas flow of 300 sccm; W_c = 1000 W; W_p = 0 W; p_c = 90 mTorr, t_{dep} = 60 s

3.3 Spin-coating and release of thin SU-8 films

Two steps are critical in the fabrication of thin SU-8 structures by the presented release method. Both are directly related to the surface properties of the deposited fluorocarbon and have been considered during the optimization of the release-coating:

- Spin-coating: Spreading of thin resist films during spin-coating is governed by a force balance between centripetal and viscous forces. If the surface free energy of the fluorocarbon coating is very low and the resist itself has a very low viscosity, the viscous forces are too weak to keep a significant amount of resist on the wafer. Most of the resist slides off the wafer. The centripetal forces prevail over viscous forces which results in incomplete wetting of the substrate by the SU-8

- Device release: The adhesion of the processed SU-8 might improve on fluorocarbon coatings with high surface free energy and specific chemical composition. The stiction of the SU-8 film to these surfaces might considerably decrease the release yield of the devices

3.3.1 Materials and method

For the evaluation of the spin coating procedure, the percentage of resist coverage of the wafer was defined as spin-coating yield. To determine this parameter on different fluorocarbon coatings, a UV-photolithography process with SU-8 2002 was performed (*Figure 3.1-1(b)*). For these experiments, fluorocarbon coatings were deposited at various pressures in the range of 5–90 mTorr, while the other parameters were constant (W_c = 300 W, W_p = 0 W, f = 120 sccm, t_{dep} = 60 s). The choice of these parameters was a result of the experiments in *Section 3.2*. The spin-coating of the SU-8 was done at 1000 rpm for 30 s with an acceleration of 5000 rpm/s resulting in a film thickness of 2.3 µm. The resist was processed according to *Process A* described in *Section 2.6 (Appendix B)*. A mask defining 364 cantilever chips distributed uniformly over the whole wafer area was used for the UV-exposure. After processing of the thin SU-8 film, the number of reproduced chips was counted and the spin-coating yield was calculated.
For the evaluation of the actual release yield of the cantilever chips, a 160-µm-thick chip body was defined in a second step of photolithography (*Figure 3.1-1(c)*) using the parameters of *Process A*[*] (*Appendix B*). The addition of this thick polymer structure allowed the mechanical release and the handling of the thin cantilevers in a manner required by real applications. The finished polymer chips were released mechanically by tweezers (*Figure 3.1-1(d)*). Cantilevers with four different dimensions were used to determine the release yield from a particular fluorocarbon coating. For each dimension, five chips with an array of nine cantilevers were released, and the number of cantilevers which remained intact was counted. Similar to the described fabrication process for the cantilever chips, a two-step photolithography process with SU-8 was performed to fabricate large chips (2 x 5 cm^2) with an array of 40 polymer membranes. The square membranes were 1.7 µm thick and had a base length of 2 mm. For the evaluation of the membrane release yield, three membrane arrays were released from each fluorocarbon coating by the use of razor blades.

3.3.2 Spin-coating

Some initial spin-coating experiments on fluorocarbon coatings identified the ramp-up acceleration as a very critical parameter. Accelerations as high as 5000 rpm/s resulted in improved wetting of the substrate as they allowed overcoming the surface tension of the photoresist. *Figure 3.3-1* shows the spin-coating yield as a function of the chamber pressure p_c during plasma polymerization. On fluorocarbon coatings deposited at $p_c \geq 30$ mTorr, the spin-coating yield was close to 100%. If the deposition was done at $p_c < 30$ mTorr, the wetting of the substrates was incomplete. A comparison with the surface free energy γ_s for the same deposited fluoropolymers *Figure 3.2-1* shows that $\gamma_s >$ 16 mJ/cm^2 was required to allow for reliable spin-coating of 2.3-µm-thick SU-8 films. As expected, fluorocarbon-coated substrates with higher surface free energies showed improved wetting by the SU-8. In other experiments, spin-coating of uniform SU-8 films with thickness down to 500 nm was easily achieved on fluorocarbon coatings deposited in the high-pressure regime.

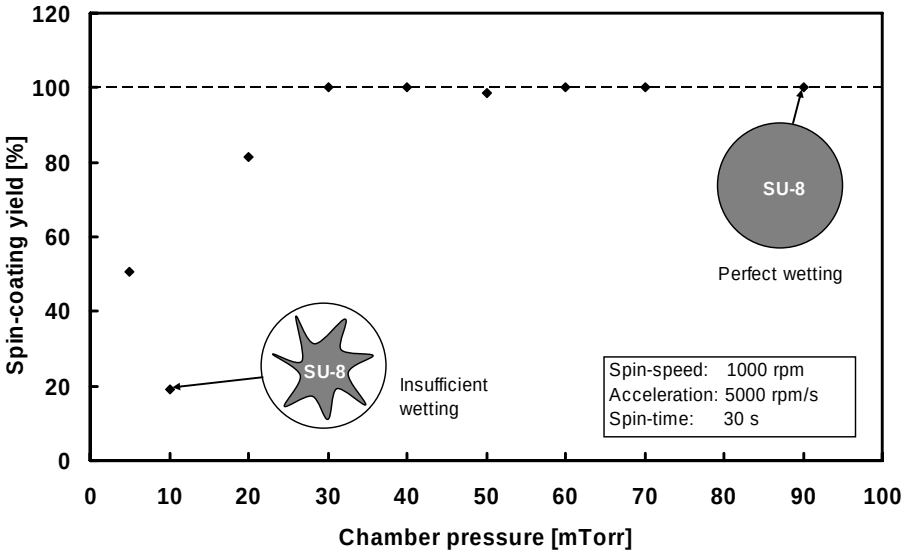

Figure 3.3-1 Spin-coating of SU-8 2002 on fluorocarbon layers 5 days after deposition at variable chamber pressu-re (other parameters see Figure 3.2-1)

3.3.3 Release

Figure 3.3-2(a)-(c) shows a released SU-8-chip with an array of nine cantilevers (L = 200 µm, w = 50 µm, t = 2.3 µm). *Figure 3.3-3(a)* summarizes the release-yield for two selected cantilever dimensions. A 1.7-µm-thick SU-8 membrane with a base length of 2 mm is shown on *Figure 3.3-2(d)*. *Figure 3.3-3(c)* presents the yield membranes of these dimensions.
In general, strain-induced rupture at the base of the cantilevers caused destruction of some cantilevers during the release. The same was observed for the release of the membranes. This failure was caused by a too good adhesion of the thin SU-8 film to the fluorocarbon coating. The released cantilevers in *Figure 3.3-2* are slightly deformed at the clamping point. This issue is discussed in detail in *Chapter 5*.
For the release of all structures, the same behaviour in dependence on the chamber pressure during plasma deposition was observed. On fluorocarbon coatings deposited at very low pressures ($p_c < 20$ mTorr), the release-yield is high and then slowly decreases until the release becomes almost impossible if the deposition was done at 30-40 mTorr. In comparison with *Figure 3.2-1* this can be explained by an increase in the surface free energy in the same pressure regime. Layers with a low surface free energy seem to show an improved release yield because of the lower adhesion between

SU-8 and fluorocarbon. In the high-pressure regime (p_c > 40 mTorr), the release peaks in an excellent release yield for both, cantilevers and membranes. This behaviour can not be explained by a change in surface free energy. *Figure 3.2-1* shows that the surface free energy for fluorocarbon coatings remains almost constant in the high-pressure regime. It is assumed that the reason for the peak of around 60 mTorr is a change of the chemical composition of the surface that has no measurable influence on the surface free energy.
A detailed analysis of the surface by spectroscopy is needed to allow further conclusions on the important change in release yield. Nevertheless, release coatings deposited in the range of 60-70 mTorr offer optimal properties for reliable spin-coating of thin SU-8 films combined with a device release with excellent yield.
Further, it has to be considered that bulk and surface properties of polymers can change with time. For example, a steady chemical reaction of the SU-8 with the fluorocarbon coating might decrease the release yield. Therefore, identical release experiments were performed three weeks after the processing was finished. *Figure 3.3-3(b)* shows that there is no decrease of the release yield. This allows for storage or shipping of the devices on the processing substrate and a release of the polymer chips at the actual time of use.

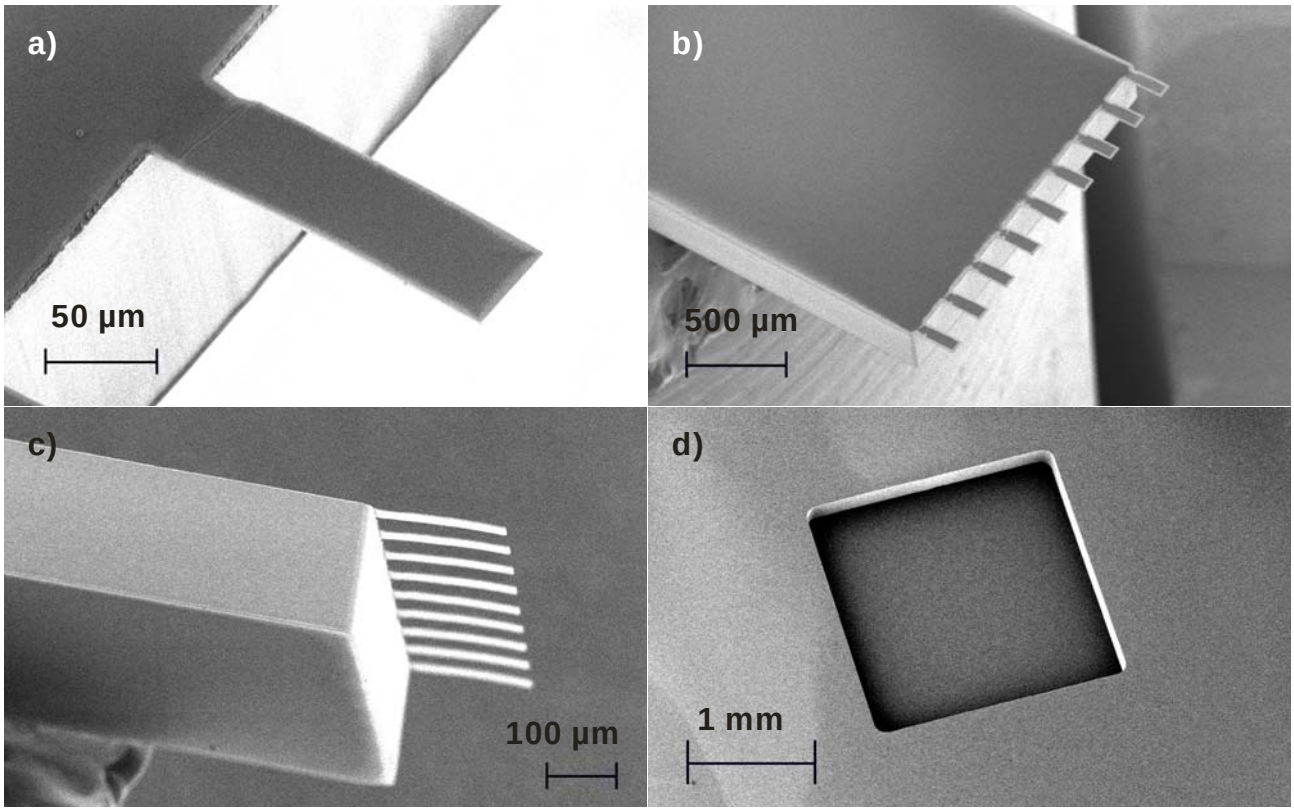

Figure 3.3-2: (a)-(c) Released array of SU-8 cantilevers t = 2.3 µm; w = 50 µm; L = 200 µm; (d) 2x2 mm² SU-8 membrane with t = 1.7 µm

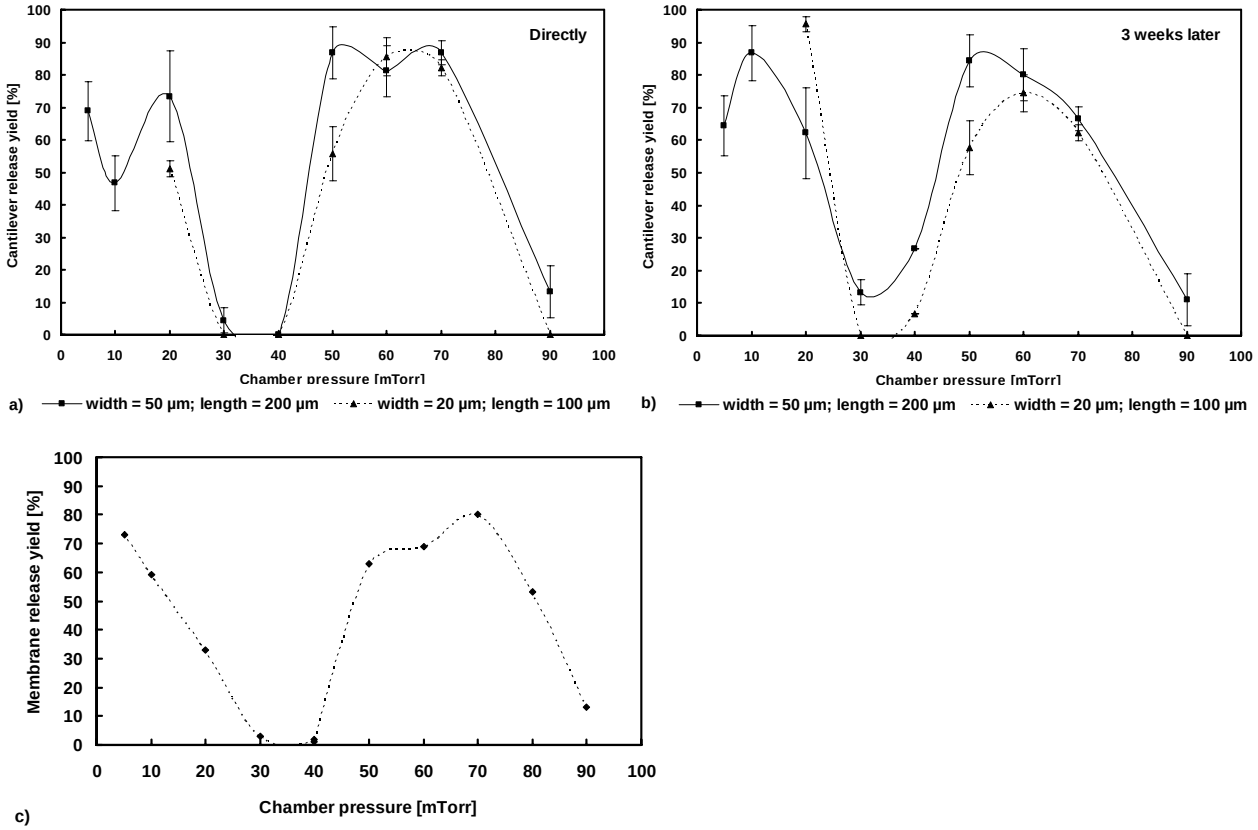

Figure 3.3-3: Release yield on fluorocarbon coatings deposited at variable chamber pressure (other parameters see Figure 3.2-1): 2.3-µm-thick SU-8 cantilevers with two different dimensions released directly after processing (a) and 3 weeks later (b); (c) 1.7-µm-thick square membranes with base-length of 2 mm released directly after processing

3.4 SU-8 backside passivation

The contact angles of the test liquids described in *Section 3.2* were measured on both sides of the released SU-8 films and the free energy of the polymer surfaces was calculated. The water contact angle on the SU-8 surface that was not in contact with the fluorocarbon during processing (SU-8 topside) was 78±5º. *Figure 3.4-1* demonstrates that the opposite surface (SU-8 backside) becomes considerably more hydrophobic for all the investigated films. The change in contact angle of the SU-8 is a result of chemical reaction of the fluorocarbon coating with the photoresist during cross-linking.

Figure 3.4-2(a) shows water contact angles of fluorocarbon coatings before SU-8 processing (filled line; see also *Figure 3.2-1*). These values are compared to the ones measured on the fluorocarbon after the release of the SU-8 films and on the SU-8 backside (dashed lines). *Figure 3.4-2(b)* shows the surface free energies for the same surfaces. The water contact angle on the SU-8 backside is different from the one measured on the as-deposited fluorocarbon. For depositions at low pressures (p_c < 40 mTorr), the contact angle on the SU-8 backside exceeds the one measured after fluorocarbon deposition. This can be explained by a difference in bulk and surface properties of the coatings in this pressure range. The surface of the plasma-polymerized fluorocarbon reacts with the SU-8. During the mechanical release of the thin SU-8 films, the fluorocarbon coating partly delaminates and sticks to the resist and fresh material is exposed. On the backside of the released

SU-8 film, the bulk properties of the fluorocarbon coating sticking to the cantilever surface are measured. This conclusion is supported by the contact angle measurements on the fluorocarbon coated substrate after release of the SU-8 structures. There, the contact angles correspond precisely to the values measured on the SU-8 backside.

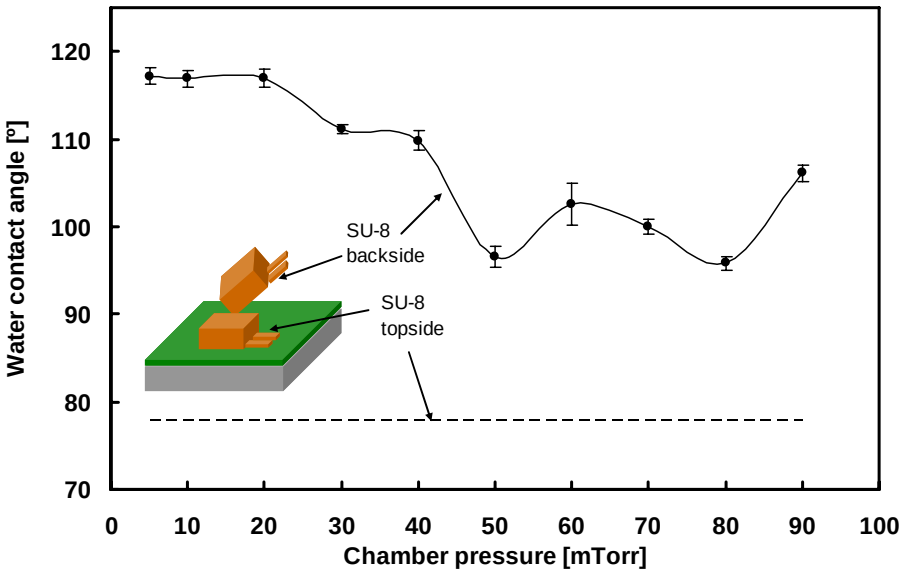

Figure 3.4-1: Water contact angles measured on both sides of SU-8 films processed on fluorocarbon coatings

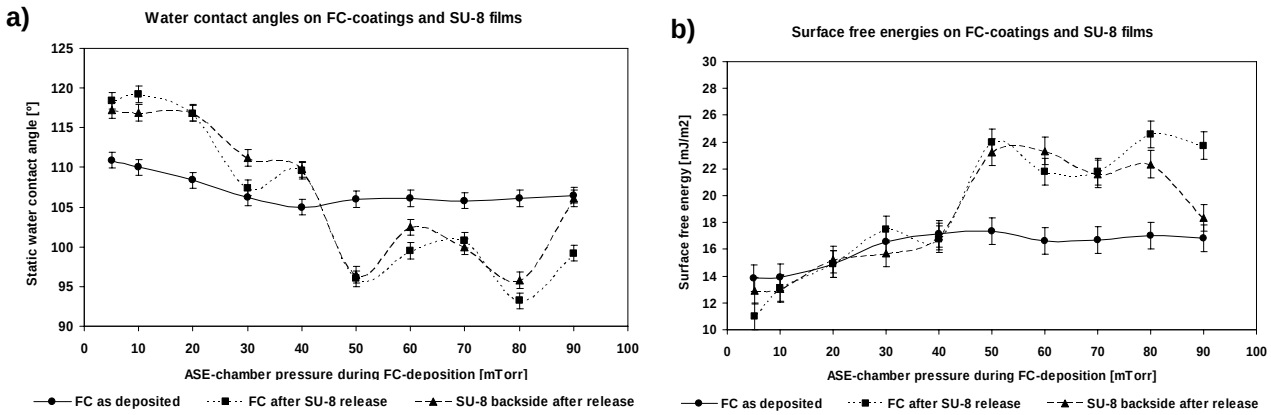

Figure 3.4-2: Comparison of water contact angles (a) and surface free energies (b) of different surfaces; the filled line shows the values measured on the fluorocarbon before SU-8 processing. The dashed lines are values on the SU-8 backside and on the fluorocarbon after processing and release of the SU-8 films.

3.5 Standard recipes

Based on the experiments described in the previous sections two standard recipes were defined for the fabrication of SU-8 devices. *Table 3.5-1* is an overview of the processing parameters and the characteristics of the two standard recipes.
Table 3.5-2 summarizes processing possibilities with the two standard recipes. Most of these results are based on process experience of members of the Nanoprobes groups using the standard recipes and are not discussed here. In general, the spin-coating of SU-8 2005 resulted in perfect resist films independent of the deposited fluorocarbon coating. Single tests showed that spin-coating of thin

films of SU-8 dissolved in gammabutyrolactone (GBL) resulted in insufficient resist-coverage of the substrate. This is explained by the higher surface tension of GBL compared to CP [78]. Therefore, only SU-8 with the solvent cyclopentanone (CP) was used for the fabrication of SU-8 chips in the context of this thesis.

Table 3.5-1: Deposition parameters and fluorocarbon characterisation

Parameter	Dry_tef	Wet_tef
Pressure [mTorr]	5	60
Gas flow [sccm]	120	120
Coil power [W]	300	300 (350)[1]
Platen power [W]	0	0
Deposition time [s]	60	60
Surface energy [mJ/m^2]	13,8±0,1	16,6±0,1
Contact angle water [°]	110,9±0,4	106,1±0,5
Contact angle ethylene glycol[°]	93,4±0,6	86,8±0,6
Contact angle diiodomethane[°]	87,3±0,4	82,4±0,3
Deposition rate [nm/min]	≈ 25	not measurable

[1] Final value had to be changed to 350 W due to problems with the ASE; no influence on spin-coating and release was observed

Table 3.5-2: Processing on fluorocarbon

Process	Dry_tef	Wet_tef
Spin-coating of SU-8 2002 (CP solvent)	Bad coverage (51%)	Good coverage
Spin-coating of SU-8 2005 (CP solvent)	Good coverage	Good coverage
Spin-coating of SU-8 2 (GBL solvent)	Bad coverage	Bad coverage
SU-8 processing t ≤ 3 µm (SU-8 2002)	Bad release	Possible
SU-8 processing t = 3.5-6 µm	Possible	Possible[1]
SU-8 processing t > 6 µm (SU-8 2005)	Possible	Delamination
Lithography AZ 5214e, 1,5µm [132]	Possible	Possible
Lithography AZ 4562, 9,5 µm [132]	Partial delamination	Partial delamination
Metal deposition 100 nm Au, Al [132]	Possible	Possible
Metal deposition 100 nm Ti, Ni [132]	Possible	Delamination
Metal deposition 100 nm Pt, Cr [132]	-	Delamination

[1] Delamination of large structures [133]

3.6 Conclusion

The variation of the parameters of a C_4F_8-plasma in a DRIE reactor allows the fine tuning of the surface free energy and the thickness of fluorocarbon antistiction coatings. The obtained increase in surface free energy for fluorocarbon deposited in the high-pressure regime resulted in perfect wettability of the substrate by low viscosity SU-8 photoresist. The improvement was sufficient to achieve uniform spin-coating of SU-8 layers with thicknesses down to 500 nm. Further, it was demonstrated that a fluorocarbon deposition at pressures of 60-70 mTorr results in fluorocarbon surfaces with excellent properties for the release of thin SU-8 devices such as cantilevers and membranes. The fact that a small variation of the chamber pressure is decisive for successful processing demonstrates the importance of total control of the plasma chamber conditions. The optimized method allows for the dry release of large SU-8 structures in a few seconds. The

processing time is significantly reduced compared to fabrication methods where the structures are released by sacrificial layer etching. Finally, it was shown that the surface layer of the fluorocarbon coatings reacts with the SU-8 during processing, which leads to an increase of the water contact angle on the backside of the released devices. This process-integrated backside-passivation is of large interest applications of SU-8 cantilevers in biosensing as it prevents unspecific absorption of biomolecules on one side of the cantilevers [50].

4 SU-8 thin film processing

4.1 Goal of the process optimization

In *Chapter 1* the selection of SU-8 as material for the complete fabrication of the flapperchip has been motivated. The most critical step is the processing of the thin SU-8 film that defines the actual flapper. The sensor concept and the challenges described in *Section 1.6* lead to the process specifications presented in *Table 4.1-1*.
Compared to thick-film processing, the number of publications on processing of thin SU-8 films is very restricted. In conventional approaches as presented in *Section 2.6.1*, processes optimized for thicker films have simply been adapted. Typically, the same process temperatures were used but the bake-times were shortened and the UV-exposure-dose was reduced [76]. Lithographic resolution is improved as the film thickness is reduced. On the other hand, structural stability of thin films is an issue and residual stress results in cracking or delamination from the substrate.
Therefore, an experimental study on thin film processing of SU-8 was performed. In *Section 4.3* and *Section 4.4* the influence of the processing steps on film stress, photolithographic resolution and stability towards development were investigated. Fourier Transform infrared spectroscopy (FT-IR) measurements of the cross-linking of the SU-8 are presented in *Section 4.5*. As the final goal of this experimental investigation, an optimized process for the patterning of the thin SU-8 film during fabrication of the flapperchip is defined in *Section 4.6*. This process was compared to conventional processing of thin SU-8 films described in *Chapter 2*. The influence of the processing on the refractive index of the SU-8 is briefly discussed in *Section 4.7*.

Table 4.1-1: Goals and specifications for the SU-8 thin film processing

Challenge	Goal	Process specification
High flapper actuation	Low thickness	$t \leq 5$ µm
No leakage before actuation	No initial out-of-plane bending	No residual stress gradients
	No cracking	Low residual stress High cross-linking
	Low gap width	Trench resolution ≤ 3 µm
Dry release from fluorocarbon	Structural stability	High cross-linking
	No delamination during processing	Low residual stress
Time-stability	Low ageing	High cross-linking

4.2 Materials and method

Some of the processing parameters were kept constant for all the experiments. Standard Silicon wafers were used as a substrate. SU-8 2002 was spin-coated without previous cleaning or surface treatment of the substrate. The spin-coating was done at 1500 rpm during 30 s with an acceleration of 5000 rpm/s to achieve a nominal thickness of 2 µm. Ramping rate to the final bake temperatures was constant at 2˚C/min and the wafers were left on the hotplate for 2 h after the end of the actual bake to allow for cool-down to ambient temperature.
In several series of experiments the parameters of soft-bake, exposure and post-exposure-bake (PEB) presented in *Section 2.3* were varied. For each set of parameters, two samples were processed in parallel resulting in a total number of about 140 processed wafers for this process optimization. The first sample was patterned by exposure in hard contact mode through a mask. The mask design

included test-structures of various dimensions to allow the monitoring of the lithographic resolution of the corresponding process (*Figure 4.2-1*). Imaging of lines and trenches with the SEM followed by image treatment (ImageTool, University of Texas Health Science Center, Texas) were used for this purpose. The second sample was flood-exposed and used for the measurement of thickness, refractive index and film stress. Thickness and refractive index of the SU-8 were measured with a spectrophotometer (FilmTek, SCI, California) that allowed automatic mapping on wafer scale samples. For the evaluation of the in-plane stress, the radius of curvature of the silicon substrate before and after processing of the SU-8 was measured with a profilometer (Dektak8, Veeco, Germany) and the residual film stress was calculated as described in *Section 2.5*. For each sample, three stress measurements were performed.

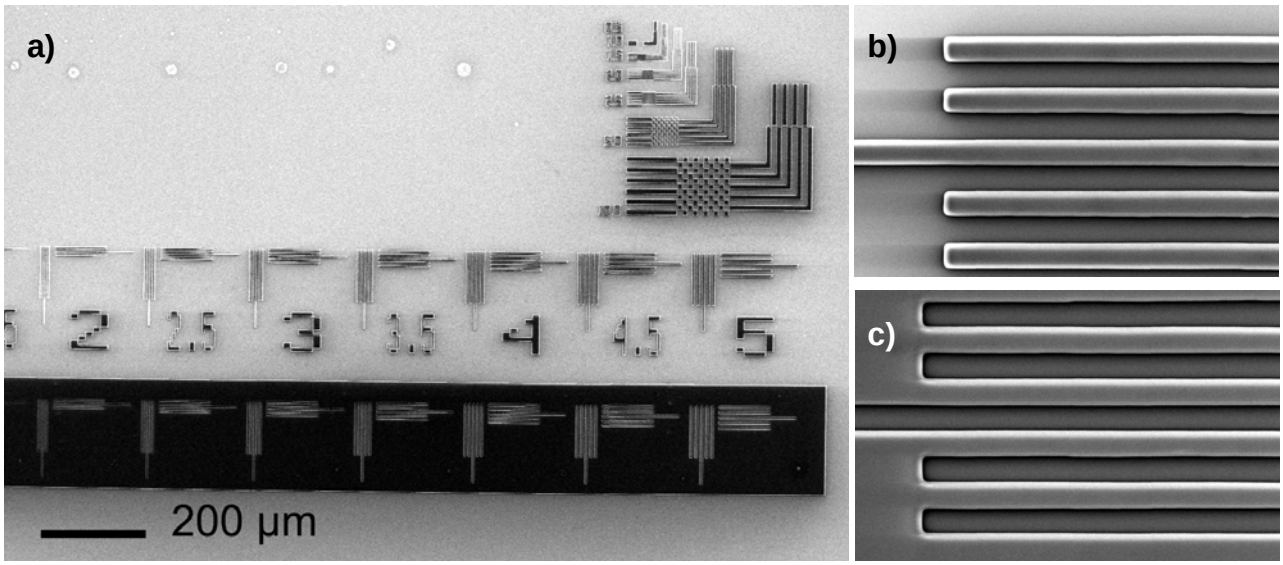

Figure 4.2-1: (a) Structures for monitoring of line- and trench-resolution; the number indicates the width of the lines and trenches in µm; (b) 5-µm-lines; (c) 5-µm-trenches

4.3 Influence of solvent content

In a first part of the optimization, the influence of the solvent content on the processing of the thin SU-8 films was investigated. For this purpose, the soft-bake parameters presented in *Section 2.3.2* were varied. Exposure dose was D = 200 mJ/cm^2, PEB-temperature T_{PEB} = 40˚C and PEB-time t_{PEB} = 60 min were constant for all the experiments. The selection of a PEB at low temperature should allow for low thermal stress as discussed in *Section 2.5*. In a first experimental series of the soft-bake optimization, the soft-bake temperature T_{SB} was varied between 20-60˚C. The soft-bake time t_{SB} was kept constant at 10 minutes. In a second series of experiments, the soft-bake was completely replaced by a solvent evaporation at ambient temperature (T_{SB} = 20ºC). For these samples, an evaporation time t_{evap} was defined as the waiting time between spin-coating and exposure of the SU-8 films. This parameter was varied from 5 minutes to 4 hours.

4.3.1 Residual stress and film thickness

Figure 4.3-1(a) shows the measured thickness and the tensile film stress for samples processed at different T_{SB}. *Figure 4.3-1(b)* represents the same parameters as a function t_{evap}. The measurements

show that the thickness of the SU-8 films decreases with an increase of T_{SB} and t_{evap}. On the other hand, the tensile film stress decreases with a decrease of T_{SB} and t_{evap}. Stress measurements on samples soft-baked at $T_{SB} > 40$ °C were impossible due to the non-uniformity of the SU-8 films.
The temperature and the duration of the soft-bake determine the residual concentration of solvent in the SU-8 at the moment UV-exposure and the onset of cross-linking. Higher T_{SB} and longer t_{SB} result in a lower solvent content due to enhanced evaporation of the cyclopentanone. The observed behavior of the film thickness is only partly explained by higher shrinkage due to enhanced solvent evaporation at higher T_{SB} or longer t_{evap}. The solvent loss during SB for films with comparable thickness is below 5% [78]. The considerable decrease of thickness at $T_{SB} > 40$ °C has to be a result of partial development due to insufficient cross-linking of the photoresist. It has been shown by other authors that the residual solvent content during polymerization has an influence on the processing results for SU-8 [94]. This is explained by the mechanisms presented in *Section 2.2.3*. Low solvent content reduces the diffusion of the photo-acid and the mobility of the monomers in the polymer matrix. This reduces the cross-linking density of the SU-8 particularly if the PEB is done at low temperatures. In the case of thin SU-8 films, the high volatility of the solvent leads to a very fast decrease of the solvent content even at ambient temperature [134]. Typically, there is a solvent gradient in the SU-8 because solvent evaporation takes place at the interface SU-8-air. Due to the reduced solvent content, the cross-linking density at the top of the SU-8 film is lower and non-cross-linked monomers are removed during the development step.
Higher residual solvent content seems to result in lower film stress. This behavior might be the result of a combination of several effects described in *Section 2.5*. The higher mobility of the SU-8 monomers at higher solvent content probably allows improved relaxation of the intrinsic stress during polymerization. The stress measurements on *Figure 4.3-1(b)* seem to be correlated to the thickness of the SU-8. Thinner films show a considerable increase in film stress. This indicates that partial development of the SU-8 results in tensile stress. Therefore, the film stress could be directly related to the development step in PGMEA.

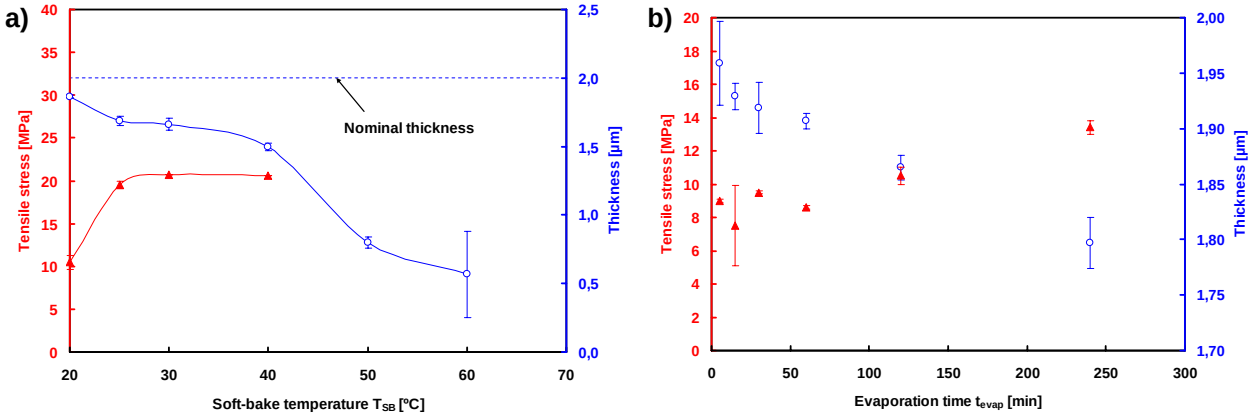

Figure 4.3-1: Influence of soft-bake temperature [t_{SB} = 10 min] (a) and evaporation time (b) on thickness (○) and stress (▲) for 2-µm-thick SU-8; D = 200 mJ/cm²; T_{PEB} = 40 °C; t_{PEB} = 60 min

4.3.2 Lithographic resolution

Figure 4.3-2 shows optical microscope pictures of SU-8 chess-board patterns with a nominal base-length of 10 µm. The experiments were performed in the second part of the soft-bake optimization

and the only variable was the evaporation time t_{evap}. For t_{evap} = 5 min loss of resolution due to broadening of the SU-8 structures was observed. On the other hand, t_{evap} = 4 h results in partial development of the square pattern.
These experiments demonstrate the influence of the residual solvent content on the lithographic resolution. A higher amount of solvent due to shorter t_{evap} facilitates diffusion of the photo-acid into non-exposed areas during the PEB and therefore leads to blurring of the original mask pattern. Lower solvent content hinders complete cross-linking of the exposed photoresist and leads to partial development at the edges which is similar to the observations of the previous section.
A practical issue is stiction between mask and photoresist if the exposure is done in hard contact mode. For 2-µm-thick SU-8 films t_{evap} < 15 min resulted repeatedly in stiction of the substrate to the mask after exposure as a result of the high solvent content in the resist.

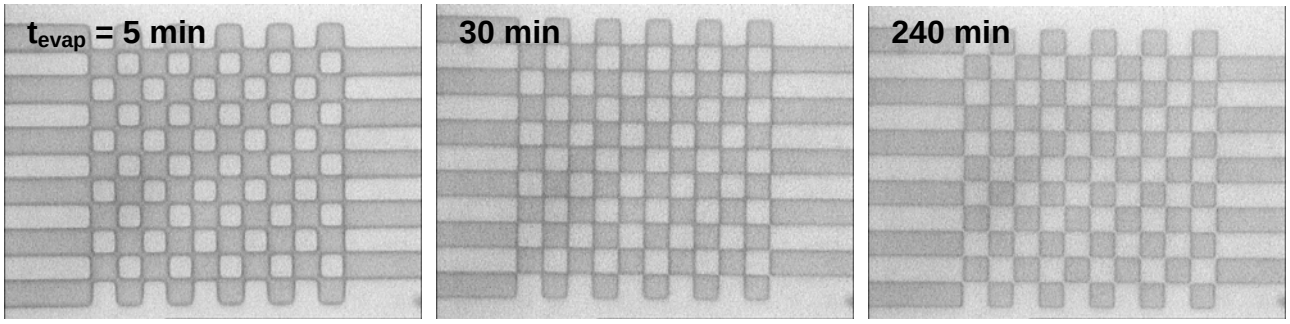

Figure 4.3-2: Resolution patterns for different t_{evap}. The nominal side-length of the squares is 10 µm; t_{evap}=5 min: The SU-8 pattern (dark grey) is blurred due to acid diffusion into non-exposed areas; t_{evap}=30 min: Good resolution; t_{evap}=240 min: Insufficient cross-linking results in partial development of the SU-8.

4.3.3 Conclusion

The residual solvent content is rarely discussed in literature but it has an important influence on the cross-linking of thin SU-8 films. High solvent content facilitates the cross-linking reaction of the SU-8. This is a result of enhanced acid diffusion and higher mobility of the SU-8 monomers. Conventionally, a soft-bake is done in SU-8 processing. For thin SU-8 films, evaporation of the solvent is fast. Therefore, the soft-bake step was replaced by a short evaporation time at ambient temperature between spin-coating and exposure of the photoresist. This resulted in lower tensile film stress and less partial development of the SU-8. On the other hand, higher solvent content leads to deterioration of the lithographic resolution and to stiction of the substrate to the mask upon exposure. The duration of the solvent evaporation has to be adjusted depending on film thickness.

4.4 Influence of exposure and post-exposure-bake

In the second part of the process optimization, exposure dose D, PEB-temperature T_{PEB} and PEB-time t_{PEB} were the explored variables. As a result of the conclusions of the previous section, t_{evap} = 30 minutes was introduced for all the experiments. For the design of experiments (DoE) of an initial series of screening experiments, the software MODDE (Umetrics, Sweden) was used. There, a Central Composite Face (CCF) design consisting of 17 experiments was selected, three of them being the center-points used for the evaluation of the reproducibility. This design allows for

response surface modeling wit both second order and interaction terms. The modeling was carried out using MODDE. The models were simplified through removal of insignificant terms and the exclusion of experimental results that were improbable based on statistical testing. The experimental range was D = 150-250 mJ/cm^2, T_{PEB} = 30-50˚C and t_{PEB} = 30-120 min.
The initial screening experiments allowed the identification of the most important parameters influencing the processing of thin SU-8 films with selected residual solvent content. Additional experiments were performed extending the parameter range to 100 ˚C for T_{PEB} and to 500 mJ/cm^2 for D. For comparison, samples were fabricated with *Process A* described in *Section 2.6.1*. There, the exposure dose was 250 and 500 mJ/cm^2.

4.4.1 Residual stress and film thickness

T_{PEB} was identified as the most important process parameter influencing the residual stress in thin SU-8 films. The same is valid for the film thickness. *Figure 4.4-1(a)* represents the tensile film stress for samples processed at two different exposure doses with the extended range for T_{PEB}. *Figure 4.4-1(b)* shows the result of the thickness measurements for the same experiments. Two temperature domains can be identified:

$T_{PEB} < 50$ ºC: The thickness of the SU-8 considerably decreases with a decrease in temperature and in parallel the stress increases

$T_{PEB} \geq 60$ºC: The thickness of the SU-8 is more or less constant and the tensile film stress increases linearly with temperature

Between the two temperature domains there is a process window where a minimum of tensile film stress is observed. The behaviour of the film stress is similar for samples processed at different exposure doses. However, the absolute stress values are considerably lower at D = 500 mJ/cm^2 compared to the ones at D = 200 mJ/cm^2. Further, the film thickness is higher for higher D. The duration of the PEB has only minor influence on film thickness and stress. Longer t_{PEB} results in a slight decrease of the tensile stress and a higher thickness of the SU-8.

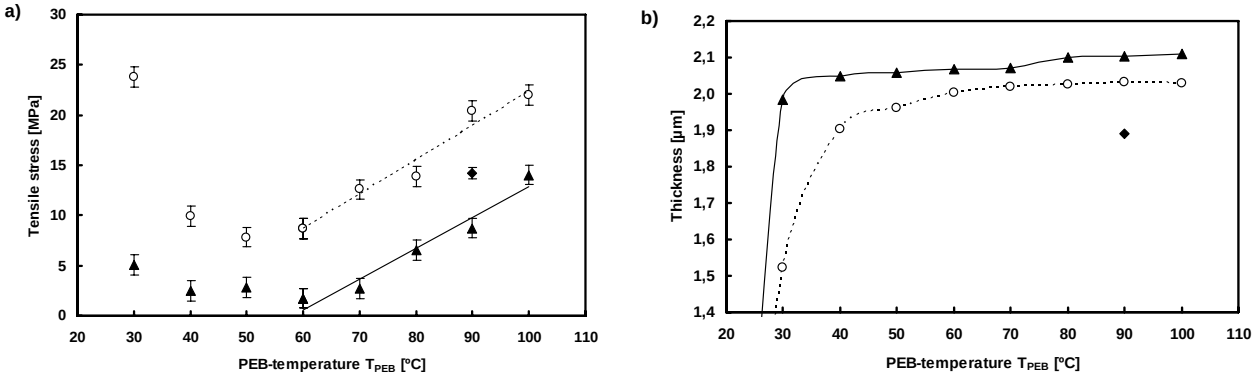

Figure 4.4-1: Influence of T_{PEB} on tensile stress (a) and thickness (b); (○) D = 200 mJ/cm^2; (▲) D = 500 mJ/cm^2; t_{PEB} = 1 h; for comparison the value for Process A is shown (◆)

For $T_{PEB} < 50$ ºC, thermal stress is expected to be low following *Equation 2.5-2*. Nevertheless, the film stress is high in this temperature domain. Similar to the observations made during the soft-bake optimization of *Section 4.3* this can be correlated to a reduced film thickness. The thermal energy seems to be too low to achieve sufficient cross-linking and partial development of the SU-8 results

in high intrinsic stress. The thickness measurements in *Figure 4.4-1(b)* show that there is less partial development of the SU-8 for $T_{PEB} < 50$ ºC if the exposure dose is increased to 500 mJ/cm^2. Higher D corresponds to a higher photo-acid concentration and therefore the cross-linking at identical bake conditions is improved.
For $T_{PEB} \geq 60$ºC, intrinsic stress due to partial development is reduced and thermal stress is assumed to be dominant. The linear behaviour of the tensile stress in *Figure 4.4-1(a)* in this temperature domain follows the one predicted by *Equation 2.5-2* for a solidified polymer film on a silicon substrate subjected to thermal processing. This equation can be used to estimate the coefficient of thermal expansion (CTE) α_{SU8} of the SU-8:

$$\alpha_{SU8} = \alpha_{Si} + \beta \frac{(1-\nu_{SU8})}{E_{SU8}} \qquad \text{PEB} \qquad (4.4\text{-}1)$$

Here, β is the slope of the linear approximation for $T_{PEB} \geq 60$ºC in *Figure 4.4-1*. The Young's modulus $E_{SU8} = 3$ GPa [102] and the Poisson's ratio $\nu_{SU8} = 0.26$ [103] are assumed to be constant for the cross-linked polymer film. The CTE of silicon is $\alpha_{Si} = 2.6*10^{-6}$ K^{-1}. With *Equation 4.4-1* it is:

D = 200 mJ/cm^2:	$\beta = 0.344$ MPa/K	$\alpha_{SU8} = 88.5*10^{-6}$ K^{-1}
D = 500 mJ/cm^2:	$\beta = 0.306$ MPa/K	$\alpha_{SU8} = 79.2*10^{-6}$ K^{-1}

The calculated values are in a first approximation independent of D and in the same order of magnitude as the values reported in literature [100, 105].
For the samples processed at $T_{PEB} \geq 60$ºC, the explanation of the offset in the stress values measured for different exposure dose is not very intuitive and probably related to a difference in polymerization kinetics during the temperature ramping of the PEB. During the slow temperature ramping to the actual T_{PEB}, polymerization is initiated and long polymer chains and loosely cross-linked domains are formed. The temperature where the conversion of epoxy groups becomes high enough to form a cross-linked polymer network could be defined as polymerization temperature T_p. For $T < T_p$ the Young's modulus of the SU-8 is assumed to be zero and the resist is stress-free. T_p could also be called the stress-free temperature. In the idealized case $T_p = T_{PEB}$, complete polymerization occurs during the PEB. There, *Equation 2.5-2* can be used to estimate the increase of thermal stress during the cool-down to ambient temperature T_o. The stress-build-up during cool-down is schematically illustrated by the blue line on
Figure 4.4-2 for a $T_{PEB} = 80$ºC. The experiments have shown that polymerization already occurs at relatively low temperature and probably in most cases it is $T_p < T_{PEB}$. There, the temperature increase from T_p to T_{PEB} results in thermal expansion of the partially polymerized SU-8. The result is a kind of stress-hysteresis with a compressive stress component that has to be deduced from the value predicted by *Equation 2.5-2*. It is expected that T_p is lower for higher D due to the enhanced polymerization as discussed above for the low-temperature domain. Therefore, the compressive stress component increases with D. This kind of stress-hysteresis is illustrated in
Figure 4.4-2 for D = 500 mJ/cm^2 (green curve) and D = 200 mJ/cm^2 (red curve). Some additional experiments showed that faster ramping leads to a considerable increase in thermal stress. For a fast ramping the time for partial polymerization is reduced and T_p is probably shifted to higher values. The presented model is a rather simplified one, as mechanical properties will change during ramping and cool-down. Nevertheless, it demonstrates that exposure dose and temperature slopes

during PEB are important process parameters influencing the stress during processing of thin SU-8 films.

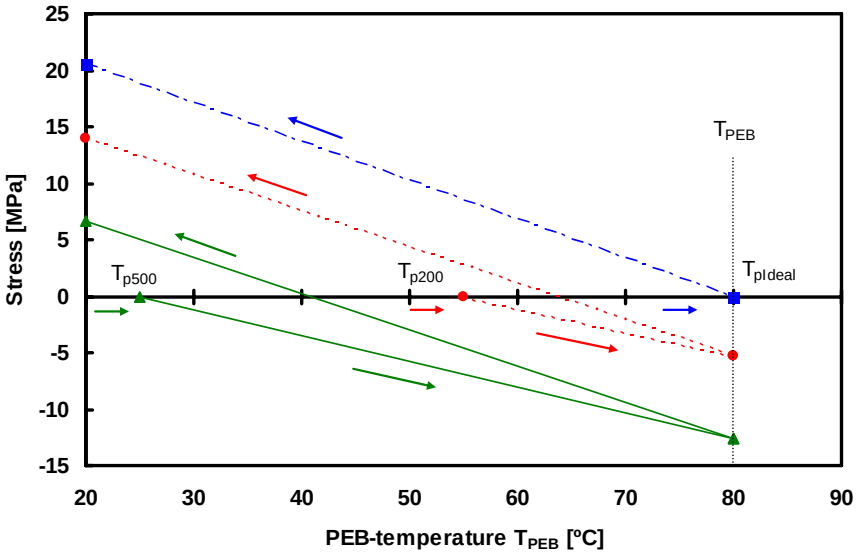

Figure 4.4-2: Schematical representation of stress hysteresis during PEB; T_p = stress-free temperature; Blue: Idealized case; Red: D = 200 mJ/cm²; Green: D = 500 mJ/cm²

For comparison, the values of thickness and tensile stress for samples processed with *Process A* are also represented on *Figure 4.4-1*. The measured values are identical for exposure doses of 250-500 mJ/cm^2. The value of tensile stress is about 14 MPa, which is assumed to be thermal stress due to the PEB at 90ºC. The thickness of the SU-8 is considerably lower compared to the samples processed without soft-bake. This is explained by the volume loss due to evaporation of most of the solvent during soft-bake at T_{SB} = 90ºC.

4.4.2 Lithographic resolution

The experimental investigation identified the exposure dose D as the most important parameter influencing the lithographic resolution. T_{PEB} also should be considered to obtain the desired resolution whereas t_{PEB} was less significant in the investigated range.
Figure 4.4-3 shows measurements of the dimensions of trenches and lines with a nominal width of 5 µm to demonstrate the influence of D and T_{PEB} on the lithographic resolution. A loss of resolution was observed with an increase of D and T_{PEB}. For the low exposure doses of 150-250 mJ/cm^2 the behaviour is similar. *Figure 4.4-4* shows a typical result for patterns obtained at D = 200 mJ/cm^2. A T_{PEB} < 50ºC results in partial development due to insufficient cross-linking. For T_{PEB} > 70ºC, line-broadening and decreased trench-width is observed. The higher D the lower is T_{PEB} where nominal trench- or line-width is reached. The high dose of D = 500 mJ/cm^2 results in overexposure independent of T_{PEB}. Higher t_{PEB} leads to a slight decrease of the resolution.
The important influence of the exposure dose on the resolution follows the expectations as it is the key parameter for all photolithographic processes [74]. High D leads to line-broadening and to a reduced trench-width due to optical effects such as diffraction at the mask and reflection on the substrate [91]. For the high value of D = 500 mJ/cm^2 these optical effects are dominant. The experiments at lower D demonstrate that besides the optical effects, photo-acid diffusion into non-exposed areas is an important issue for processing of chemically amplified photoresists such as SU-

8. The observations are explained by the polymerization mechanisms presented in *Section 2.2.3.* At high T_{PEB} the mobility of the photo-acid is increased and leads to a loss of resolution. Longer t_{PEB} allows for continued photo-acid diffusion although the effect is not as important as for the temperature.

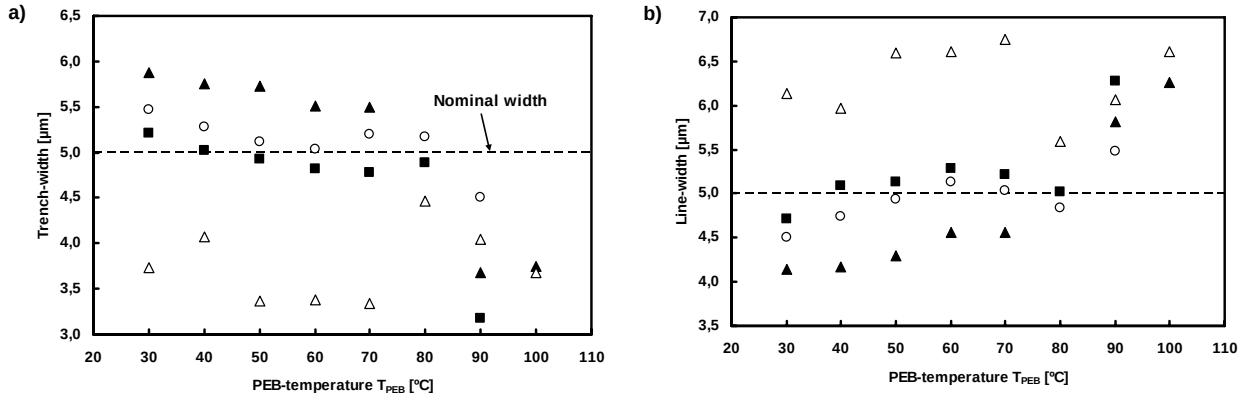

Figure 4.4-3: Influence of T_{PEB} on dimension of trenches (a) and lines (b) with nominal width 5 µm; exposure dose D: (▲) 150 mJ/cm²; (○) 200 mJ/cm²; (■) 250 mJ/cm²; (△) 500 mJ/cm²

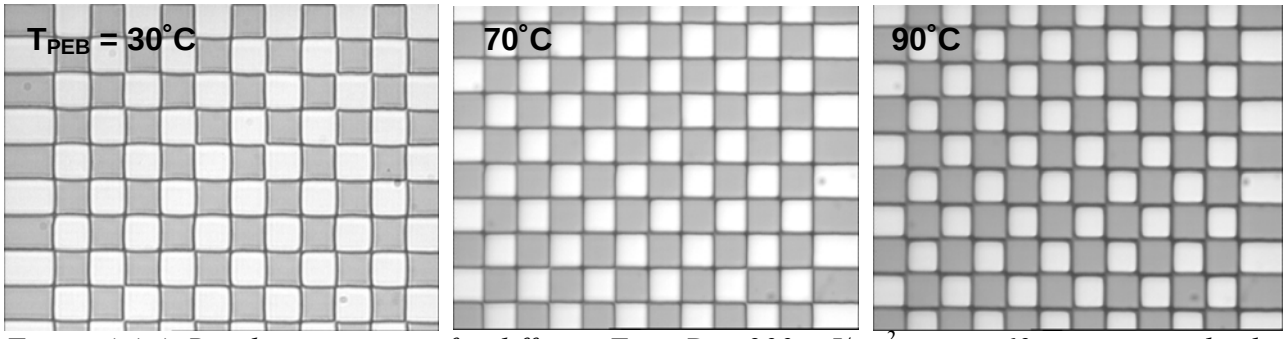

Figure 4.4-4: Resolution patterns for different T_{PEB}; D = 200 mJ/cm², t_{PEB} = 60 min; nominal side-length of the squares is 10 µm; T_{PEB} = 30ºC: Insufficient cross-linking results in partial development of the SU-8 (dark grey); T_{PEB} = 70ºC: Good resolution; T_{PEB} = 90ºC: The pattern is blurred due to acid diffusion into non-exposed areas

4.4.3 Change of film stress with time

The residual film stress discussed in Section 4.4-1 was re-evaluated at different times after processing. The samples were stored in the cleanroom at ambient temperature in air. *Figure 4.4-5* shows the change of film stress with time for SU-8 processed at different T_{PEB} with D = 500 mJ/cm². There, the measurements presented in *Figure 4.4-1(a)* were repeated after storage of 3 weeks and 3 months. Similar to previous discussions, two temperature domains can be identified.

$T_{PEB} < 50$ ºC: The film stress in the SU-8 increases with time and the increase is more important at lower TPEB

$T_{PEB} \geq 60$ºC: The film stress considerably decreases with time and in an approximation stress-free after storage of 3 months

In *Section 2.5.4*, different sources for the change of stress in the SU-8 with time were discussed. For $T_{PEB} < 50$ ºC, the increase of stress is probably explained by further cross-linking of the SU-8. This effect is more important the lower the initial cross-linking density of the polymer. For $T_{PEB} \geq 60$ºC, physical ageing can only partially explain the decrease of film stress. Relaxation of intrinsic stress in epoxy resists at $T < T_g$ is a very slow process [113, 114]. Therefore, creep is a more probable explanation for the observed relaxation of the measured film stress in the high temperature domain. Creep is the plastic deformation of the polymer due to long-term exposure to extrinsic stress. In the case of the SU-8 film processed at high temperature on the silicon substrate, thermal stress is generated during the cool-down after the PEB. During storage, slow sliding of the polymer chains results in relaxation of the film stress.

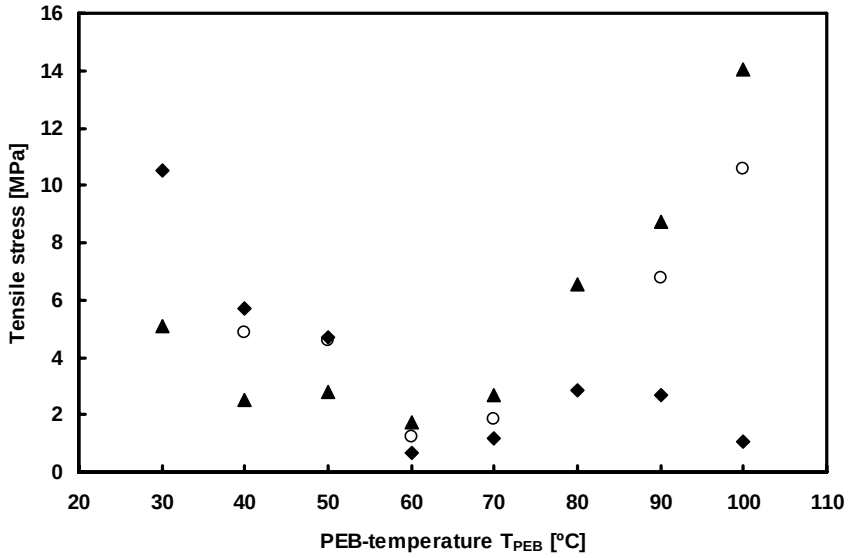

Figure 4.4-5:
Tensile stress at measured after different times of storage: (▲) 1 day; (○) 3 weeks; (◆) 3 months; D = 500 mJ/cm²; t_{PEB} = 1 h;

4.4.4 Conclusions

The experiments show that T_{PEB} is the main parameter influencing the stress and the cross-linking of thin SU-8 films. For $T_{PEB} < 50$ºC, partial development due to insufficient cross-linking results in high intrinsic film stress. For $T_{PEB} \geq 60$ºC, the difference in coefficient of thermal expansion between substrate and SU-8 results in higher tensile stress for samples processed at higher T_{PEB}. Higher T_{PEB} has a negative impact on the lithographic resolution due to enhanced diffusion of photo-acid into non-exposed areas. Processing at T_{PEB} = 50-60ºC seems to be suitable to minimize residual film stress and to prevent loss of resolution.
The exposure dose D should be high to improve cross-linking and reduce film stress. On the other hand, high exposure dose has a negative influence on the lithographic resolution. A value of D = 250 mJ/cm² easily results in a trench resolution of 2 µm for 2-µm-thick SU-8 films.
Repeated measurements on stored samples showed considerable changes of film stress with time. The results indicate that SU-8 with low cross-linking further polymerizes during storage. Thermal stress due to processing on a silicon substrate at high temperature is probably released by slow plastic deformation of the SU-8 films (creep). These issues have to be investigated in further detail.

4.5 Fourier-Transform infrared spectroscopy

Fourier-Transform infrared (FT-IR) spectroscopy is a common method for the characterization of organic materials. Several authors have earlier reported FT-IR measurements to demonstrate the influence of the process parameters on the conversion of the epoxy-groups of the SU-8 [91, 135, 136]. Here, the method was used to investigate the cross-linking achieved with the new processing approach.

4.5.1 Materials and methods

The measurements were done in transmission mode and due to the limited sensitivity of the instrument (Perkin Elmer, Germany) the film thickness had to be increased to 5 µm compared to the experiments in the previous sections. SU-8 2005 was spin-coated at 2000 rpm for 30 s with an acceleration of 5000 rpm/s. The solvent evaporation time was increased to 2 h due to the higher film thickness. Based on the results of *Section 4.4*, the PEB was performed during 60 min at a temperature of 50˚C. For comparison with the new approach, SU-8 films with the same thickness were prepared using *Process A*. For both processes, samples flood-exposed with 250 mJ/cm^2 and with 500 mJ/cm^2 were characterized with FT-IR. Completely non-cross-linked SU-8 was used as a reference for the FT-IR measurements. For this purpose, SU-8 monomer solution without the photo-initiator (Microresist, Germany) was spin-coated to a thickness of 5 µm and soft-baked for 60 min at 100ºC to remove the solvent.

4.5.2 Results and discussion

Figure 4.5-1 represents part of the recorded FT-IR spectra of SU-8. The relevant peaks for the spectral analysis are summarized in *Table 4.5-1*. The spectra have been normalized to the absorption peak of the aromatic C-C stretching of the SU-8 monomer that is situated at 1500 cm^{-1}. This peak is independent of processing parameters as the monomer backbone is not modified during cross-linking [135]. In *Section 2.2.3* the polymerization of SU-8 was described. During the cross-linking of SU-8 the epoxy groups of the monomers are opened and ether-bonds and OH-groups are formed instead. The peaks at 861 cm^{-1} and 910 cm^{-1} are assigned to C-O stretching of respectively cis- and trans-epoxy-groups [137]. Both peaks are visible for the non-cross-linked monomer sample (*Figure 4.5-1(a)*) and show reduced amplitude for polymerized SU-8 (*Figure 4.5-1(b)-(e)*). The lower amplitude of the absorption peaks for the new process compared to *Process A* shows that the new approach results in higher conversion of the epoxy-groups. For the new process, the peak amplitude slightly decreases for D = 500 mJ/cm^2 compared to D = 200 mJ/cm^2. This indicates the improved cross-linking at higher exposure dose. In parallel, the intensity of the C-O stretching band characteristic of ethers and secondary alcohols (respectively 1000-1230 cm^{-1} and 1000-1290 cm^{-1}) increases for the SU-8 samples processed by the new process (*Figure 4.5-1(d)-(e)*), which is another consequence of the improved efficiency of cross-linking.
Furthermore, an absorption band around 1750 cm^{-1} is present only in the FT-IR spectrum of SU-8 films processed with the new process (*Figure 4.5-1(d)-(e)*). This band can be assigned to the SU-8 solvent cyclopentanone that shows an absorption band in this spectral region [138]. For the samples processed with a soft-bake step this band is absent (*Figure 4.5-1(b)-(c)*). This observation is in good

agreement with the hypothesis that the removal of the soft-bake results in higher residual solvent content in the SU-8 films.

Table 4.5-1: Relevant peaks of the SU-8 FT-IR spectra

Wavenumber [cm^{-1}]	Characteristic vibration	SU-8 processing effect on the peak intensity
861	C-O stretching of cis substituted epoxy-rings	↘ with crosslinking
910	C-O stretching of trans substituted epoxy-ring	↘ with crosslinking
1000-1230	C-O-C stretching in ethers	↗ with crosslinking
1000-1290	C-O stretching in phenols and secondary alcohols	↗ with crosslinking
1500	aromatic C-C stretching (in-ring)	→ with crosslinking
1700-1750	C=O stretching cyclopentanone (solvent)	↘ with solvent evaporation

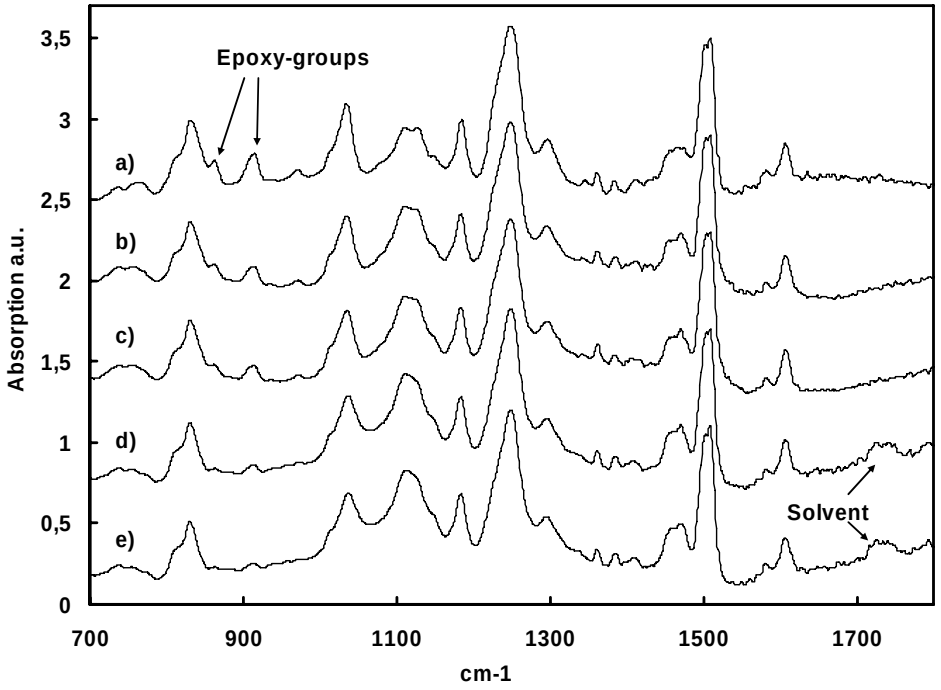

Figure 4.5-1: FT-IR spectra of 5-µm-thick SU-8 films: (a) SU-8 monomer Process A : (b) D = 250 mJ/cm² (c) D = 500 mJ/cm² New process : (d) D = 250 mJ/cm² (e) D = 500 mJ/cm²

4.5.3 Conclusion

The FT-IR measurements confirm the influence of the solvent content on the processing of SU-8. Higher solvent content due to a replacement of the soft-bake step with a solvent evaporation at ambient temperature allows for higher mobility of photo-acid and SU-8 monomers. The result is a higher conversion of the epoxy-groups of the thin SU-8 films. The FT-IR spectra demonstrate that this is the case even if the processing is done at a lower temperature T_{PEB} = 50˚C compared to T_{PEB} = 90˚C in *Process A*. For the new process, the cross-linking density increases at higher exposure dose.

4.6 Optimized processing of thin SU-8 films

Table 4.6-1 summarizes the influence of the different process parameters on the responses investigated in *Section 4.3* to *Section 4.5*. This overview allows the adjustment of the parameters depending on the requirements for the specific application and on the film thickness. In *Table 4.1-1* high cross-linking, low residual stress, low residual stress gradients and a trench-resolution of 3 µm were presented as specifications for the processing of the thin SU-8 layer defining the flapper. The residual stress is minimal for T_{PEB} = 50ºC. The selection of a set of parameters aiming for increased cross-linking unfortunately results in a lower resolution. There, a trade-off has to be made. With these considerations an optimized *Process B* is defined in *Table 4.6-2*. *Table 4.6-3* is an overview of some responses for *Process A* and *Process B* that have been investigated during the thin film experiments. For the lithographic resolution there is no difference between the two approaches. In the following, the two processes are compared regarding the issues of cracking and delamination.

Table 4.6-1: Summary of the influence of processing parameters on the investigated responses

Parameter	**Response (if corresponding parameter is increased)**			
	Thickness	**Residual stress**[2]	**Cross-linking**	**Resolution**[3]
Solvent content[1]	↗	↘	↗	↗
Exposure dose	↗	↘	↗	↗
PEB-time	↗	↘	↗	↗
T_{PEB} < 50 ºC	↗	↘	↗	↗
T_{PEB} > 50 ºC	↗	↗	↗	↗

[1] The solvent content is regulated by the evaporation time or the soft-bake parameters
[2] The residual stress is tensile
[3] An increase corresponds to a loss of resolution

Table 4.6-2: Process B - Optimized process for thin SU-8 films

Process step	**Equipment**	**Parameters: SU-8 2002 (SU-8 2005)**
Spin-coating	KS Spinner	see *Table 2.6-1*
Solvent evaporation	-	30 min (2 h)
Exposure	KS Aligner	250-500 mJ/cm^2
Post-exposure bake	Hotplate	60 min, 50ºC; ramping 2ºC/min
Development	PGMEA	2 min FIRST, 2 min FINAL
Rinse	Isopropanol	30 s

Table 4.6-3: Comparison of the characteristics of process A and process B

Process		**Process A**		**Process B**	
Exposure dose [mJ/cm^2]		**250**	**500**	**250**	**500**
SU-8 2002	**Thickness [nm]**	1869±8	1902±8	1974±5	2067±1
	Residual stress [MPa]	14.3±0.1	14.2±0.6	6.3±1.7	2.9±0.5
	Line resolution [µm]	2.0±0.5	-	2.5±0.5	4.6±0.5
	Trench resolution [µm]	3.5±0.5	-	2.5±0.5	4.8±0.5
SU-8 2005	**Thickness [µm]**	5.03±0.04	5.16±0.08	5.53±0.05	5.51±0.01
	Residual stress [MPa]	11.5±0.1	13.5±0.2	4.2±0.1	-
	Line resolution [µm]	3.5±0.5	4.0±0.5	3.5±0.5	-
	Trench resolution [µm]	4.0±0.5	5.0±0.5	4.0±0.5	-

4.6.1 Cracking

In *Table 4.1-1,* low residual stress and high cross-linking were defined as requirements to reduce cracking of the SU-8. 5-µm-thick SU-8 films were prepared with *Process A* and *Process B* to evaluate if this goal was achieved. A mask in hard contact mode and a dose of 250 mJ/cm^2 were used for the exposure. The mask design included critical features such as concave corners which typically are sites for the initiation of cracks (*Section 2.5.5*).
Figure 4.6-1 shows optical images of the resulting SU-8 patterns. The sample fabricated with *Process A* shows cracking at the concave corners. The absence of cracking for the film patterned with *Process B* is a direct visualization of the improved cross-linking discussed in *Section 4.5* and the reduced residual stress as presented in *Table 4.6-3*.

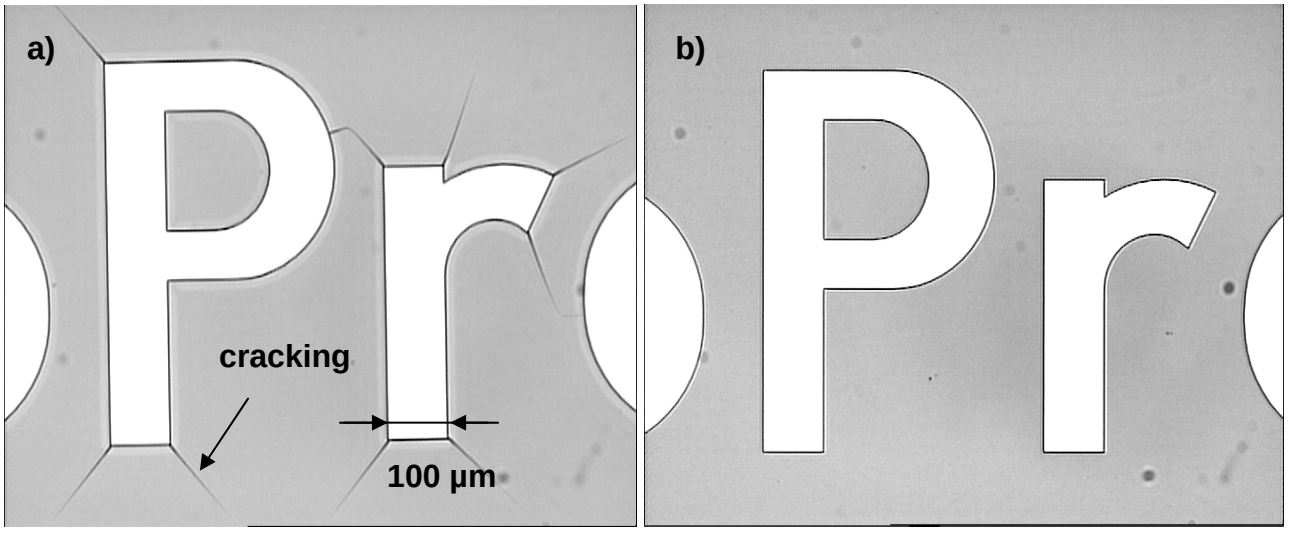

Figure 4.6-1: Optical images of 5-µm-thick SU-8: (a) Process A; (b) Process B

4.6.2 Delamination

The two processes were used by Michael Lillemose in a specific application for another PhD-project in the Nanoprobes-group. There, the goal was the use of SU-8 as an etch mask for the patterning of polyaniline films by oxygen plasma. The critical issue for this application is the low adhesion between the SU-8 and the polyaniline. Tensile stress in the SU-8 film results easily in delamination of the structures.
First, gold electrodes were patterned on a silicon substrate by a standard lift-off process. A polyaniline film with thickness of 300 nm was deposited by spin-coating and baked on a hotplate. On top of the unstructured polymer, a 2-µm-thick SU-8 film was patterned using *Process A* and *Process B*. The resolution was not a critical issue and therefore a high exposure dose of 625 mJ/cm^2 was used.
Figure 4.6-2 shows that the issue of delamination was solved with the optimized processing approach. These results are very promising for the fabrication of the flapper chip because the presented situation is similar to the one where the thin SU-8 flapper is patterned on top of the fluorocarbon release layer. There, delamination would considerably reduce the fabrication yield.

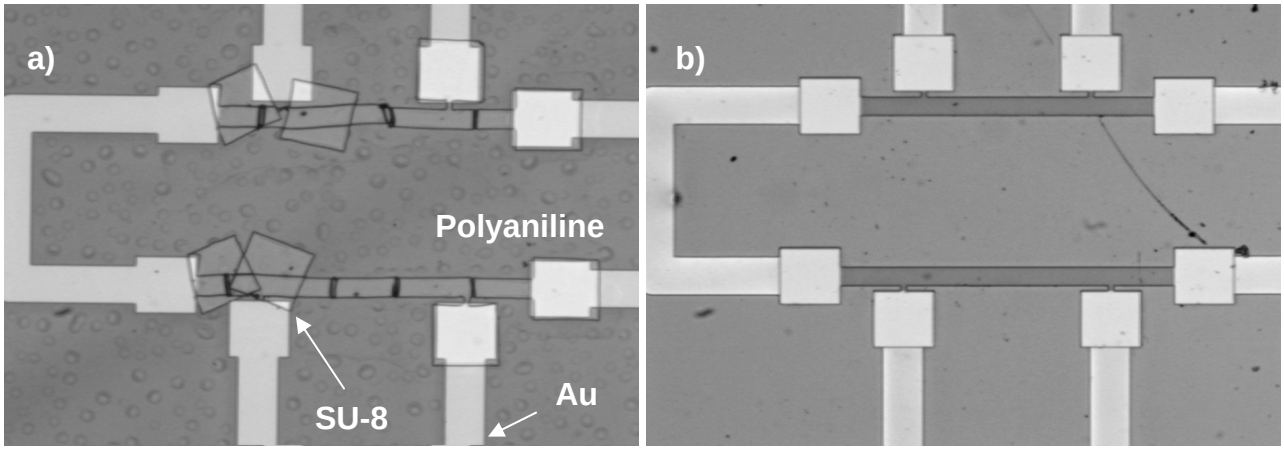

Figure 4.6-2: SU-8 patterned on top of a polyaniline film; (a) Process A results in delamination; (b) Process B leads to perfect overlap of the SU-8 with the Au-electrode pads.

4.7 Refractive index

In principle, the refractive index n of the SU-8 has no influence on the functionality of the flapperchips because the optical properties of the SU-8 are not explored in this application. On the other hand, this parameter allows for additional conclusions on the processing of SU-8 films as it is a measure for the optical density of the material.
Figure 4.7-1 shows a comparison of thickness and refractive index measured after each processing step for *Process A* and *Process B*. A suggested behaviour for the two approaches is schematically illustrated on *Figure 4.7-2*. For *Process A*, the refractive index significantly increases during the soft-bake. Solvent evaporation results in densification of the film, which is confirmed by the thickness measurements in *Figure 4.7-1(b)*. During the PEB, refractive index and thickness are more or less constant because the film is cross-linked without further change of volume or mass. For *Process B*, solvent evaporation during the waiting time between spin-coating and exposure is reduced and a considerable amount of solvent is expected to remain in the resist. Densification of the film during this step is smaller than for *Process A*, which results in a higher thickness and a lower refractive index. The thickness remains constant during further process steps. As illustrated in *Figure 4.7-2*, fast formation of the polymer network probably hinders shrinkage of the polymer.

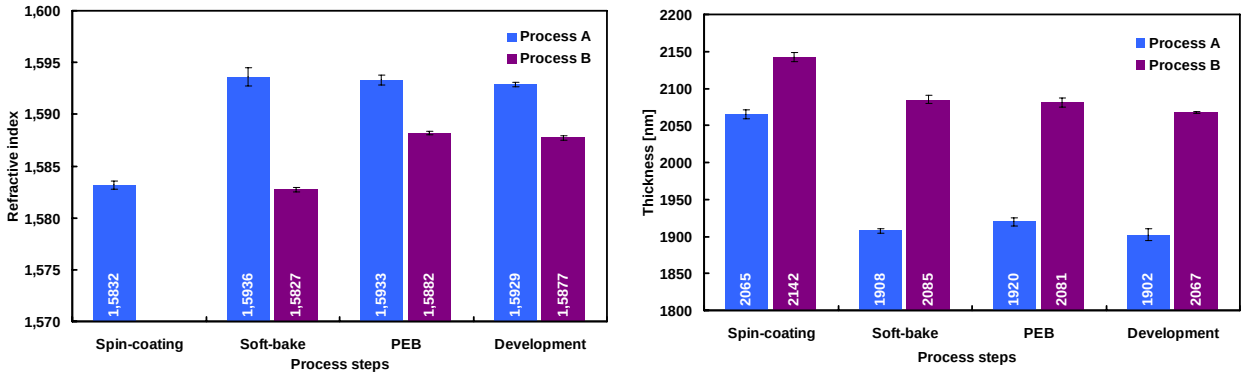

Figure 4.7-1: Comparison of refractive index (a) and thickness (b) after the different process steps of Process A and Process B for 2-µm-thick SU-8 films; D = 500 mJ/cm^2

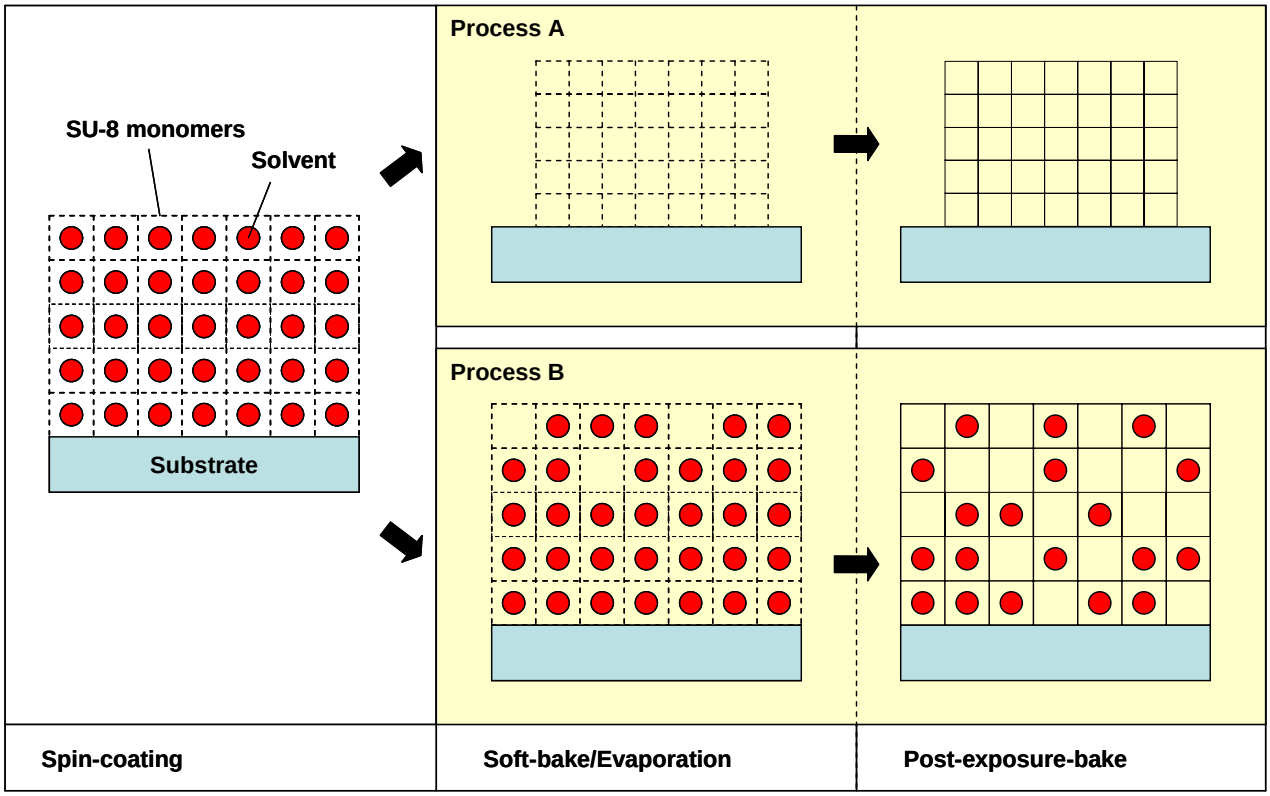

Figure 4.7-2: Schematical illustration of the polymerization with Process A and Process B. Interrupted lines indicate non-cross-linked SU-8, filled lines the cross-linked polymer

In conclusion, the measurements show that the refractive index of the SU-8 is influenced by the residual solvent content during cross-linking. The measured value for all the films processed in *Section 4.3* to *Section 4.5* was n = 1.585-1.589 compared to n ≈ 1.593 for *Process A*. The results indicate that control of the processing parameters might allow tuning of the optical properties of the SU-8. Other authors have demonstrated that this could be of interest for the fabrication of optical devices [139]. In this context, it will be important to investigate if the free volume assumed for *Process B* enhances re-absorption of solvent molecules in the polymer film. This might result in swelling and intrinsic stress which would be a problem for the operation of cantilever-based sensors.

4.8 Conclusion

The results of the experimental investigation of processing of thin SU-8 films allow the prediction of the influence of the processing parameters on process responses such as residual stress, structural stability, cross-linking density and refractive index. With the gained knowledge on SU-8 processing an optimal resist process can be designed depending on the specific application. Although the conclusions are based on processing of thin films, the observations might even be used for the process design for thick SU-8 films.
Based on the requirements for the fabrication of the thin SU-8 flapper specified in *Table 4.1-1* an optimized thin film process was defined as *Process B*. This process was compared to the conventional *Process A* presented in *Section 2.6*. The optimized processing results in lower residual stress which reduces cracking and delamination of the SU-8. Further, FT-IR measurements demonstrated the improved cross-linking of the SU-8. This should have a positive impact on the

mechanical and chemical stability of the SU-8. The lithographic resolution of the two processes is comparable and can be adjusted with the exposure dose.
The change of film properties with time was only discussed very briefly. The measurements showed that the film stress can change considerably during storage. Extended long-term studies on SU-8 films and devices should be performed to conclude on this important issue. The short discussion of *Section 4.7* on the refractive index shows that the density of the SU-8 films depends on the processing. This might have an influence on solvent absorption and swelling of the resist which is critical for the fabrication of devices operated in liquid.

5 Fabrication of SU-8 cantilevers

5.1 Goal of the process optimization

In *Chapter 4* the processing of thin SU-8 films was investigated in detail. The goal of the process optimization described in this chapter was to go one step further and to optimize the fabrication of arrays of thin SU-8 cantilevers. The cantilever chips served as model system for the flapperchip. This had the advantage that test masks with a large number of chips and a variety of cantilever dimensions could be used giving access to a large number of process data. The results should allow the definition of an optimized process for the fabrication of multi-layered cantilever-based sensors such as the flapperchip.
A first goal of the experiments was to ensure that the thin film processing of SU-8 meets the specifications defined in *Table 4.1-1* which could not be investigated in the previous chapter. An eventual gradient of residual stress in the thin SU-8 has to be minimized as it directly results in bending once the film is released from the substrate. For the fabrication of the autonomous sensor, low initial deflection of the lid is essential to avoid a release of the marker solution before the actual actuation. However, low cantilever bending is also a requirement for the alignment of the laser in most measurement setups using optical readout. Further, the release yield of the cantilevers from the fluorocarbon coating was investigated. This parameter is closely related to the structural stability of the thin SU-8 film but other factors might influence the release of the SU-8 structures from the substrate. Finally, the evaluation of cantilever bending and release yield as a function of storage time should allow conclusions on the time-stability of the photoresist and the shelf-life of the devices. Typically, it should be possible to store cantilever chips for some months between fabrication and use.
In *Section 5.3* and *Section 5.4* the influence of the post-exposure-bake conditions on the different process responses was evaluated. An additional hard-bake step was introduced in *Section 5.5* and the influence of the hard-bake parameters was investigated in *Section 5.6*. In *Section 5.7*, an optimized process for the fabrication of thin SU-8 cantilevers was defined and the process results were compared to the ones achieved with the conventional *Process B* described in *Section 2.6*.
In all the experiments, one has to be careful with conclusions on thin film processing as the setup is more complex than in *Chapter 4* due to the addition of a chip body on top of the SU-8 cantilever layer. In *Section 5.8*, the influence of the processing of the thick SU-8 layer on the fabrication of thin SU-8 cantilevers is demonstrated with some additional experiments.

5.2 Materials and method

The fabrication of the cantilever chips followed the scheme illustrated in *Figure 3.1-1*. In all the experiments the silicon substrate was coated with fluorocarbon using the recipe wet_tef2 developed in *Chapter 3*. For the definition of the cantilevers, SU-8 2002 was spin-coated to a nominal thickness of 2 µm using the parameters defined in *Table 2.6.1*. The solvent evaporation was done according to *Process B* described in *Table 4.6-2*. The exposure dose was fixed at 500 mJ/cm^2 and test masks with cantilevers of various dimensions were used. Each chip had an array of 8 or 9 cantilevers. Typically, the length of the cantilevers was L = 200-500 µm and the width w = 50-100 µm. The patterning of the thin SU-8 film was followed by a second step of SU-8 photolithography to define the chip body. For the fabrication of the chip body, Process B* described in *Table 2.6-2* was used. The resulting thickness of the chip body is about 185 µm. The thick-film processing was

done at low temperature to minimize an increase of the thermal stress in the thin SU-8 film. In the course of the optimization a total of 58 wafers were processed.
The measured responses were the release yield, the bending of the cantilevers and the quality of the chips. The release yield was evaluated with the method described in *Section 3.3.1*. For the specific cantilever dimension five chips with arrays of cantilevers were released from the substrate and the percentage of successfully released cantilevers was calculated. In some cases the evaluation of the release is difficult and rather qualitative.
In principle, the term bending implies a curvature of the beam. In the context of the experiments, cantilever bending was defined as the deflection of the free-standing end of the cantilever independent of the bending profile. Initially, the bending of the cantilevers was measured the SEM. There, charging effects rendered imaging difficult. To avoid this, the cantilevers were coated with a thin gold film. Comparison of the bending profile before and after gold coating showed, that even a very short metal deposition at ambient temperature has an influence on the bending of the thin SU-8 cantilevers. Finally, optical imaging of the side-profile followed by image treatment was chosen for the measurement of the cantilever bending. As a convention, positive values of bending describe an upward deflection of the cantilever as illustrated on *Figure 5.2-1*.

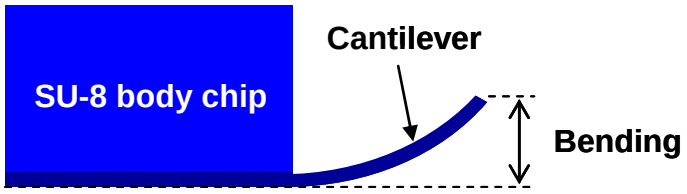

Figure 5.2-1: Illustration of a cantilever chip; the value of cantilever bending is positive

Table 5.2-1: Process B - Low temperature processing of 185-µm-thick SU-8 films*

Process step	Equipment	Parameters
Spin-coating	KS Spinner	100 rpm/s, 400 rpm; 30 s; 100 rpm/s, 800 rpm; 60 s
Soft-bake	Hotplate	10 h, 40ºC; ramping 2ºC/min
Exposure	KS Aligner	4x450 mJ/cm^2
Post-exposure bake	Hotplate	10 h, 40ºC; ramping 2ºC/min
Development	PGMEA	15 min FIRST, 15 min FINAL
Rinse	Isopropanol	30 s

5.3 Post-exposure-bake on the hotplate

In a first series of experiments, the influence of the post-exposure-bake temperature T_{PEB} on the described process responses was evaluated. The starting point for the experiments was *Process B* where T_{PEB} was varied in the range of 50-90ºC.

5.3.1 Replication of mask pattern

In *Chapter 4* the influence of increasing T_{PEB} on the lithographic resolution was discussed. At higher temperature diffusion of photo-acid into non-exposed areas was observed. Here, optical inspection of the non-released devices showed that T_{PEB} = 90˚C results in diffusion patterns at the border of the cantilevers (*Figure 5.3-1)*. The finger-like SU-8 structures on the substrate at the edged of the SU-8 are visible on the SEM-image taken at high resolution (*Figure 5.3-2*).

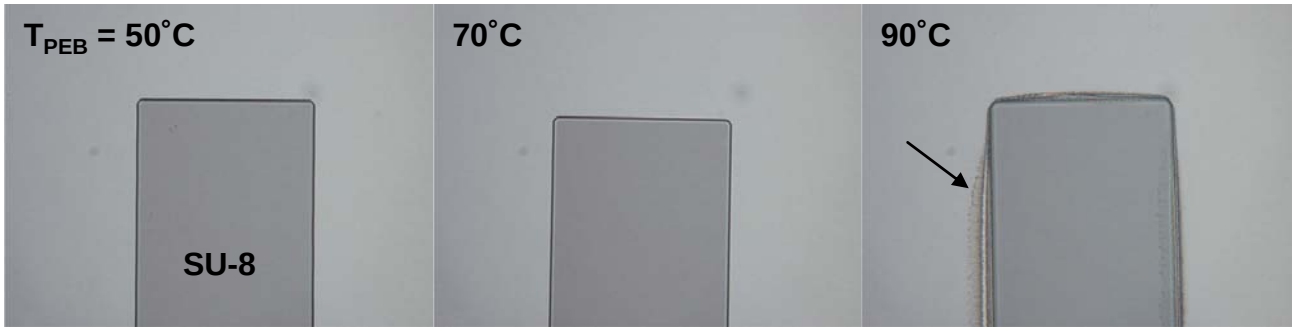

Figure 5.3-1: Optical images of the apex of non-released cantilevers (w = 100µm); the arrow indicates diffusion patterns

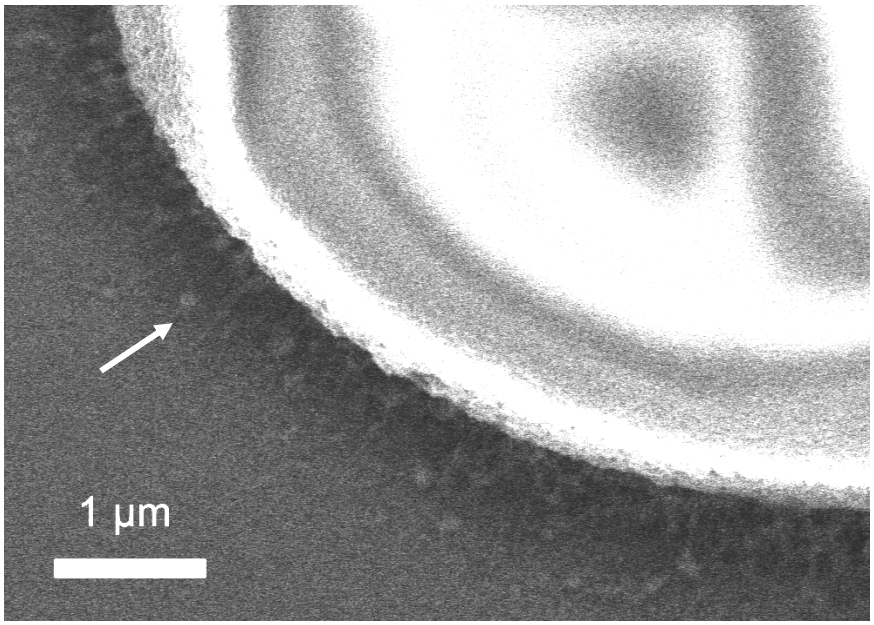

Figure 5.3-2: SEM-image of the diffusion patterns obtained at the edge of the SU-8 at T_{PEB} = 90˚C

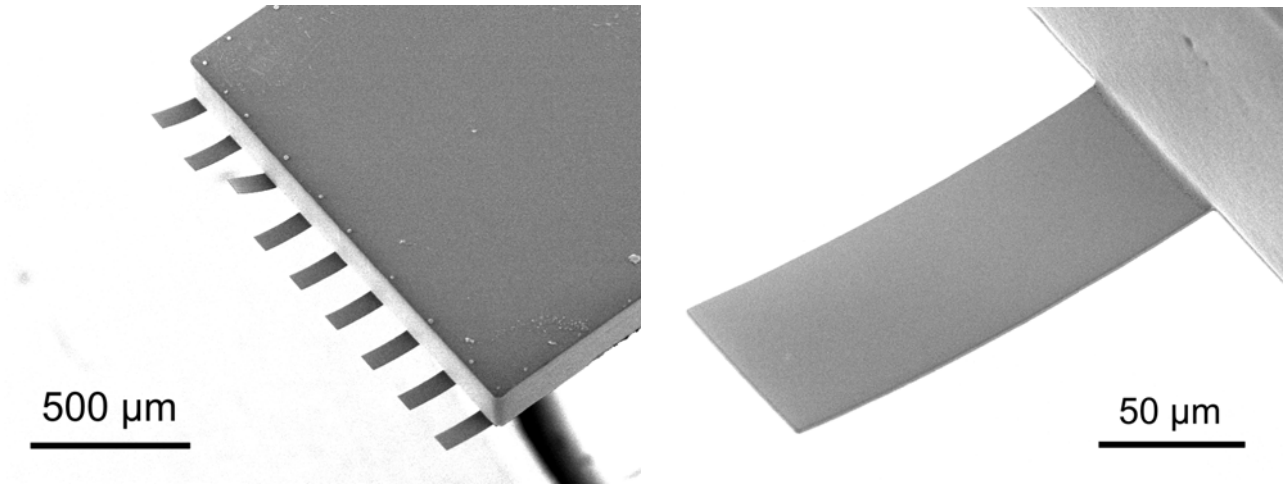

Figure 5.3-3: Array of 2-µm-thick cantilevers processed at T_{PEB} = 50˚C; L = 200 µm, w = 70 µm; the cantilevers are bending slightly upwards

5.3.2 Release of the cantilevers

Figure 5.3-3 shows SEM-images of a chip with an array of 200-µm-long cantilevers fabricated with *Process B* at T_{PEB} = 50˚C. The devices were successfully released from the fluorocarbon substrate. *Figure* 5.3-4 presents the release yield for cantilevers with a length L = 300 µm processed at different T_{PEB}. In the selected parameter range, the release from the fluorocarbon coating works well independent of T_{PEB} and is not affected by the observed diffusion patterns.

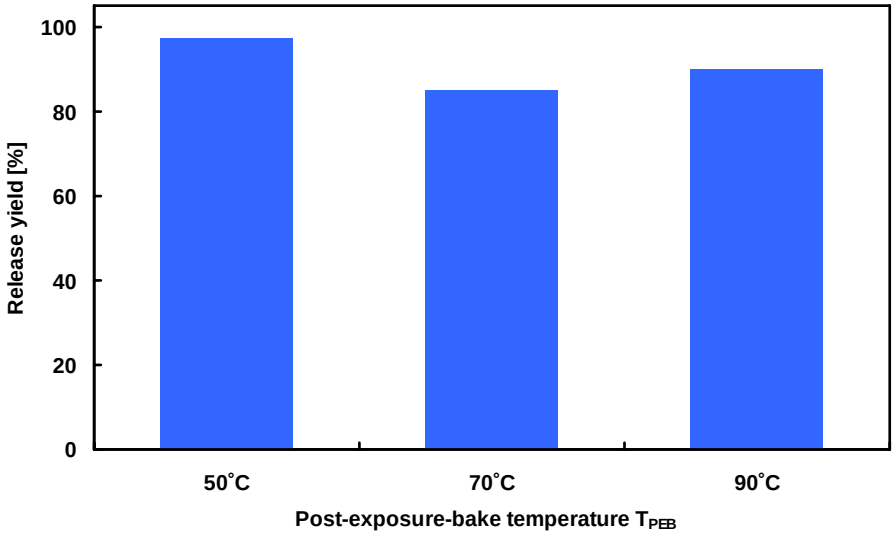

Figure 5.3-4: Release yield for cantilevers processed at different T_{PEB}; L = 300 µm; w = 100 µm

5.3.3 Cantilever bending

Figure 5.3-5 shows the circular bending profile of two 500-µm-long cantilevers processed at different T_{PEB}. The measurements of the bending for cantilever with two different lengths are summarized in *Figure 5.3-6*. *Process B* results in high cantilever bending (*Figure 5.3-5(a)*). With an increase of T_{PEB} a considerable decrease of the bending is observed. For T_{PEB} = 90˚C and a cantilever length of 300 µm the bending is below 10 µm.

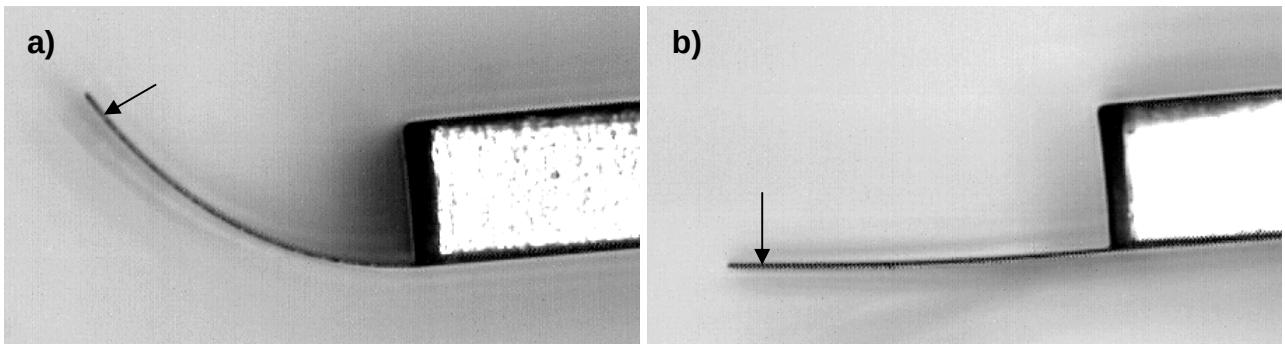

Figure 5.3-5: Side-view of cantilevers processed at T_{PEB} = 50˚C (a) and 90˚C (b); L = 500 µm

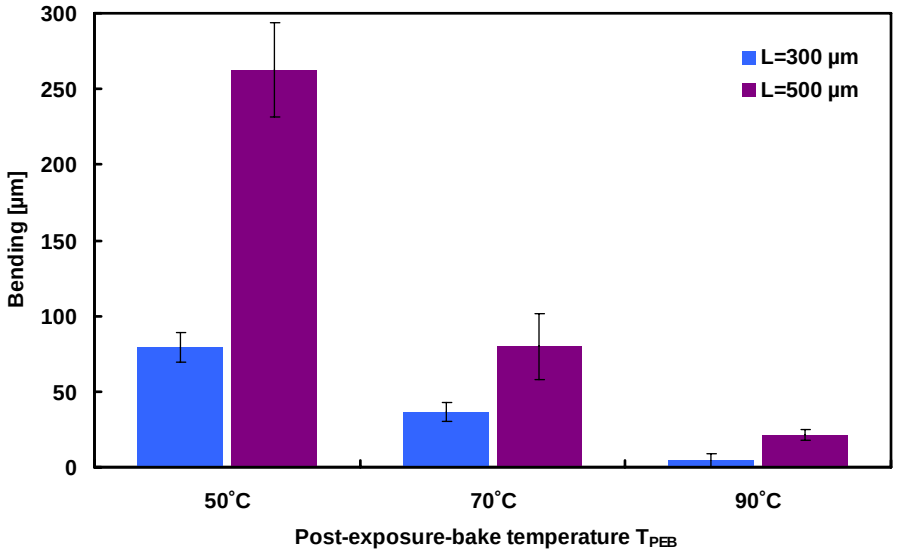

Figure 5.3-6: Bending of cantilevers processed at different T_{PEB}; w = 100 µm

5.3.4 Residual stress gradients

In *Chapter 4* an optimized process was defined for non-released SU-8 films was defined and one of the goals was the reduction of the residual film stress. Processing at T_{PEB} = 50˚C resulted in minimal tensile in-plane stress (*Figure 4.4-1*). The results on the cantilever bending demonstrate that residual stress and gradients of residual film stress are only partly correlated and have to be discussed separately.

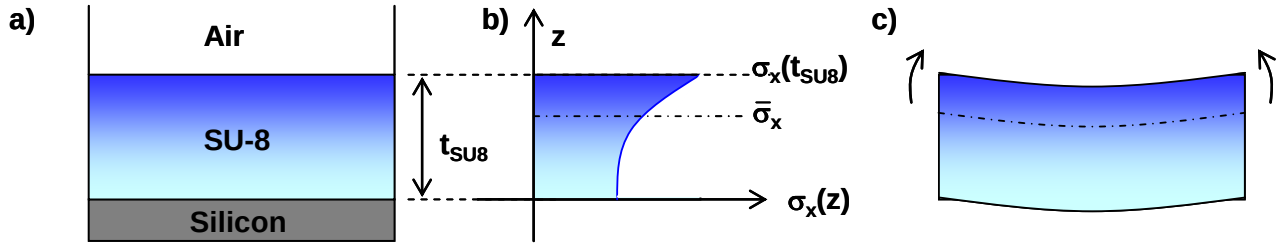

Figure 5.3-7: (a) Schematic of SU-8 processed on Si, t_{SU8} = film thickness; (b) example of a stress profile in the SU-8 film; (c) the residual stress gradient results in bending after removal from the Si

Figure 5.3-7(a) shows schematically the situation for an SU-8 film with thickness t_{SU8} processed on a silicon substrate. It is assumed that the stress in the film plane is constant:

$$\sigma_x = \sigma_y \qquad (5.3\text{-}1)$$

The film stress for the non-released substrate measured in *Chapter 4* is the mean value of the in-plane stress:

$$\overline{\sigma_x} = \frac{1}{t_{SU8}} \int_0^{t_{SU8}} \sigma_x(z)\,dz \qquad (5.3\text{-}2)$$

On the other hand, there might be a gradient of film stress normal to the film plane as illustrated on *Figure 5.3-7(b)*:

$$\frac{\delta\sigma_x(z)}{\delta z} \neq 0 \qquad (5.3\text{-}3)$$

Following Stoney's equation discussed in *Section 2.5*, this stress gradient results in a circular bending of the film particularly when it is released from the silicon substrate (*Figure 5.3-7(c)*). Therefore, free-standing structures such as cantilevers allow for direct visualization of residual stress gradients in the cantilever material. The circular bending profiles observed in the experiments suggest that the deflection of the cantilevers is related to residual stress gradients in the SU-8 film.
In *Chapter 2,* the influence of different process steps on cross-linking density, mechanical properties and residual film stress of the SU-8 was discussed. Sameoto et al. have used SU-8 cantilevers to show the influence of processing parameters on residual stress gradients in the resist [140]. They concluded, that processing gradients result in non-uniform material properties and gradients of residual stress. A removal of residual stress gradients as described by *Equation 5.3-3* requires a minimization of processing gradients throughout the film thickness. Three main sources for residual stress gradients as a result of SU-8 processing can be identified:

- Gradients in UV-radiation during exposure lead to different concentrations of photo-acid and to a variation of the cross-linking density
- Temperature gradients during the PEB result in a variation of cross-linking density and in a difference of thermal stress
- Gradients of solvent content result in non-uniform cross-linking and gradients of intrinsic stress due to a difference in volume

The gradient in UV-radiation is assumed negligible due to the low thickness of the SU-8 and the low absorption of the resist at the exposure wavelength [65]. The reduced thermal conductivity of the SU-8 compared to Si and the air flow in the cleanroom will result in a temperature gradient in the SU-8 film during the PEB on a hotplate. Finite element analysis of this situation with COMSOL Multiphysics showed that the temperature difference ΔT between the two SU-8 surfaces is very small. For $T_{PEB} = 90^{\circ}C$ it is $\Delta T < 0.02^{\circ}C$ and for $T_{PEB} = 50^{\circ}C$ it is even $\Delta T < 0.01^{\circ}C$.
Therefore, it is assumed that the most important processing gradient is related to a non-uniform solvent content throughout the film thickness. Between spin-coating and exposure and also during the first part of the PEB solvent molecules will diffuse from the bulk of the resist film to the interface air-SU-8 where they evaporate. The evaporation process is diffusion-limited which means that the solvent content at the polymer surface is much lower than in the bulk [78]. In *Chapter 4* it was shown, that the solvent content has an important influence on the cross-linking of the SU-8, particularly when the PEB is done at low temperature. As a consequence, the cross-linking density will be lower close to the SU-8 surface than in the bulk. This situation is represented in *Figure 5.3-8* with a simplified model of a two layered polymer cantilever where the bulk and the surface region have a different cross-linking density. As discussed in *Section 2.4.4*, this results in a higher coefficient of thermal expansion (CTE) in the bulk α_b than the CTE of the surface region α_s (*Figure 5.3-8(a)*). During the cool-down from the PEB the bi-layered cantilever bends due to the thermal stress caused by a difference in the coefficient of thermal expansion (*Figure 5.3-8(b)*) as described in *Section 2.5*.
In reality, the situation is much more complex as the gradient of the properties is continuous. Nevertheless, the results on the cantilever bending as a function of T_{PEB} might be explained by a

change of the gradient in cross-linking density. At T_{PEB} = 50˚C the surface region with low cross-linking is large which results in higher bending. With an increase of T_{PEB} the cross-linking improves, the gradient of the CTE is minimized and the cantilevers bend less. In the optimal case, the thermal and mechanical properties are uniform throughout the whole cantilever thickness and the residual stress gradient is zero.

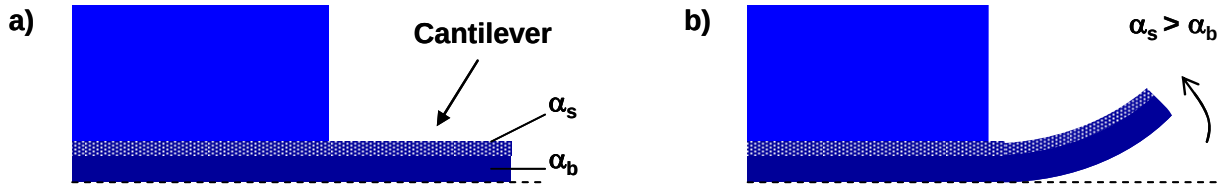

Figure 5.3-8: (a) Model of a cantilever with two SU-8-layers of different cross-linking density after the PEB; the CTE of the surface region α_s is higher than the one of the bulk α_b; (b) cool-down after the PEB results in thermal stress because $\alpha_s > \alpha_b$; the cantilever bends upwards

5.3.5 Change of properties with time

The release yield and the cantilever bending were re-evaluated after storage of the non-released devices in air for 5 months at a temperature of 22˚C. Similar to the results presented on the optimization of the fluorocarbon coating the release yield for 200-µm-long cantilevers slightly increased with storage and was close to 100% independent of T_{PEB}.
Figure 5.3-9 shows the measurements of cantilever bending after storage in comparison to the values measured directly after processing. For the samples processed at low T_{PEB} a considerable change in cantilever bending is observed (*Figure 5.3-10*). The bending is less significant after storage than directly after processing. In *Section 4.4.3*, decrease of film residual film stress was observed for SU-8 films processed at T_{PEB} > 50˚C. This was explained with creep, which means that thermal stress was released by plastic deformation of the SU-8. In case of the cantilever samples, the films have undergone an additional temperature cycle during the processing of the thick SU-8 film, which makes a direct comparison to the previous experiments impossible (see *Section 5.8*). Nevertheless, creep might result in stress relaxation and reduced bending. Another explanation is that cross-linking gradients are reduced with time due to continued polymerization. It will be interesting to see if the change of properties will continue for a longer storage time or if a stable state was reached.

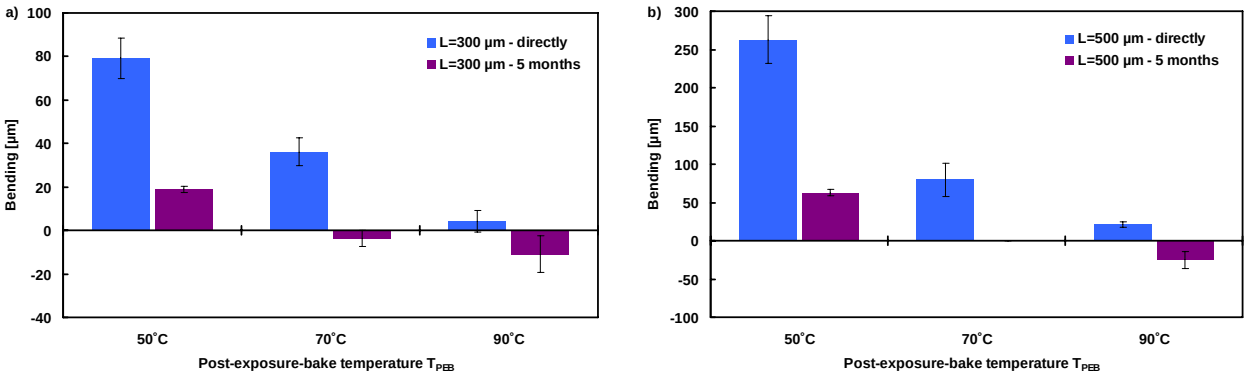

Figure 5.3-9: Cantilever bending measured directly after processing and after 5 months of storage for samples processed at different T_{PEB}; w = 100 µm

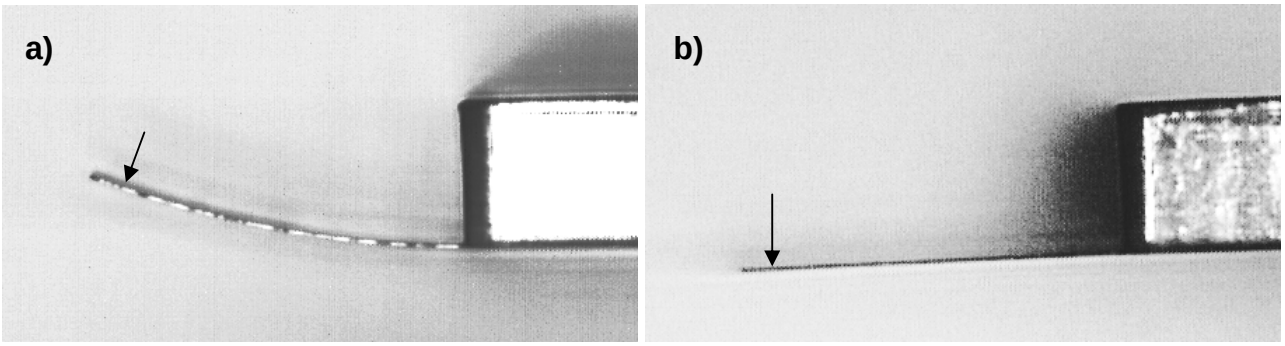

Figure 5.3-10: Deflection profile of cantilevers cross-linked at T_{PEB} = 70˚C released directly after processing (a) and after 5 months of storage (b); L = 500 µm, w = 100 µm

5.3.6 Conclusion

The fabrication and dry release of cantilever chips using the optimized Process B of the previous chapter was possible. On the other hand, the cantilevers show huge bending for samples processed at T_{PEB} = 50˚C. An increase of the T_{PEB} reduces the cantilever bending without affecting the release of the chips. Higher T_{PEB} results in more uniform cross-linking of the thin SU-8 film. Therefore, the material properties show less variation throughout the film thickness and gradients in residual film stress are smaller. Cross-linking gradients in the SU-8 have to be further reduced to minimize the cantilever bending. After some months of storage the cantilevers are in general straighter than directly after processing and can be released more easily. The change of bending is probably a combination of relaxation of residual stress and more uniform cross-linking density due to continued polymerization during storage. A T_{PEB} > 70˚C has a negative effect on the replication of the original mask pattern. The photo-acid diffuses in non-exposed areas which is not suitable for the fabrication of the flapperchip.

5.4 Post-exposure-bake in the oven

The goal of these experiments was to investigate if a long post-exposure-bake in an oven reduces cross-linking gradients in the SU-8. An oven is a more uniform processing environment than a hotplate because the temperature of the SU-8 and the evaporation of the solvent are not affected by the air-flow in the cleanroom. A practical advantage of an oven is that batch processing is possible where the number of wafers that can be processed simultaneously on a hotplate is limited. A long PEB of 15 h was done and T_{PEB} was varied from 50-90˚C. No temperature ramping or controlled cool-down was possible.

5.4.1 Release of the cantilevers

Figure 5.4-1 represents the release yield for cantilevers with a length of 200 µm and a width of 70 µm. Even for these short cantilevers, the release became difficult for samples processed at T_{PEB} > 50˚C. *Figure 5.4-2* shows images taken with an optical microscope after development of the thin SU-8 film processed at different temperatures. For T_{PEB} = 50˚C, the original mask pattern is correctly replicated. At higher T_{PEB} the SU-8 also polymerized in non-exposed areas as a result of enhanced diffusion of the photo-acid. For T_{PEB} = 90 ˚C, the diffusion length is around 35 µm which

corresponds to 2-3 µm/h. This value compares well to the results presented in *Section 4.4.2* for a PEB of 60 minutes on a hotplate. As a consequence of the partial cross-linking of the SU-8 outside the actual cantilever pattern, the release yield decreases with an increase of T_{PEB}.

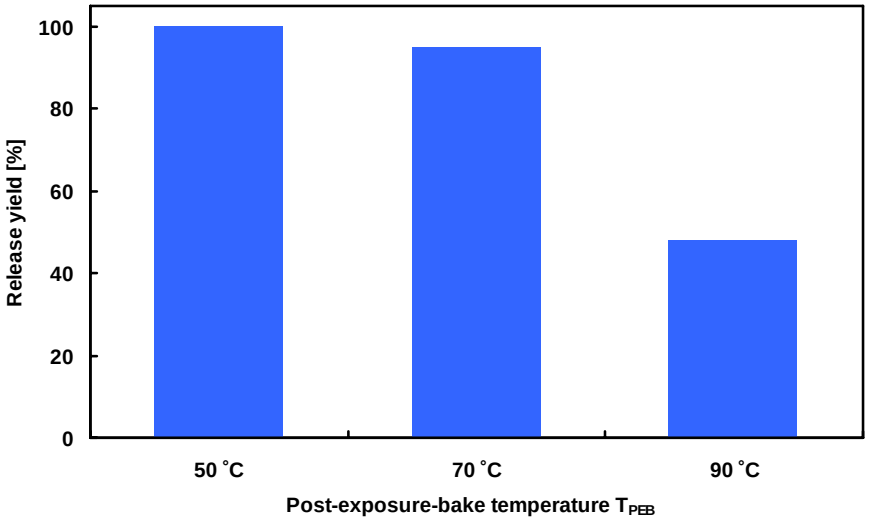

Figure 5.4-1: Release yield for cantilevers processed in an oven for 15h at different T_{PEB}; L = 200 µm; w = 70 µm

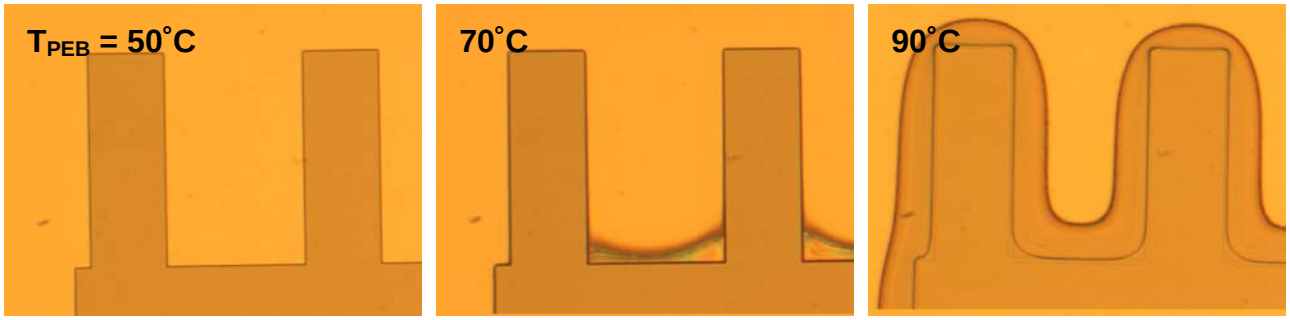

Figure 5.4-2: SU-8 pattern after processing at different T_{PEB} in the oven; for T_{PEB} = 50°C the mask pattern is correctly replicated

5.4.2 Cantilever bending

As a result of the difficulties with the release, the bending of the cantilevers was not analyzed in detail. The general impression was that the long PEB in the oven results in reduced bending compared to the PEB on a hotplate. For cantilevers processed at T_{PEB} = 90°C, most of the cantilevers were deformed during the release due to the diffusion patterns. Some chips could be released together with the thin SU-8 film cross-linked outside the original mask pattern (*Figure 5.4-3(a)*) and the cantilevers showed very low bending (*Figure 5.4-3(b)*).

5.4.3 Conclusion

During the long PEB in the oven photo-acid diffuses into non-exposed areas for T_{PEB} > 50°C. The result is a deterioration of the original lithographic pattern and a decrease of the release yield. On the other hand, cantilever processed at higher T_{PEB} seem to bend less straight which confirms the results of *Section 5.3*.

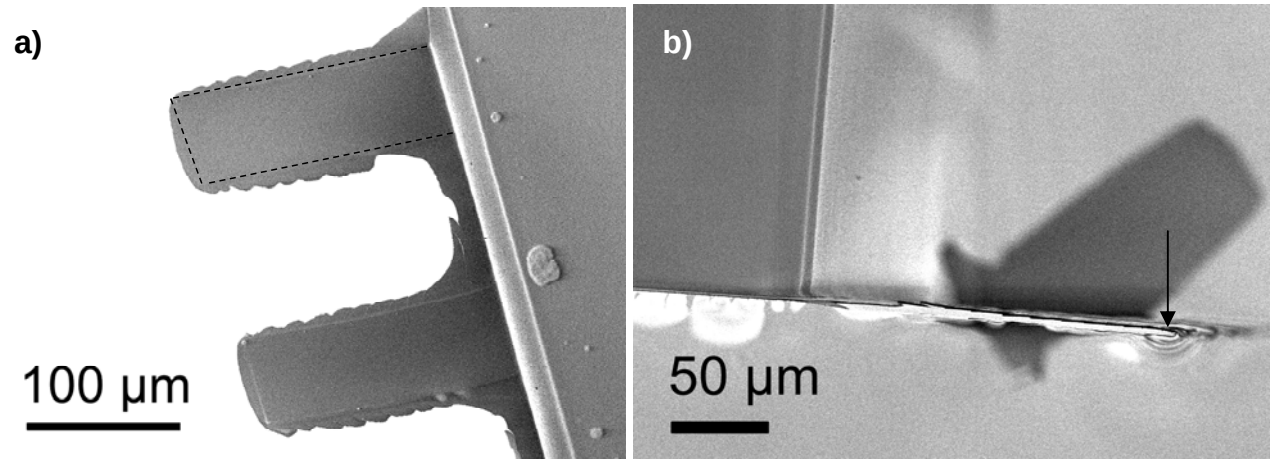

Figure 5.4-3: Devices processed in an oven at T_{PEB} = 90˚C; L = 200 µm, w = 70 µm; (a) replication of the original mask pattern (interrupted line) is affected by diffusion; (b) side-profile

5.5 Introduction of a hard-bake in the oven

The results of the two previous sections show that a higher T_{PEB} results in less bending of the cantilevers. On the other hand, the release yield and the lithographic resolution are better for structures processed at low T_{PEB}. Therefore, it might be beneficial to do the cross-linking of the SU-8 in two steps. First, the SU-8 is pre-polymerized during a short PEB at low temperature. There, the cross-linking has to be sufficient to ensure stability towards development. After removal of the non-cross-linked SU-8, the samples are exposed for a second time to UV-light to activate the rest of the photo-initiator. This step is followed by a long hard-bake in an oven at a temperature $T_{HB} > T_{PEB}$ to achieve further polymerization of the SU-8. This process should allow for high cross-linking density without negative influence on the release yield or the lithographic resolution.
For the experiments, cantilever chips were fabricated using the same process parameters as in *Section 5.3*. The PEB was done on a hotplate during 60 minutes at different T_{PEB}. After development the samples were dried in air for 2 h. The dose for the second exposure was 500 mJ/cm^2 and no mask was used. For all the samples the hard-bake was done in an oven at T_{HB} = 120˚C during 15 h. The high T_{HB} and the long duration of the hard-bake should allow high cross-linking of the SU-8 and minimal cross-linking gradients throughout the film thickness.

5.5.1 Effect of the hard-bake on cross-linking of the SU-8

For the evaluation of the effect of the hard-bake on the cross-linking, 5-µm-thick SU-8 films were processed with the same parameters as for the patterning of the cantilever layer but without using a photolithographic mask. These samples were used for analysis by Fourier-Transform infrared spectroscopy as described in *Section 4.5*.
Figure 5.5-1 is the FT-IR-spectra for a sample with and without hard-bake in comparison to the non-cross-linked monomer. In the spectra of the hard-baked SU-8 (*Figure 5.5-1(c)*) the peaks at 861 cm^{-1} and 910 cm^{-1} are completely removed demonstrating the high conversion of the epoxy-groups. In parallel, the intensity of the C-O stretching band characteristic of ethers (1000-1230 cm^{-1}) and secondary alcohols (1000-1290 cm^{-1}) increases for this sample which is another consequence of the improved cross-linking.

In *Section 4.5*, the absorption band around 1750 cm^{-1} in the FT-IR spectrum of SU-8 films processed with Process B was assigned to the SU-8 solvent cyclopentanone. For the sample processed with a hard-bake step the intensity of this band significantly lower. This observation suggests that solvent residuals in the SU-8 are evaporated during the hard-bake at high temperature.

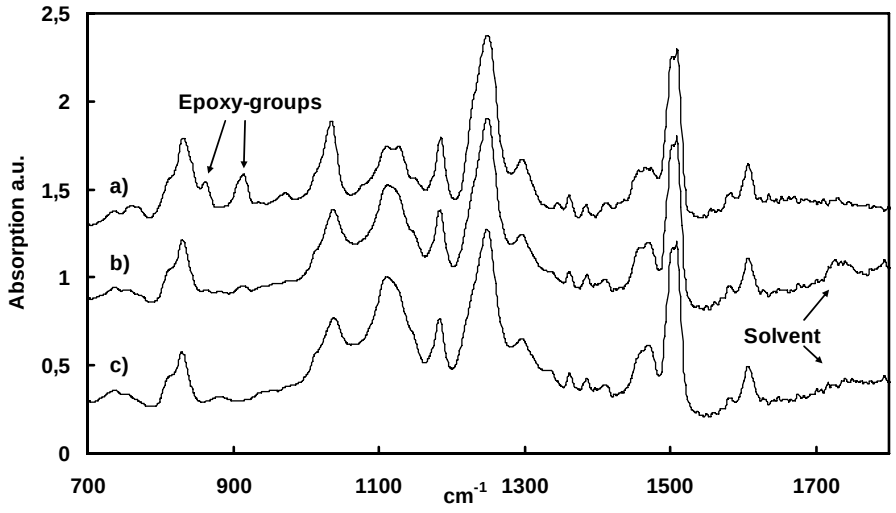

Figure 5.5-1: FT-IR-spectra of 5-µm-thick SU-8 films: (a) SU-8 monomer (b) Process B (c) Process B with hard-bake at 120˚C

5.5.2 Release of the cantilevers

Figure 5.5-2 represents the release yield with and without hard-bake for 300-µm-long cantilevers that were pre-polymerized at different T_{PEB}. The results without hard-bake were discussed in *Section 5.3* and are shown for comparison. For $T_{PEB} < 90˚C$, the release yield slightly remains close to 100%. For the sample processed at $T_{PEB} = 90˚C$, the release yield decreased due to the hard-bake. This is explained by the formation of diffusion patterns in non-exposed areas as shown on *Figure 5.3-1*. Apparently, the thin finger-like SU-8 structures are acting like glue at the edges of the cantilevers which affects the release of the cantilevers.

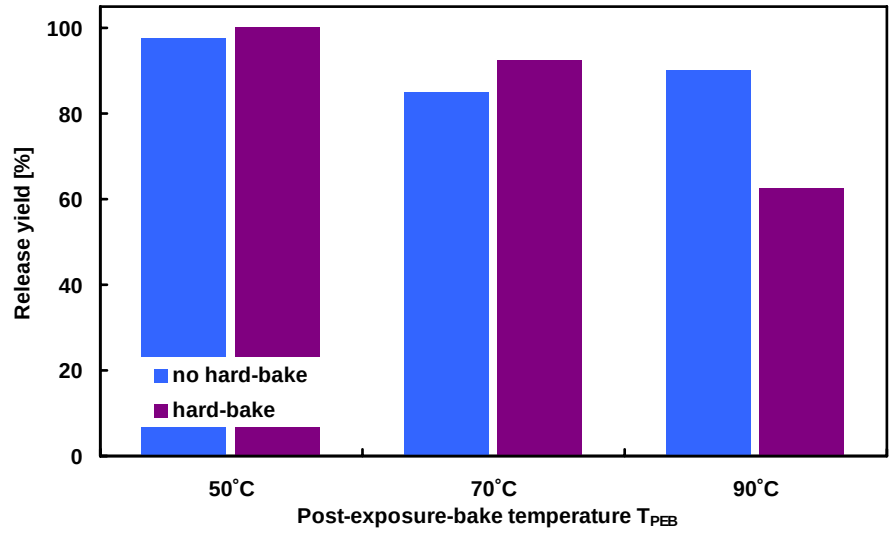

Figure 5.5-2: Release yield for cantilevers processed without and with hard-bake; L = 300 µm; w = 100 µm

5.5.3 Cantilever bending

Figure 5.5-3 summarizes the measurements of cantilever bending for samples with and without hard-bake pre-polymerized at different T_{PEB}. The results demonstrate a considerable effect of the hard-bake on residual stress gradients in the SU-8 films. For T_{PEB} = 50˚C, the bending considerably decreases with a hard-bake. For higher T_{PEB}, the bending is affected by the additional bake step but *Figure 5.5-3* allows no conclusion if an improvement was achieved.
Here, the bending profiles before and after the hard-bake have to be considered. Without a hard-bake, the bending of the cantilevers is circular and can be described by a radius of curvature R (*Figure 5.5-4(a)*). In *Section 5.3.4* it was concluded that the bending is a result of cross-linking gradients in the SU-8. For samples processed with hard-bake, the side-profile shows no real curvature of the cantilever (*Figure 5.5-4(b)*) which is observed for all values of T_{PEB}. The long hard-bake at high temperature seems to result in more uniform cross-linking of the SU-8 and the removal of residual stress gradients. The term bending might be misleading in the discussion for the hard-baked samples. For these cantilevers, it would be more precise to call the measured negative value the end-point deflection. The deflection is mainly a result of plastic deformation at the cantilever base (circle on *Figure 5.5-4(b)*) during the mechanical release from the substrate. The adhesion to the fluorocarbon seems to increase during the hard-bake at high temperature which results in difficulties with the release of the cantilevers. For T_{PEB} < 90˚C this had no direct effect on the release yield observed in *Figure 5.5-2*. Apparently, the mechanical strength of the hard-baked SU-8 is high enough to allow for the release of the cantilevers but not sufficient to prevent plastic deformation.

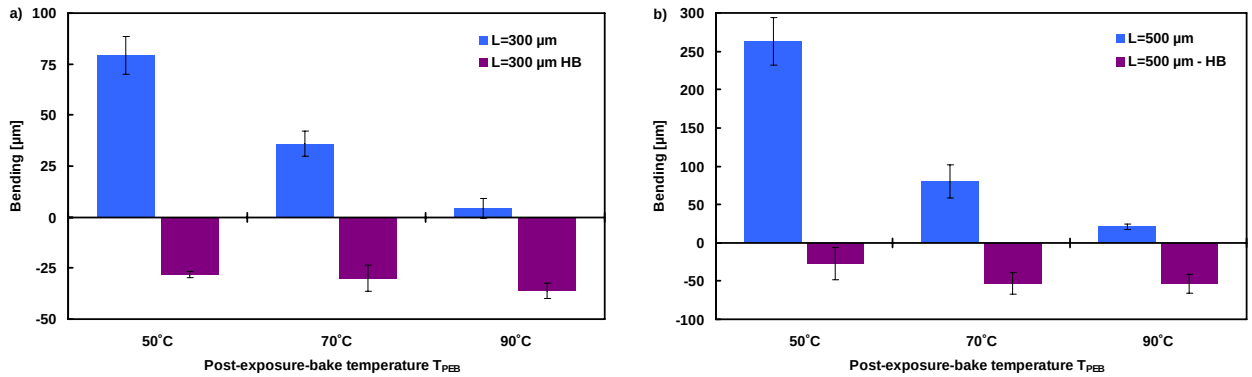

Figure 5.5-3: Bending of cantilevers processed without and with hard-bake (HB); w = 100 µm

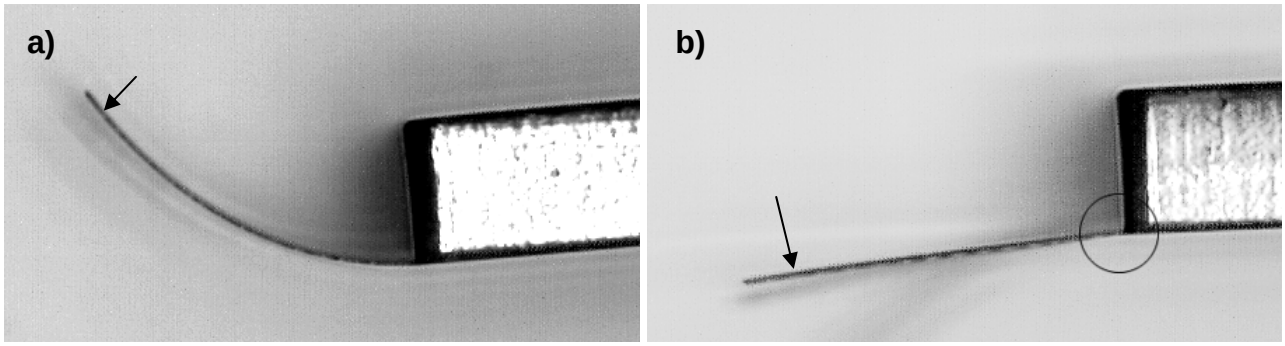

Figure 5.5-4: Cantilevers processed at T_{PEB} = 50˚C without (a) and with (b) hard-bake at T_{HB}=120˚C; L = 500 µm; w = 100 µm; the circle indicates plastic deformation

5.5.4 Change of properties with time

Figure 5.5-5 compares the release yield for the hard-baked samples measured after 5 months of storage to the values obtained directly after processing. For $T_{PEB} \leq 70^{\circ}C$, the release was improved with time and the yield was 100%. On the other hand, the release of the SU-8 cantilevers from the sample processed at $T_{PEB} = 90^{\circ}C$ was impossible due to stiction of the structures to the fluorocarbon. The finger-like diffusion patterns seem to react chemically with the release coating.
The values of cantilever bending are more or less unchanged for samples released after 5 months of storage. The cantilevers are still very straight but show plastic deformation at the clamping to the chip body. In comparison to the devices fabricated without hard-bake (*Figure 5.3-9*) the improved cross-linking due to the long hard-bake at high temperature is expected to result in reduced creep and ageing of the SU-8.

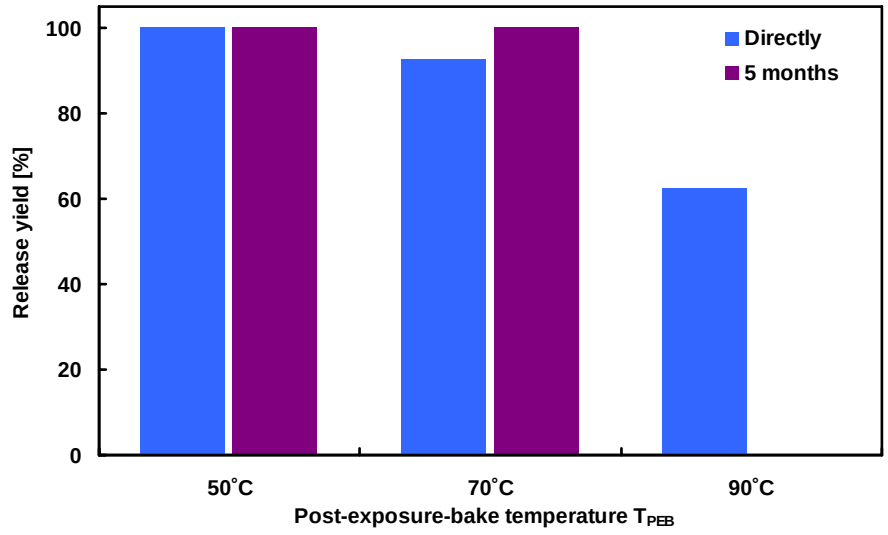

Figure 5.5-5: Release of cantilevers fabricated with a hard-bake at T_{HB}=120°C directly after processing and 5 months later; L = 300 µm, w = 100 µm

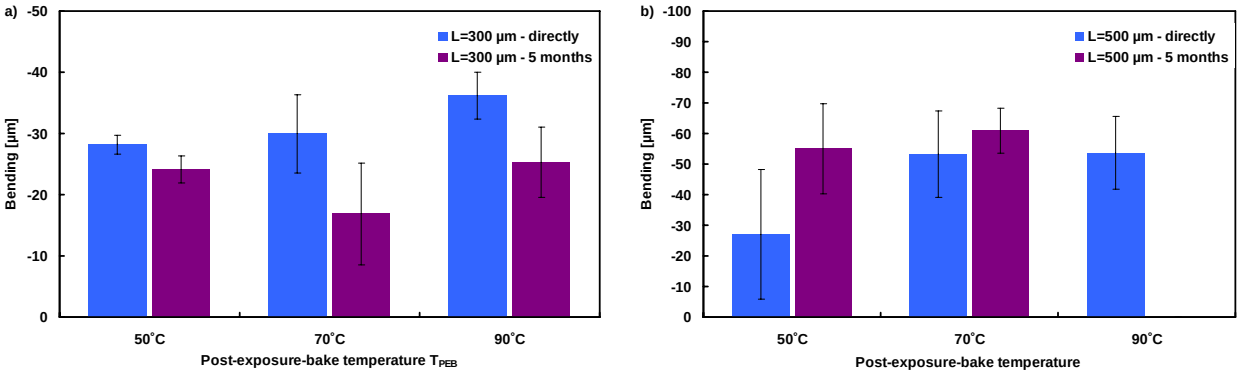

Figure 5.5-6: Comparison of hard-baked devices released directly after processing and 5 months later; release of cantilevers with L = 500 µm processed at T_{PEB} = 90°C was impossible

5.5.5 Hard-bake after release of the cantilevers

For some samples, it was evaluated if a hard-bake after the release of the devices could replace the one introduced after the development of the first layer. This would avoid the observed decrease of

the release yield due to stiction to the fluorocarbon substrate. Devices fabricated with *Process B* were hard-baked for 2h in the oven at a temperature of 120˚C. *Figure 5.5-7* shows 300-µm-long cantilevers before and after the bake step. Similar to the results presented previously in this section, the curvature of the cantilever is significantly lower for the hard-baked sample. On the other hand, the hard-bake results in contraction of the chip body. The cantilever is deflected out-of-plane as its movement is not longer restricted by the substrate.

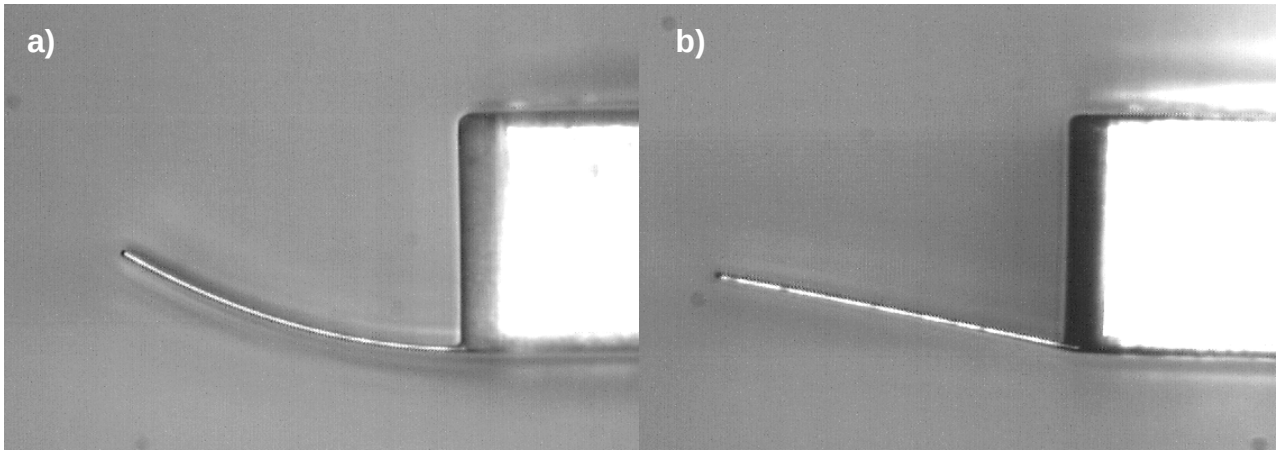

Figure 5.5-7: Cantilever processed at T_{PEB}=50˚C before (a) and after (b) hard-bake in oven (2h at 120˚C) after the release from the fluorocarbon; L = 300 µm

5.5.6 Conclusion

The introduction of a hard-bake at T_{HB} = 120˚C in an oven after development of the thin SU-8 film reduces the bending of the cantilevers due to a removal of cross-linking gradients in the resist. FT-IR measurements showed that the cross-linking of the SU-8 is improved and that solvent residuals are evaporated. This is expected to improved time-stability of the devices as ageing and creep are reduced. On the other hand, the release of the devices is more critical as stiction to the substrate leads to plastic deformation of the cantilevers at the base. Processing at low T_{PEB} followed by a hard-bake at high temperature is recommended to prevent formation of diffusion patterns that affect the release yield and the lithographic resolution. A hard-bake after release of the devices is no alternative. There, contraction of the chip body results in significant out-of-plane deflection of the cantilevers.

5.6 Variation of hard-bake conditions

In a final series of experiments on the processing of the thin SU-8 film the influence of the hard-bake temperature T_{HB} was investigated. For all the samples the pre-polymerization was done on a hotplate at T_{PEB} = 50˚C during 60 minutes. After the PEB the SU-8 was developed, dried in air for 2 h and flood-exposed with a dose of 500 mJ/cm^2. This step was followed by a hard-bake in the oven during 15 h and T_{HB} was varied from 90˚C to 200˚C.

5.6.1 Release of the cantilevers

The release yield for the cantilevers is close to 100% for chips processed at $T_{HB} \leq 120^{\circ}C$. The release becomes more difficult for devices fabricated at higher T_{HB} due to stiction to the substrate. For $T_{HB} = 200^{\circ}C$, the release of 500-µm-long cantilevers becomes impossible and shorter cantilever are heavily deformed during the release. Apparently, the processing at higher temperature leads to chemical reaction of the SU-8 with the fluorocarbon.

5.6.2 Cantilever bending and release of cantilevers

The bending of the cantilevers was evaluated for the samples processed at different T_{HB}. *Figure 5.6-1* is a summary of the results. The introduction of a hard-bake minimizes the cantilever bending compared to the sample processed without hard-bake independent of T_{HB}. On the other hand, the quality of the released devices is strongly influenced by the value of T_{HB}. In contrary to the expectations, an increase of T_{HB} results in higher cantilever bending. *Figure 5.6-2* shows that a hard-bake at $T_{HB} = 90^{\circ}C$ results in very straight cantilevers compared to significant cantilever bending at $T_{HB} = 150^{\circ}C$.
The measured bending of the cantilevers is a combination of two effects. Similar to the previous section, stiction to the fluorocarbon substrate during the release results in plastic deformation at the base of the cantilevers. On the other hand, the cantilevers processed at higher T_{HB} effectively show a negative curvature as shown in *Figure 5.6-2(b)*.
In *Section 5.3.4* a bi-layered model was introduced to explain the bending of the SU-8 cantilevers after the PEB. Due to non-uniform cross-linking during the PEB the surface region has a higher CTE than the bulk ($\alpha_s > \alpha_b$). Therefore, devices released after the cool-down to ambient temperature show positive bending. *Figure 5.6-3* illustrates the situation where the cantilever is subjected to an additional hard-bake step. Reheating of the bi-layered cantilever to T_{PEB} would result in straight cantilevers. If the temperature is further increased the direction of the bending is changed (*Figure 5.6-3(b)*). The negative bending is higher the higher the difference between T_{PEB} and T_{HB}. At the hard-bake temperature T_{HB} the SU-8 is uniformly cross-linked and ideally gradients in the material properties are removed ($\alpha_s = \alpha_b$). The strained polymer network is stabilized and the cantilever remains bent after cool-down (*Figure 5.6-3(c)*).

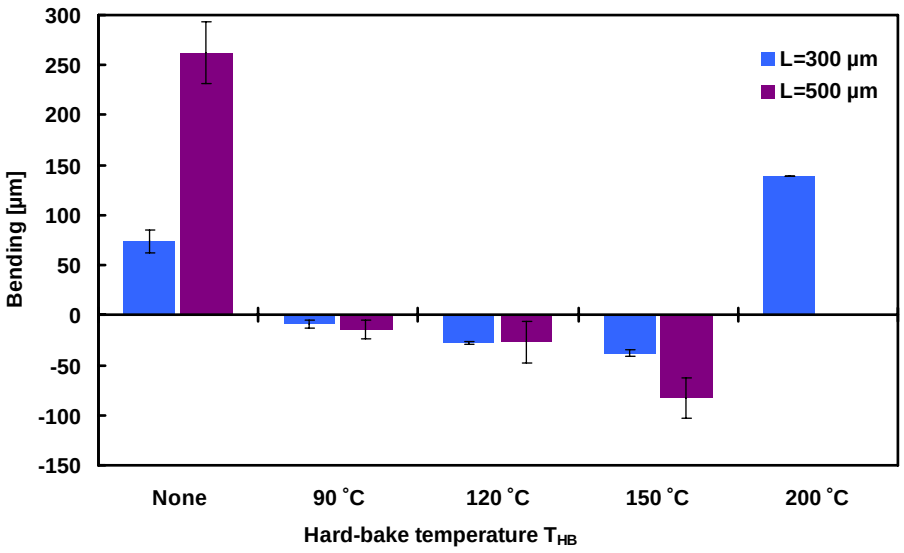

Figure 5.6-1: Cantilever bending for processing at variable T_{HB}; w = 100 µm

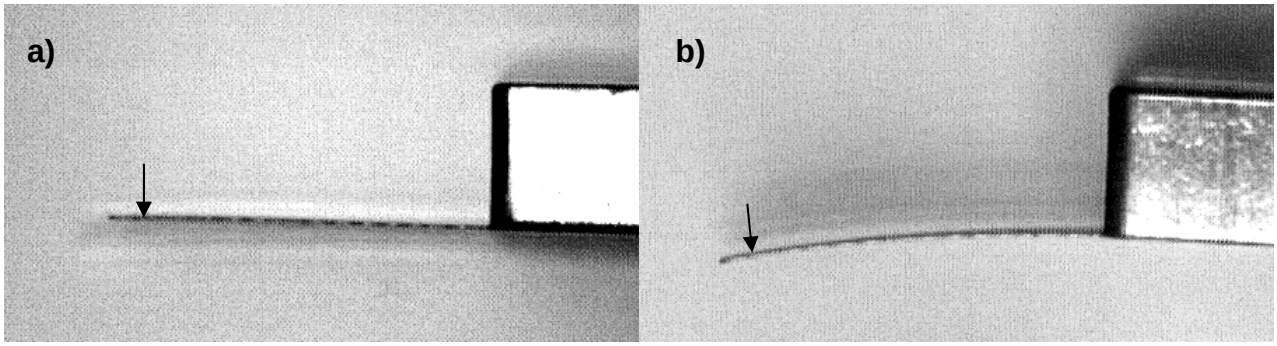

Figure 5.6-2: Side-profile of cantilever fabricated with (a) T_{HB} = 90˚C and (b) T_{HB} = 150˚C

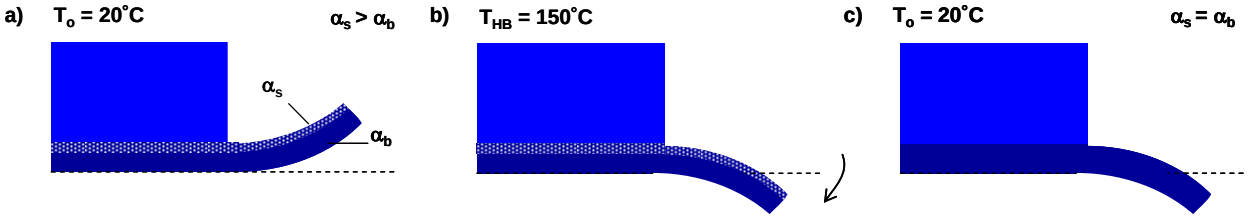

Figure 5.6-3: (a) Bi-layered SU-8 cantilever due to non-uniform cross-linking during PEB as described in Section 5.3.4; (b) Thermal stress results in change of cantilever bending as $T_{HB} > T_{PEB}$; (c) Material properties are uniform at the end of the hard-bake and the bending remains

5.6.3 Change of properties with time

The release and the bending of the cantilevers was evaluated after 4 months of storage and compared to the values obtained directly after processing. The release yield was close to 100% even for the devices processed at T_{HB} = 200˚C that initially could not be removed from the substrate. *Figure 5.6-4* shows the results on cantilever bending. For $T_{HB} \leq 120$˚C the parameter is more or less unchanged. For T_{HB} = 150˚C the bending measured after storage is lower than directly after processing which is probably related to relaxation of residual stress. The significant change for T_{HB} = 200˚C is explained by less plastic deformation during the release from the substrate.

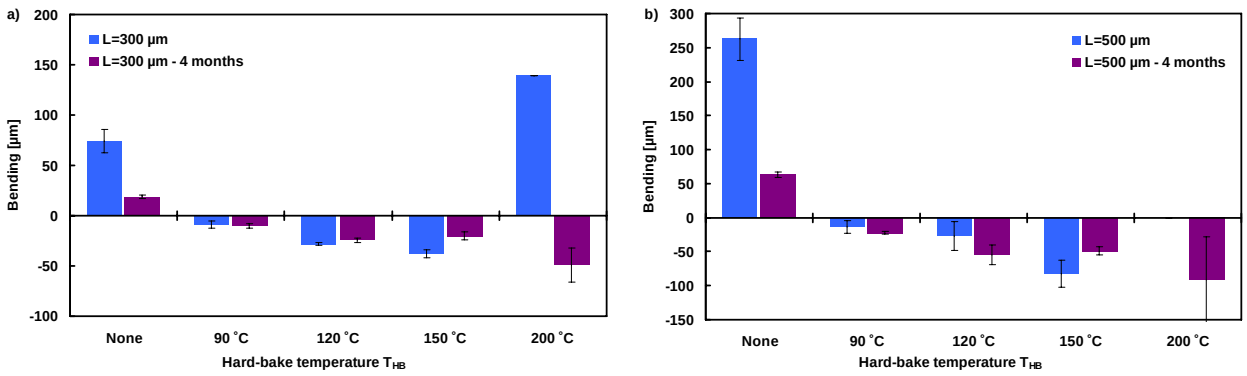

Figure 5.6-4: Comparison of the bending of cantilever processed at variable T_{HB} released directly after processing and 4 months later

5.6.4 Conclusion

A hard-bake at T_{HB} = 90-120ºC results in high release yield, low cantilever bending and low change of these properties after a storage for several months. At higher T_{HB} the cross-linking might be improved but a negative bending is observed and the release yield decreases.

5.7 Optimized and conventional fabrication of thin SU-8 cantilevers

In *Chapter 4*, an optimized process for thin SU-8 films was defined (*Process B*, *Table 4.6-2*). This process featured high structural stability, low residual stress and high lithographic resolution. The experiments in *Section 5.3* and *Section 5.5* demonstrated that *Process B* is well-suited for the fabrication of SU-8 cantilevers if a hard-bake in the oven is added after the development of the SU-8. In *Section 5.6* different hard-bake temperatures were tested and it was concluded on an optimal range for this parameter. In *Table 4.6-2*, the optimized thin film process (*Process C*) for the fabrication of SU-8 cantilevers is defined. In the following, *Process C* will be compared to the conventional thin film process for the fabrication of thin SU-8 cantilevers (*Process A, Table 2.6-3*). In both cases, the fabrication of the chip body is done with the *Process B** described in *Table 2.6-2*.

Table 5.7-1: Process C - Optimized process for the fabrication of 2-µm-thick SU-8 cantilevers

Process step	Equipment	Parameters: SU-8 2002
Process B	-	see *Table 4.6-2*
Drying in air	-	2 h
2nd Exposure	KS Aligner	Flood-exposure; 500 mJ/cm^2
Hard-bake	Oven	15 h, 90ºC

5.7.1 Introduction of a hard-bake for conventional processing

In *Section 4.5* the epoxy conversion for *Process A* and *Process B* was measured with FT-IR spectroscopy and it was demonstrated that *Process B* results in a higher degree of polymerization of the SU-8. A second series of FT-IR measurements in *Section 5.5.1* proved that the introduction of a hard-bake results in further improvement of the cross-linking of the SU-8 for *Process B*. To complete this study, it should be evaluated if the cross-linking is dependent of the initial process or if it is only the hard-bake that determines the final conversion of the epoxy groups. Therefore, samples were prepared with *Process A* followed by a hard-bake in the oven for 15h at 120˚C. *Figure 5.7-1* shows the results of FT-IR measurements on 5-µm-thick SU-8 films with and without hard-bake. Indeed the intensity of the peaks characteristic for un-openend epoxy-groups decreases for the hard-baked sample. On the other hand, a comparison with *Figure 5.5-1* shows that even with the hard-bake the cross-linking is not as high as for *Process C*. Therefore, it is concluded that the additional bake step only partially compensates for differences in cross-linking as a result of earlier process steps.

5.7.2 Release of the cantilevers

Figure 5.7-2(a) is a comparison of the release yield for the different processes directly after processing. No measurement for the cantilevers with L = 500 µm was done for *Process B*. For

Process A with and without hard-bake, the release is clearly more difficult than for the other processes. *Figure 5.7-3* shows that a lot of SU-8 residues remain on the fluorocarbon substrate after the release of the cantilevers fabricated with *Process A*. Similar to earlier the results presented in *Figure 5.3-1*, the high T_{PEB} resulted in the formation of diffusion patterns at the edge of the thin SU-8 film which have a negative impact on the release yield. Compared to this, almost no residues are left after the release of the cantilevers for the optimized *Process C*. Storage of the samples for 5 months resulted in an improved release for all the samples. On the other hand, the release yield for *Process A* is still lower than for the other processes where it was 100%.

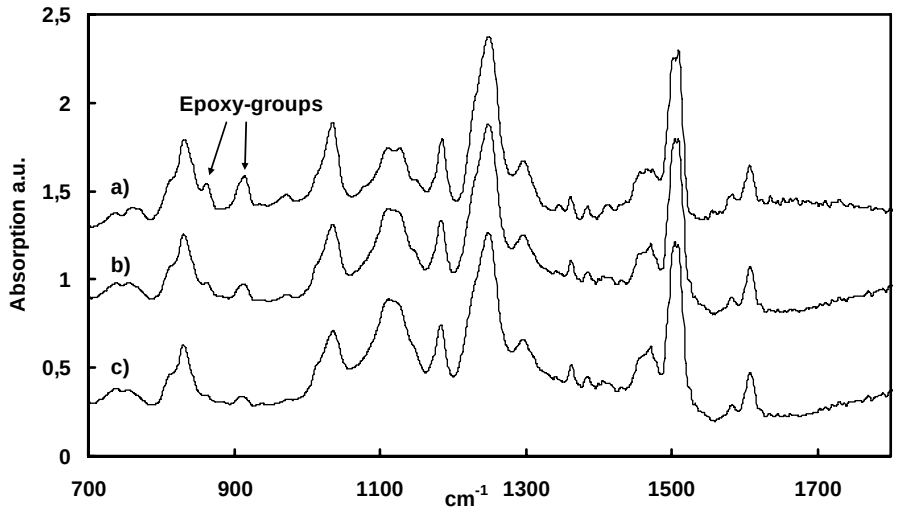

Figure 5.7-1: FT-IR-spectra of 5-µm-thick SU-8 films. (a) SU-8 monomer; (b) Process A; (c) Process A with hard-bake at 120˚C

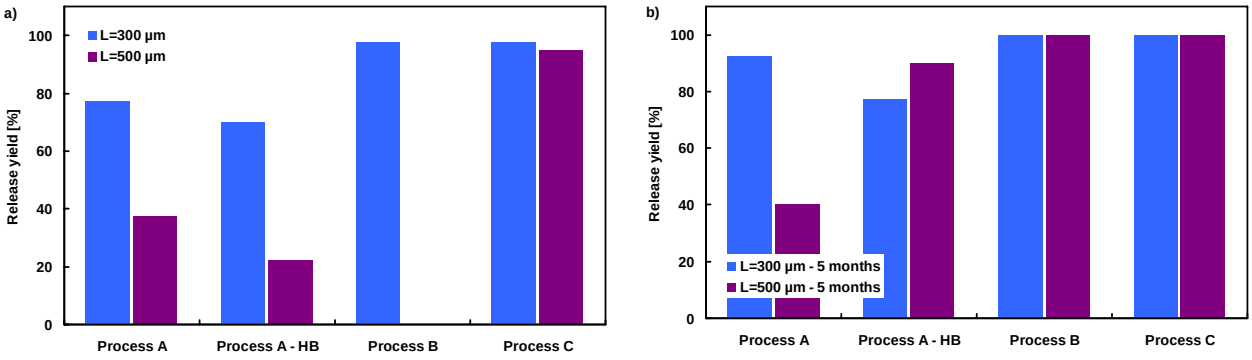

Figure 5.7-2: Release yield for the different processes directly after processing and 5 months later

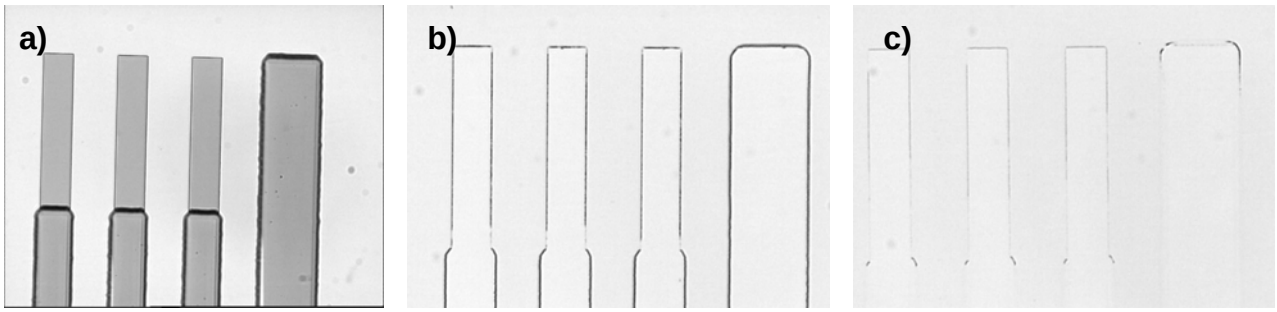

Figure 5.7-3: Optical images of fluorocarbon substrates before (a) and after release of cantilevers fabricated with (a) Process A and (c) Process B; SU-8 residues are visible

5.7.3 Cantilever bending

Finally, the bending of the cantilevers was compared. *Figure 5.7-4* and *Figure 5.7-5* show that the optimized *Process C* results in very straight cantilevers compared to the other processes. For Process A, the curvature of the cantilevers was reduced by an additional hard-bake similar to the results described in *Section 5.5* for *Process B*. There, plastic deformation of the cantilevers during the release was the main factor influencing the cantilever bending. For the measurements after 5 months of storage the results are similar, the cantilever bending is smallest for the devices fabricated with *Process C*.

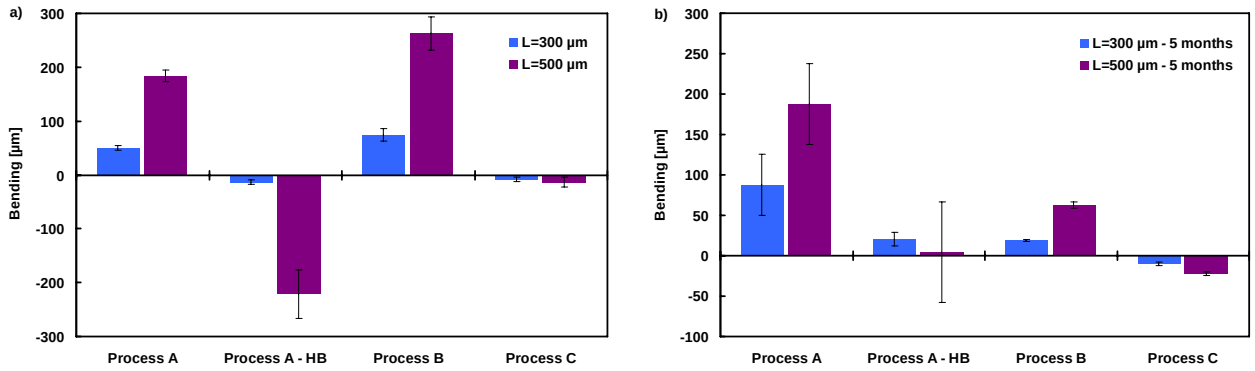

Figure 5.7-4: Comparison of the cantilever bending for the different processes directly after processing (a) and after 5 months of storage (b)

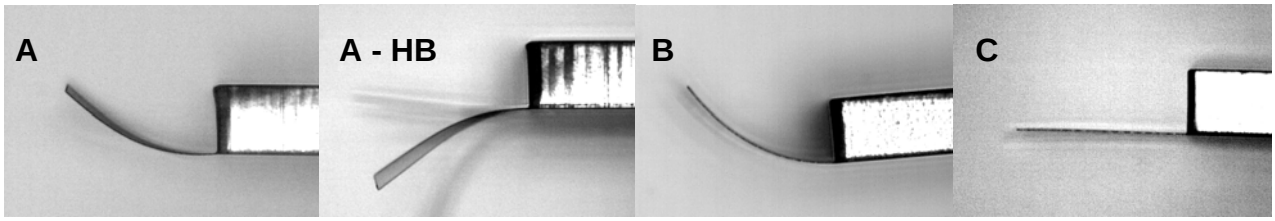

Figure 5.7-5: Bending profile directly after fabrication; L = 500 µm

5.7.4 Conclusion

Compared to conventional processing, the optimized *Process C* results in high cross-linking of the SU-8, excellent release yield and low cantilever bending. The properties proved to be stable for storage at ambient temperature for 5 months. *Figure 5.7-6* shows SEM-images of arrays of 2-µm-thick SU-8 cantilevers with a length of 500 µm fabricated with *Process C*. The initial bending of the devices is about 20 µm which is a considerable improvement compared to more than 200 µm for the non-optimized processes. Further, the results of the process optimization might be transferred for the fabrication of other devices. *Figure 5.7-7* shows 5.6-µm-thick cantilevers with a length of 500 µm fabricated with *Process C*. The only modification was an increase of the evaporation time for the thin SU-8 film from 30 min to 2 h. For these devices, the release yield is 100% and the bending is below 10 µm.

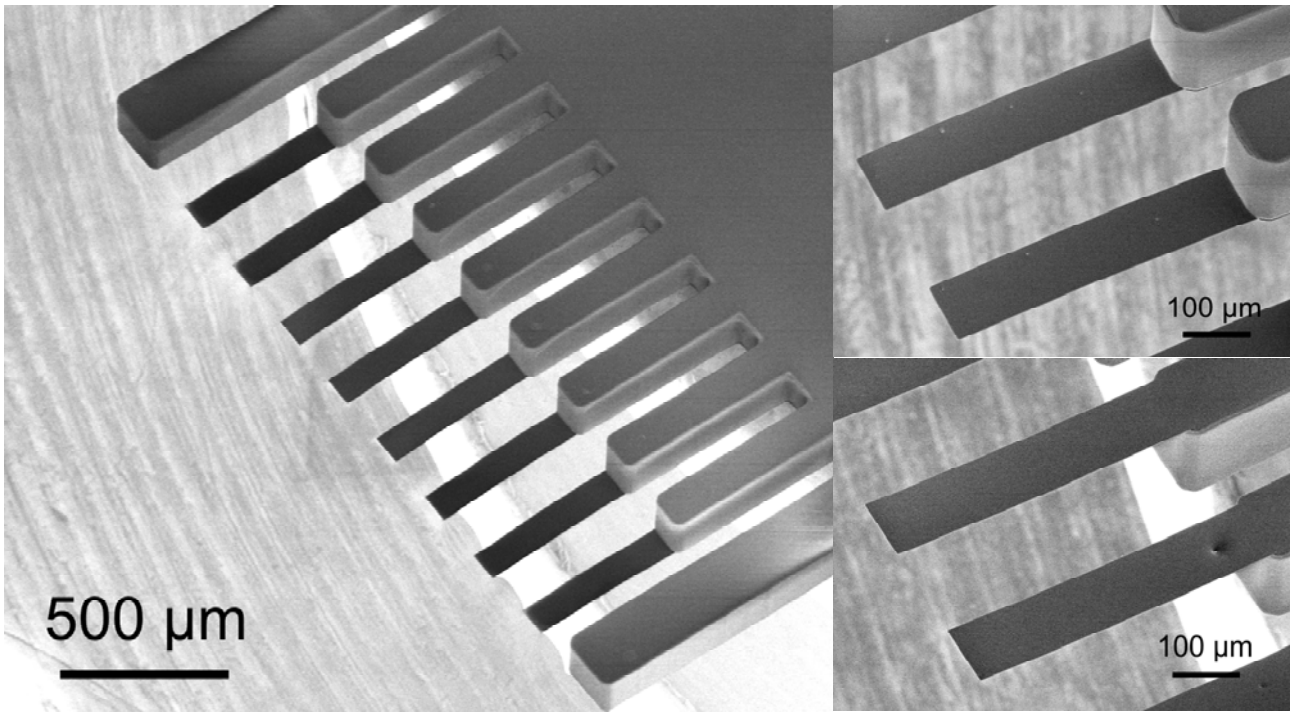

Figure 5.7-6: Array of 2-µm-thick SU-8 cantilevers fabricated with the optimized process C; L = 500 µm, w = 100 µm, pitch = 150 µm

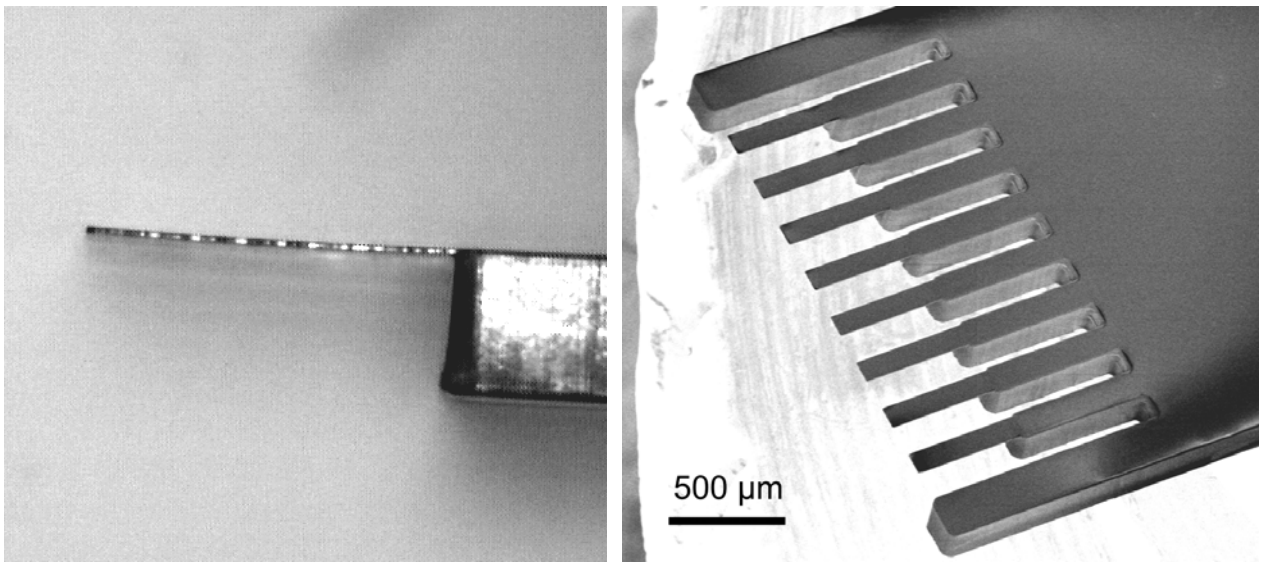

Figure 5.7-7: 5.6-µm-thick SU-8 cantilevers fabricated with the optimized process C; L = 500 µm

5.8 Influence of thick-film processing

In all the experiments presented above the process parameters for the fabrication of the thick chip body was done with *Process B*[*] described in *Table 2.6-2*. On the other hand, the processing of the second layer of SU-8 might have a direct impact on the quality of the cantilevers and on the fabrication yield. The fabrication of the chip body implies additional steps of temperature processing and exposure to UV-light which might modify the properties of the thin SU-8 film.

In this section, the influence of the processing parameters of the thick SU-8 film on the fabrication of the SU-8 cantilevers is discussed. For all the experiments, the temperature for the soft-bake and the PEB was always identical and a bake temperature T_B was defined. The bake temperature, exposure dose and the length of the soft-bake were varied. The discussion in the following sections will focus on T_B because this parameter was identified as the most important one influencing the fabrication of the thin SU-8 cantilevers.

5.8.1 Residual stress in the thin SU-8 film

The same methods as described in *Section 4.2* were used to demonstrate changes of the residual stress in the thin SU-8 film as a result of further temperature cycling during the processing of the second SU-8 layer. 2-µm-thick SU-8 films were fabricated with *Process C* defined in *Table 4.6-2*. For the exposure no mask was used and the hard-bake was done at T_{HB} = 120˚C. For comparison, a sample without hard-bake was prepared. The second layer of SU-8 was spin-coated on top of the first one to simulate the real situation for the cantilever layer. The film was not exposed to UV-light but soft-bake, post-exposure-bake and development were done according to *Process B**. The bake temperature was varied T_B = 40-80˚C.
Figure 5.8-1 shows the measurements of the residual stress in the thin SU-8 film after the different processing steps. The value measured after the development of the SU-8 (first layer) compares well to the one presented in *Table 4.6-3* for the same process. The bake at high temperature results in a very reproducible increase of thermal stress. The residual stress in the thin SU-8 film decreases for all the samples during processing of the second layer. This is probably explained by physical ageing of the SU-8 as discussed in *Section 2.5.4*. After the hard-bake, the SU-8 is cooled-down very fast and the polymer is in a structural non-equilibrium. Stress relaxation is expected to be very slow at room temperature [113]. The temperature cycling during the processing of the thick SU-8 might accelerate the annealing of the thin film and the approach of the equilibrium. In principle, this effect is expected to be higher at higher T_B but this is not directly confirmed by the measurements. In conclusion, the processing of the second layer has an influence on the residual stress of the first layer. Further ageing of the hard-baked samples during storage for 4 months at ambient temperature was not detected. On the other hand, the sample processed without hard-bake shows a huge increase of residual stress with time. This is attributed to further cross-linking of the SU-8 during storage which demonstrates the improvement of time-stability with the introduction of the hard-bake step.

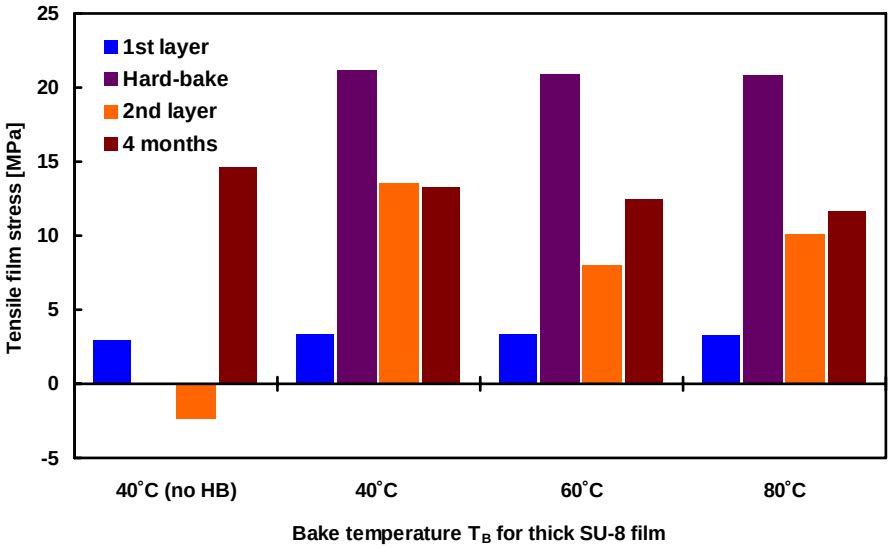

Figure 5.8-1: Residual stress in the thin SU-8 film after different processing steps

5.8.2 Replication of mask pattern

For the evaluation of the release yield and the cantilever bending, SU-8 cantilevers were fabricated with the same parameters as described in the previous section but using the two photolithographic masks. Although the film thickness is 100x higher than for the cantilever layer, it is expected that the behaviour of the resist as a function of the processing parameters is similar. *Figure 5.8-2* shows for example that the width of the thick SU-8 chip body was larger for processing at higher temperature T_B due to diffusion of photo-acid. Further, the measurements on *Figure 5.8-3* demonstrate that the gap between the cantilevers was reduced if a higher exposure dose was used. In principle, bad replication of the mask pattern for the thick layer has no influence on the functionality of the cantilevers. On the other hand, the formation of finger-like structures at the cantilever base and on the substrate was observed (*Figure 5.8-4*) which might influence the release of the devices and the bending of the cantilevers.

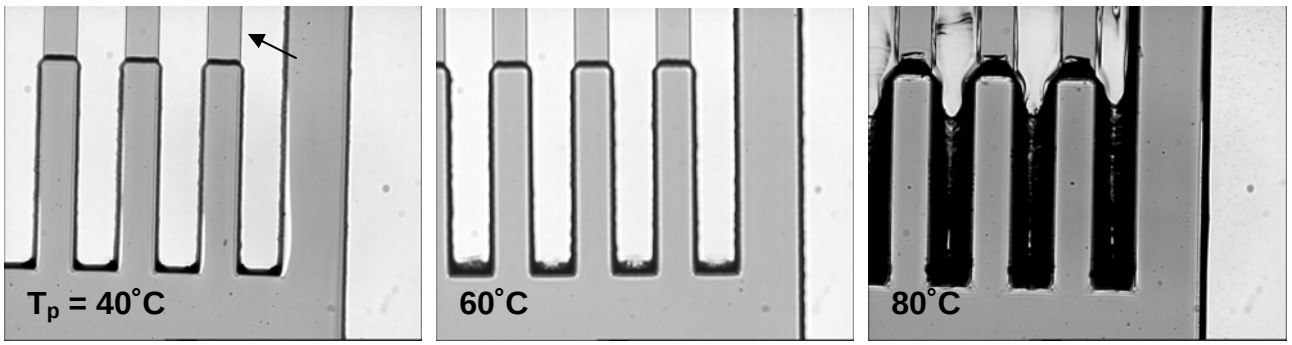

Figure 5.8-2: Top-view of the thick SU-8 processed at different T_B with the cantilevers (arrow)

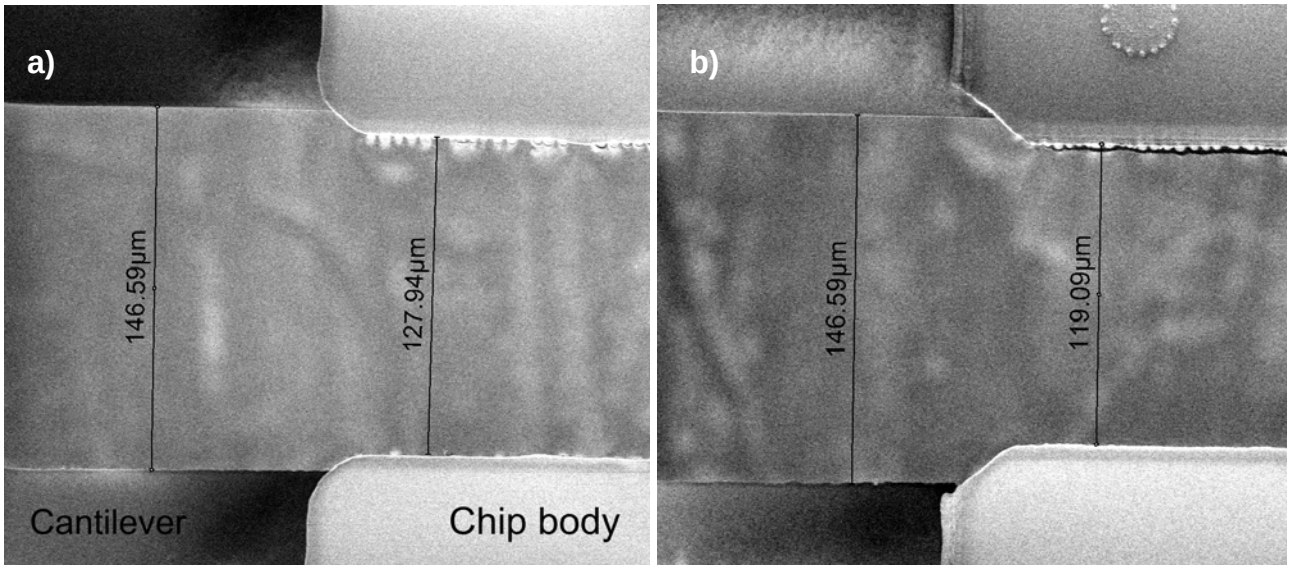

Figure 5.8-3: SEM-topview of the gap between two cantilevers; nominal width = 150 µm; the exposure dose for the thick film was varied: (a) D = 900 mJ/cm^2; (b) D = 1800 mJ/cm^2; T_B = 50˚C

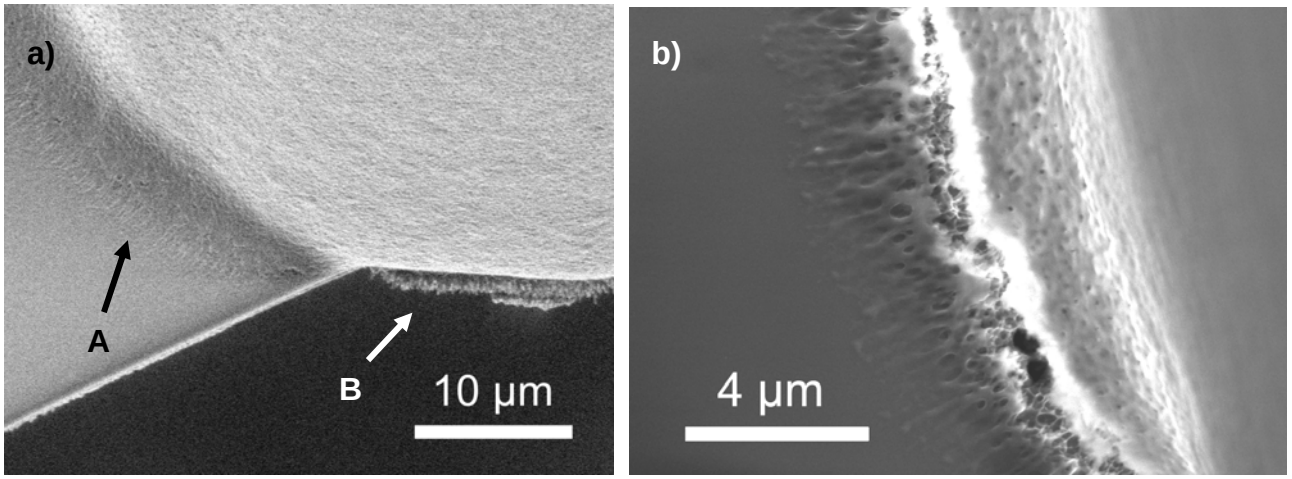

Figure 5.8-4: (a) The second layer shows finger-like diffusion patterns onto the first layer (A) and onto the fluorocarbon substrate (B); (b) close-up view of (A)

5.8.3 Shrinkage of the chip body

In *Chapter 2* it was discussed that the SU-8 shrinks during soft-bake and during PEB due to solvent evaporation and cross-linking. The experiments in *Section 5.5.5* showed that the shrinkage of the thick SU-8 film had an important effect on the cantilever bending for released chips. For non-released devices, delamination of the cantilevers from the fluorocarbon due to contraction of the thick SU-8 was observed. Limited delamination due to shrinkage of the thick SU-8 might be beneficial for the release of the cantilevers. The contraction of the chip body probably explains the increase of the release yield with storage time. On the other hand, it can result in cracking at the cantilever base (*Figure 5.8-5*) or in plastic deformation (*Figure 5.8-6*) depending on the mechanical stability of the thin SU-8 film.
It is assumed that the shrinkage of the chip body is influenced by the processing parameters for the thick SU-8 film. Higher exposure dose seemed to result in less delamination. This is probably related to faster stabilization of the polymer network during the PEB and reduced shrinkage of the chip body. Therefore, a relatively high exposure dose is used for the patterning of the thick SU-8 compared to the one recommended by the producer [76].

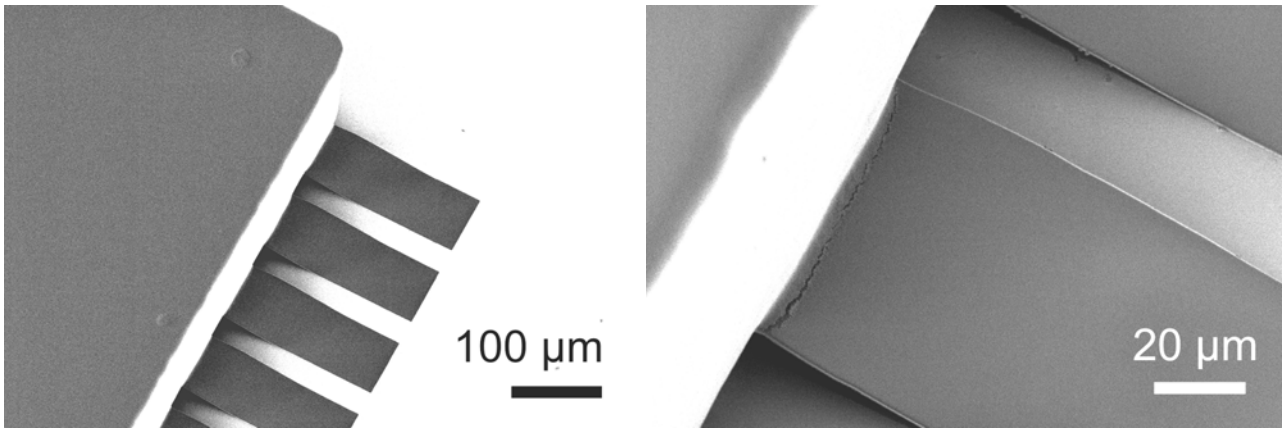

Figure 5.8-5: Lift-off and crack formation at the cantilever base due to contraction of the chip body

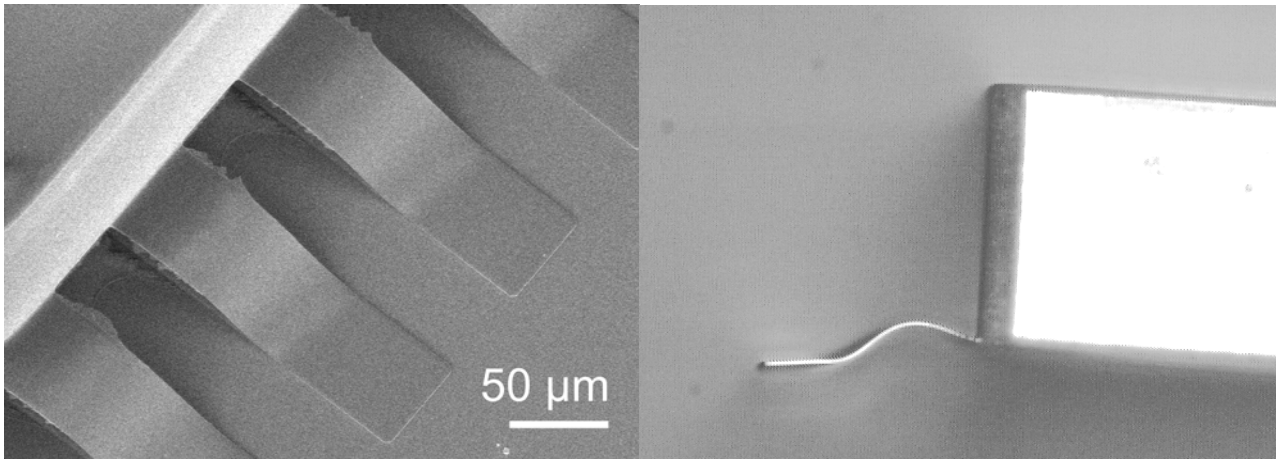

Figure 5.8-6: Plastic deformation of the cantilevers due to contraction of the chip body

5.8.4 Release of the cantilevers

Figure 5.8-7(a) shows that the release yield was lower if the soft-bake and the post-exposure-bake of the thick SU-8 film were done at high T_B. *Figure 5.8-8* presents optical images of fluorocarbon substrates before and after the release of the cantilevers. For T_B = 40˚C, it was barely possible to identify the place where the chips were situated (*Figure 5.8-8(b)*). For T_B = 80˚C, a lot of SU-8 residues were left on the substrate defining the outline of the cantilevers and the chip body (*Figure 5.8-8(c)*).
The processing of the second layer results in the formation of diffusion patterns at the edges of the chip body (*Figure 5.8-4*). Further, thick SU-8 seems to cross-link at the edge of the thin SU-8 film even in areas where it was not exposed to UV-light. Probably, diffusion of photo-acid from the first layer is responsible for this polymerization. Both effects are larger for processing at higher T_B. The SU-8 residues are responsible for the decrease in release yield similar to the diffusion patterns in the thin SU-8 film observed in *Section 5.3*. Due to the same reason, an increase of the exposure dose resulted in a slight decrease of the release yield. Further, traces on the substrate in *Figure 5.8-8(b)* indicate chemical reaction of the SU-8 solvent with the fluorocarbon at T_B = 80˚C.
After 4 months of storage (*Figure 5.8-7(b)*), the release yield approaches 100% for most of the samples except for the one processed at T_B = 80˚C. This is in agreement with previous observations.

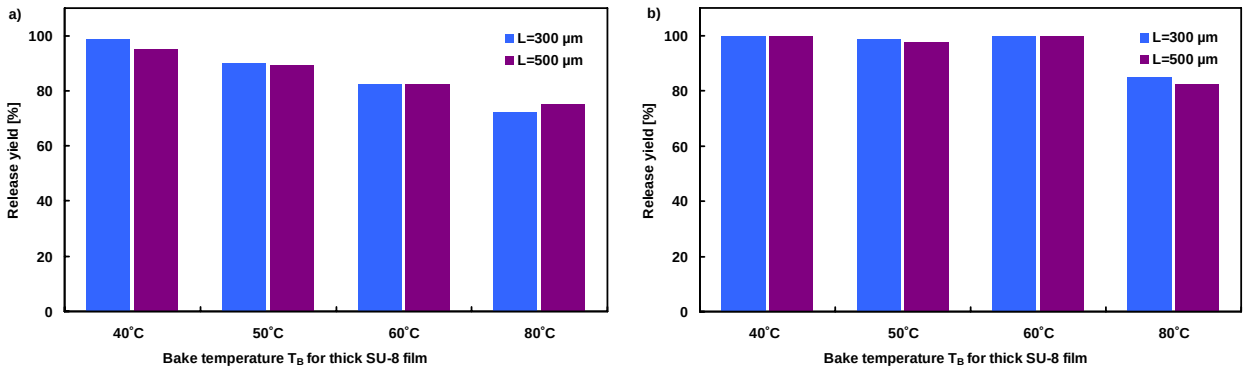

Figure 5.8-7: Release yield directly after processing and 4 months later for cantilevers fabricated with variable process conditions for the thick SU-8 film

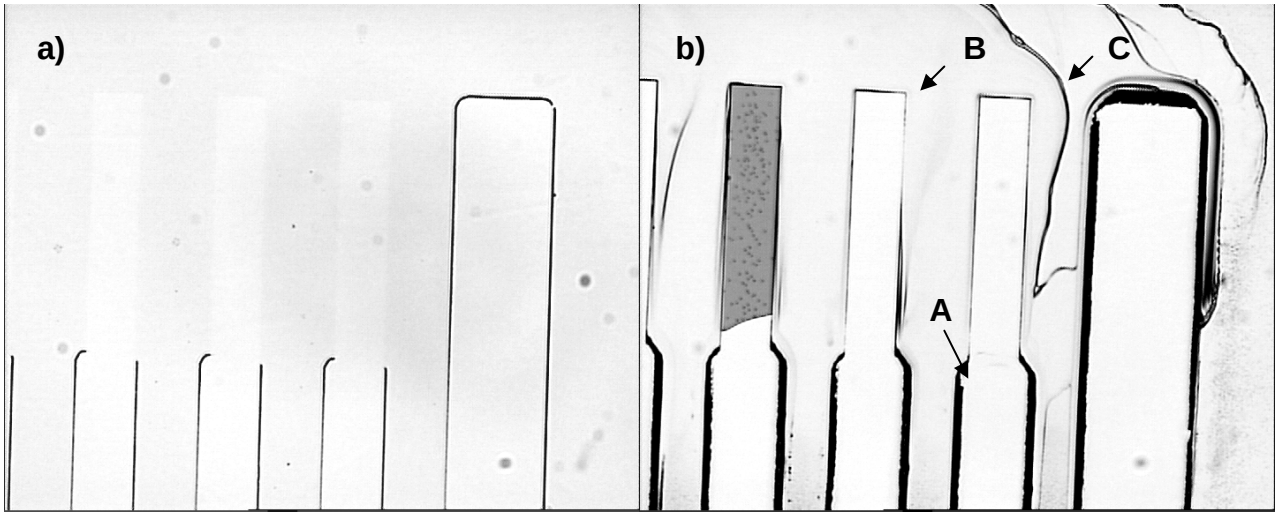

Figure 5.8-8: Optical images of fluorocarbon substrates after release of cantilevers fabricated with variable process temperature for the thick SU-8 film; (a) T_p = 40˚C; (b) T_p = 80˚C; A: Diffusion patterns of the thick SU-8 film; B: Cross-linking of thick SU-8 at the edge of the thin film; C: Traces indicating chemical reaction with the fluorocarbon

5.8.5 Cantilever bending

Figure 5.8-9 summarizes the results on cantilever bending for samples where the thick SU-8 film was processed at different T_B. Directly after processing, the bending for the samples processed at T_B > 40˚C is affected by the mechanical release. The released devices show plastic deformation at the clamping to the chip body which is expressed by the large error bars on *Figure 5.8-9(a)*.
Figure 5.8-9(b) and *Figure 5.8-10* show the results for cantilevers released after 4 months of storage. There, an influence of the bake temperature of the thick SU-8 film on the bending of the cantilevers is observed. For T_B < 50˚C the cantilevers show a negative bending and the values become positive for T_B > 50˚C. This behaviour can be explained by the shrinkage of the thick SU-8 during processing. Higher temperature results in higher contraction of the chip body which pulls the cantilevers upwards. The best results are achieved for T_B = 50˚C. It is interesting that the optimal value for T_B seems to be identical to the optimal T_{PEB} defined for the thin SU-8 film. Particularly for the thick film there might be a relation to the glass transition temperature T_g of the non-cross-linked resist which is around 50˚C [100]. For T_B > T_g, reflow of the thick SU-8 is facilitated which enhance contraction of the resist during polymerization.

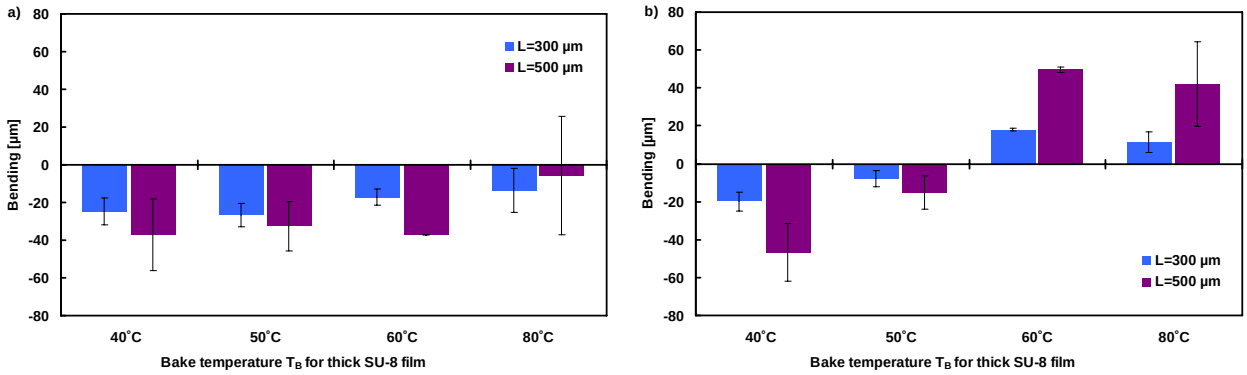

Figure 5.8-9: Cantilever bending (a) directly after processing and (b) after 4 months of storage

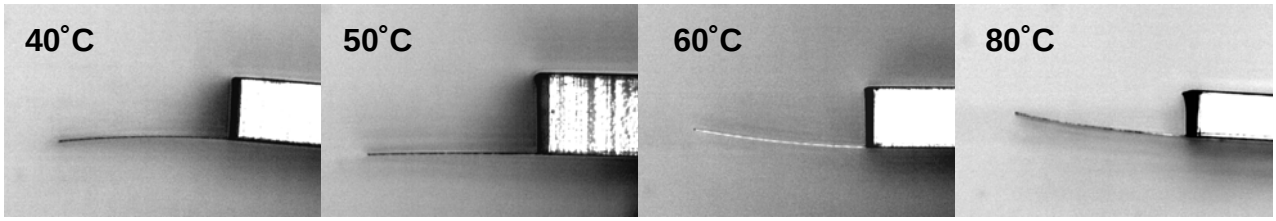

Figure 5.8-10: Bending profiles of 500-µm-long cantilevers released after 4 months of storage; the process temperature T_B of the thick film was varied from 40-80˚C

5.8.6 Conclusion

The processing of the thick SU-8 film has more influence on release yield and cantilever bending than expected. Fabrication of the SU-8 chip body results in the formation of diffusion patterns at the edges of the structures and in reaction with the fluorocarbon which affect the release of the devices. Further, contraction of the chip body might lead to the formation of cracks at the cantilever base and to cantilever bending. Both effects are minimized for processing at a temperature T_B = 50˚C. This conclusion completes the definition of an optimized process for the fabrication of SU-8 cantilevers chips with two steps of photolithography. The detailed process sequence is placed in *Appendix B*.

5.9 Conclusions

The fabrication thin SU-8 cantilevers was optimized experimentally. The cantilever bending decreased with processing at higher PEB-temperature. On the other hand, photo-acid diffusion increased with T_{PEB} and lead to a bad replication of the mask patterns and a reduced release yield. The introduction of a long hard-bake in an oven at high temperature after development of the SU-8 solved these issues. The additional bake step resulted in improved cross-linking and in a reduced bending of the cantilevers due to the removal of residual stress gradients in the thin SU-8 film. Further, solvent residues in the resist are removed. A hard-bake temperature of 90-120˚C proved to be optimal. At higher temperatures the SU-8 started to react with the fluorocarbon release coating which affected the release yield for the devices. There, the limitations of the selected release method are shown. Slight stiction of the polymer to the substrate already resulted in plastic deformation of the thin cantilevers. Change of the properties during storage of non-released devices was investigated in detail. In general, the release yield improved during storage. Further, high cross-linking was essential for a low change of the properties with time. Therefore, the optimized process with hard-bake proved to be very stable.
The temperature cycling during the fabrication of the SU-8 chip body had an influence on the release and the bending of the cantilevers. The results demonstrate that addition or change of consecutive process steps in principle requires further process optimization. This can be very time-consuming and is definitively a disadvantage for processing with SU-8 compared to traditional materials in microfabrication.
Nevertheless, the reproducible fabrication of arrays with 2-µm-thick cantilevers with a length of 500 µm with an initial bending of only 20 µm was possible with the optimized process. Following *Equation 1.1-1*, these devices are theoretically as sensitive for the measurement of surface stress changes as silicon cantilevers with a thickness of 300 nm.

6 Surface stress measurements with optical readout

6.1 NOSE-setup and IBM-chips

The group of Prof. Güntherodt and Dr. Gerber at the University of Basel (Switzerland) was one of the pioneering groups using microcantilevers for the measurement of surface stress [11, 25, 29]. They developed the so-called Nanotechnology Olfactory Sensors (NOSE) system that allows the parallel optical readout on an array of eight cantilevers [22, 23, 141]. There, vertical cavity surface emitting lasers (VCSELs) are aligned to the apex of the cantilevers and the beam deflections are measured with a linear position-sensitive detector (PSD) as shown in *Figure 6.1-1*. The researchers in Basel use commercially available cantilever chips from IBM (Rüschlikon, Switzerland). The cantilevers are fabricated in silicon and have length of 500 µm, a width of 100 µm and a thickness of 600 nm to 12 µm depending on the application. Due to the characteristic sensor design these cantilever arrays will be called "IBM-chips". The NOSE-setup has an integrated microfluidic system with a liquid chamber with dimensions adapted to the ones of the IBM-chips.

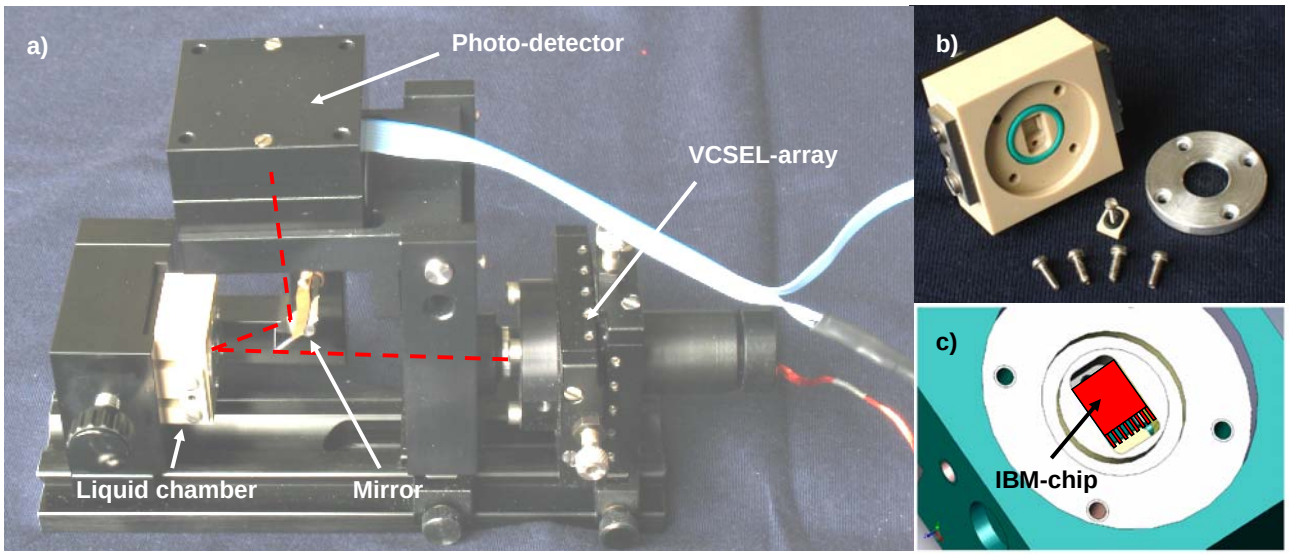

Figure 6.1-1: (a) NOSE-setup with optical read-out and integrated liquid handling system; (b)-(c) IBM-chips are clamped in a micromachined cavity of the liquid chamber [142]

Recently, the Nanoprobes group achieved a NOSE-setup for the measurement of surface stress in liquid. One of the goals is the fabrication of IBM-chips using SU-8. Ransley and co-authors have used SU-8 to fabricate chips for the same setup but their devices were quite bulky with a thickness of more than 10.8 µm [44]. The main challenges for the fabrication of the IBM-chips with SU-8 include:

- The cantilever thickness has to be $t \leq 5$ µm to achieve a sensitivity of the sensors comparable to the original IBM-chips
- Optical readout of the cantilever bending requires high intensity of the laser light reflected from the polymer surface
- The possibilities of alignment of the VCSELs to the cantilever tips are limited and therefore there should be no initial bending of the cantilever
- Surface functionalization of the polymer cantilevers

The NOSE-setup allows for direct comparison of the devices with the original cantilever chips fabricated by IBM in terms of sensitivity, reproducibility and selectivity for the measurement of surface stress.

6.2 Design of the IBM-chips

The design of the devices is adapted to the NOSE-setup and the dimensions are in principle identical to the ones of the original IBM chips [11]. The masks for a first generation of IBM-chips were designed by Daniel Eils and Maria Nordström in June 2007. Based on the experiences with these chips, the design of the IBM-chips was slightly modified in February 2008. The design of the second generation of the devices is illustrated in *Figure 6.2-1*.
Three layers of SU-8 are used for the fabrication of the IBM-chips. The cantilevers are defined in a 5.6-µm-thick film of SU-8. On each chip an array of eight cantilevers with a width w = 100 µm and a pitch of 250 µm is placed. The number of cantilevers and the spacing are given by the array of VCSEL's for the optical readout. The cantilever length was varied in the range of L = 100-500 µm.
Two thick layers of SU-8 are used for the definition of the chip body required for the handling of the cantilevers. The two SU-8 films have a thickness of 30 µm and 500 µm respectively and the final dimension of the chip is 2.5 x 3.75 mm^2. The high thickness of the chip body was required for the clamping of the chips in the NOSE-setup. *Figure 6.2-1* highlights some design features of the chip body which will be briefly discussed in the following:

- Cantilever clamping: In *Chapter 5*, mechanical release of thin SU-8 cantilevers often resulted in plastic deformation at the clamping point of the cantilevers (*Figure 5.5-4*). Initial experiments showed that a two-step process for the fabrication of the chip body improves the fabrication yield for arrays of thin SU-8 cantilevers. The main purpose of the intermediate SU-8 layer is the mechanical stabilization of the cantilever base. Further, the alignment of this SU-8 layer to the thin cantilever layer during patterning is more accurate than for the 500-µm-thick SU-8 film. This allows a more precise definition of the actual length of the cantilevers
- Sidebars: To protect the cantilevers during release and handling of the chips, a bar with a width of 175 µm is placed on each side of the cantilever array
- Tweezer spacings: On each side of the chip body a u-shaped spacing with a width of 1.2 mm was placed to allow for handling of the chip with a tweezer
- Stress release holes: Holes with a diameter of 200 µm were patterned in the bulky third layer to minimize the contraction of the chip body and to release stress
- Compensation for diffusion: The formation of diffusion patterns at the edges of the thick SU-8 chip body resulted in a decrease of the release yield for cantilever chips fabricated in *Chapter 5*. Therefore, the size of the original mask pattern for the chip body was reduced to compensate for this broadening of the resist

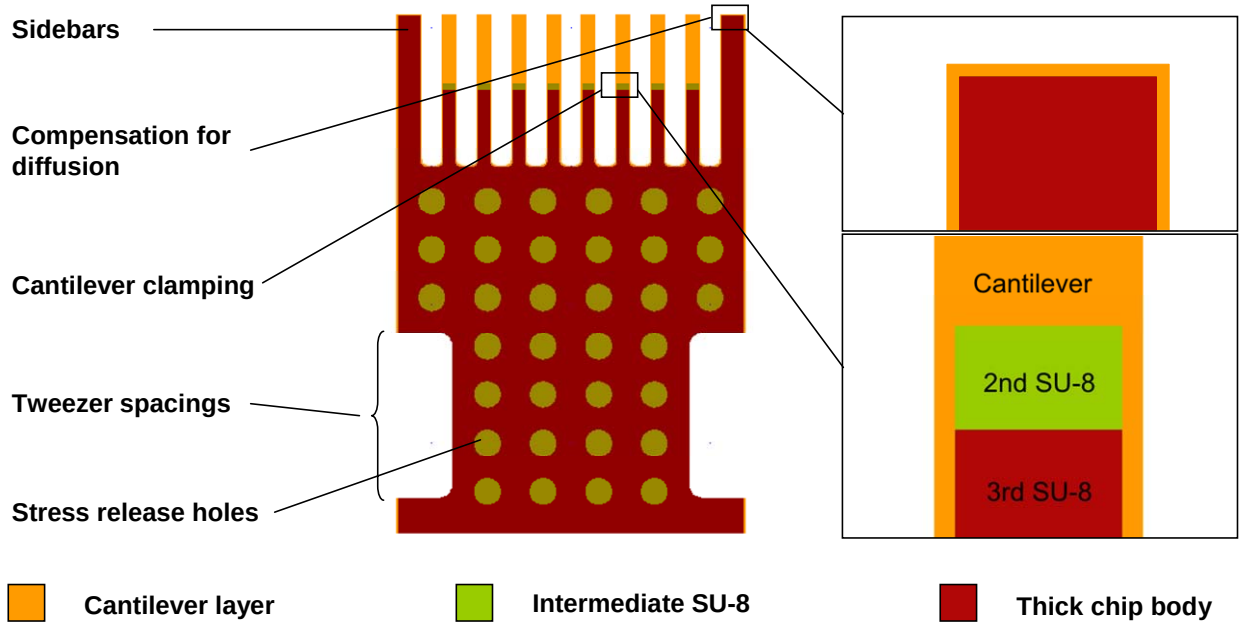

Figure 6.2-1: Design of the IBM-chip fabricated with three layers of SU-8

6.3 Fabrication of the IBM-chips with SU-8

The fabrication of the IBM-chips follows the scheme illustrated in *Figure 3.1-1*. The optimized process sequence for the fabrication of 2-µm-thick SU-8 cantilevers developed in *Chapter 5* (see *Appendix B*) was slightly modified. The thickness of the SU-8 film defining the cantilevers was increased to 5.6 µm. The hard-bake of the thin SU-8 was done at T_{HB} = 120˚C to ensure high cross-linking and reduce residual solvent content. Further, an additional step of SU-8 photolithography was introduced after patterning of the thin cantilever layer. Finally, the spin-coating of the third layer of SU-8 was done in two steps to achieve the required thickness of 500 µm. The detailed process sequence for the fabrication of the IBM-chips is described in *Appendix C*.

6.3.1 Fabrication results and discussion

Figure 6.3-1 shows the SU-8 IBM-chip with the design described in *Figure 6.2-1*. The fabrication yield for the IBM-chips with 5.6-µm-thick cantilevers is 100% and plastic deformation of the cantilevers is rarely observed. *Figure 6.3-1(c)* presents an alternative chip design with a complete protection bar surrounding the cantilever array. This design proved to be particularly practical for the release and the handling of the cantilevers. For the optical evaluation of the cantilever bending, chips without the sidebars were included in the mask design. The cantilevers with a length of 500 µm are bending 76±3 µm downwards (*Figure 6.3-2(a)*) which is more than twice as much as the value obtained in *Section 5.5.3* for 2-µm-thick cantilevers processed with a hard-bake at the same temperature. The results demonstrate some of the challenges of the processing with SU-8. The use of process recipes for the fabrication of cantilevers with other thicknesses is not possible without a certain readjustment of the parameters.

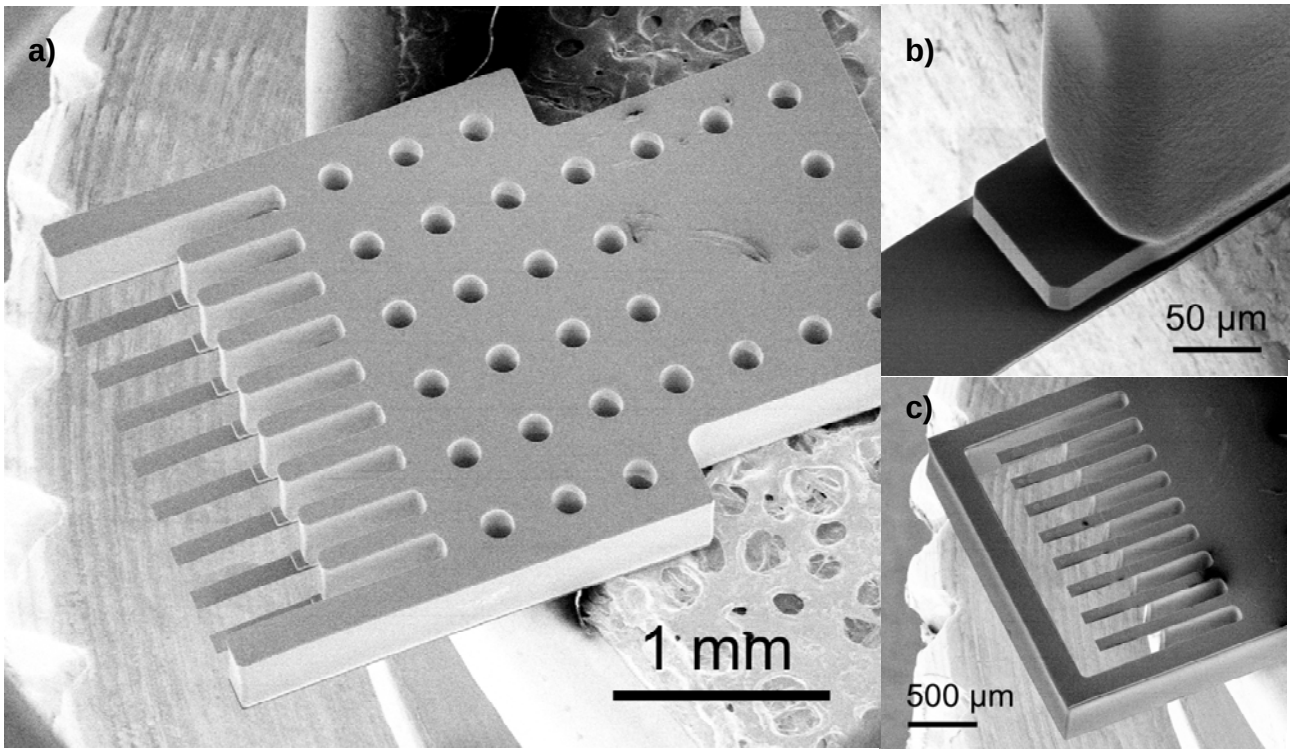

Figure 6.3-1: (a) IBM-chip with an array of eight cantilevers; length = 500 µm; (b) close-up view of the clamping point with the intermediate SU-8 layer; (c) design with complete protection bar

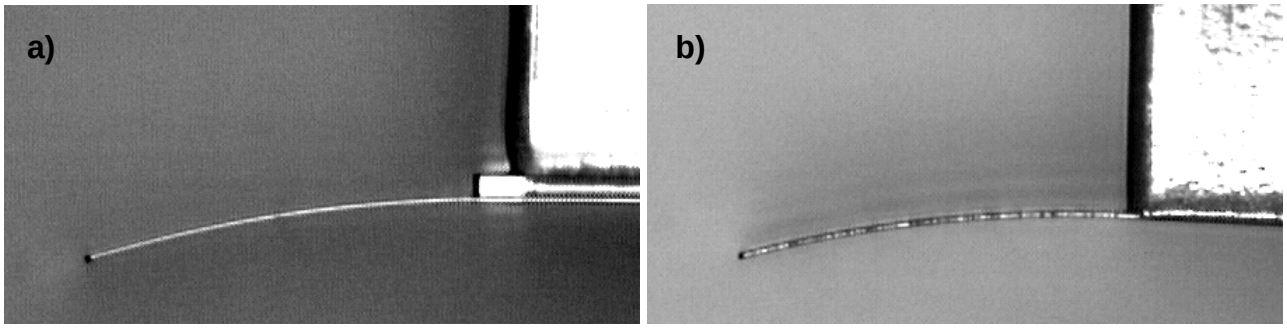

Figure 6.3-2: Comparison of the bending of 500-µm-long cantilevers fabricated with three (a) and two (b) layers of SU-8

In *Section 5.8*, the influence of the processing of the thick SU-8 film on the cantilever bending was demonstrated. It was concluded that the introduction of additional processing steps with temperature cycling is critical as it can accelerate physical ageing of the film or promote further polymerization. Compared to the cantilever chips fabricated in *Chapter 5*, the introduction of the intermediate SU-8 layer for the IBM-chips might have an influence on the residual stress gradients in the SU-8. Therefore, IBM-chips without the intermediate layer were fabricated. *Figure 6.3-2* compares the bending of cantilevers fabricated with a two-layer and a three-layer process. For both processes the deflection of 500-µm-long cantilevers is 75 µm which probably excludes the introduction of the intermediate layer as the main reason for the high cantilever bending.
In *Figure 5.7-7* perfectly straight cantilevers with identical thickness of 5.6 µm were presented. There, a hard-bake temperature T_{HB} = 90˚C was used compared to T_{HB} = 120˚C for the IBM-chips. Apparently, the value of the hard-bake temperature has more influence on the cantilever bending if the thickness of the cantilevers is increased. Following the discussion in *Section 5.6* and the

corresponding illustration in Fig.5.6-3, higher cross-linking gradients as a result of the PEB might explain the negative bending observed in *Figure 6.3-2* after completed processing.
Figure 6.3-3 shows the cantilever bending in dependence of the storage time at ambient temperature. It is clearly observed that the bending decreases with time. This behavior could be related to different phenomena. This is probably explained with stress relaxation through creep and physical ageing as discussed in detail in *Chapter 5*.

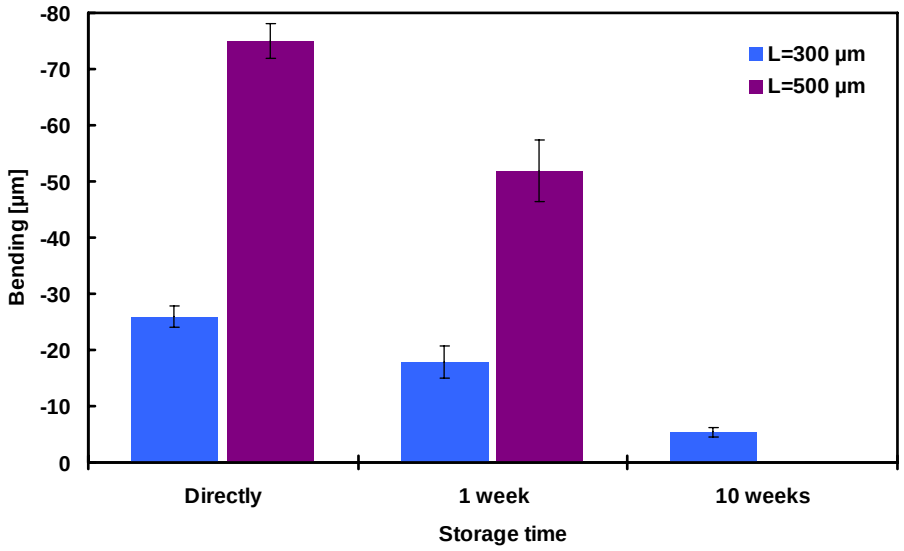

Figure 6.3-3: Bending of 5.6-µm-thick SU-8 cantilevers after different times of storage on the substrate; for L = 500 µm and storage of 10 weeks no measurement was done

6.3.2 Introduction of hard-bake after processing

Other authors have proposed that the introduction of an additional hard-bake step after completed fabrication but before the release results in SU-8 cantilevers with low bending [143]. Indeed, similar experiments showed that the bending of the cantilevers is considerably reduced after a hard-bake of the non-released devices for 2 h in the oven at 120˚C. *Figure 6.3-4* and *Figure 6.3-5* compare the bending of SU-8 cantilevers with and without the final bake step. The 300-µm-long cantilever processed without hard-bake (*Figure 6.3-4(a)*) shows a bending of 20±2 µm where the hard-baked structure (*Figure 6.3-4(b)*) is perfectly straight. Probably, the introduction of the additional temperature cycle accelerates the stress relaxation discussed in *Section 6.3.1* for the stored samples.

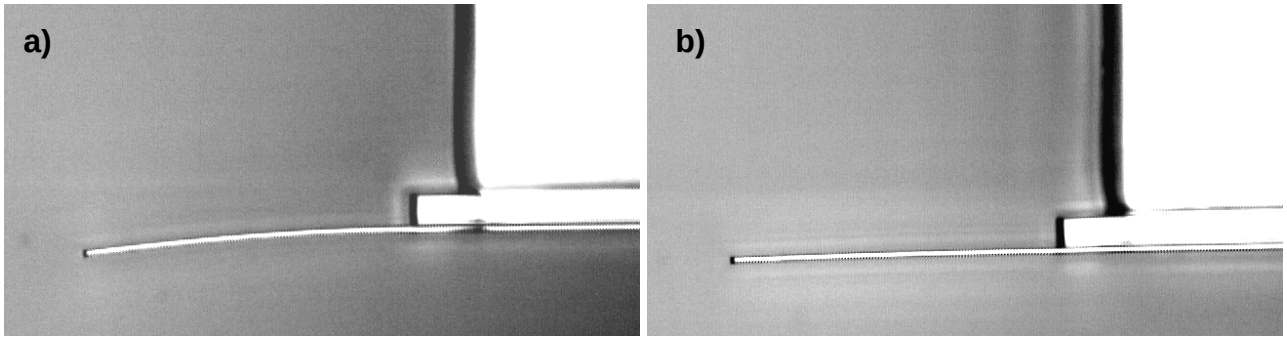

Figure 6.3-4: Cantilever bending without(a) and with (b) final hard-bake step; L = 300 µm

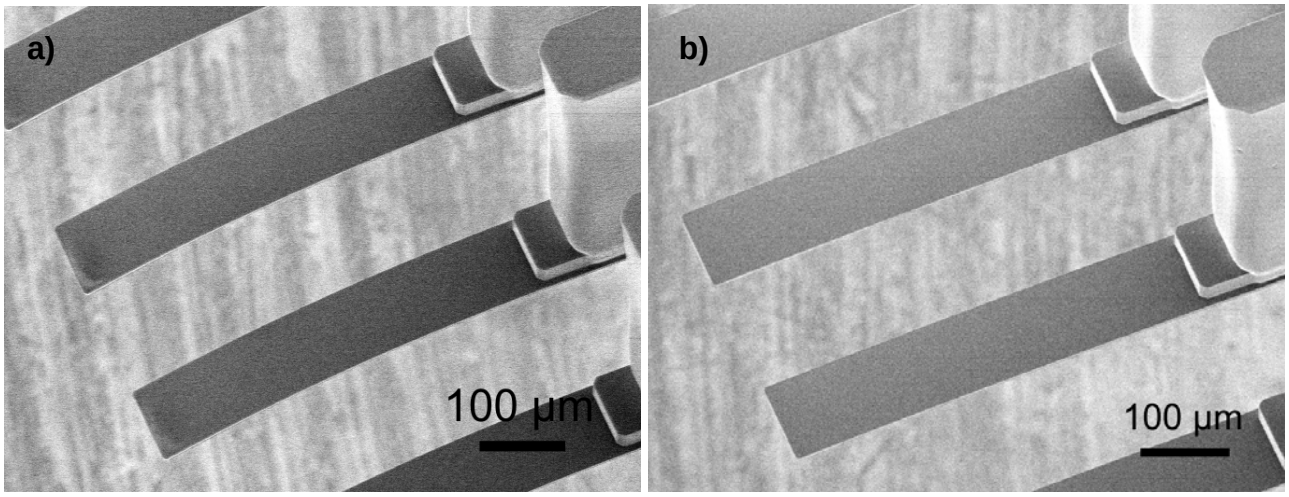

Figure 6.3-5: Cantilevers processed without (a) and with (b) final hard-bake step; L = 500 µm

6.4 Process-integrated metal coating

There are two motivations to coat the fabricated cantilever-based sensors with metal. Typically, Au coatings are used to enhance the reflection for optical-readout and to allow the surface functionalization by thiols as discussed in *Section 6.5*. In collaboration with the University of Basel, Dr. Maria Nordström from the Nanoprobes group performed some initial experiments using SU-8 IBM-chips of the first generation. It was concluded that the light reflected from the pure SU-8 surface is insufficient for optical readout of the cantilever deflection in the NOSE-setup. Au films with a thickness $t_{AU} > 30$ nm were required for measurable reflection of the laser beams from the cantilever surface.
There are two possibilities to deposit an Au layer on a cantilever-based sensor. Typically, gold is deposited on single cantilevers just before use. This provides fresh Au but the process is very time-consuming and the characteristics of the Au can vary from one chip to the other. Alternatively, Au patterning on wafer-scale can be integrated in the fabrication process. In this approach, photolithography is used for the structuring of the Au. There, the metal is exposed to various chemicals such as resist and developer that can contaminate the surface. This contamination might be difficult to remove and results in difficulties for the functionalization of the surface. In the following, two approaches of process-integrated metal coating of the IBM-chips are presented and discussed.

6.4.1 Metal coating A – Lift-off after processing of the thin SU-8 film

The traditional process-integrated approach for the coating of SU-8 cantilevers with metals such as gold is represented on *Figure 6.4-1*. The processing of the thin SU-8 film on the fluorocarbon substrate is followed by a standard step of photolithography with metal lift-off to define the metal patterns on the top-side of the cantilevers. After this step, the chip body is defined in the thick SU-8 layer.
The drawback of this approach is that the high temperature during metal deposition induces thermal stress in the thin SU-8 film. This can result in cracks in the SU-8 or bending of the cantilevers [116, 144]. *Figure 6.4-2* shows IBM-chips fabricated with the process illustrated on *Figure 6.4-1*. The complete fabrication of IBM-chips with *Metal coating A* is described in *Appendix C*. The

cantilevers are coated with 50 nm Au and 5 nm Ti serve as adhesion layer between the SU-8 and the Au. The cantilevers are bending 70-80 µm downwards. This is mainly explained by the thermal stress as it was earlier described by *Equation 2.5-2*. The SU-8 has a higher coefficient of thermal expansion (CTE) than Au and therefore contracts more during the cool-down after the deposition of the metal. Compared to the pure SU-8 cantilevers discussed in *Section 6.3.*, the addition of a final hard-bake step has no effect on the bending.
Different solutions have been proposed to avoid the bending of the cantilevers due to the thermal stress generated during the metal deposition on the SU-8 [145]. Probably, the most promising approach is to avoid a complete metal coating of the cantilever. In principle, a small reflective pad at the apex of the cantilever should be sufficient as mirror for optical readout. *Figure 6.4-3* shows SEM-images of IBM-chips with circular Au pads. The cantilevers are perfectly straight although a metal deposition step was included. Initial tests in the NOSE-setup showed that enough light is reflected from the mirror pads although the alignment of the VCSELs is more challenging for these chips. There, the surface functionalization has to be done directly on the polymer which will be discussed in *Section 6.5*.

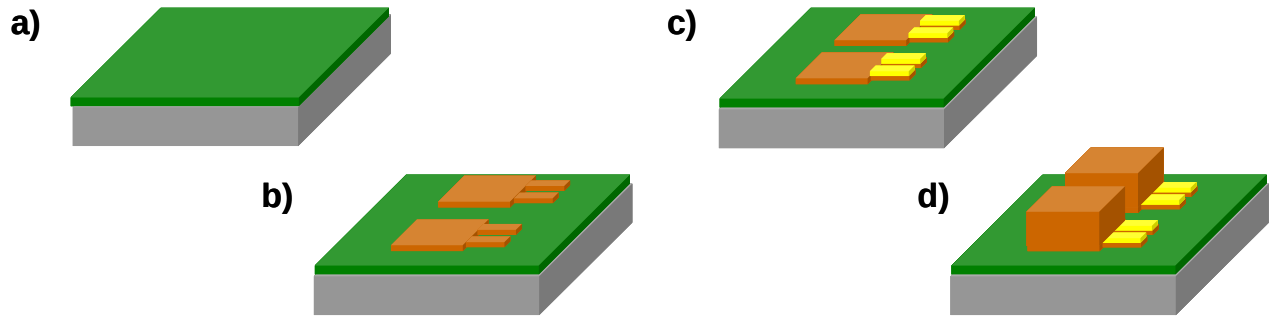

Figure 6.4-1: Metal coating A: (a) Fluorocarbon deposition; (b) Photolithography of first layer of SU-8; (c) Metal patterning by lift-off; (d) Definition of the thick SU-8 chip body

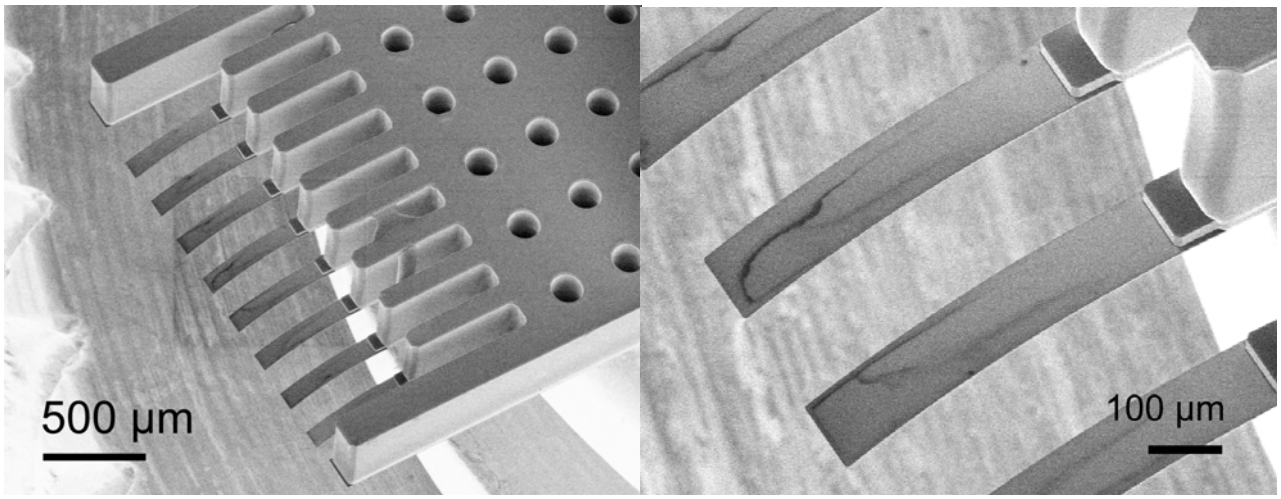

Figure 6.4-2: Array of cantilevers completely coated with 50 nm Au on the top-side; L = 500 µm

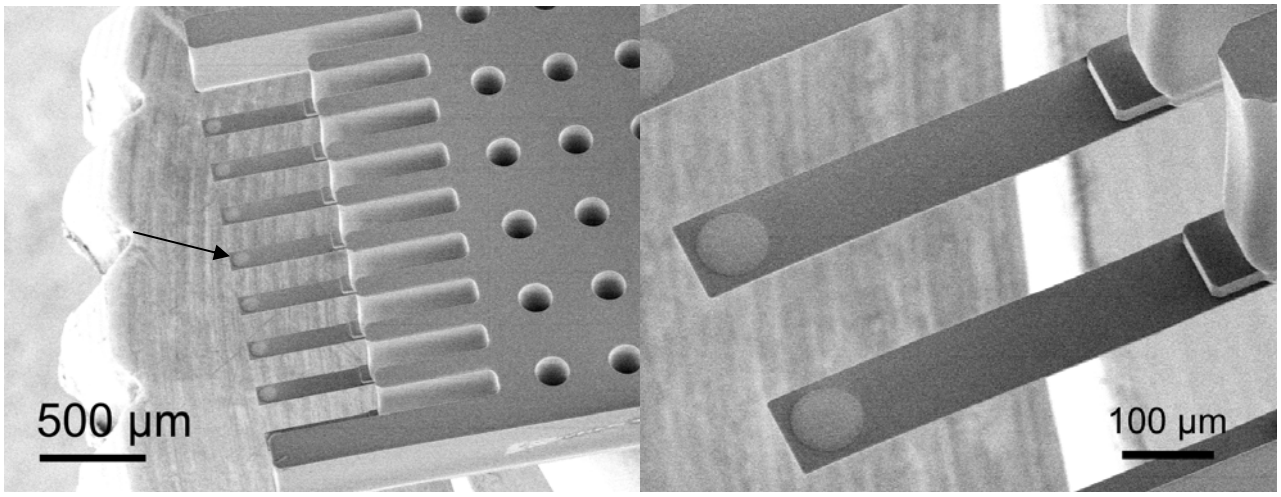

Figure 6.4-3: IBM-chip with circular Au pads at the apex of the cantilevers (arrow); L = 500 µm

6.4.2 Metal coating B – Lift-off before processing of the thin SU-8 film

Figure 6.4-4 shows an alternative approach to achieve process-integrated coating of the devices with metal. There, the step of metal patterning is done directly on the fluorocarbon. After the metal lift-off the SU-8 chip is processed as described in *Section 7.3*. Kim et al. demonstrated a similar approach for process-integrated metal coating of SU-8 using a self-assembling monolayer for the dry release [122].

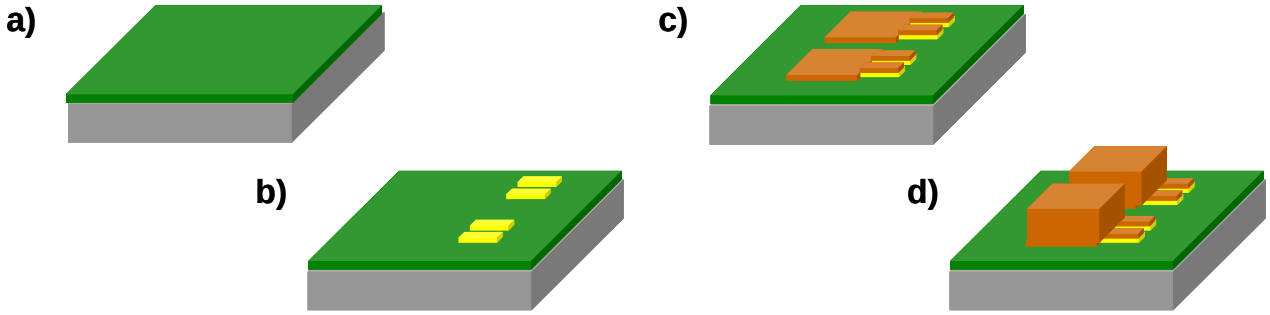

Figure 6.4-4: Metal coating B: (a) Fluorocarbon deposition; (b) Metal patterning by lift-off; (c) Photolithography of first layer of SU-8; (d) Definition of the thick SU-8 chip body

The advantage *Metal coating B* is that the thermal cycling during metal deposition has no effect on the SU-8. On the other hand, the adhesion of the metal to the fluorocarbon might be an issue. Patterning without delamination of photoresist (*Figure 6.4-5(a)*) or metal (*Figure 6.4-5(b)*) has to be possible but the adhesion should be low enough to allow for a release of the metal after completed chip fabrication. The dry release of various metals was investigated in a student project at DTU Nanotech [132]. The yield for the fabrication of metal-coated cantilevers depends on the fluorocarbon coating similar to the release of pure SU-8 devices discussed in *Chapter 3*. *Figure 6.4-6* shows IBM chips fabricated with the approach illustrated in *Figure 6.4-4*. There, 50 nm Au and 5 nm Ti were deposited on the fluorocarbon coating. The complete process sequence for the fabrication of IBM-chips with *Metal coating B* is described in *Appendix C*. The cantilevers are bending 20-25 µm which is less than for the approach presented in the previous section. Further, the

cantilevers are bending upwards which demonstrates that the bimorph effect is still an issue. As discussed above, the replacement of the complete gold coating (*Figure 6.4-6(b)*) by mirror pads at the apex of the cantilevers (*Figure 6.4-6(c)*) is a suitable solution. In this case, eventual bending of the cantilever could be removed by a hard-bake before the release as presented in *Section 6.3.2* resulting in perfectly straight cantilevers.

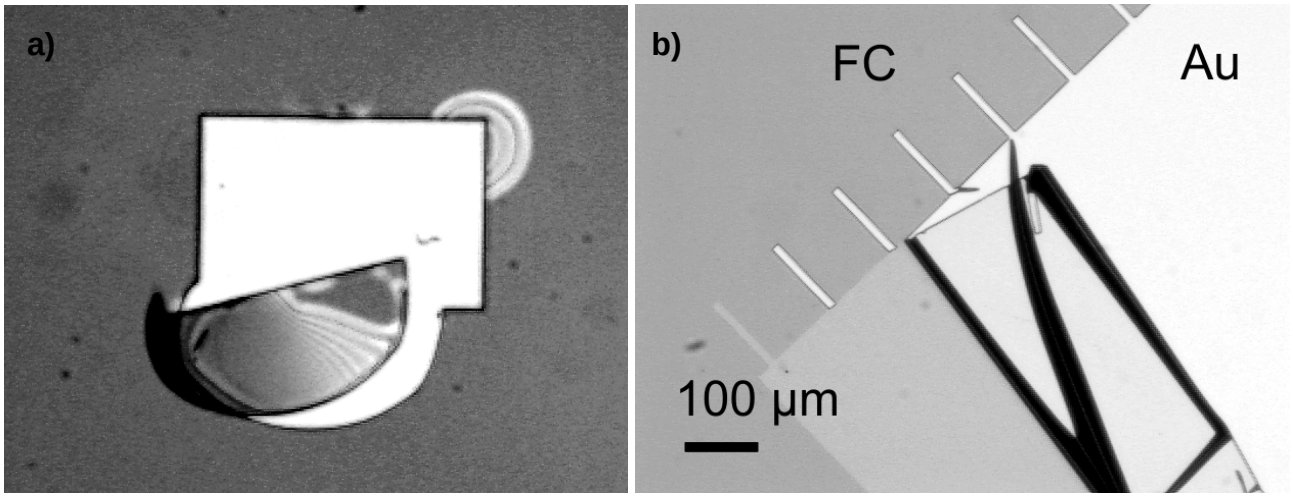

Figure 6.4-5: (a) Delamination of photoresist from the fluorocarbon; (b) Delamination of Au patterns with a thickness of 100 nm from the fluorocarbon (FC) after lift-off

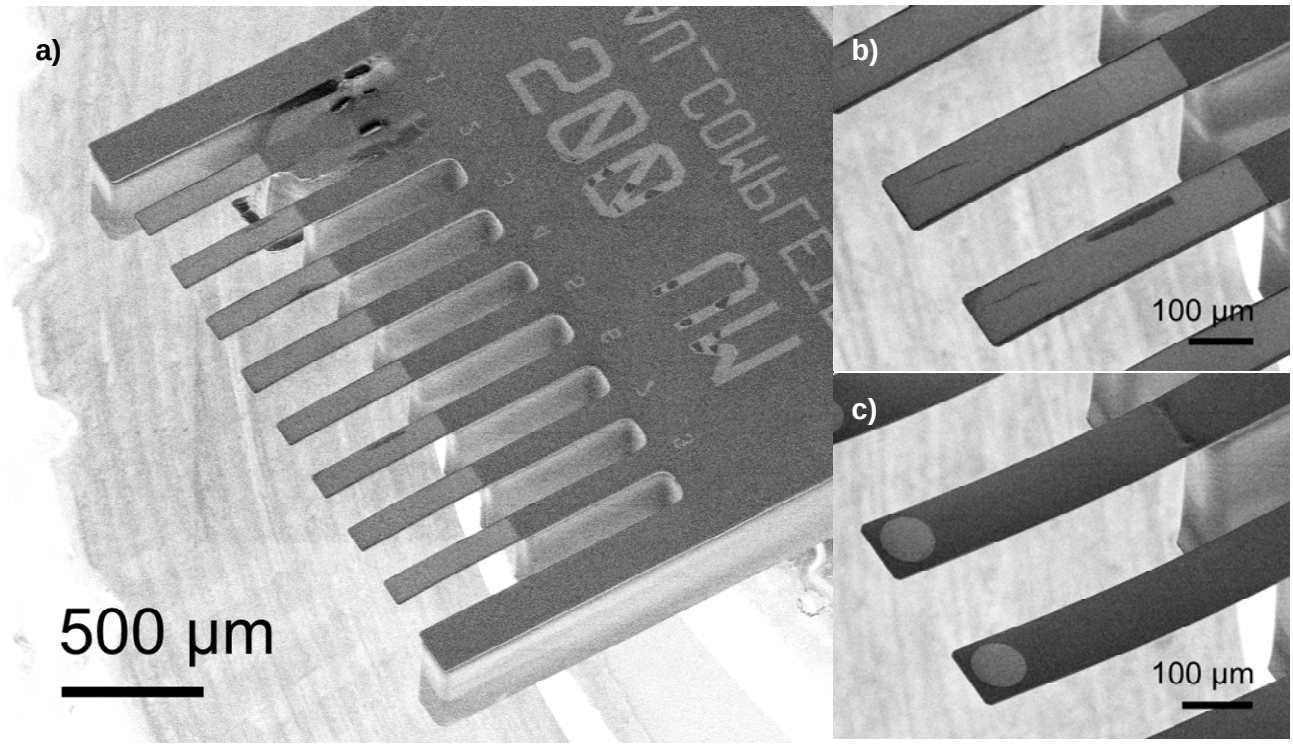

Figure 6.4-6: (a)-(b) Array of SU-8 cantilevers coated with 50 nm Au on the backside; (c) Au pads at the apex of the cantilevers

6.4.3 Metal surface contamination

The presence of contaminants on the Au surface is an issue if the metal is used as an anchor for surface functionalization by thiols, a method that is discussed in *Section 6.5*. Compared to deposition of fresh Au on single chips directly before use, the cleanliness of the metal surface might be affected by the two process-integrated approaches presented in *Section 6.4.1* and *Section 6.4.2*. Therefore, a study on the metal surface contamination was performed in collaboration with Dr. Gabriela Blagoi of the Nanoprobes group.
Direct measurement of the Au contamination on cantilevers is difficult. Therefore, contact angle measurements with water were performed on different surfaces simulating the Au coatings of the cantilevers after completed processing in the cleanroom. The following surfaces were prepared:

Au: 50 nm Au were evaporated on a Si substrate less than 30 minutes before the contact angle measurement were performed

Au-SU-8: *Metal coating A* might result in Au contamination during the definition of the SU-8 chip body (*Figure 6.4-1(d)*):

- 50 nm Au were evaporated on a Si substrate
- Spin-coating of the thick SU-8 film
- Bake for 20 h on a hotplate at 50˚C simulating the thick film processing
- Development in PGMEA and rinse with IPA

Au-FC: *Metal coating B* might result in Au contamination with fluorocarbon due to contact with the release layer during the complete chip fabrication:

- Fluorocarbon deposition with recipe wet_tef or dry_tef (*Table 3.5-1*)
- Definition of large Au patterns (2x5 cm^2) by lift-off; 50 nm Au, 5 nm Ti
- Processing of two SU-8 films with *Process B* (*Table 4.6-3*) and *Process B** (*Table 5.2-1*) using flood-exposure
- Release of complete SU-8 film from fluorocarbon resulting in a 200-µm-thick SU-8 wafer with Au patterns (*Figure 6.4-7(a)*)

Furthermore, the effect of several cleaning methods was evaluated to allow conclusions about the stability of eventual Au contamination. The cleaning of Au deposited on polymer cantilevers is particularly critical. Cleaning methods involving wet chemistry such as piranha solution or aqua regia are quite aggressive and also attack the polymer substrate itself. Oxygen plasma induces thermal stress in the polymer. The most suitable method is based on the oxidation of the organic contaminantes in UV-ozone equipment [21]. Here, the effect of 30 min of UV-ozone cleaning (PR-100 UV ozone photoreactor, UVP Inc.) was investigated. Furthermore, samples were immersed for 2 h in 10% Deconex solution followed by a rinse with MilliQ-water. Deconex 11 is a detergent that is commonly used for the cleaning of surfaces contaminated with organic compounds [146]. Measurements of the static water contact angle on a contact angle meter (DSA10, Krüss GmbH, Germany) were used to evaluate the contamination of the different Au surfaces (*Figure 6.4-7(b)*).
Figure 6.4-8 summarizes the results of the contact angle measurements on the different surfaces. The contact angle on freshly deposited gold was 76±2˚. After cleaning with the two methods, the Au contact angle significantly decreased. A considerable amount of experimental and theoretical work has been published and conclusions whether the surface of Au is hydrophilic or hydrophobic

are rather controversial. Smith states that clean Au is hydrophilic and that less than a monolayer of carbonaceous contamination results in contact angles of 50° [147]. It is concluded that the Au surface has carbonaceous contamination even if no further process steps are performed after metal deposition. The contact angle on *Metal coating A* (Au-SU-8) is identical to the one of freshly deposited Au before and after cleaning. The contamination of the Au surface during processing of the thick SU-8 seems to be minimal and can be reduced by cleaning in UV-ozone.
The two surfaces resulting from *Metal coating B* (Au-wet_tef and Au-dry_tef) are hydrophobic after release from the substrate. This indicates that both coatings are heavily contaminated with fluorocarbon residues from the release coating. The values measured on the Au coatings are identical to the ones measured in *Section 3.4* on the SU-8 backside after release from the substrate (*Figure 3.4-1*). In agreement with these results, the contact angle on Au-dry_tef is slightly higher than on Au-wet_tef. It can be concluded, that any material processed on the fluorocarbon release layer will be covered by a thin film of fluorocarbon after release. This fluorocarbon coating seems to be quite stable and was only partially removed by cleaning.

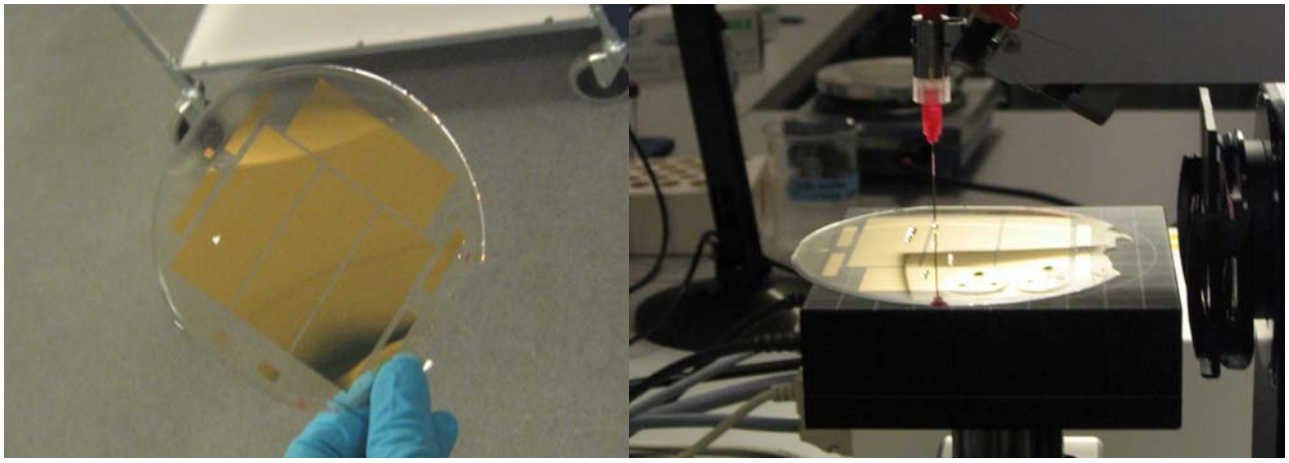

Figure 6.4-7: (a) 200-µm-thick SU-8 wafer fabricated with Metal coating B after release from the fluorocarbon; (b) The large Au patterns are used for contact angle measurements

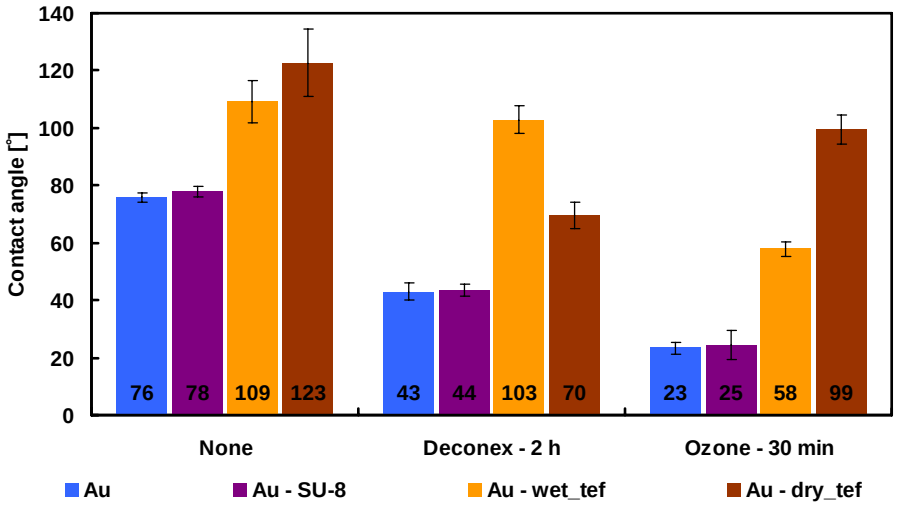

Figure 6.4-8: Measurements of water contact angle on Au coatings directly after fabrication and after cleaning with two different procedures

6.4.4 Conclusion

Two process-integrated approaches for metal coating of the IBM-cantilevers were introduced. *Metal coating B*, where the metal deposition is done before the actual processing of the SU-8, results in less bending of the coated cantilevers. The optimal solution in terms of bending for both approaches is the replacement of a complete Au coating with a reflective Au pad at the apex of the cantilever. The metal contamination due to the two processes was evaluated. *Metal coating A* is only to a minor degree contaminated after processing and should be suitable for direct surface functionalization. In case of *Metal coating B*, the Au is in direct contact with the fluorocarbon release layer during processing which results in significant surface contamination. It is expected that *Metal coating B* can only be used as a reflective layer but not for the functionalization of the surface.

6.5 Process-integrated surface functionalization

The functionality of a biosensor is defined by the receptors immobilized on the sensor surface. Therefore, the process of the immobilization of the receptor molecules to the sensor surface is called surface functionalization. The receptor layer directly affects the selectivity, reproducibility and sensitivity of the sensor. In case of the cantilevers actuated by surface stress, one wants to deposit a thin, uniform and compact layer of receptor molecules. Covalent attachment of the receptors is preferred compared to physisorption to improve the stability of the layer and to achieve a high force transduction to the cantilever. Further, it is important to ensure that the immobilization technique preserves the recognition ability of the receptor molecules [148].

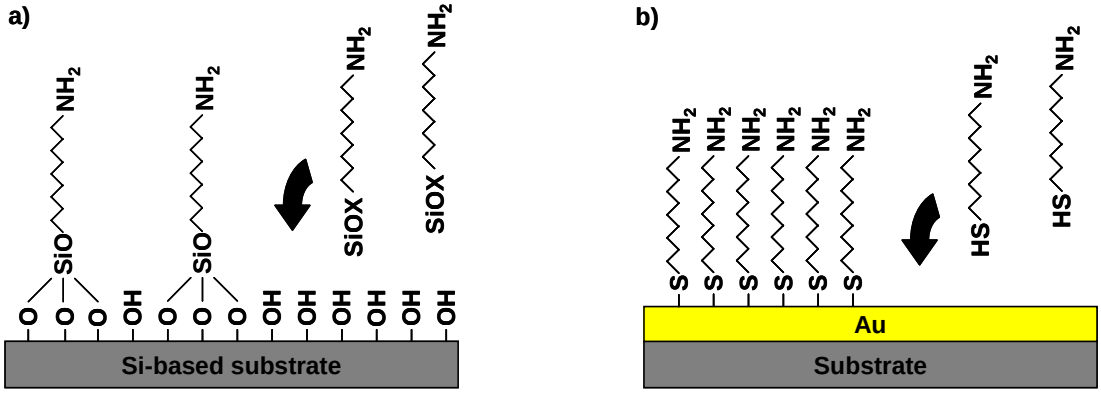

Figure 6.5-1: Surface functionalization of different substrates: (a) Silanization of surfaces with hydroxyl-groups; (b) Thiol-based immobilization on gold coating

Two methods are commonly used for the covalent attachment of molecules to the sensor surface. In both methods, self-assembly assists the formation of a uniform, densely packed and robust coating as illustrated in *Figure 6.5-1* [149]. Silicon-based substrates can be functionalized by silanization where molecules with silane (-SiOR') groups are linked to the hydroxyl (-OH) groups present on the substrate (*Figure 6.5-1(a)*) [150, 151]. The availability of OH-groups on the SU-8 is limited and therefore silanization is difficult [152]. A possible way to increase the number of reactive sites is surface activation in oxygen plasma but typically plasma treatments result in stress in the polymer due to heating processes.

Alternatively, Au surfaces are used as anchor for the immobilization of molecules with thiol (-SH) end-groups (*Figure 6.5-1(b)*) [153, 154]. Berger et al. first introduced alkanethiols on Au as a model system for the study of surface stress measurements with cantilevers [25]. In the following years, thiol-chemistry was established as the most common method for the functionalization of cantilever-based biosensors [26, 29]. In the Nanoprobes group, this method has been implemented for the measurement of surface stress with both silicon-based and SU-8 cantilevers [21, 55]. The reactivity and the morphology of the Au coating are heavily dependent on the methods and conditions used for the deposition. It was demonstrated that these characteristics have a direct influence on the measured surface stress [155]. This adds a lot of additional challenges for the Au coating of the cantilevers, in particular if the metal evaporator is not exclusively dedicated to this purpose. Some other issues related to Au coating of SU-8 cantilevers were discussed in *Section 6.4*.
Due to the limitations of the two described methods, the surface functionalization of SU-8 without the need for metal coating or surface activation was evaluated. Other authors have demonstrated UV-mediated grafting of poly(acrylic acid) and water-soluble monomers onto the SU- surface. A spatial resolution of 2 µm was achieved [156]. However, this method relies on the residual photo-acid generator of the SU-8 polymer which might be limiting for its use on fully cross-linked SU-8 films. Here, an alternative method is briefly discussed and the details are published elsewhere [157]. The approach allows chemical patterning of the SU-8 with high resolution and can be integrated in the fabrication process in the cleanroom.

6.5.1 Materials and methods

The method is based on Antraquinone (AQ) photolinkers. These molecules are highly reactive when irradiated in the UV-A range [158]. The AQ-E photolinker contains an electrophilic group that reacts with amino and thiol groups at different pH. A simplified schematic of the reaction between the antraquinone (AQ-E) derivative used the experiments and the SU-8 surface (R-H) is presented in *Figure 6.5-2*. The AQ linkers attach with the O atom to the substrate, forming a new C-O bond. Therefore, the electrophile group of the AQ photolinkers is available for further immobilization of biomolecules. AQ photolinkers with other end-groups are available which makes this approach very modular.

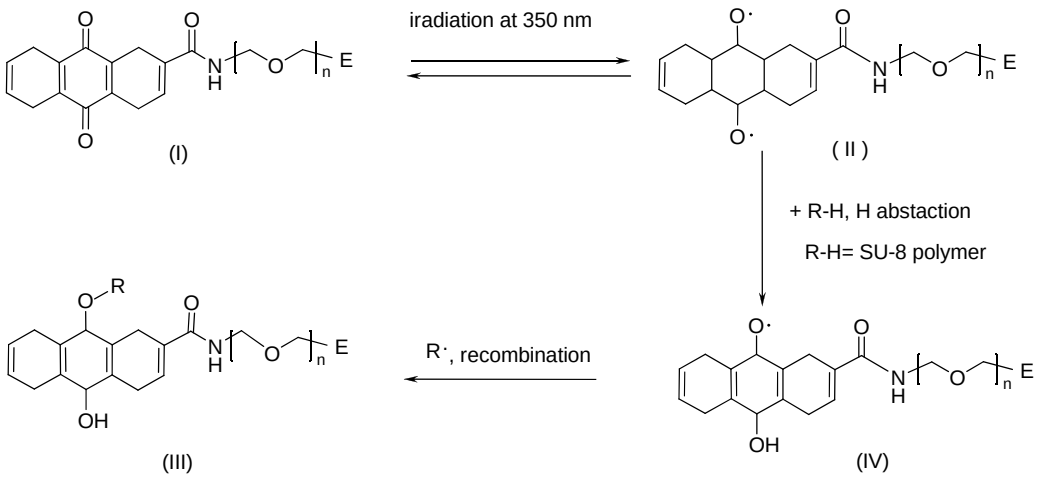

Figure 6.5-2: Simplified photoreaction between the antraquinone (AQ) based photolinker modified with electrophile group (E) and SU-8 polymer surface (R-H)

The goal was the use of a standard UV aligner for photochemical patterning of the surface. Therefore, the dry functionalization scheme illustrated in *Figure 6.5-3* was developed. First, the SU-8 surface was incubated overnight with 50 µg/ml AQ-E and dried in air. Then, the substrate is exposed using a standard photolithographic mask. After exposure for 10 min the substrate is extensively cleaned in order to remove non-specifically adsorbed AQ-E. The samples were immersed in a solution of Alexa 647-cadaverine where the free amino group of this fluorescently labelled biomolecule reacted with the grafted electrophile (E) moieties on the SU-8 surface. The resulting patterns were imaged using a fluorescent scanner or a fluorescence microscope.

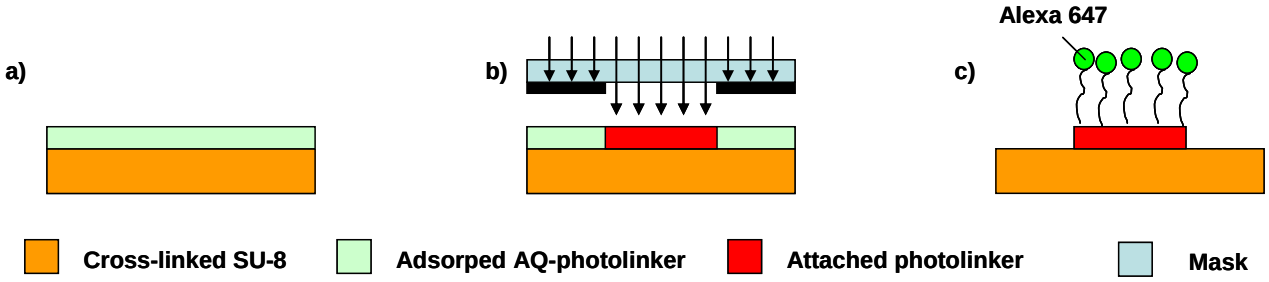

Figure 6.5-3: Photochemical surface functionalization of SU-8: (a) Antraquinone (AQ) photolinker is dried on the SU-8; (b) UV-activation of the AQ photolinker (c) rinse and immobilization of Alexa 647 cadaverine biomolecule with fluorescent label

6.5.2 Results and discussion

Figure 6.5-4 shows various fluorescent patterns realized on unstructured SU-8 substrates. *Figure 6.5-4(c)* is a fluorescence microscopy image of the same resolution structures as used for the thin film optimization in *Chapter 4*. A line resolution of 1.5 µm was achieved.
In order to investigate the stability of the generated pattern, the substrates were extensively rinsed and sonicated in ethanol. The fluorescence signal from the rinsed surface was only reduced by 2% which indicates that the labelled biomolecules were selectively and stably immobilised.

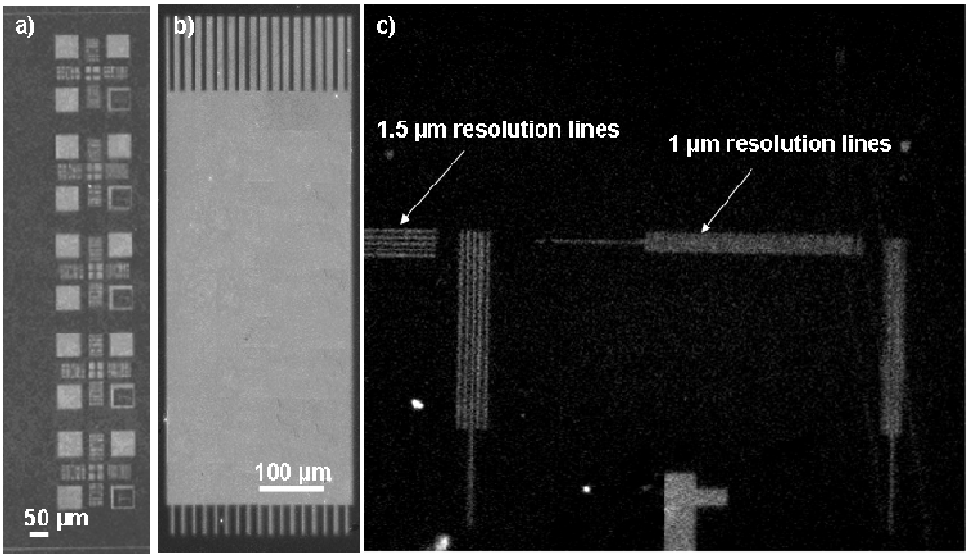

Figure 6.5-4: Fluorescence images of patterns of: (a) Alignment marks; (b) Chip with cantilevers (c) Resolution test structures (compare to Fig.4.2-1); a resolution of 1.5 µm was demonstrated

6.5.3 Conclusion

A reliable and straightforward method for photochemical functionalization and immobilization of biomolecules on a SU-8 photoresist surface was presented using AQ photolinkers. The approach has several advantages. The used AQ photolinkers are non toxic and water soluble molecules, eliminating possible safety issues. The method allows definition of chemical patterns by the use of a photolithographic mask. An adapted protocol of the functionalization method was fully compatible with cleanroom processing and high resolution on wafer-scale was achieved using an UV-aligner and a standard photolithographic mask.

6.6 Surface stress measurements

In collaboration with the University of Basel (Switzerland), the fabricated SU-8 IBM-chips were used for surface stress measurements with the NOSE-setup. The measurements were performed by Dr. Gabriela Blagoi of the Nanoprobes group. The goal was a direct comparison of the specificity and molecular sensitivity of the fabricated SU-8 IBM-chips to the one reported by McKendry et al. obtained with the same setup [159]. These authors used silicon cantilevers with the same dimensions but with a thickness of 1 μm for the measurement of surface stress change generated upon DNA-hybridization.

6.6.1 Materials and method

IBM-chips fabricated with Metal coating A were used for the measurement. These devices were selected based on the conclusions on the Au contamination because the Au was used as anchor for functionalization using thiol-chemistry. The cantilever thickness was 5.5 μm and the devices were coated with 50 nm Au. No cleaning in UV-ozone was done because this resulted in cantilever bending. The cantilevers were functionalized with thiolated single-stranded DNA. The same synthetic 12mer oligonucleotides were used as reported by McKendry [159]. Thiolated probe BioB2 TGC TGT TTG AAG and complementary targets BioB2C CTT CAA ACA GCA were obtained from Microsynth (Balgach, Switzerland). The thiol-modification with a 5_HS$(CH_2)_6$ linker enables covalent binding to Au-coated cantilever surfaces. For the reference cantilevers unspecific 12mer oligonucleotides (AC)6 2 Bio-B2 50-SH-(CH2)6-TGCTGT TTG AAG-30 were purchased. 1 M NaCl sodium citrate hybridization (SSC) buffer was used. The functionalization of the cantilever array was done by immersion in microcapillaries.
Prior to the experiments, a calibration test was performed to asses the functionality of the cantilevers. A heat pulse of 2°C was applied for 30 s with a Peltier-element mounted directly below the cantilever array. After calibration, different concentrations of target DNA were injected automatically at various flow rates. All measurements were performed at 23°C. After binding, hybridized oligonucleotides could be denatured chemically by purging the cell with dehybridization agents, 30% urea salts in buffer.

6.6.2 Results and discussion

During the calibration-test, all the cantilevers showed an approximate deflection of 535 nm. This is explained by the bimorph effect as SU-8 and Au have different coefficients of thermal expansion (CTE). The deflection δ at the free end of a cantilever is given by [160]:

$$\delta = (\alpha_{SU8} - \alpha_{Au}) \frac{3L^2 (t_{SU8} + t_{Au})}{\frac{E_{SU8} t_{SU8}^3}{E_{Au} t_{Au}} + 4t_{SU8}^2 + 6t_{SU8} t_{Au} + 4t_{Au}^2 + \frac{E_{Au} t_{Au}^3}{E_{SU8} t_{SU8}}} \Delta T \qquad (6.6\text{-}1)$$

E_{SU8}	= Young's modulus SU-8 = 5 GPa	E_{Au}	= Young's modulus Au = 78 GPa
α_{SU8}	= CTE SU-8 (*Section 4.4*) = 52 ppm/K	α_{Au}	= CTE Au = 14 ppm/K
t_{SU8}	= thickness of cantilever = 5.5 µm	t_{Au}	= thickness of Au coating = 50 nm
ΔT	= temperature difference = 2°C	L	= length of cantilever = 500 µm

With *Equation 6.6-1* and the described values the theoretical deflection is δ = 1.2 µm which is significantly more than effectively measured during the Peltier-test. A possible explanation is that the measurement is not done completely at the apex of the cantilever and that the actual value of L is lower. On the other hand, Young's modulus and CTE of the SU-8 are values from literature (see *Chapter 2*) and are probably different for the fabricated cantilevers.
The data in *Figure 6.6-1* shows the result of a surface stress measurement where 1µM BioB2C was injected during 20 min followed by a rinse with buffer. The delay in the signals is due to the time the reagents need to pass the microfluidic system. The BioB2C binds covalently to the complementary BioB2 sequence immobilized on the surface. The hybridization reaction results in a change of surface stress and the cantilever bends downwards. A cantilever deflection of 70 nm was observed. According to *Equation 1.2-1* this corresponds to a surface stress σ = 11 mN/m. This value is in agreement with published values [159]. On the other hand, the actual cantilever deflection at the same value of surface stress is higher than for the silicon devices. This demonstrates suggests that the limit of detection will be lower with the SU-8 IBM-chips.

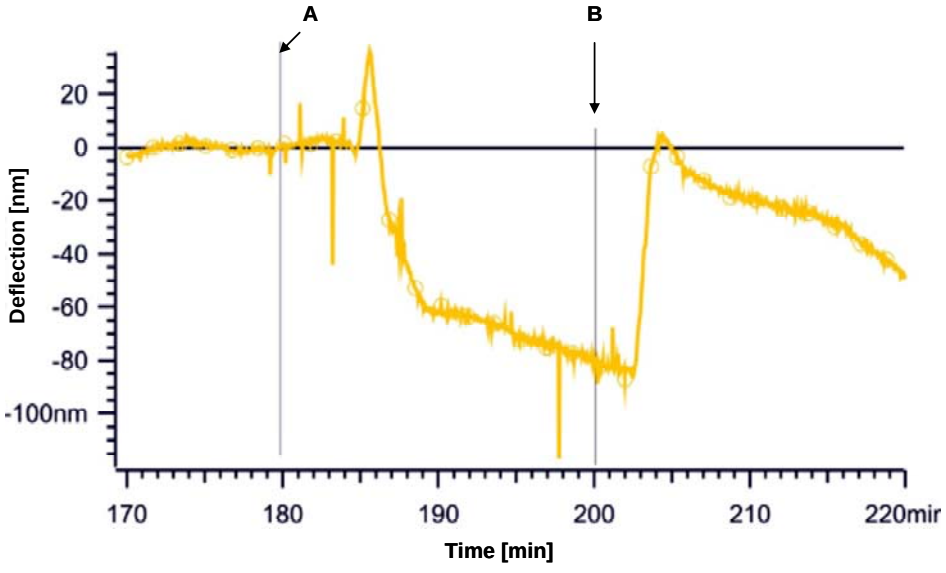

Figure 6.6-1: Surface stress measurement with IBM-chips: A: Injection of 1 µM complementary DNA; B: Rinse with buffer

6.7 Conclusion

The optimized processes developed in the previous chapters were used for the fabrication of cantilever chips for surface stress measurement with optical read-out. For this purpose, metal coatings had to be integrated on the cantilevers to allow for reflection of the laser beams. Two process-integrated approaches were implemented. In both cases, complete coating of the cantilevers with a 50 nm thick Au film results in bending. Alternatively, only a small reflective pad was placed at the apex of the cantilever. This still allowed for optical read-out and the bending of the cantilevers due to fabrication was significantly reduced. The surface contamination of the metal as a result of the cleanroom fabrication was evaluated. Au surfaces that are in contact with the release layer during fabrication are heavily contaminated with fluorocarbon. Therefore, these metal coatings are not suitable for surface functionalization with thiol-chemistry. Finally, a new method for direct functionalization of the SU-8 surface was discussed. This method is compatible with clean-room processes and allows photochemical patterning on wafer-scale using a standard UV aligner.
In conclusion, the two sensor designs illustrated in *Figure 6.7-1* are suggested for surface stress measurements with the NOSE-setup. Both devices feature metal coating for optical-readout, surface functionalization and backside-passivation as an integral part of cleanroom fabrication on wafer-scale.

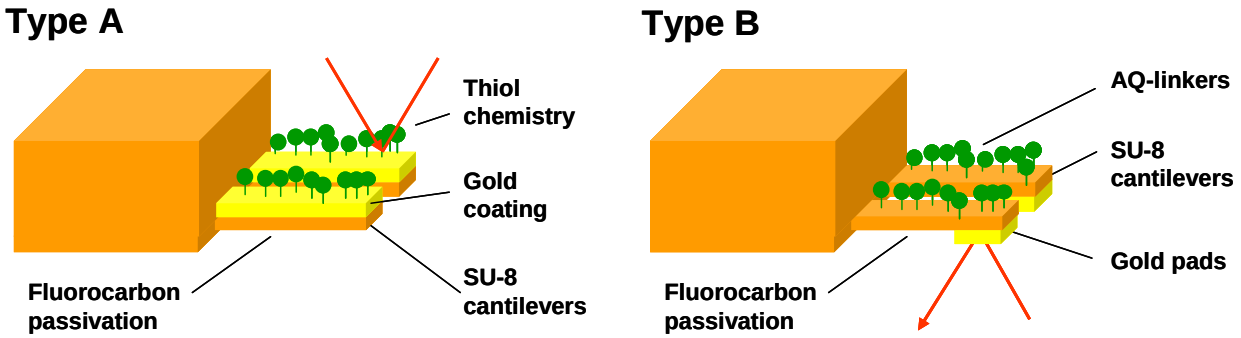

Figure 6.7-1: Two sensor design for surface stress measurement with optical read-out including metal coating, surface functionalization and backside passivation

Type A is fabricated with *Metal coating A* as described in *Section 6.4-1*. The Au covers the complete cantilever and serves simultaneously as reflective layer and as anchor for surface functionalization. Immobilization of thiols is possible due to acceptable surface contamination of the Au. The backside of the SU-8 cantilever is passivated by fluorocarbon as demonstrated in *Chapter 3*. First measurements of surface stress due to hybridization of DNA using IBM-chips of *Type A* were presented in *Section 6.6*.
For *Type B*, *Metal coating B* described in *Section 6.4-2* is used. There, only the apex of the cantilever is coated with Au to minimize cantilever bending. AQ-photolinkers are used for direct photochemical surface functionalization of the top-side of the cantilevers. This step can be done before or after the release of the devices from the substrate. The backside of the SU-8 cantilevers and the Au pads are inherently passivated with fluorocarbon as shown in *Chapter 3* and *Section 6.4.3*. In near future, sensors of *Type B* will be tested with the NOSE-setup. There, the influence of the functionalization step on the cantilever bending has to be evaluated as the long exposure with UV-light might induce stress in the SU-8.

7 Design and fabrication of the autonomous sensor

The concept of the autonomous sensor was introduced in *Section 1.5*. The design requirements and the related challenges for the fabrication of this device were described in *Section 1.6*. Most issues have been addressed during the process optimizations presented in the previous chapters. Here, the results on the optimized dry release method, the redesigned processing of the thin SU-8 film and the optimized fabrication of cantilever chips are combined for the design and the fabrication of the flapperchip. Particular focus is on the integration of the flapper in a microfluidic system that allows systematic testing of the sensor concept with high throughput. Therefore, batch fabrication of the flapperchips is further promoted by the combination of bonding- and release-processes on wafer-scale.

7.1 Design of the chips

7.1.1 Design of microfluidic system

For the cantilever-chips presented in *Chapter 6* the fabrication of a microfluidic system for the transport of the analyte solution was not required. There, the IBM-chips were simply clamped into a predefined chip holder of the NOSE-setup which provides the channels for liquid handling. In more advanced devices such as the SU-8 chip fabricated by Alicia Johansson, the cantilevers were integrated in microfluidic system with a single channel used for the introduction of the analyte [55]. For the testing of the flapperchip, a more complex microfluidic system is required as illustrated in *Figure 7.1-1*. A first microchannel is filled with the marker solution (M) and simulates the liquid container closed by the lid. A second channel is used for the analyte solution (A). Both microfluidic systems are separated by the lid that is functionalized with the receptor molecules (red). If the flapper is functionalized on the opposite side, the channels for marker and analyte solution can easily be exchanged. Further, free optical access with a camera and eventually a laser beam is desirable for visualization of the color change and quantification of the flapper deflection.

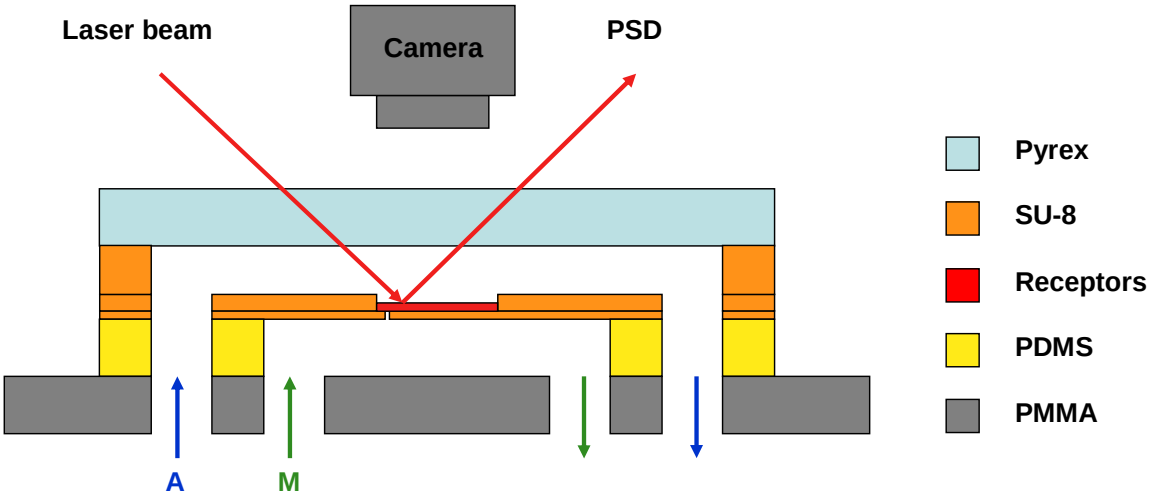

Figure 7.1-1: Schematic of the flapperchip with two microfluidic channels for analyte (A) and marker (M) solution. A position sensitive diode (PSD) is used to measure the flapper deflection.

Figure 7.1-2 shows the top-view of the different parts of the microfluidic system. The two microchannels are overlapping in the center of the chip where the flapper is situated once the parts are assembled as shown on *Figure 7.1-1*. The Pyrex cover (*Figure 7.1-2(a)*) seals the upper channel and allows for optical read-out. The core part is the flapperchip fabricated in the cleanroom using SU-8 (*Figure 7.1-2(b)*). Design and fabrication of the chip are discussed in the following sections. Bonding of the Pyrex cover to the SU-8 flapperchip can be integrated in microfabrication, which will be discussed in *Section 7.3*. The second microchannel is defined in Polydimethylsiloxane (PDMS), an elastomer that also ensures sealing (*Figure 7.1-2(c)*). The base plate with the microfluidic interconnections is fabricated with Polymethylmethacrylate (PMMA) (*Figure 7.1-2(d)*). The design and fabrication of these two parts are briefly described in *Section 7.6*.

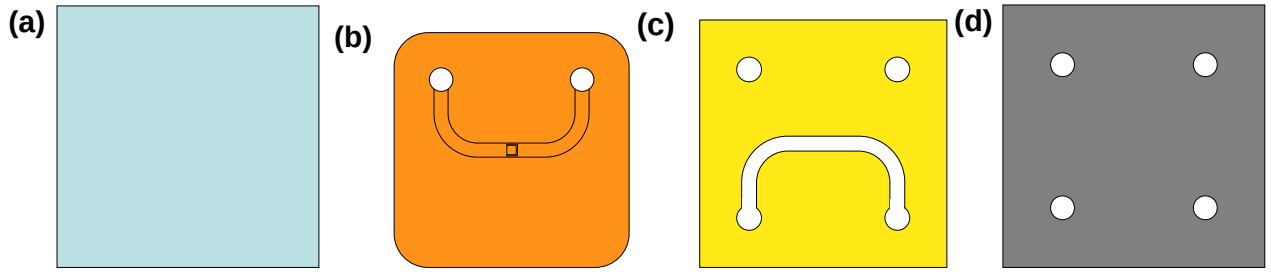

Figure 7.1-2: Top-view of different layers schematically represented in Figure 7.1-1: a) Pyrex cover, b) SU-8 flapperchip, c) PDMS channel, d) PMMA base plate

7.1.2 Design of the SU-8 flapperchip

Figure 7.1-3 shows the design of the flapperchip fabricated with three layers of SU-8. The chips are relatively large with a total size is 1x1 cm^2 to provide enough area for the four microfluidic interconnections and the optical read-out.

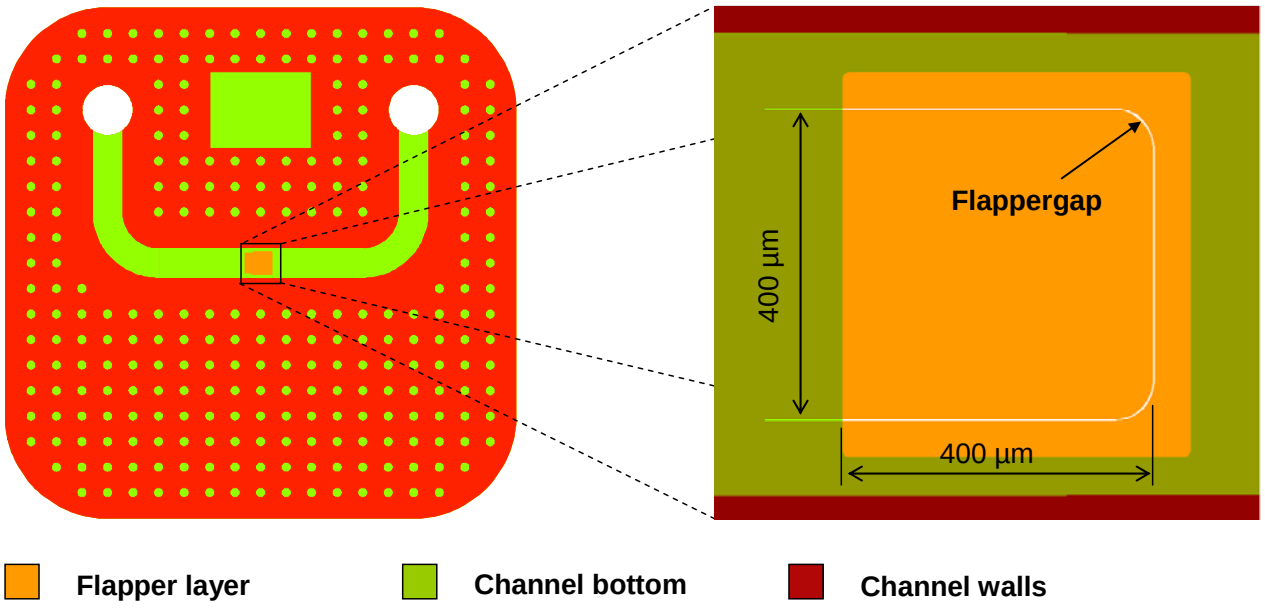

Figure 7.1-3: Design of the flapperchip with three layers of SU-8

The flapper is placed in the center of the chip and it is defined in the first layer of SU-8. A 4-inch wafer includes 35 chips with some variations of the design and the placement of the flappers. The standard devices had flappers with a length L = 400 µm and a width w = 400 µm. The thickness t of the flappers was 2 µm, 3.7 µm or 5.6 µm. Based on the results of *Chapter 4* on processing of the thin SU-8 film, two different masks were designed. For a film with t = 2 µm, the expected trench-resolution at an exposure dose of 250 mJ/cm^2 is 3 µm (*Table 4.6-3*). This value was chosen as the nominal width of the flappergap on the mask. For t = 5.6 µm, the lithographic resolution decreases and therefore the nominal width of the flappergap on the mask designed for this SU-8 thickness was 8 µm. For the intermediate thickness of 3.7 µm both masks could be used depending on the selected exposure dose. The second layer of SU-8 serves as a reinforcement of the channel bottom and has a thickness of 65µm. Only a small window at the location of the flapper in the center or the chip is open. The third layer has a thickness of 250 µm. The design includes a U-shaped microchannel with a width of 600 µm and a large circular well at each end serving as fluid inlet and outlet. Similar to the IBM-chips, circular holes with a diameter of 200 µm were evenly distributed on the chip area to allow for release of the film stress in the thick SU-8.

7.2 Fabrication of the SU-8 flapperchip

7.2.1 Process steps

The process sequence for the fabrication of the flapperchip is illustrated in *Figure 7.2-1*. The processing is similar to the one used for the fabrication of the IBM-chips in *Chapter 5*.

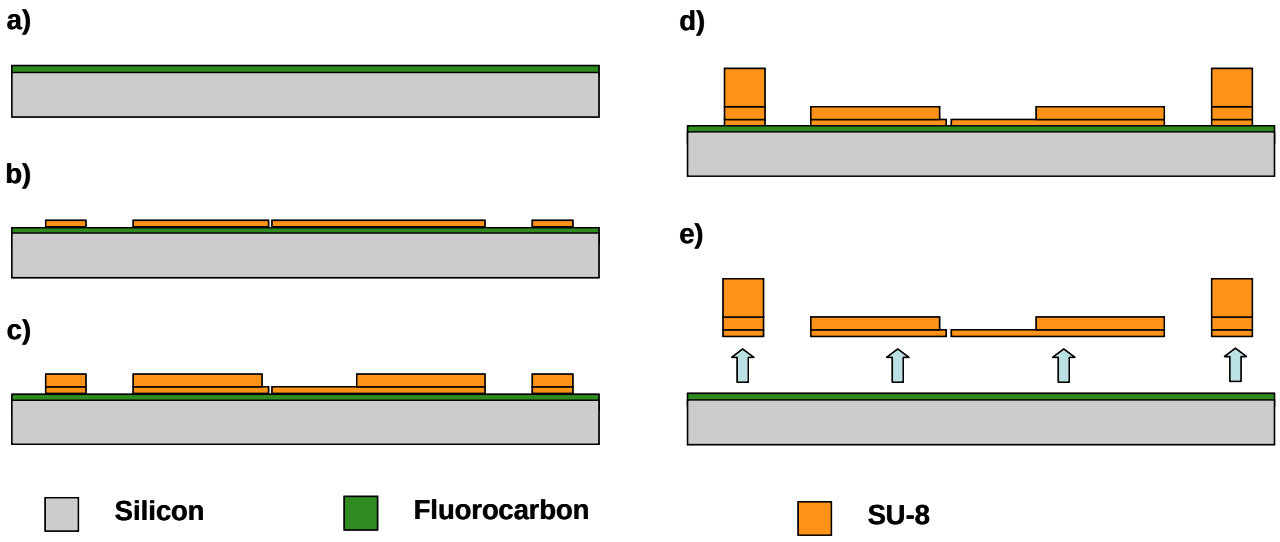

Figure 7.2-1: Process flow for the fabrication of the flapperchip: (a) Deposition of fluorocarbon coating; (b)-(d) three steps of UV-lithography with SU-8 to define the flapper (b), the channel bottom (c) and the channels walls (d); (e) Mechanical release of the flapperchip with a razor blade

The silicon substrates were coated with fluorocarbon using the recipe wet_tef described in *Section 3.5* (*Figure 7.2-1(a)*). Three consecutive steps of SU-8 photolithography were performed for the definition of flapper, channel bottom and channel walls respectively (*Figure 7.2-1(b)-(d)*). For the patterning of the first layer of SU-8, the optimized *Process C* (*Appendix B*) was used. The exposure dose was reduced to D = 250 mJ/cm^2 to ensure that the flappergap remained open. Finally, the chips

were released from the substrate using a razor blade (*Figure 7.2-1(e)*). The detailed process parameters are given in *Appendix D*.

7.2.2 Fabrication results and discussion

Figure 7.2-2 is a top-view of the center of the flapperchip with the three layers of SU-8. In terms of lithographic resolution and quality of the structures the fabrication followed the expectations. No cracks were observed in the SU-8. The trench resolution was better than 3 µm for the 2-µm-thick SU-8 and about 5 µm for the 5.6-µm-thick films which resulted in open flappergaps for all the devices (*Figure 7.2-2(b)*).
Figure 7.2-3 shows a flapper with a thickness of only 2-µm that was successfully released from the substrate. The bending of the devices was low but in general the release yield was much lower than for the cantilever chips in *Chapter 5*. The area of the flapper is larger compared to cantilevers which increases the adhesion force between the fluorocarbon and the SU-8. Furthermore, the handling of the flapperchip during mechanical release is difficult and the use of a razor blade induces a lot of lateral movement compared to the release of the cantilever chips with a tweezer. The released devices typically showed plastic deformation or cracks at the clamping point of the flapper as shown in *Figure 7.2-3(b)*.
The flappers with a thickness t = 5.6 µm showed a negative bending identical to the IBM-chips shown in *Section 6.3*. There, it was concluded that the introduction of a final bake step before the release resulted in reduced bending of 5-µm-thick cantilevers. This observation was confirmed for the fabrication of the flapperchips. A hard-bake in the oven at 120˚C for 2 h results in less bending of the flappers with the same thickness as shown in *Figure 7.2-4*. Further, the release yield for the flappers was considerably improved. During this additional temperature cycle the thick chip body seems to contract and thereby to assist the release of the flapper from the substrate.

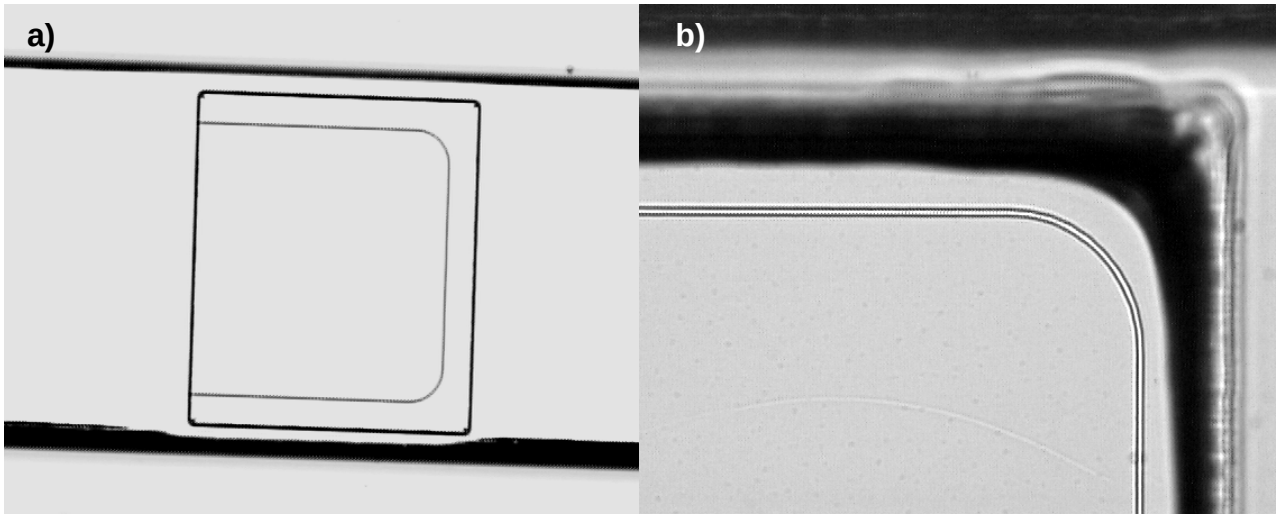

Figure 7.2-2: (a) 2-µm-thick flapper before release; (b) the flappergap with w = 3 µm is open

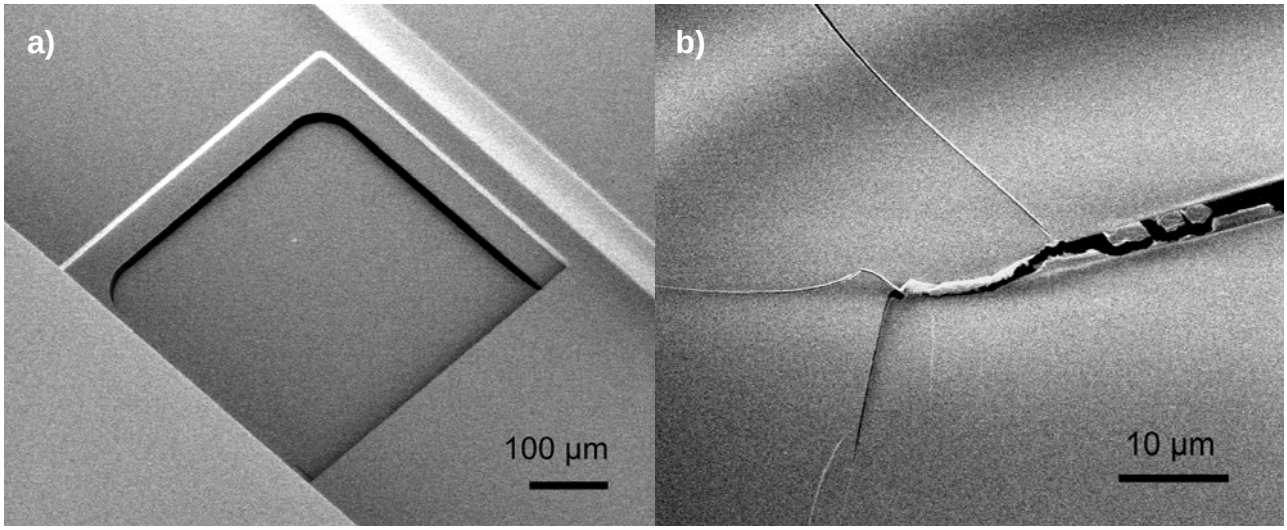

Figure 7.2-3: (a) Released flapper with t=2 µm; (b) the mechanical release results in plastic deformation and cracks at the clamping point

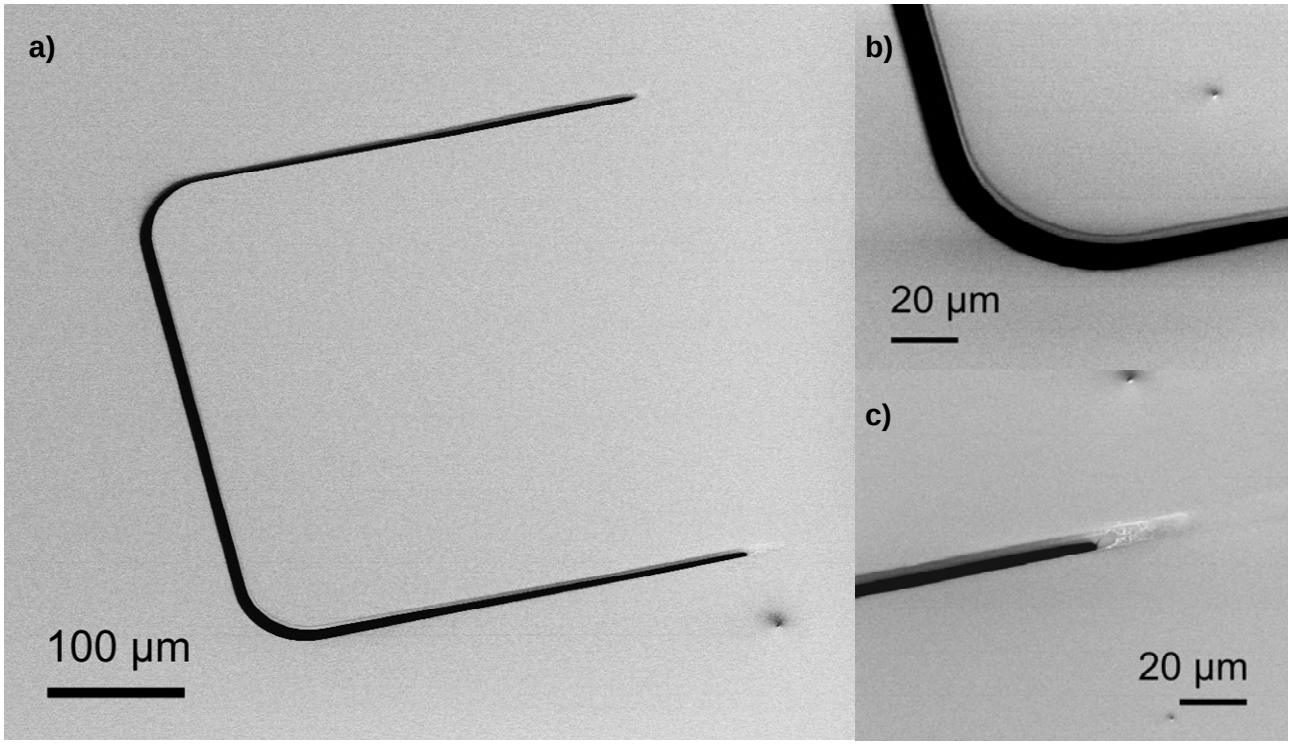

Figure 7.2-4: (a) Flapper released after additional hard-bake in oven at 120˚C for 2 h; t=5.6 µm; flapper shows low bending (a) and no cracks at the clamping point (c)

7.3 Cover bonding and release on wafer-scale

In *Figure 7.1-1* the microfluidic system where the top channel is closed by a Pyrex cover was presented. In the past, different approaches have been introduced to achieve tight sealing in similar systems:

- Mechanical clamping: The two parts are pressed together and typically a soft PDMS layer is required to avoid leakage between the two parts
- Single chip bonding: A Pyrex is cut into pieces and a cover is bonded to the released SU-8 flapperchip by means of glue
- Wafer-scale bonding: A complete Pyrex wafer is bonded to the non-released SU-8 chips

The first solution was chosen by Daniel Häfliger for the proof-of-concept with the flapper [59]. There, leakage was an issue and the pressure required for tight sealing often resulted in broken glass covers. The advantage of this approach is that the same microfluidic parts can be used for the measurement with several chips. The other approaches solve the issue with leakage by replacing the PDMS with a permanent sealing. Single-chip bonding resulted in a low yield probably due to insufficient pressure during the bonding [55].
In the interest of batch processing such an approach was chosen for the sealing of the flapperchips. A large amount of work has been published on wafer-scale bonding for closure of SU-8 microchannels. Several authors used Pyrex substrates with a thin SU-8 film as bonding layer as a cover [67, 117, 161]. For the actual bonding procedure, a large variety of processes was reported. Due to the rigidity of the Pyrex, the main challenge was to ensure uniform bonding on wafer-scale [162]. Therefore, alternative solutions using more flexible substrates were suggested [163, 164]. In the reported methods, the bonding was typically done for large microfluidic systems and an eventual release of the structures from the substrate was uncritical. Recently, Maria Nordström from the Nanoprobes group developed a method for combined bonding and release of thin SU-8 cantilevers on wafer scale [56]. Here, this process was slightly modified for the bonding of a Pyrex cover to the flapperchips.

7.3.1 Process steps

Figure 7.3-1 illustrates the different process steps. A Pyrex wafer was cleaned and an SU-8 bonding layer with a thickness of 8 µm was spin-coated (*Figure 7.3-1(b)*). The experiments in Chapter 4 showed that high solvent content improved the cross-linking of thin films. Therefore, no soft-bake was performed but the spin-coating was immediately followed by flood-exposure with a dose D = 1000 mJ/cm^2. The bonding of the Pyrex substrate to the wafer with the SU-8 flapperchips was done directly after the exposure (*Figure 7.3-1(c)*). A setup originally designed for hot embossing (520 Hot Embosser, EV Group, Austria) was used for this purpose (*Figure 7.3-2*). The two substrates were placed in the setup and the chamber was evacuated. A pressure of 2000 N was applied to ensure good contact between the two substrates upon polymerization of the bonding layer. The substrates were heated to the bonding temperature of 90˚C with a slow ramping of 2˚C/min. At this temperature SU-8 was cross-linked during 1 h. After cool-down to ambient temperature the substrates were separated mechanically with the SU-8 flapperchips bonded to the Pyrex wafer (*Figure 7.3-1(d)*). In principle, the silicon substrate could be reused for the fabrication of a new batch of flapperchips after cleaning.

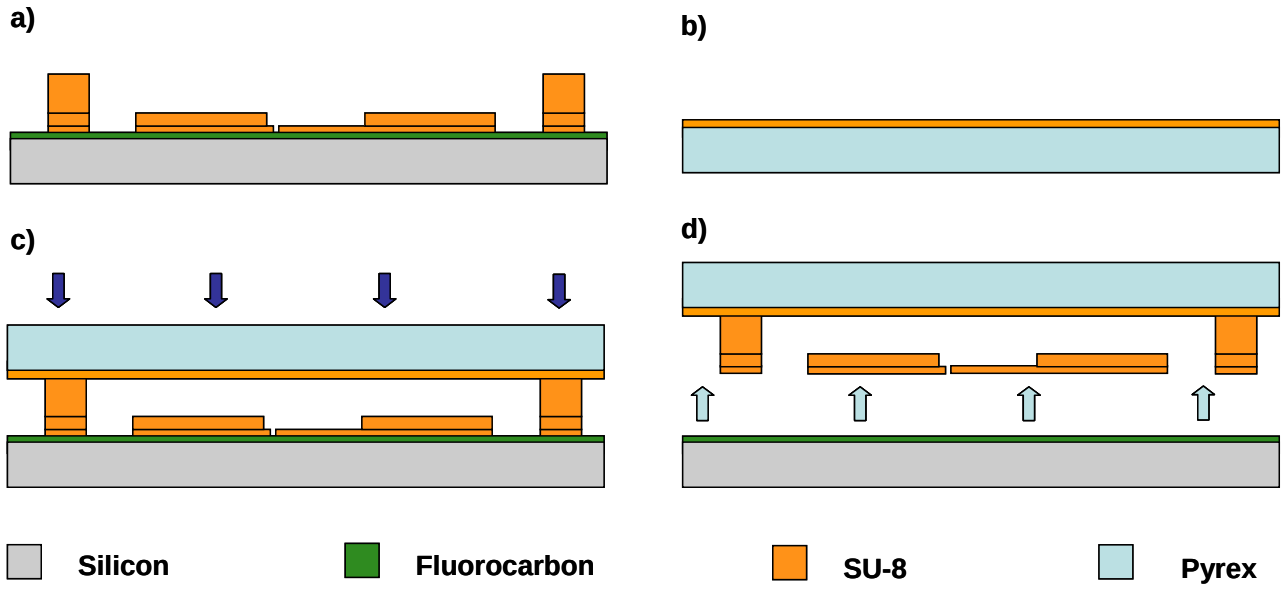

Figure 7.3-1: Process sequence for wafer bonding: (a) SU-8 flapperchip after fabrication; (b) SU-8 bonding layer on Pyrex; (c) Bonding of the two wafers; (d) Release of the chips on wafer-scale

7.3.2 Fabrication results and discussion

Measurements with a profilometer showed that the thickness of the thick SU-8 film was higher at the edge of the wafer. The result of this edge-bead was a non-uniform contact force and therefore insufficient bonding in the center of the wafer. This was partially solved by inserting a small carbon pad below the center of the Silicon substrate during bonding. A series of experiments for the optimization of the uniformity of the thick SU-8 film was performed. Long soft-bake times at low temperature typically improved the uniformity of the thickness on wafer-scale. Further, the leveling of the hotplates turned out to be a critical issue.
With these optimizations, the wafer-scale release of flapperchips with the described method was possible. *Figure 7.3-3(a)* shows a Pyrex wafer after bonding and separation from the silicon substrate. *Figure 7.3-3(b)* is a SEM-image of one of the flappers. In general the release yield was improved and the plastic deformation of the flappers was less significant compared to single chips released with a razor blade. This is probably due to reduced shear forces when the release is done with the rigid Pyrex wafer as handle.

7.3.3 Wafer dicing

The fabrication of the SU-8 flapperchips was concluded by dicing of the Pyrex wafer with an automatic saw (DAD321, Disco, USA) after bonding. In principle, this process is straightforward and allows the dicing of a wafer with 35 chips in 15 minutes. On the other hand, during cooling of the blade by water is required during sawing. The heavy flow of water is a problem for the dicing of chips with fragile MEMS-devices and results in contamination of the surfaces.
Some attempts were made to do the dicing of the Pyrex before the separation from the silicon substrate. There, the shear force of the blade was too high and the complete Pyrex wafer delaminated during dicing. Coverage of the critical flapper devices with AZ-resist is an option but

in contradiction to the goal of batch processing. Alternative methods for the wafer dicing would be wet etching or laser machining.

7.3.4 Conclusion

Wafer-scale bonding and release of the SU-8 flapperchips using a Pyrex cover was demonstrated. The release yield for the flappers is increased compared to the release of single chips with a razor blade. Nevertheless, the release remains the critical step in the fabrication of the flapperchips. Compared to the IBM-cantilevers in *Chapter 6*, the flappers have a larger area and therefore the stiction to the fluorocarbon substrate is increased.

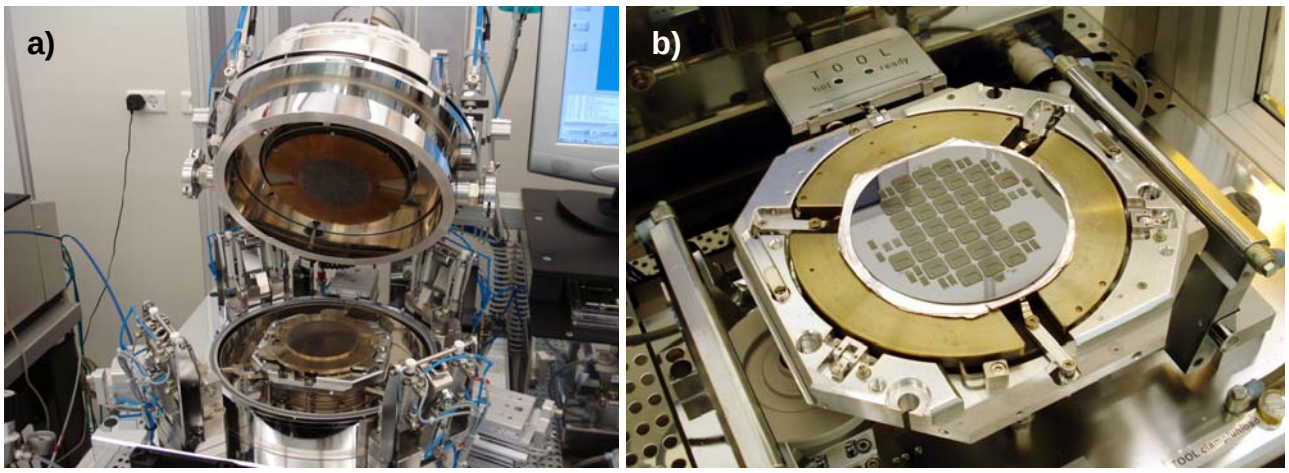

Figure 7.3-2: (a) Hot-embossing-setup used for wafer-scale bonding (b) the Pyrex wafer is manually aligned to the silicon substrate with the flapperchips

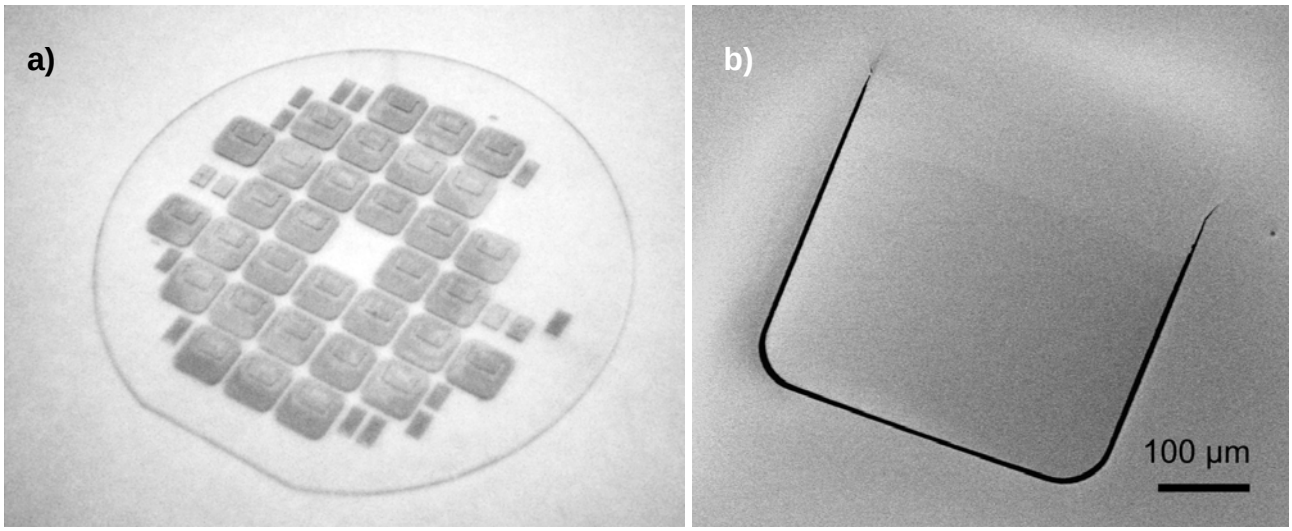

Figure 7.3-3: (a) Pyrex wafer with flapperchips after separation from silicon substrate; (b) SEM-image of a 2-µm-thick flapper after wafer-scale bonding and release

7.4 Alternative release methods

As a consequence of the low yield for the release of the flappers from the fluorocarbon, alternative release methods were evaluated. The concept was a combination of the optimized dry release with the wet etch of a sacrificial polymer layer. *Figure 7.4-1* illustrates two different methods that further are called *Method A* and *Method B*. In both cases, the sacrificial layer is deposited onto the fluorocarbon coating (*Figure 7.4-1(a)*). This step is followed by the fabrication of the SU-8 flapperchips as described in *Section 7.2* (*Figure 7.4-1(b)*).
In *Method A*, the sacrificial layer is partially etched after completed SU-8 processing using wet chemistry (*Figure 7.4-1(c1)*). The purpose of this process step is the release of the flapper before the mechanical dry release of the chip body from the fluorocarbon substrate (*Figure 7.4-1(d2)*). The advantage of this combined approach compared to a simple wet etch of a sacrificial layer is that the process is very fast because the chip body is not completely under-etched. Further, the fluorocarbon coating on the silicon substrate should prevent stiction of the flappers to the substrate.
In *Method B*, the sequence of wet and dry release is inverted. The sacrificial layer is released from the fluorocarbon substrate together with the flapperchip (*Figure 7.4-1(c2)*). The sacrificial layer serves as reinforcement of the thin flapper structure during mechanical release. After this, the removal of the sacrificial layer can be done on wafer-scale (*Figure 7.4-1(d2)*). Alternatively, the stripping of the sacrificial layer on single chips after the dicing step is possible. There, the protective coating is an additional advantage as it might prevent damage of the flapper by the cooling water or contamination of the surface.

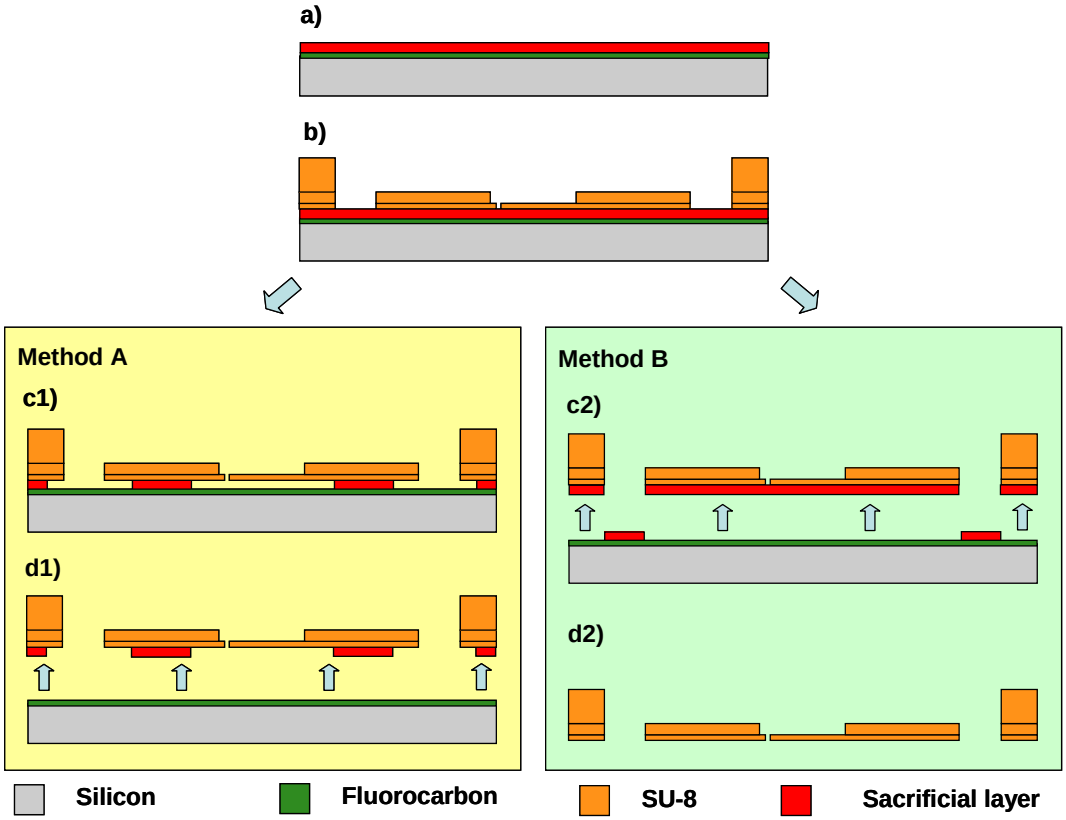

Figure 7.4-1: Alternative release of the flapperchips: a) spin-coating of sacrificial layer; b) fabrication of SU-8 flapperchip; Method A: c1) wet etch of sacrificial layer; d1) dry release from fluorocarbon; Method B: c2) dry release from fluorocarbon; d2) wet etch of sacrificial layer

For both methods described above, there are several requirements for the sacrificial layer:

- Film deposition: Possibility of spin-coating on the fluorocarbon substrate
- Compatibility with SU-8 processing: Chemical resistance towards SU-8 solvent and developer and thermal stability up to a temperature of about 100˚C
- Wet etching: Wet chemistry for the removal of the layer after processing with a fast etch rate (> 1 μm/min) and without affecting the SU-8 structures

The use of several polymers for the wet release of SU-8 structures was reported. Spin-coated films of standard positive photoresist [165, 166], polystyrene [166, 167] or lift-off-resist [168] have been introduced as sacrificial layers. Polystyrene was previously tested in the Nanoprobes group and the results were not satisfying [169].

7.4.1 Sacrificial layer of positive tone photoresist AZ 5214e

Standard positive tone photoresist AZ 5214e (Hoechst-Celanese) was evaluated as sacrificial layer for the fabrication of SU-8 structures. Spin-coating of the resist onto the fluorocarbon and wet etching with Acetone are easily possible. On the other hand, the photoresist is not compatible with the processing of the SU-8 [169]. The photoresist is dissolved by the solvent and the developer of the SU-8. Therefore, the photoresist was protected by a thin metal coating.
A photoresist film with a thickness of 2.2 μm was spin-coated on the fluorocarbon substrate. Preliminary experiments showed that a hard-bake of the photoresist at 120˚C was required to avoid out-gassing during further fabrication steps. The bubbles on *Figure 7.4-2(a)* are a result of this outgassing. The resist was covered by a metal film of 50 nm aluminum and the fabrication of the flapperchips on top of the protective metal layer was successful.
For the testing of *Method A*, the protective aluminum layer had to be removed using NaOH. The following wet etch of the sacrificial layer of photoresist with Acetone was not possible. Apparently, the resist was strongly polymerized during the different temperature steps which rendered dissolution impossible.
The dry-release step of *Method B* was possible. *Figure 7.4-2(b)* shows a flapper that was removed from the fluorocarbon substrate together with the sacrificial resist layer. The release of the flappers improved compared to processing without sacrificial layer but, similar to *Method A,* the final removal of the resist was impossible.

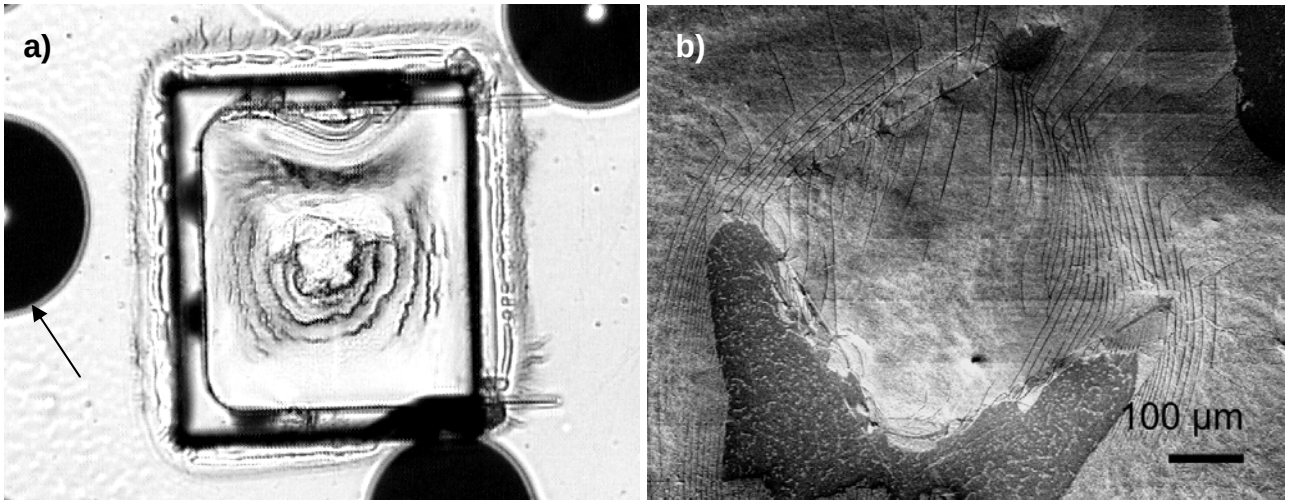

Figure 7.4-2: (a) Flapper fabricated on a sacrificial layer of AZ 5416e covered by Aluminum: Out-gassing of the photoresist resulted in bubbles (arrow); (b) SEM-image of device processed with Method B: The photoresist is released with the SU-8 chip

7.4.2 Sacrificial layer of lift-off-resist LOR 20B

The use of a lift-off-resist (LOR) for the fabrication and release of SU-8 microcantilevers was demonstrated by Claus Jeppesen at DTU Nanotech [168]. The resist is based on polydimethylglutarimide and are therefore compatible with the wet chemistry involved in processing of normal photoresist and SU-8 [76]. Further, the etch rate can be controlled by the processing parameters of the LOR and by the selection of the chemicals used for the removal.
LOR 20B (MicroChem, USA) was spin-coated during 60 s at 2000 rpm with an acceleration of 1500 rpm/s. The wetting of the fluorocarbon was excellent and the measured thickness was 3.2±0.2 µm. The resist was soft-baked on a hotplate for 10 min at only 150˚C which should allow for a high etch rate. The fabrication of the flapperchip on the LOR-coated substrate was easily achieved. For the etching, Microposit MF-319 Developer (Shipley Company LCC) was used at ambient temperature. This product is based on Tetramethylammonium hydroxide (TMAH) at low concentration.
Figure 7.4-3 shows a flapper processed according to *Method A* after etching of the LOR for 5 min (*Figure 7.4-1(c1)*). The opening of the flappergap is large enough to give access for the developer and to allow under-etch of the SU-8 with an etch rate > 10 µm/min. After wet release of the flappers, the chips were mechanically lifted-off from the fluorocarbon. The method resulted in a significant increase of the release yield for the devices. However, considerable bending of the flappers was observed (*Figure 7.4-3(b)*).
Release of the flapperchips using *Method B* was investigated. The adhesion of the LOR to the fluorocarbon is very low and the dry release of the devices was possible. *Figure 7.4-4* shows 5.6-µm-thick cantilevers fabricated on the same substrate as the flapperchips. The structures are nicely covered by the LOR and are almost perfectly straight with a bending < 10 µm (*Figure 7.4-5(a)*). Immersion of the cantilevers for 5 min in MF-319 resulted in a complete removal of the LOR but also in an increase of the bending of 100-120 µm (*Figure 7.4-5(b)*). The same effect was observed for the flapperchips presented on *Figure 7.4-6* before and after final etching of the LOR. Apparently, residual stress gradients in the SU-8 are different for processing with and without the sacrificial layer. Another explanation for the increased bending is the absorption of the developer in the SU-8 during the etching of the LOR.

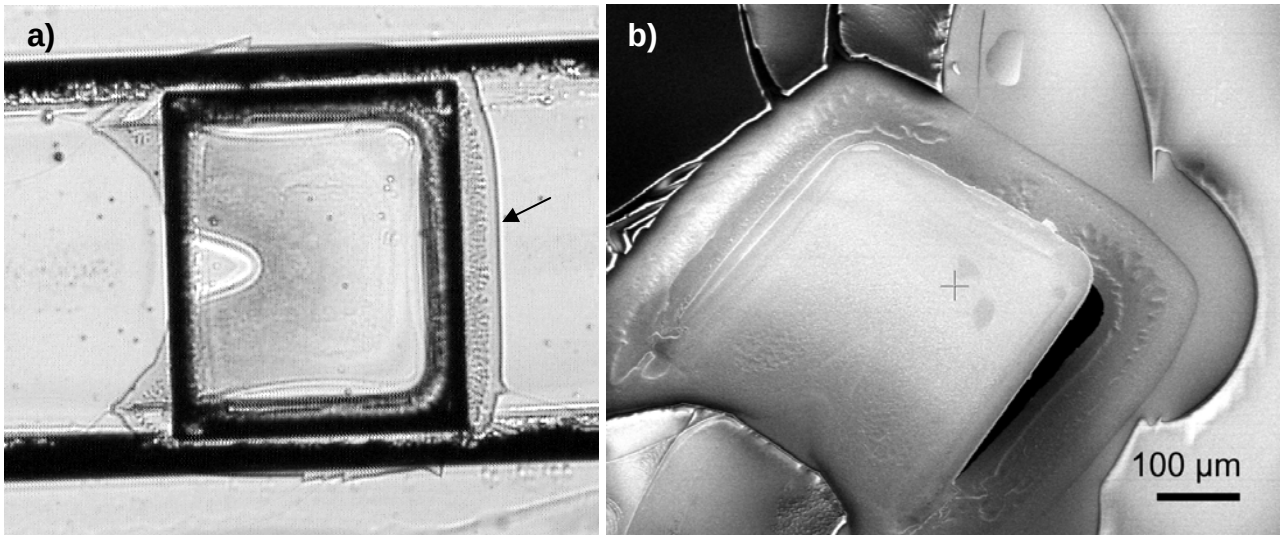

Figure 7.4-3: Flapper fabricated on a sacrificial layer of LOR released with Method A: (a) Sacrificial etch of LOR results in undercut of the SU-8 (arrow); (b) Device after dry release

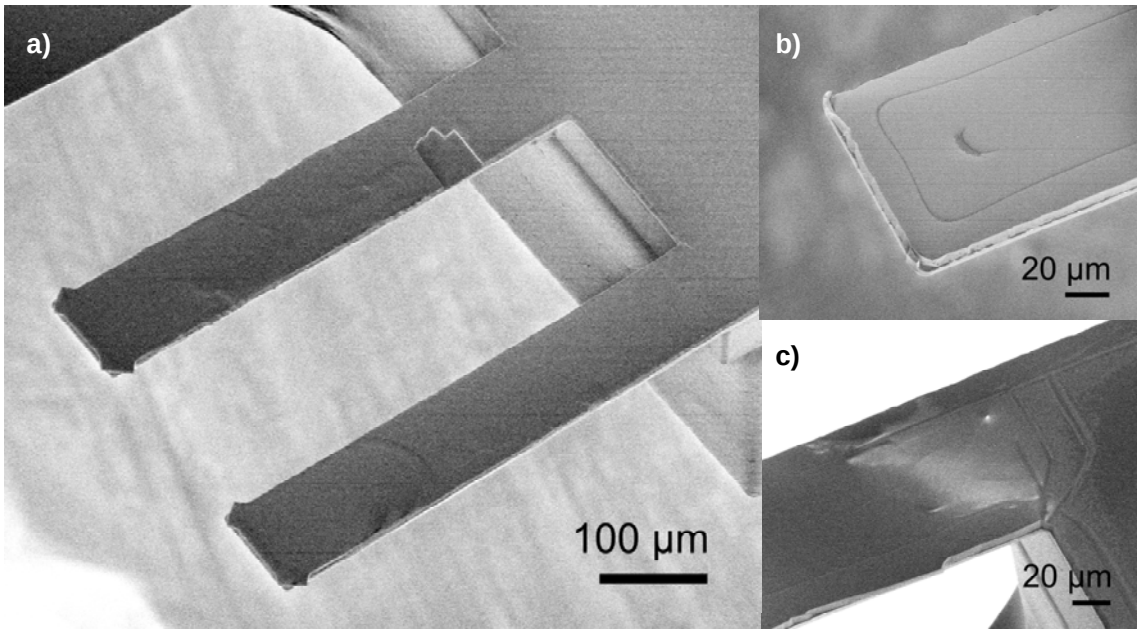

Figure 7.4-4: 5.6-µm-thick SU-8 cantilevers covered with LOR; the resist adheres well to the SU-8 and no cracking is observed at the cantilever base (c); L = 500 µm, w = 100 µm

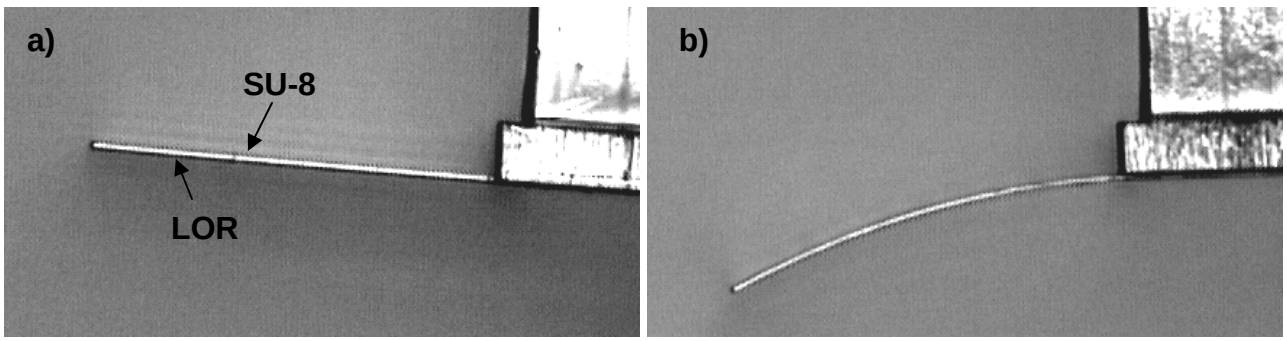

Figure 7.4-5: 5.6-µm-thick cantilever before (a) and after (b) removal of 3.2 µm LOR; L = 500 µm

7.4.3 Conclusion

The combination of wet etching of a sacrificial layer with the developed dry release method was investigated. AZ 5416e was not suitable as sacrificial layer due to the incompatibility of the resist with the processing of the SU-8. The use of lift-off-resist was more promising. There, sacrificial etch of the LOR before the dry release of the SU-8 chips from the substrate was beneficial for the release yield of the flappers. Further, dry release of flappers and cantilevers coated with LOR was possible with a high yield and low initial bending of the devices. In all the experiments with the LOR, the bending of the structures increased upon removal of the resist which is a major drawback of this method. On the other hand, *Figure 7.4-6* demonstrates for the first time the actuation of a flapper using an organic coating.

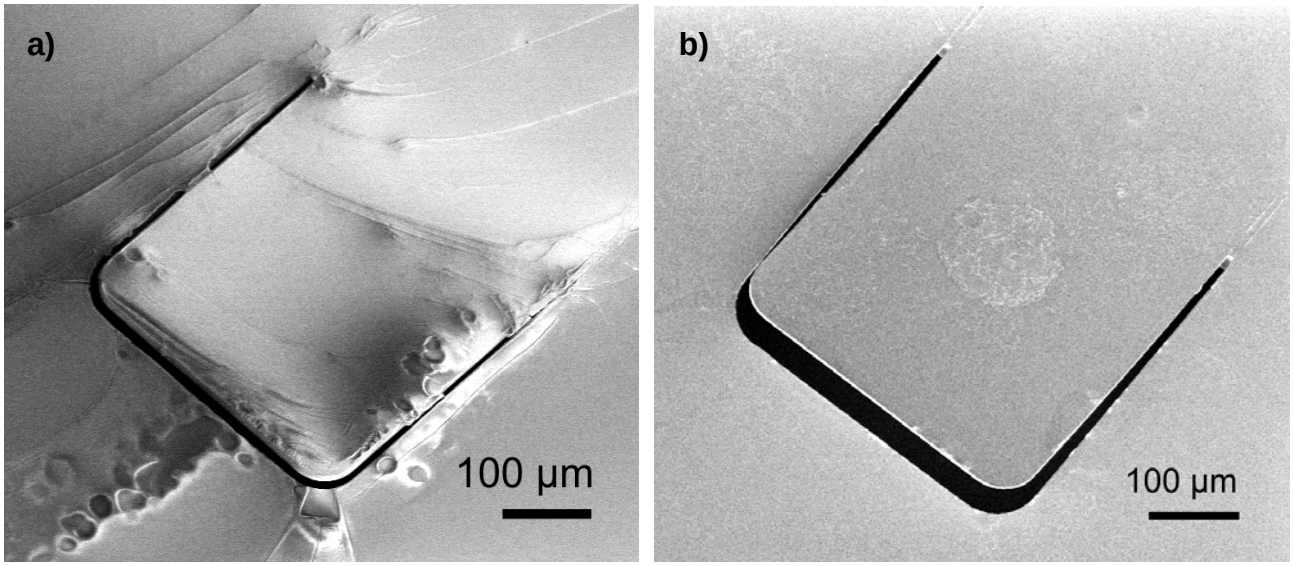

Figure 7.4-6: 5.6-µm-thick flapper before (a) and after (b) removal of 3.2 µm LOR

7.5 Process-integrated coating with biopolymer

In *Section 7.4*, the good adhesion of an organic sacrificial layer to the SU-8 allowed for a process-integrated coating of the flappers. Stripping of the organic coating resulted in high actuation of initially closed flappers (*Figure 7.4-6*). In a final series of experiments, the introduction of a more functional material for the coating of the flappers was investigated. A biopolymer was chosen for this purpose.

Biopolymers are fabricated from natural resources such as starch or cellulose [170]. The applications include fabrication of sutures or stents or the use as packaging material [171]. The advantage of biopolymers is that they are biodegradable through hydrolysis or by enzymes. Testing of biodegradability is typically very time-consuming because the samples have to be buried in the ground for several weeks or months. There, alternative test methods could allow for faster advances in the development of biopolymers.

Figure 7.5-1 illustrates the concept of actuation of the autonomous sensor. The flapper is initially closed and coated with a thin film of biopolymer. Biodegradation of the film results in actuation of the flapper and in a release of the marker solution. Possible applications of such a device are:

- Environmental testing: Systematic investigation of the influence of parameters such as temperature or pH-value on the degradation rate
- Degradation in the human body: Biopolymers are used as scaffold materials for implants; time-limited stability of the materials in this environment is important
- Drug release: Degradation by specific enzymes in the digestive system could trigger the local release of drugs

In collaboration with Dr. David Plackett at DTU-Risø, L-polylactide (PLLA) was selected for a first test of process-integrated coating of the flapper. Polylactic acid or polylactide is a biodegradable, thermoplastic, aliphatic polyester derived from renewable resources, such as corn starch or sugarcanes [172, 173]. PLLA is mainly degraded through hydrolysis but enzymatic degradation with proteinase K has been reported [174].

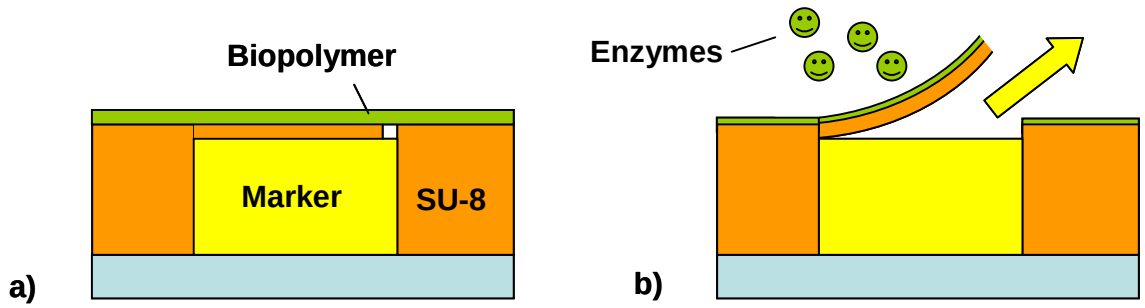

Figure 7.5-1: (a) the closed flapper is coated with biopolymer (b) enzymatic degradation of the coating results in actuation of the flapper and in release of the marker solution

7.5.1 Materials and method

L-polylactide L-9000 (Biomer, Germany) was achieved in granular form. The polymer was dissolved in dichloromethane assisted by 1 h of agitation in an ultrasonic bath. The final concentration was 1% of PLLA. The fabrication process followed *Method B* presented in *Figure 7.4-1*. Instead of a sacrificial layer, 3 ml PLLA-solution were spin-coated during 30 s at 1000 rpm. The wetting of the fluorocarbon substrate was excellent and the measured film thickness was 717±60 nm. Initial experiments showed that the Biomer film is not compatible with the SU-8 processing. Therefore, a titanium film with thickness of 30 nm was deposited as a protective coating, similar to the aluminum film used in *Section 7.4.1*. This step was followed by the fabrication of the SU-8 flapperchip (*Figure 7.4-1(b)*). Finally, the chips were released from the fluorocarbon (*Figure 7.4-1(c2)*).

7.5.2 Fabrication results and discussion

Figure 7.5-2 shows 5.6-µm-thick cantilevers after the release. The initial bending of the cantilevers was 30-40 µm. The structures are covered by PLLA which demonstrates that the integration of the biodegradable coating in the fabrication of the flapperchip is possible. On the other hand, the release of the flappers was difficult. The adhesion of the structures to the fluorocarbon was too high and the flappers mostly remained on the substrate. Some flappers could be released from the

substrate with parts of the biopolymer coating (*Figure 7.5-3*). Probably, the increase of the thickness of the PLLA film would improve the stability of the coating and result in a higher release yield.

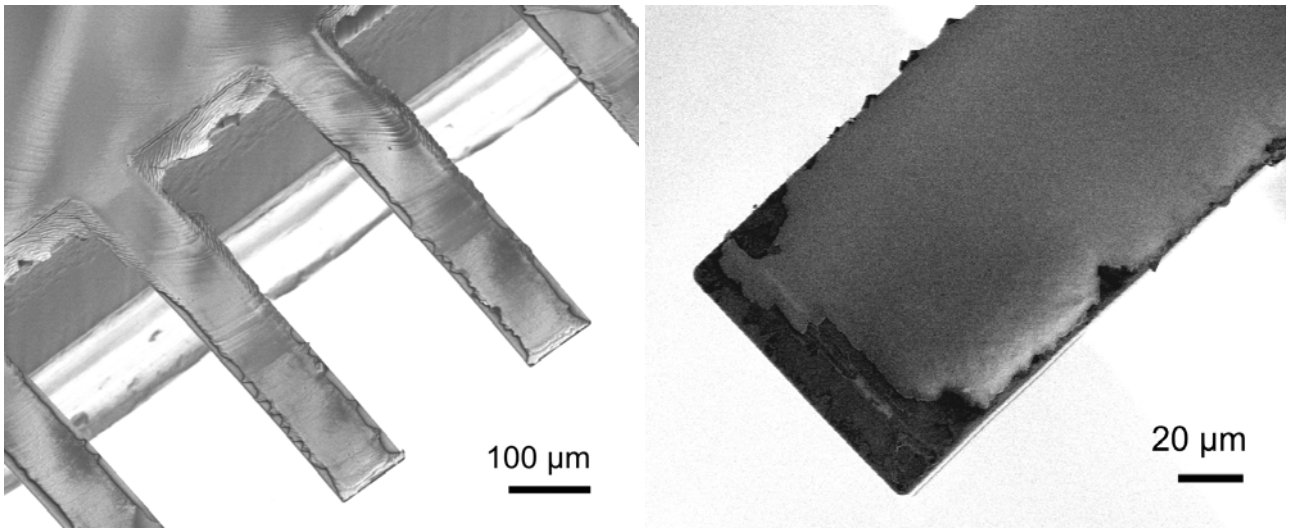

Figure 7.5-2: 5.6-µm-thick cantilevers covered with 600 nm PLLA; L = 500 µm, w = 100 µm

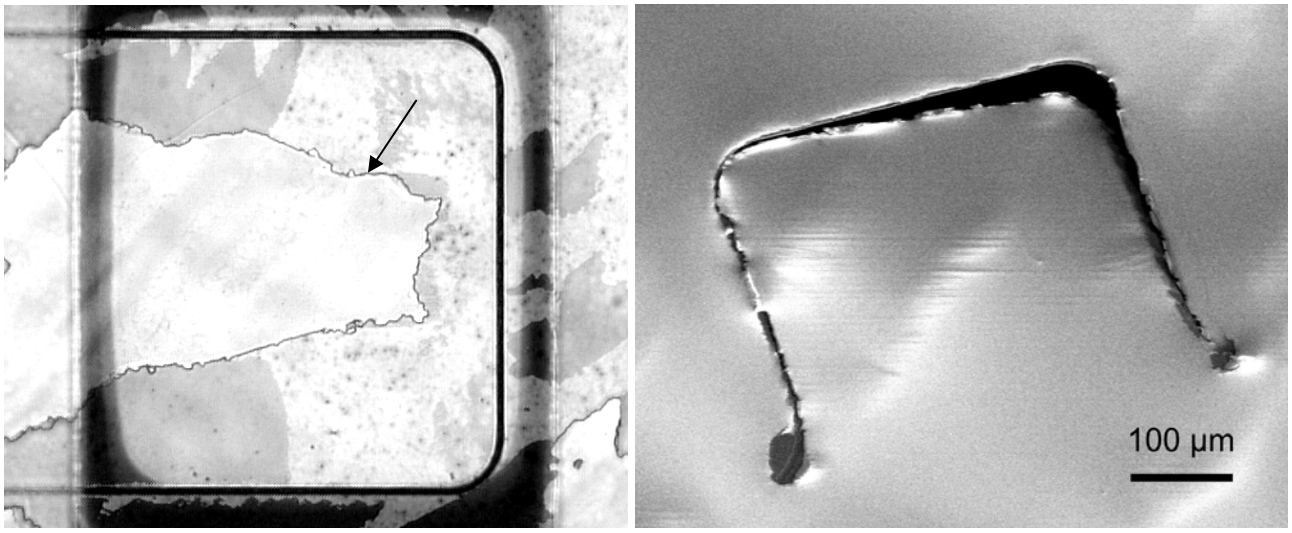

Figure 7.5-3: (a) Optical image of released SU-8 flapper partially coated with PLLA (arrow) (b) SEM-image of flapper coated with PLLA, SU-8 thickness 5.5 µm

7.5.3 Conclusion

The experiments showed that the concept of the alternative release methods presented in *Section 7.4* can be used for the fabrication of cantilevers and flappers with organic coatings. PLLA was introduced in cleanroom fabrication and the first results are promising. Further optimization of the process-integrated coating of the flapperchips with the selected polymer is required.
Alternatively, manual dispensing was used to deposit PLLA on single flapperchips. *Figure 7.5-4* shows that the flapper is coated by the biopolymer and that the flappergap is sealed. This method is suitable for coatings that are not compatible with the fabrication of the flapperchip.

A further implementation of the presented concept could lead the way for the fabrication of devices for the monitoring of enzymatic biodegradation of polymers. Possible applications are the testing of biodegradability of new polymers or the release of drugs in the human body triggered by specific enzymes.

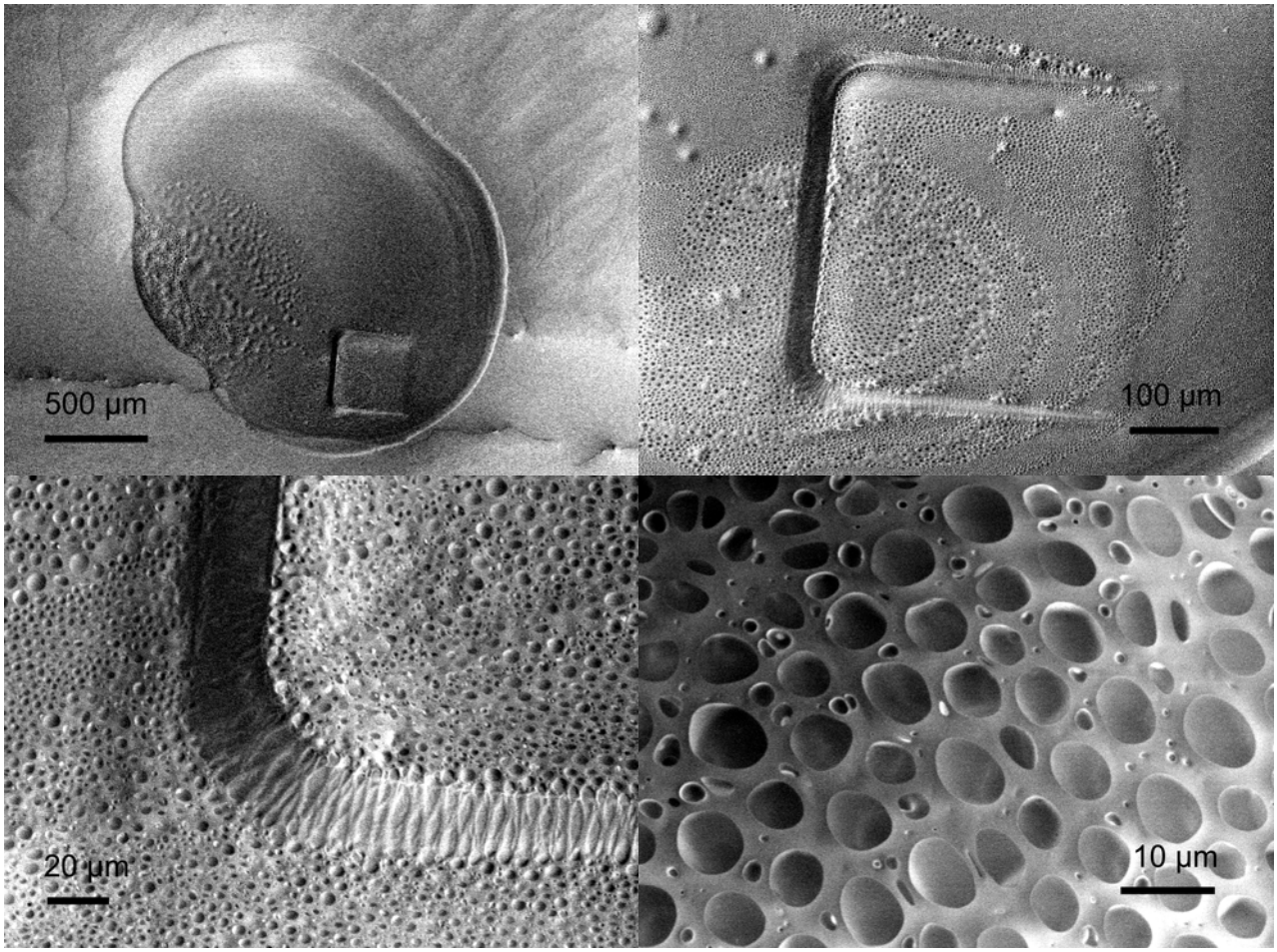

Figure 7.5-4: 5.6-µm-thick flapper after release and deposition of PLLA by dispensing

7.6 Measurement setup

The design of the microfluidic system was illustrated in *Figure 7.1-1*. In *Section 7.2* and *Section 7.3* the fabrication of the flapperchip and the bonding to the Pyrex cover were demonstrated. In collaboration with Oliver Geschke at DTU Nanotech, Marco Grünefeld fabricated a microfluidic system providing the second microfluidic channel and the microfluidic interconnections for the introduction of analyte and marker solution [175]. The assembly of the microfluidic system is illustrated in *Figure 7.6-1*.

The different parts of the setup are made of polymers and were machined with a CO_2-laser. The test system consists of a PMMA base plate with a dimension of 4x4 cm^2. On the top of the base plate, four metal pins are integrated to allow for the self-alignment of the chips. There, the PDMS with the micromachined channel is placed (*Figure 7.6-1(a)*). The PDMS ensures the sealing between SU-8 flapperchip and PMMA base plate. The flapperchip with the Pyrex cover on the top is aligned to the PDMS (*Figure 7.6-1(b)*). Finally, a cover plate is mechanically fixed with screws to ensure tight sealing of the system (*Figure 7.6-1(c)*). The cover plate was made of PMMA and had a window in

the center to improve optical read-out. Four hollow metal pins on the bottom of the base plate are used for the connection to silicone tubes (*Figure 7.6-1(d)*). For testing, these tubes can be connected to a syringe pump.
The functionality of the system was demonstrated with some test chips. A flow rate of up to 2.5 ml/min was possible without leakage even after several hours of operation. The exchange of the test chips was straightforward and could be done in a few minutes. The design of the system is modular and would allow the testing of other chips than the autonomous sensor.
A measurement setup for the characerization of the flapperchips was developed in collaboration with Danish Micro Engineering (DME, Gladsaxe, Denmark) as shown in *Figure 7.6-2(a)*. The setup is equipped with a laser for the measurement of the deflection of the flapper and with a camera for the monitoring of the colour change upon actuation. The microfluidic system was easily clamped in the setup after assembly (*Figure 7.6-2(b)*).

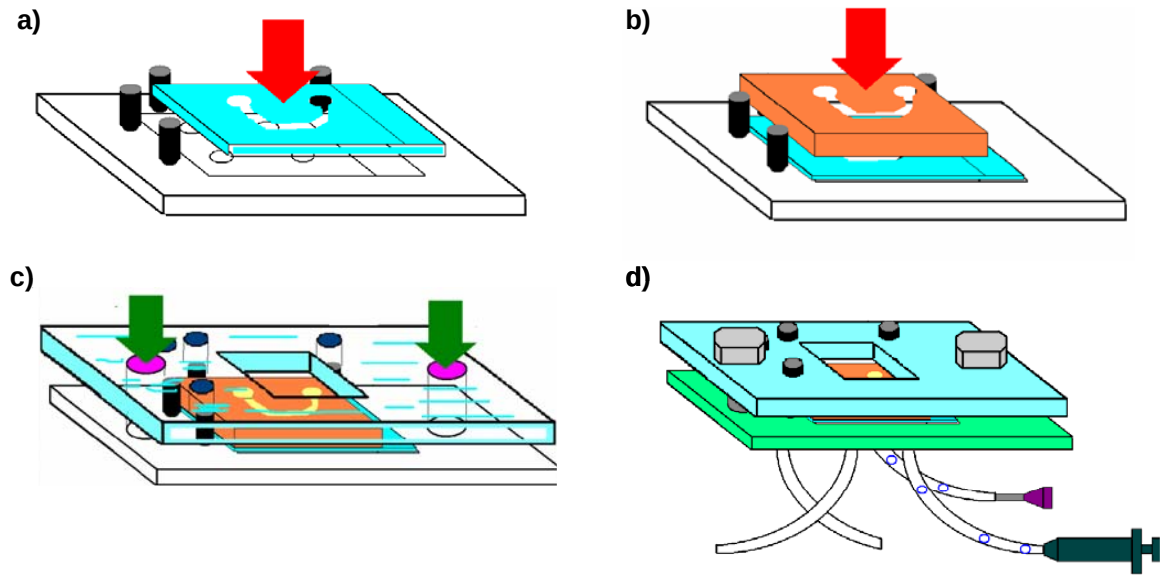

Figure 7.6-1: Assembly of microfluidic system: (a) PDMS with microchannel on PMMA base-plate; (b) Flapperchip with bonded Pyrex cover on top-side; (c) Mechanical clamping with PMMA cover-plate; (d) Microfluidic interconnection with tubes on the bottom-side

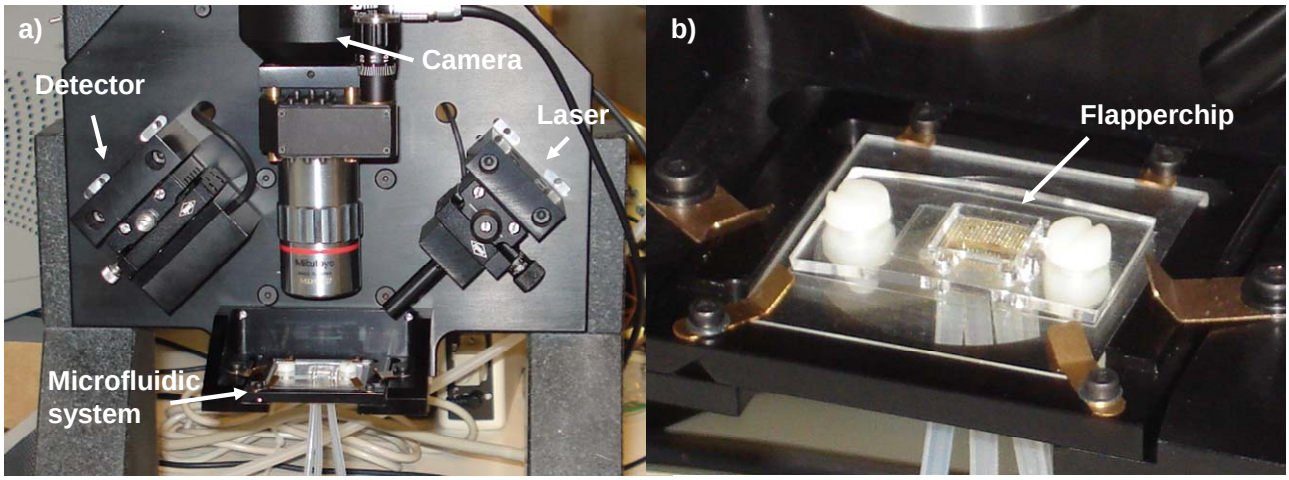

Figure 7.6-2: (a) Setup for optical read-out with laser and camera; (b) Microfluidic setup with flapperchip in the center and tubes on the bottom-side

7.7 Conclusion

The processes developed in the previous chapters were successfully implemented for the fabrication of the flapperchip. Release of flappers with a base length of 400 µm and a thickness of only 2 µm was demonstrated and the structures showed low initial bending. On the other hand, the release of the flappers is still a challenge. The adhesion of the flapperchips is increased compared to the smaller cantilevers which results in plastic deformation upon release. Furthermore, a razor blade has to be used for the removal of the large flapperchips from the substrate which results in shear forces that have a negative impact on the release yield. The implementation of alternative release methods increased the release yield but the approaches had other drawbacks.
Compared to the cantilever chips, the flapper had to be integrated in a complete microfluidic system. Two channels were required for the transport of the analyte and the coloured marker solution respectively. The first channel was fabricated with SU-8 and closed by thermal bonding in the cleanroom. There, a Pyrex substrate was used for wafer-scale bonding and release of the flapperchips. The second microfluidic channel was defined by laser machining outside the cleanroom. The two parts were easily assembled and the complete microfluidic system can be clamped in measurement setup designed for systematic testing of the autonomous actuation.
First steps towards an application were presented. The process-integrated coating of the flappers with L-polylactide was demonstrated. This polymer is biodegradable through hydrolysis or by enzymes. In near future, the testing of these devices in the described setup is planned. The proof-of-concept of an autonomous actuation of the flapper by biodegradation could lead the way for new applications in the field of material testing, food quality monitoring or controlled drug release.

8 Conclusion and Outlook

The goal of this thesis was the proof-of-concept of a cantilever-based sensor for the autonomous measurement of surface stress. A liquid channel filled with a coloured marker solution and closed by a thin polymer flapper. One surface of the device is functionalized with receptor molecules. Specific binding of analyte to the receptors results in a change of surface stress. As a consequence, the flapper bend mechanically and the marker solution is released. This colour change is detected by eye or with an optical microscope. The actuation of the device is autonomous, which means that no external energy source is required for the read-out and the actuation.

The main challenge is to achieve sufficient actuation of the flapper to release the marker solution. For cantilevers of typical dimensions, surface stress changes due to biomolecular interactions result in bending below 1 µm. For the actuation of the flapper, this value has to be increased by a reduction of the thickness of the flapper. This required optimization of the design and fabrication of the sensor. The negative epoxy photoresist SU-8 was chosen for the fabrication of the complete sensor. The advantage of this polymer compared to traditional silicon-based materials is that its Young's modulus is about 50 times lower. This allows for high actuation of cantilever-based sensors due to changes in surface stress. On the other hand, the fabrication of cantilevers with SU-8 is a challenge. Residual stress results in cracking and bending of the devices as the thickness is reduced. Further, stiction and deformation of the cantilevers is an issue using conventional wet or dry release methods.

In a first part of the thesis, the fabrication process of SU-8 cantilever chips was redesigned. A plasma-polymerized fluorocarbon coating was introduced for the dry release of polymer chips. The fluorocarbon deposition was optimized to allow spin-coating and release of thin SU-8 films. An review of publications on fabrication with SU-8 showed, that no process optimizations on thin film processing have been reported. Therefore, the influence of processing parameters on residual stress, cross-linking density, structural stability, lithographic resolution and refractive index on SU-8 films with a thickness of 2 µm was investigated in detail. Redesign of the process allowed considerable improvements in terms of cross-linking and residual stress. With the presented results, design of thin film processes based on the requirements of a specific application is possible. Here, arrays of thin SU-8 cantilevers were fabricated. Further process optimization was required to minimize out-of-plane bending of the cantilevers and to achieve high fabrication yield. The introduction of a hard-bake step improved cross-linking of the SU-8 and residual stress gradients were reduced. With the optimized process, the fabrication of arrays of 2-µm-thick SU-8 cantilevers with a length of 500 µm an initial bending of less than 20 µm was demonstrated. To the best of the author's knowledge no polymer-based cantilevers of similar characteristics have been reported before. Theoretically, these devices have the same sensitivity for surface stress measurements as silicon cantilevers of the same dimensions but with a thickness of 300 nm. Stability of the devices upon storage for several months was investigated and minimal influence was observed for devices fabricated with the optimized process. However, additional experiments on ageing should be performed.

The dry release method and the optimized SU-8 processing were used for the fabrication of cantilever chips for the measurement of surface stress with optical read-out. The chip design was adapted to the NOSE-setup achieved from the University of Basel where eight VCSELs are used for the measurement of the cantilever deflections. The reflectivity of SU-8 was insufficient for the optical read-out and the cantilever had to be coated with 50 nm Au. Two methods were investigated to achieve process-integrated metal coating of the cantilevers. Unfortunately, both approaches result

in bending of the cantilevers. This issue is solved by the replacement of the complete Au coating of the cantilevers with a small mirror pad at the apex. There, 5-µm-thick devices with a length of 500 µm were fabricated with a yield of 100% and an initial bending below 10 µm.
Additionally to their function as reflective layer, Au coatings commonly serve as anchor for the functionalization of the cantilever surface with thiol chemistry. There, the cleanliness of the Au is a critical issue. The surface contamination of the Au as a result of the different fabrication approaches was evaluated. Organic contamination of the Au was observed, in particular for Au that was in contact with the release layer during processing. Nevertheless, first surface stress measurements with Au-coated SU-8 cantilevers were possible. DNA-hybridization resulted in cantilever bending of 80 nm. Further, a photochemical method for the direct functionalization of the SU-8 was briefly discussed. This method allows for the replacement of the Au coating and solves the issues related to metal deposition and contamination. Another advantage is that wafer-scale surface functionalization can be done as an integral part of cleanroom fabrication.

Finally, the flapperchip was designed and fabricated. The fabrication and release of flappers with an area of 400x400 μm^2 and a thickness of only 2 µm was demonstrated. On the other hand, the release was challenging due to the increased size of the chips. The thin SU-8 flapper had to be integrated in a microfluidic system that allows testing of the sensor. For this purpose, a Pyrex cover was thermally bonded to the SU-8 structures. The wafer-scale release of the flapperchips bonded to the Pyrex was possible and resulted in a significant increase of the release yield. Alternative release methods combining dry and wet release steps were evaluated to further improve the fabrication yield for the flapperchips. In general, the release improved but the methods had other drawbacks. Finally, methods for coating of the flappers with a biopolymer were evaluated. Degradation of the biopolymer coating through hydrolysis or enzymes is expected to result in a high actuation of the flappers. Unfortunately, measurements with the fabricated devices were not possible in the context of this thesis.

The great versatility of SU-8 for microfabrication was demonstrated. During the experimental work related to this thesis, films with thicknesses from 500 nm - 500 µm were used for fabrication of cantilevers, membranes, chips, microchannels or even complete SU-8 wafers. The resist was further used for bonding and sealing of microfluidic system. Some general conclusions related to SU-8 processing are possible. The experiments showed that the careful control of the parameters is essential. The processes are very reproducible but at the same time quite sensitive to minimal changes. Further, one has to consider that the properties of the SU-8 might change during additional temperature cycling in the fabrication process.

In future, systematic characterization of the IBM-chips with surface stress measurements in the NOSE-setup will be performed. There, the issues of Au contamination have to be solved or ideally the Au will be replaced by the direct photochemical functionalization of the SU-8. Related to the measurements, the swelling of the polymer due to solvent absorption should be investigated. This might be a major issue for the use of SU-8 for the measurement of surface stress in liquid.

The main efforts of future work will concentrate on measurements with the flapperchips. In March 2008 a setup dedicated to the characterization of the flapperchip was achieved. The setup provides a laser beam for the optical readout of the flapper deflection and a high precision camera for the monitoring of the color change. In combination with the developed microfluidic system, this setup should allow systematic testing of the sensor concept. There, particularly the approach with the biopolymer coating will be pursued. The first step is a proof-of-concept of autonomous actuation by

degradation of a thin biopolymer film. This would open new possibilities as a large number of different biopolymers with different degradation mechanisms are available.

In conclusion, the main achievement of this thesis was the optimization of existing and new processes for the fabrication of thin cantilever-based surface stress sensors with the polymer SU-8. The efforts were directed towards the fabrication of sensor for autonomous read-out of a change in surface stress.

Bibliography

[1] G. Binnig, C. F. Quate, C. Gerber, *'Atomic Force Microscope'*, Physical Review Letters, **56** (1986) 930

[2] http://sahussain.wordpress.com/2007/11/03/can-we-see-the-atomic-dimension/, 25.03.2008

[3] J. K. Gimzewski, C. Gerber, E. Meyer, R. R. Schlittler, *'Observation of a chemical reaction using a micromechanical sensor'*, Chemical Physics Letters, **217** (1994) 589

[4] J. R. Barnes, R. J. Stephenson, M. E. Welland, C. Gerber, J. K. Gimzewski, *'Photothermal Spectroscopy with Femtojoule Sensitivity Using a Micromechanical Device'*, Nature, **372** (1994) 79

[5] T. Thundat, R. J. Warmack, G. Y. Chen, D. P. Allison, *'Thermal and ambient-induced deflections of scanning force microscope cantilevers'*, Applied Physics Letters, **64** (1994) 2894

[6] T. Thundat, G. Y. Chen, R. J. Warmack, D. P. Allison, E. A. Wachter, *'Vapor Detection Using Resonating Microcantilevers'*, Analytical Chemistry, **67** (1995) 519

[7] G. Y. Chen, T. Thundat, E. A. Wachter, R. J. Warmack, *'Adsorption-induced surface stress and its effects on resonance frequency of microcantilevers'*, Journal of Applied Physics, **77** (1995) 3618

[8] H. J. Butt, *'A sensitive method to measure changes in the surface stress of solids'*, Journal of Colloid and Interface Science, **180** (1996) 251

[9] S. J. O'Shea, M. E. Welland, T. A. Brunt, A. R. Ramadan, T. Rayment, *'Atomic force microscopy stress sensors for studies in liquids'*, Journal of Vacuum Science & Technology B: Microelectronics and Nanometer Structures, **14** (1996) 1383

[10] D. R. Baselt, G. U. Lee, R. J. Colton, *'Biosensor based on force microscope technology'*, (1996) 789

[11] H. P. Lang, R. Berger, F. Battiston, J. P. Ramseyer, E. Meyer, C. Andreoli, J. Brugger, P. Vettiger, M. Despont, T. Mezzacasa, L. Scandella, H. J. Güntherodt, C. Gerber, J. K. Gimzewski, *'A chemical sensor based on a micromechanical cantilever array for the identification of gases and vapors'*, Applied Physics A: Materials Science & Processing, **66** (1998) S61

[12] M. Tortonese, R. C. Barrett, C. F. Quate, *'Atomic resolution with an atomic force microscope using piezoresistive detection'*, Applied Physics Letters, **62** (1993) 834

[13] J. Thaysen, A. Boisen, O. Hansen, S. Bouwstra, *'Atomic force microscopy probe with piezoresistive read-out and a highly symmetrical Wheatstone bridge arrangement'*, Sensors and Actuators A: Physical, **83** (2000) 47

[14] T. Itoh, T. Suga, *'Piezoelectric force sensor for scanning force microscopy'*, Sensors and Actuators A: Physical, **43** (1994) 305

[15] P. F. Indermuhle, G. Schurmann, G. A. Racine, N. F. de Rooij, *'Fabrication and characterization of cantilevers with integrated sharp tips and piezoelectric elements for actuation and detection for parallel AFM applications'*, Sensors and Actuators A: Physical, **60** (1997) 186

[16] C. L. Britton, R. L. Jones, P. I. Oden, Z. Hu, R. J. Warmack, S. F. Smith, W. L. Bryan, J. M. Rochelle, *'Multiple-input microcantilever sensors'*, Ultramicroscopy, **82** (2000) 17

[17] D. R. Baselt, B. Fruhberger, E. Klaassen, S. Cemalovic, C. L. Britton, S. V. Patel, T. E. Mlsna, D. McCorkle, B. Warmack, *'Design and performance of a microcantilever-based hydrogen sensor'*, Sensors and Actuators B: Chemical, **88** (2003) 120

[18] N. Blanc, J. Brugger, N. F. de Rooij, U. Durig, *'Scanning force microscopy in the dynamic mode using microfabricated capacitive sensors'*, journal of Vacuum Science & Technology B: Microelectronics and Nanometer Structures, **14** (1996) 901

[19] G. Shekhawat, S.-H. Tark, V. P. Dravid, *'MOSFET-Embedded Microcantilevers for Measuring Deflection in Biomolecular Sensors'*, Science, **311** (2006) 1592

[20] R. Raiteri, H.-J. Butt, *'Measuring Electrochemically Induced Surface Stress with an Atomic Force Microscope'*, Journal of Physical Chemistry, **99** (1995) 15728

[21] R. Marie, *'Nucleic acids reactions investigated by cantilever-based sensor'*, PhD-Thesis, Technical University of Denmark, Lyngby (2003)

[22] H. P. Lang, R. Berger, C. Andreoli, J. Brugger, M. Despont, P. Vettiger, C. Gerber, J. K. Gimzewski, J. P. Ramseyer, E. Meyer, H. J. Guntherodt, *'Sequential position readout from arrays of micromechanical cantilever sensors'*, Applied Physics Letters, **72** (1998) 383

[23] M. K. Baller, H. P. Lang, J. Fritz, C. Gerber, J. K. Gimzewski, U. Drechsler, H. Rothuizen, M. Despont, P. Vettiger, F. M. Battiston, J. P. Ramseyer, P. Fornaro, E. Meyer, H. J. Guntherodt, *'A cantilever array-based artificial nose'*, Ultramicroscopy, **82** (2000) 1

[24] F. M. Battiston, J. P. Ramseyer, H. P. Lang, M. K. Baller, C. Gerber, J. K. Gimzewski, E. Meyer, H. J. Guntherodt, *'A chemical sensor based on a microfabricated cantilever array with simultaneous resonance-frequency and bending readout'*, Sensors and Actuators B: Chemical, **77** (2001) 122

[25] R. Berger, E. Delamarche, H. P. Lang, C. Gerber, J. K. Gimzewski, E. Meyer, H.-J. Guntherodt, *'Surface Stress in the Self-Assembly of Alkanethiols on Gold'*, Science, **276** (1997) 2021

[26] R. Raiteri, M. Grattarola, H.-J. Butt, P. Skladal, *'Micromechanical cantilever-based biosensors'*, Sensors and Actuators B: Chemical, **79** (2001) 115

[27] R. Raiteri, G. Nelles, H. J. Butt, W. Knoll, P. Skladal, *'Sensing of biological substances based on the bending of microfabricated cantilevers'*, Sensors and Actuators B-Chemical, **61** (1999) 213

[28] G. Wu, R. H. Datar, K. M. Hansen, T. Thundat, R. J. Cote, A. Majumdar, *'Bioassay of prostate-specific antigen (PSA) using microcantilevers'*, Nat Biotech, **19** (2001) 856

[29] J. Fritz, M. K. Baller, H. P. Lang, H. Rothuizen, P. Vettiger, E. Meyer, H.-J. Güntherodt, C. Gerber, J. K. Gimzewski, *'Translating Biomolecular Recognition into Nanomechanics'*, Science, **288** (2000) 316

[30] G. Wu, H. Ji, K. Hansen, T. Thundat, R. Datar, R. Cote, M. F. Hagan, A. K. Chakraborty, A. Majumdar, *'Origin of Nanomechanical Cantilever Motion Generated from Biomolecular Interactions'*, Proceedings of the National Academy of Sciences of the United States of America, **98** (2001) 1560

[31] K. M. Hansen, H. F. Ji, G. H. Wu, R. Datar, R. Cote, A. Majumdar, T. Thundat, *'Cantilever-based optical deflection assay for discrimination of DNA single-nucleotide mismatches'*, Analytical Chemistry, **73** (2001) 1567

[32] M. D. Antonik, N. P. Dcosta, J. H. Hoh, *'A biosensor based on micromechanical interrogation of living cells'*, Ieee Engineering in Medicine and Biology Magazine, **16** (1997) 66

[33] R. Pechmann, J. M. Kohler, W. Fritzsche, A. Schaper, T. M. Jovin, *'The Novolever: A new cantilever for scanning force microscopy microfabricated from polymeric materials'*, Review of Scientific Instruments, **65** (1994) 3702

[34] G. Genolet, J. Brugger, M. Despont, U. Drechsler, P. Vettiger, N. F. de Rooij, D. Anselmetti, *'Soft, entirely photoplastic probes for scanning force microscopy'*, Review of Scientific Instruments, **70** (1999) 2398

[35] X. Wang, K. S. Ryu, D. A. Bullen, J. Zou, H. Zhang, C. A. Mirkin, C. Liu, *'Scanning Probe Contact Printing'*, Langmuir, **19** (2003) 8951

[36] A. Gaitas, Y. B. Gianchandani, *'An experimental study of the contact mode AFM scanning capability of polyimide cantilever probes'*, Ultramicroscopy, **106** (2006) 874

[37] A. W. McFarland, M. A. Poggi, L. A. Bottomley, J. S. Colton, *'Production and characterization of polymer microcantilevers'*, Review of Scientific Instruments, **75** (2004) 2756

[38] A. W. McFarland, M. A. Poggi, L. A. Bottomley, J. S. Colton, *'Injection moulding of high aspect ratio micron-scale thickness polymeric microcantilevers'*, Nanotechnology, **15** (2004) 1628

[39] A. W. McFarland, M. A. Poggi, L. A. Bottomley, J. S. Colton, *'Injection-moulded scanning force microscopy probes'*, Nanotechnology, **16** (2005) 1249

[40] X. R. Zhang, X. Xu, *'Development of a biosensor based on laser-fabricated polymer microcantilevers'*, Applied Physics Letters, **85** (2004) 2423

[41] L. P. Lee, S. A. Berger, D. Liepmann, L. Pruitt, *'High aspect ratio polymer microstructures and cantilevers for bioMEMS using low energy ion beam and photolithography'*, Sensors and Actuators A: Physical, **71** (1998) 144

[42] J. Zou, X. Wang, D. Bullen, K. Ryu, C. Liu, C. A. Mirkin, *'A mould-and-transfer technology for fabricating scanning probe microscopy probes'*, Journal of Micromechanics and Microengineering, **14** (2004) 204

[43] M. Calleja, J. Tamayo, A. Johansson, P. Rasmussen, L. M. Lechuga, A. Boisen, *'Polymeric cantilever arrays for biosensing applications'*, Sensor Letters, **1** (2003) 20

[44] J. H. T. Ransley, M. Watari, D. Sukumaran, R. A. McKendry, A. A. Seshia, *'SU8 bio-chemical sensor microarrays'*, Microelectronic Engineering, **83** (2006) 1621

[45] T. Xu, C. Ruisheng, M. Bachman, A. G.-P. L. Guann-Pyng Li, *'Optical polymer waveguide based cantilevers for chemical and biological sensors'*, Sensors, 2005 IEEE, (2005)

[46] A. W. McFarland, J. S. Colton, *'Chemical sensing with micromolded plastic microcantilevers'*, Microelectromechanical Systems, Journal of, **14** (2005) 1375

[47] E. Manias, J. Chen, N. Fang, X. Zhang, *'Polymeric micromechanical components with tunable stiffness'*, Applied Physics Letters, **79** (2001) 1700

[48] Z. Bayindir, Y. Sun, M. J. Naughton, C. N. LaFratta, T. Baldacchini, J. T. Fourkas, J. Stewart, B. E. A. Saleh, M. C. Teich, *'Polymer microcantilevers fabricated via multiphoton absorption polymerization'*, Applied Physics Letters, **86** (2005) N.PAG

[49] M. Calleja, M. Nordstrom, M. Alvarez, J. Tamayo, L. M. Lechuga, A. Boisen, *'Highly sensitive polymer-based cantilever-sensors for DNA detection'*, Ultramicroscopy, **105** (2005) 215

[50] M. Calleja, J. Tamayo, M. Nordström, A. Boisen, *'Low-noise polymeric nanomechanical biosensors'*, Applied Physics Letters, **88** (2006)

[51] A. Boisen, *'Passive and active AFM probes - design, fabrication and characterization'*, PhD-Thesis, Technical University of Denmark, Lyngby (1997)

[52] H. Jensenius, J. Thaysen, A. A. Rasmussen, L. H. Veje, O. Hansen, A. Boisen, *'A microcantilever-based alcohol vapor sensor-application and response model'*, Applied Physics Letters, **76** (2000) 2615

[53] A. Boisen, J. Thaysen, H. Jensenius, O. Hansen, *'Environmental sensors based on micromachined cantilevers with integrated read-out'*, Ultramicroscopy, **82** (2000) 11

[54] J. Thaysen, A. D. Yalcinkaya, P. Vettiger, A. Menon, *'Polymer-based stress sensor with integrated readout'*, Journal of Physics D: Applied Physics, **35** (2002) 2698

[55] A. Johansson, *'SU-8 cantilever sensor with integrated readout'*, PhD-Thesis, Technical University of Denmark, Lyngby (2006)

[56] M. Nordström, *'Integrated optical read-out for polymeric cantilever-based sensors'*, PhD-Thesis, Technical University of Denmark, Lyngby (2007)

[57] R. Marie, H. Jensenius, J. Thaysen, C. B. Christensen, A. Boisen, *'Adsorption kinetics and mechanical properties of thiol-modified DNA-oligos on gold investigated by microcantilever sensors'*, Ultramicroscopy, **91** (2002) 29

[58] L. M. Lechuga, J. Tamayo, M. Alvarez, L. G. Carrascosa, A. Yufera, R. Doldan, E. Peralias, A. Rueda, J. A. Plaza, K. Zinoviev, C. Dominguez, A. Zaballos, M. Moreno, C. Martinez-A, D. Wenn, N. Harris, C. Bringer, V. Bardinal, T. Camps, C. Vergnenegre, C. Fontaine, V. Diaz, A. Bernad, *'A highly sensitive microsystem based on nanomechanical biosensors for genomics applications'*, Sensors and Actuators B: Chemical, **118** (2006) 2

[59] D. Haefliger, R. Marie, A. Boisen, *'Self-actuated polymeric valve for autonomous sensing and mixing'*, 13th International Conference on Solid-State Sensors and Actuators and Microsystems, TRANSDUCERS '05, Seoul, Korea, (2005) 1569

[60] A. Johansson, G. Blagoi, A. Boisen, *'Polymeric cantilever-based biosensors with integrated readout'*, Applied Physics Letters, **89** (2006) N.PAG

[61] J. D. Gelorme, R. J. Cox, S. A. R. Gutierrez, *'Photoresist composition and printed circuit boards and packages made therewith',* U.S. Patent No. 4882245 (1989)

[62] H. Lorenz, M. Despont, N. Fahrni, N. LaBianca, P. Renaud, P. Vettiger, *'SU-8: a low-cost negative resist for MEMS'*, Journal of Micromechanics and Microengineering, **7** (1997) 121

[63] M. Despont, H. Lorenz, N. Fahrni, J. Brugger, P. Renaud, P. Vettiger, *'High-aspect-ratio, ultrathick, negative-tone near-uv photoresist for MEMS applications'*, Micro Electro Mechanical Systems, 1997. MEMS '97, Proceedings, IEEE., Tenth Annual International Workshop on, (1997) 518

[64] N. LaBianca, J. D. Gelorme, K. Y. Lee, E. Cooper, E. O'Sullivan, J. Shaw, *'High aspect ratio optical resist chemistry for MEMS applications'*, Electrochemical Society Proceedings, **95-18** (1993) 386

[65] K. Y. Lee, N. LaBianca, S. A. Rishton, S. Zolgharnain, J. D. Gelorme, J. Shaw, T. H. P. Chang, *'Micromachining applications of a high resolution ultrathick photoresist'*, Journal of Vacuum Science & Technology B, **13** (1995) 3012

[66] L. J. Guerin, M. Bossel, M. Demierre, S. Calmes, P. Renaud, *'Simple and low cost fabrication of embedded micro-channels by using a new thick-film photoplastic'*, Solid State Sensors and Actuators, 1997. TRANSDUCERS '97 Chicago., 1997 International Conference on, (1997) 1419

[67] R. J. Jackman, T. M. Floyd, R. Ghodssi, M. A. Schmidt, K. F. Jensen, *'Microfluidic systems with on-line UV detection fabricated in photodefinable epoxy'*, Journal of Micromechanics and Microengineering, **11** (2001) 263

[68] K. B. Mogensen, J. El-Ali, A. Wolff, J. P. Kutter, *'Integration of Polymer Waveguides for Optical Detection in Microfabricated Chemical Analysis Systems'*, Applied Optics, **42** (2003) 4072

[69] S. Balslev, A. M. Jorgensen, B. Bilenberg, K. B. Mogensen, D. Snakenborg, O. Geschke, J. P. Kutter, A. Kristensen, *'Lab-on-a-chip with integrated optical transducers'*, Lab on a Chip, **6** (2006) 213

[70] J. D. Williams, W. Wang, *'Study on the postbaking process and the effects on UV lithography of high aspect ratio SU-8 microstructures'*, Journal of Microlithography, Microfabrication, and Microsystems, **3** (2004) 563

[71] G. Voskerician, M. S. Shive, R. S. Shawgo, H. v. Recum, J. M. Anderson, M. J. Cima, R. Langer, *'Biocompatibility and biofouling of MEMS drug delivery devices'*, Biomaterials, **24** (2003) 1959

[72] C. Friese, M. Wissmann, H. Zappe, *'Polymer-based membrane mirrors for micro-optical sensors'*, Sensors, 2003. Proceedings of IEEE, (2003) 667
[73] www.mimotec.ch, 20.04.2008
[74] M. J. Madou, '*Fundamentals of microfabrication'*, CRC Press, Boca Raton (2002)
[75] J. V. Crivello, *'The discovery and development of onium salt cationic photoinitiators'*, Journal of Polymer Science A, **37** (1999) 4241
[76] www.microchem.com, 20.04.2008
[77] www.gersteltec.ch, 20.04.2008
[78] M. Shaw, D. Nawrocki, R. Hurditch, D. Johnson, *'Improving the process capability of SU-8'*, Microsystem Technologies, **10** (2003) 1
[79] D. Johnson, Personal Communication, Lyngby (2006)
[80] J. M. Shaw, J. D. Gelorme, N. C. LaBianca, W. E. Conley, S. J. Holmes, *'Negative photoresists for optical lithography'*, IBM Journal of Research and Development, **41** (1997) 81
[81] A. Schütz, *'Untersuchungen zum Einsatz des Negativresistmaterials SU-8 in der LIGA-Technik'*, PhD-thesis, Technische Universität, Berlin (2004)
[82] G. Genolet, *'New photoplastic fabrication techniques and devices based on high aspect ratio photoresist'*, PhD-Thesis, Ecole polytechnique fédérale de Lausanne, Lausanne (2001)
[83] G. Odian, '*Principles of polymerization'*, Wiley Interscience, New York (1981)
[84] G. P. Patsis, N. Glezos, *'Probabilistic gel formation theory in negative tone chemically amplified resists used in optical and electron beam lithography'*, Journal of Vacuum Science & Technology B: Microelectronics and Nanometer Structures, **20** (2002) 1303
[85] N. Glezos, G. P. Patsis, I. Raptis, P. Argitis, M. Gentili, L. Grella, *'Application of a reaction-diffusion model for negative chemically amplified resists to determine electron-beam proximity correction parameters'*, The 40th international conference on electron, ion, and photon beam technology and nanofabrication, Atlanta, Georgia (USA), (1996) 4252
[86] T. H. Fedynyshyn, C. R. Szmanda, R. F. Blacksmith, W. E. Houck, J. C. Root, *'Relationship between resist performance and reaction order in a chemically amplified resist system'*, Proceedings of the 16th international symposium on electron, ion, and photon beams, San Diego, California (USA), (1993) 2798
[87] G. P. Patsis, N. Glezos, *'Molecular dynamics simulation of gel formation and acid diffusion in negative tone chemically amplified resists'*, Microelectronic Engineering, **46** (1999) 359
[88] A. D. Jenkins, A. Ledwith, '*Reactivity, mechanism and structure in polymer chemistry'*, Wiley Interscience, London (1974)
[89] A. L. Bogdanov, S. S. Peredkov, *'Use of SU-8 photoresist for very high aspect ratio x-ray lithography'*, Microelectronic Engineering, **53** (2000) 493
[90] C. H. Lin, G. B. Lee, B. W. Chang, G. L. Chang, *'A new fabrication process for ultra-thick microfluidic microstructures utilizing SU-8 photoresist'*, Journal of Micromechanics and Microengineering, **12** (2002) 590
[91] J. Zhang, M. B. Chan-Park, S. R. Conner, *'Effect of exposure dose on the replication fidelity and profile of very high aspect ratio microchannels in SU-8'*, Lab on a Chip, **4** (2004) 646
[92] T. A. Anhoj, A. M. Jorgensen, D. A. Zauner, J. Hubner, *'The effect of soft bake temperature on the polymerization of SU-8 photoresist'*, Journal of Micromechanics and Microengineering, **16** (2006) 1819
[93] Z. G. Ling, K. Lian, L. Jian, *'Improved patterning quality of SU-8 microstructures by optimizing the exposure parameters'*, Advances in Resist Technology and Processing XVII, Santa Clara, CA, USA, (2000) 1019
[94] T. A. Anhoj, *'Fabrication of high aspect ratio SU-8 structures for integrated spectrometers'*, PhD-Thesis, Technical University of Denmark, Lyngby (2007)

[95] G. P. Patsis, N. Glezos, E. Gogolides, *'Monte Carlo simulation of gel formation and surface and line-edge roughness in negative tone chemically amplified resists'*, Journal of Vacuum Science & Technology B: Microelectronics and Nanometer Structures, **21** (2003) 254

[96] S. Jiguet, *'Microfabrication d'objets composites fonctionnels en 3D et à haut facteur de forme, par procédés UV-LIGA et microstéréolithographie'*, Ecole polytechnique fédérale de Lausanne, Lausanne (2004)

[97] J. Zhang, K. L. Tan, G. D. Hong, L. J. Yang, H. Q. Gong, *'Polymerization optimization of SU-8 photoresist and its applications in microfluidic systems and MEMS'*, Journal of Micromechanics and Microengineering, **11** (2001) 20

[98] B. Eyre, J. Blosiu, D. Wiberg, *'Taguchi optimization for the processing of Epon SU-8 resist'*, Micro Electro Mechanical Systems, 1998. MEMS 98. Proceedings., The Eleventh Annual International Workshop on, (1998) 218

[99] H. Sang Jeen, C. Seungkeun, C. Yoonsu, M. Allen, G. S. May, *'Characterization of low-temperature SU-8 photoresist processing for MEMS applications'*, Advanced Semiconductor Manufacturing, 2004. ASMC '04. IEEE Conference and Workshop, (2004) 404

[100] R. Feng, R. J. Farris, *'Influence of processing conditions on the thermal and mechanical properties of SU8 negative photoresist coatings'*, Journal of Micromechanics and Microengineering, **13** (2003) 80

[101] K. Lian, Z.-g. Ling, C. Liu, *'Thermal stability of SU-8 fabricated microstructures as a function of photo initiator and exposure doses'*, Reliability, Testing, and Characterization of MEMS/MOEMS II, San Jose, CA, USA, (2003) 208

[102] M. Hopcroft, T. Kramer, G. Kim, K. Takashima, Y. Higo, D. Moore, J. Brugger, *'Micromechanical testing of SU-8 cantilevers'*, Fatigue & Fracture of Engineering Materials and Structures, **28** (2005) 735

[103] C. Luo, T. W. Schneider, R. C. White, J. Currie, M. Paranjape, *'A simple deflection-testing method to determine Poisson's ratio for MEMS applications'*, Journal of Micromechanics and Microengineering, **13** (2003) 129

[104] U. W. Gedde, '*Polymer physics'*, Kluwer Academic Publishers, Dordrecht (1999)

[105] H. Lorenz, M. Laudon, P. Renaud, *'Mechanical characterization of a new high-aspect-ratio near UV-photoresist'*, Microelectronic Engineering, **41-42** (1998) 371

[106] G. G. Stoney, *'The tension of metallic films deposited by electrolysis'*, Proceedings of the Royal Society London A - Materials, **82** (1909) 172

[107] S. Motahhari, J. Cameron, *'The contribution to residual stress by differential resin shrinkage'*, Journal of Reinforced Plastics and Composites, **18** (1999) 1011

[108] J. F. Gaynor, S. B. Desu, *'Stress measurement as a new technique for determining glass transition temperatures and other thermomechanical properties of polymers'*, Journal of Materials Science Letters, **13** (1994) 236

[109] S. J. Hong, S. Choi, Y. Choi, M. Allen, G. S. May, *'Characterization of low-temperature SU-8 photoresist processing for MEMS applications'*, Advanced Semiconductor Manufacturing, 2004. ASMC '04. IEEE Conference and Workshop, (2004) 404

[110] T. A. Anhoj, A. M. Jorgensen, D. A. Zauner, J. Hubner, *'Optimization of SU-8 processing for integrated optics'*, Micromachining Technology for Micro-Optics and Nano-Optics IV, San Jose, CA, USA, (2006) 611009

[111] J. Thurn, T. Hermel-Davidock, *'Thermal stress hysteresis and stress relaxation in an epoxy film'*, Journal of Materials Science, **42** (2007) 5686

[112] D. Y. Perera, *'Physical ageing of organic coatings'*, Progress in Organic Coatings, **47** (2003) 61

[113] S. Montserrat, *'Physical aging studies in epoxy resins. I. Kinetics of the enthalpy relaxation process in a fully cured epoxy resin'*, Journal of Polymer Science: Part B: Polymer Physics, **32** (1994) 509
[114] A. Lee, G. B. McKenna, *'Effect of crosslink density on physical ageing of epoxy networks'*, Polymer, **29** (1988) 1812
[115] H. Lorenz, M. Despont, N. Fahrni, J. Brugger, P. Vettiger, P. Renaud, *'High-aspect-ratio, ultrathick, negative-tone near-UV photoresist and its applications for MEMS'*, Sensors and Actuators A: Physical, **64** (1998) 33
[116] M. Nordström, *'Fabrication of cantilever chip with complementary micro channel system in SU-8 for biochemical detection'*, Master-Thesis, Technical University of Denmark, Lyngby (2004)
[117] J. Carlier, S. Arscott, V. Thomy, J. C. Fourrier, F. Caron, J. C. Camart, C. Druon, P. Tabourier, *'Integrated microfluidics based on multi-layered SU-8 for mass spectrometry analysis'*, Journal of Micromechanics and Microengineering, **14** (2004) 619
[118] S. Mouaziz, G. Boero, R. S. Popovic, J. A. B. J. Brugger, *'Polymer-based cantilevers with integrated electrodes'*, Journal of microelectromechanical Systems, **15** (2006) 890
[119] L. S. Pakula, H. Yang, H. T. M. Pham, P. J. French, P. M. Sarro, *'Fabrication of a CMOS compatible pressure sensor for harsh environments'*, Journal of Micromechanics and Microengineering, **14** (2004) 1478
[120] N. N. Noeth, Unpublished Work, Technical University of Denmark, Lyngby (2008)
[121] M. C. Cheng, A. P. Gadre, J. A. Garra, A. J. Nijdam, C. Luo, T. W. Schneider, R. C. White, J. F. Currie, M. Paranjape, *'Dry release of polymer structures with anti-sticking layer'*, Journal of Vacuum Science & Technology A: Vacuum, Surfaces, and Films, **22** (2004) 837
[122] B. J. Kim, M. Liebau, J. Huskens, D. N. Reinhoudt, J. Brugger, *'A self-assembled monolayer-assisted surface microfabrication and release technique'*, Microelectronic Engineering, **57-58** (2001) 755
[123] D. Haefliger, M. Nordstrom, P. A. Rasmussen, A. Boisen, *'Dry release of all-polymer structures'*, Microelectronic Engineering, **78-79** (2005) 88
[124] A. A. Ayon, D.-Z. Chen, R. Khanna, R. Braff, H. H. Sawin, M. A. Schmidt, *'A novel integrated MEMS process using Fluorocarbon films deposited with a Deep Reactive Ion Etching (DRIE) tool'*, Mat. Res. Soc. Symp. Proc., **605** (2000) 141
[125] C. B. Labelle, V. M. Donnelly, G. R. Bogart, R. L. Opila, A. Kornblit, *'Investigation of fluorocarbon plasma deposition from c-C[sub 4]F[sub 8] for use as passivation during deep silicon etching'*, Journal of Vacuum Science & Technology A: Vacuum, Surfaces, and Films, **22** (2004) 2500
[126] Y. X. Zhuang, A. Menon, *'Wettability and thermal stability of fluorocarbon films deposited by deep reactive ion etching'*, Journal of Vacuum Science & Technology A: Vacuum, Surfaces, and Films, **23** (2005) 434
[127] T. Shimmura, S. Soda, S. Samukawa, M. Koyanagi, K. Hane, *'Effects of fluorocarbon gas species on electrical conductivity and chemical structure of deposited polymer in SiO[sub 2] etching processes'*, Journal of Vacuum Science & Technology B: Microelectronics and Nanometer Structures, **22** (2004) 533
[128] D. K. Owens, R. C. Wendt, *'Estimation of Surface Free Energy of Polymers'*, Journal of Applied Polymer Science, **13** (1969) 1741
[129] D. H. Kaelble, K. C. Uy, *'A Reinterpretation of Organic Liquid-Polytetrafluoroethylene Surface Interactions'*, Journal of Adhesion, **2** (1970) 50
[130] W. Rabel, *'Einige Aspekte der Benetzungstheorie und ihre Anwendung auf die Untersuchung und Veraenderung der Oberflaecheneigenschaften von Polymeren'*, Farbe und Lack, **77** (1971) 997

[131] N. Amyot, J. E. Klembergsapieha, M. R. Wertheimer, Y. Segui, M. Moisan, *'Electrical and Structural Studies of Plasma-Polymerized Fluorocarbon Films'*, Ieee Transactions on Electrical Insulation, **27** (1992) 1101
[132] F. C. Mbende, J. Nagstrup, A. Lei, *'Fabrication of metal-coated polymer cantilevers by dry release method'*, 3-week-project, DTU, Lyngby (2007)
[133] R. Bhushan, *'Design and fabrication of microcantilevers for external magnetic actuation'*, Master, Technical University of Denmark, Lyngby (2007)
[134] M. Uddin, H. Chan, C. Chow, Y. Chan, *'Effect of spin coating on the curing rate of epoxy adhesive for the fabrication of a polymer optical waveguide'*, Journal of Electronic Materials, **33** (2004) 224
[135] S. K. Rath, F. Y. C. Boey, M. J. M. Abadie, *'Cationic electron-beam curing of a high-functionality epoxy: effect of post-curing on glass transition and conversion'*, Polymer International, **53** (2004) 857
[136] T. L. Tan, D. Wong, P. Lee, R. S. Rawat, A. Patran, *'Study of a Chemically Amplified Resist for X-ray Lithography by Fourier Transform Infrared Spectroscopy'*, Applied Spectroscopy, **58** (2004) 1288
[137] V. M. Parikh, '*Absorption spectroscopy of organic molecules'*, Addison - Wesley Publishing Menlo Park (1974)
[138] www.sigma-aldrich.com, 22.04.2008
[139] B. H. Ong, X. Yuan, S. C. Tjin, *'Adjustable refractive index modulation for a waveguide with SU-8 photoresist by dual-UV exposure lithography'*, Applied Optics, **45** (2006) 8036
[140] D. Sameoto, S. H. Tsang, I. G. Foulds, S. W. Lee, M. Parameswaran, *'Control of the out-of-plane curvature in SU-8 compliant microstructures by exposure dose and baking times'*, Journal of Micromechanics and Microengineering, **17** (2007) 1093
[141] H. P. Lang, M. K. Baller, R. Berger, C. Gerber, J. K. Gimzewski, F. M. Battiston, P. Fornaro, J. P. Ramseyer, E. Meyer, H. J. Guntherodt, *'An artificial nose based on a micromechanical cantilever array'*, Analytica Chimica Acta, **393** (1999) 59
[142] Images are courtesy of the University of Basel, Switzerland
[143] C. Martin, A. Llobera, A. Voigt, G. Gruetzner, G. Abadal, F. Perez-Murano, *'Opto-thermal actuation in microcantilevers made of double polymer layer'*, 33rd Int. Conference on Micro- and Nano-Engineering, Copenhagen, (2007)
[144] D. Haefliger, O. Hansen, A. Boisen, *'Self-Positioning of Polymer Membranes Driven by Thermomechanically Induced Plastic Deformation'*, Advanced Materials, **18** (2006) 238
[145] D. Haefliger, A. Boisen, *'Three-dimensional microfabrication in negative resist using printed masks'*, Journal of Micromechanics and Microengineering, **16** (2006) 951
[146] G. R. J. Artus, S. Jung, J. Zimmermann, H. P. Gautschi, K. Marquardt, S. Seeger, *Silicone Nanofilaments and Their Application as Superhydrophobic Coatings*, in A. Materials, ed., 2006, pp. 2758.
[147] T. Smith, *'The hydrophilic nature of a clean gold surface'*, Journal of Colloid and Interface Science, **75** (1980) 51
[148] T. Cha, A. Guo, X.-Y. Zhu, *'Enzymatic activity on a chip: The critical role of protein orientation'*, Proteomics, **5** (2005) 416
[149] A. Ulman, *'Formation and Structure of Self-Assembled Monolayers'*, Chemical Reviews, **96** (1996) 1533
[150] H. H. Weetall, K. Mosbach, *'Covalent coupling methods for inorganic support materials'*, Methods in Enzymology, **44** (1976) 134
[151] C. M. Halliwell, A. E. G. Cass, *'A Factorial Analysis of Silanization Conditions for the Immobilization of Oligonucleotides on Glass Surfaces'*, Analytical Chemistry, **73** (2001) 2476

[152] M. Joshi, R. Pinto, V. R. Rao, S. Mukherji, *'Silanization and antibody immobilization on SU-8'*, Applied Surface Science, **253** (2007) 3127
[153] L. H. Dubois, R. G. Nuzzo, *'Synthesis, Structure, and Properties of Model Organic Surfaces'*, Annual Review of Physical Chemistry, **43** (1992) 437
[154] J. C. Love, L. A. Estroff, J. K. Kriebel, R. G. Nuzzo, G. M. Whitesides, *'Self-Assembled Monolayers of Thiolates on Metals as a Form of Nanotechnology'*, Chemical Reviews, **105** (2005) 1103
[155] V. Tabard-Cossa, M. Godin, I. J. Burgess, T. Monga, R. B. Lennox, P. Grutter, *'Microcantilever-Based Sensors: Effect of Morphology, Adhesion, and Cleanliness of the Sensing Surface on Surface Stress'*, Analytical Chemistry, **79** (2007) 8136
[156] Y. Wang, M. Bachman, C. E. Sims, G. P. Li, N. L. Allbritton, *'Simple Photografting Method to Chemically Modify and Micropattern the Surface of SU-8 Photoresist'*, Langmuir, **22** (2006) 2719
[157] G. Blagoi, S. Keller, F. Persson, A. Boisen, M. H. Jakobsen, *'Photochemical modification and patterning of SU-8 using antraquinone photolinkers'*, to be published (2008)
[158] D. Dankbar, G. Gauglitz, *'A study on photolinkers used for biomolecule attachment to polymer surfaces'*, Analytical and Bioanalytical Chemistry, **386** (2006) 1967
[159] R. McKendry, J. Zhang, Y. Arntz, T. Strunz, M. Hegner, H. P. Lang, M. K. Baller, U. Certa, E. Meyer, H.-J. Guntherodt, C. Gerber, *'Multiple Label-Free Biodetection and Quantitative DNA-Binding Assays on a Nanomechanical Cantilever Array'*, Proceedings of the National Academy of Sciences of the United States of America, **99** (2002) 9783
[160] P. G. Datskos, N. V. Lavrik, S. Rajic, *'Performance of uncooled microcantilever thermal detectors'*, Review of Scientific Instruments, **75** (2004) 1134
[161] S. Li, C. B. Freidhoff, R. M. Young, R. Ghodssi, *'Fabrication of micronozzles using low-temperature wafer-level bonding with SU-8'*, Journal of Micromechanics and Microengineering, **13** (2003) 732
[162] F. J. Blanco, M. Agirregabiria, J. Garcia, J. Berganzo, M. Tijero, M. T. Arroyo, J. M. Ruano, I. Aramburu, K. Mayora, *'Novel three-dimensional embedded SU-8 microchannels fabricated using a low temperature full wafer adhesive bonding'*, Journal of Micromechanics and Microengineering, **14** (2004) 1047
[163] P. Abgrall, C. Lattes, V. Conedera, X. Dollat, S. Colin, A. M. Gue, *'A novel fabrication method of flexible and monolithic 3D microfluidic structures using lamination of SU-8 films'*, Journal of Micromechanics and Microengineering, **16** (2006) 113
[164] Y. Song, C. S. S. R. Kumar, J. Hormes, *'Fabrication of an SU-8 based microfluidic reactor on a PEEK substrate sealed by a 'flexible semi-solid transfer' (FST) process'*, Journal of Micromechanics and Microengineering, **14** (2004) 932
[165] L. Dellmann, S. Roth, C. Beuret, G. A. Racine, H. Lorenz, M. Despont, P. Renaud, P. Vettiger, N. F. de Rooij, *'Fabrication process of high aspect ratio elastic and SU-8 structures for piezoelectric motor applications'*, Sensors and Actuators A: Physical, **70** (1998) 42
[166] C. Luo, A. Govindaraju, J. Garra, T. Schneider, R. White, J. Currie, M. Paranjape, *'Releasing SU-8 structures using polystyrene as a sacrificial material'*, Sensors and Actuators A: Physical, **114** (2004) 123
[167] D. Sameoto, S.-H. Tsang, M. Parameswaran, *'Polymer MEMS processing for multi-user applications'*, Sensors and Actuators A: Physical, **134** (2007) 457
[168] C. Jeppesen, *'Optically actuated cantilevers'*, Master, Technical University of Denmark, Lyngby (2008)
[169] A. Johansson, *'SU-8 cantilever platform for biowire'*, Master-Thesis, Technical University of Denmark, Lyngby (2003)

[170] *'Handbook of biodegradable polymers'*, Ed. C. Bastioli, Rapra Technology Ltd., Shawbury (2005).
[171] T. Hayashi, *'Biodegradable Polymers for Biomedical Uses'*, Progress in Polymer Science, **19** (1994) 663
[172] M. Vert, G. Schwarch, J. Coudane, *'Present and Future of PLA Polymers'*, Journal of Macromolecular Science-Pure and Applied Chemistry, **A32** (1995) 787
[173] J. Lunt, *'Large-scale production, properties and commercial applications of polylactic acid polymers'*, Polymer Degradation and Stability, **59** (1998) 145
[174] M. S. Reeve, S. P. McCarthy, M. J. Downey, R. A. Gross, *'Polylactide stereochemistry: effect on enzymic degradability'*, Macromolecules, **27** (1994) 825
[175] M. Grünefeld, *'Fabrication of a test device for a fluid cell'*, Microsystems Project, Technical University of Denmark, Lyngby (2008)

Appendix A

Polymerization
of negative
epoxy-photoresist SU-8

A. Photopolymerization of SU-8

A chemically amplified epoxy resin like SU-8 polymerizes by cationic polymerization. Three steps can be identified:

1. Photoinitiation
2. Polymerization
3. Termination

In the following sections each of the three steps is discussed.

A.1. Photoinitiation

The actual mechanism of initiation of polymerization using an onium salt as photoinitiator is quite complex [1]. The photoactive cation PA^+ of the onium salt is excited upon exposure to radiation (see *Equation A.1-1*). The excited cation is decomposed and free radical, cationic and cation-radical fragments are formed simultaneously. These photolysis-products are highly reactive species and react therefore further with other resin components (R) to give protonic acids (Brønsted-acids) and other byproducts (R') (see *Equation A.1-2*). Therefore, the whole mechanism is also called a photoacid-generation.

$$PA^+MtX_n^- \xrightarrow{h\nu} [PA^+MtX_n^-]^* \qquad \text{(A.1-1)}$$

$$[PA^+MtX_n^-]^* + R \longrightarrow HMtX_n + R' \qquad \text{(A.1-2)}$$

The composition and the stability of the metal halide anion MtX_n^- determine the strength of the acid resulting of the photolysis and therefore its efficiency as an initiator of the polymerization. *Figure A.1-1* identifies the critical functions that can be assigned to the anion and the cation portion in an onium salt photoinitiator.

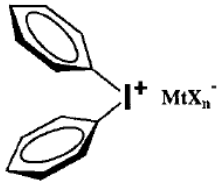

CATION	ANION
DETERMINES PHOTOCHEMISTRY	DETERMINES POLYMER CHEMISTRY
λ_{max}	acid strength
molar absorption coefficient	nucleophilicity (ion pairing)
quantum yield	anion stability
photosensitization	initiation efficiency
thermal stability	propagation rate constants

Figure A.1-1: Anatomy of an onium salt photoinitiator[1]

The formed protonic acids should be strong, shifting the equilibrium in *Equation A.1-3* to the deprotonized state:

$$HMtX_n \longleftrightarrow H^+ + MtX_n^- \qquad \text{(A.1-3)}$$

Triarylsulfonium-Hexafluoroantimonium salt is used as photoinitiator in SU-8. Therefore, *Equation A.1-1* becomes:

$$Ar_3S^+SbF_6^- \xrightarrow{h\nu} [Ar_3S^+SbF_6^-]^* \qquad \text{(A.1-4)}$$

Ar represents the aryl-groups on the photochemically active cation. Crivello identifies a homolytic (*Equation A.1-5*) and a heterolytic (*Equation A.1-6*) cleavage reaction from this excited state, where the heterolytic cleavage pathway is dominant [1]:

$$[Ar_3S^+SbF_6^-]^* \longrightarrow Ar_2S^{\cdot +}SbF_6^- + Ar^{\cdot} \qquad \text{(A.1-5)}$$

$$[Ar_3S^+SbF_6^-]^* \longrightarrow Ar_2S + Ar^+SbF_6^- \qquad \text{(A.1-6)}$$

Both pathways are summarized in an equation similar to *Equation A.1-3* resulting in a strong acid and reaction byproducts:

$$[Ar_3S^+SbF_6^-]^* + R \longrightarrow HSbF_6 + R' \qquad \text{(A.1-7)}$$

As mentioned above, the high stability of the anion SbF_6^- is decisive for the efficiency of initiation.

In summary, the critical conditions for a successful photo-initiation are:

- The intensity I_a absorbed by the photoactive cation PA^+ at the chosen wavelength has to be high enough to form reactive species
- The concentration and the reactivity of the formed species and the stability of the anions has to be sufficient to generate a high concentration of catalytic protons

A.2. Polymerization

As the actual initiation step of the cationic polymerization the catalytic protons resulting of the photoinitiation will interact with the monomer M by delocalisation of a π-electron and a positive charge is formed on the monomer:

$$H^+ MtX_n^- + M \longrightarrow HM^+ MtX_n^- \qquad \text{(A.2-1)}$$

The cationic polymerization takes place by chain propagation at the polymer cation that was formed as a result of *Equation A.2-1*. The positive charge on the monomer M is a site for further electron delocalization on epoxy groups of other monomers. This leads to the formation of a polymer chain:

$$HM^+ MtX_n^- + nM \longrightarrow HM_nM^+ MtX_n^- \qquad \text{(A.2-2)}$$

In case of the SU-8, the catalytic protons are attacking the oxygen of the epoxy-groups on the SU-8 monomer, which are partially negatively charged due to the free electron pairs. The epoxy-ring is opened and a positive charge is formed on the carbon atom [2]:

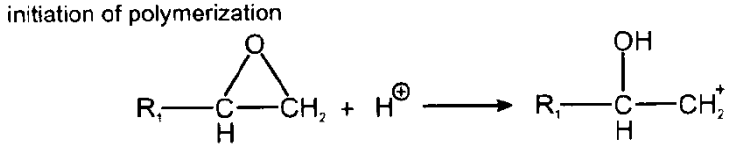

(A.2-3)

The non-saturated carbon of the opened ring on the carbo-cation is place for further polymerization. The addition of monomers according to *Equation A.2-2* leads to cross-linking through the formation of ether-bindings [2]:

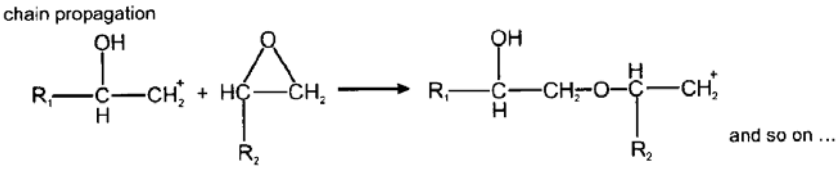

(A.2-4)

The cross-linking leads to the formation of polymer clusters and finally to a gel state.

A.3. Termination

Termination of the propagating chain occurs by reaction with anions, solvent molecules or other species present in the reaction system but it never involves the reaction with another carbocation [3]. It is also possible that a reaction which terminates the growth of a propagating chain can generate a new propagating species (see *Equation A.3-1*). The following mechanisms are most common:

Chain transfer reaction (proton transfer to a monomer molecule):

$$HM_nM^+\ MtX_n^- + M \longrightarrow M_{n+1} + HM^+\ MtX_n^- \qquad \text{(A.3-1)}$$

Spontaneous termination (regeneration of initial protonic acid):

$$HM_nM^+\ MtX_n^- \longrightarrow M_{n+1} + H^+\ MtX_n^- \qquad \text{(A.3-2)}$$

For these two reactions the kinetic chain is not terminated since a new propagating species is regenerated.

Cation-anion recombination (covalent bond):

$$HM_nM^+\ MtX_n^- \longrightarrow HM_nM\ MtX_n \qquad \text{(A.3-3)}$$

If the anion is a strong nucleophile, then subsequent reaction with the carbo-cation will take more rapidly than further reactions with monomers and the termination described in *Equation A.3-3* will

be dominant. This shows that the use of cationic initiators with highly stable anions reduces termination processes and allows cationic polymerization to proceed under ambient conditions.

[1] J. V. Crivello, *'The discovery and development of onium salt cationic photoinitiators'*, Journal of Polymer Science A, **37** (1999) 4241

[2] G. Genolet, J. Brugger, M. Despont, U. Drechsler, P. Vettiger, N. F. de Rooij, D. Anselmetti, *'Soft, entirely photoplastic probes for scanning force microscopy'*, Review of Scientific Instruments, **70** (1999) 2398

[3] G. Odian, '*Principles of polymerization'*, Wiley Interscience, New York (1981)

Appendix B

Fabrication of
thin SU-8 cantilevers

Process: **Process A**
Operator: **Stephan Keller**
Last revision: **30.04.2008**
Substrates: **Silicon <100>, 100mm, 525µm, single side**
Description: **Conventional fabrication of thin SU-8 cantilevers**

Step Nº	Description	Equipment	Program/Parameters	Target	Remarks
1	RELEASE COATING WITH FLUOROCARBON				
1.1	Stock out				
1.2	C4F8-passivation	Z2/ASE	wettef2 (120sccm, 350W, 0W, 60mTorr, 60s)		
2	SU-8 FIRST LAYER SPINNING				
2.1	SU-8 spin-coating	Z3/KS Spinner	1500rpm, 30s, 5000rpm/s	2 µm	SU-8 2002
2.2	SU-8 soft-bake	Z3/Hotplate	10 min, 60ºC, 10ºC/min; 10 min, 90ºC, 10ºC/min		
3	SU-8 FIRST LAYER PHOTOLITHOGRAPHY - PROCESS A				
3.1	SU-8 exposure	Z3/KS Aligner	2x250 mJ/cm2, HC		Cantilevers
3.2	Post-exposure bake	Z3/Hotplate	10 min, 60ºC, 10ºC/min; 10 min, 90ºC, 10ºC/min		
3.3	SU-8 development	Z3/Developer	2 min FIRST, 2 min FINAL		PGMEA
3.4	Rinse	Z3/Developer	Isopropanol, Air dry		
4	SU-8 SECOND LAYER SPINNING - PROCESS A*				
4.1	SU-8 spin-coating	Z3/KS Spinner	500rpm, 15s, 100rpm/s; 1000rpm, 30s, 200rpm/s	150µm	SU-8 2075, 8s, 42psi
4.2	SU-8 soft-bake	Z3/Hotplate	30 min, 60ºC, 10ºC/min; 60 min, 90ºC, 10ºC/min		
5	SU-8 SECOND LAYER PHOTOLITHOGRAPHY				
5.1	SU-8 exposure	Z3/KS Aligner	6x300mJ/cm2, sub 800µm, al 150µm, exp 150µm		GlobalWEC, Prox
5.2	SU-8 soft-bake	Z3/Hotplate	30 min, 60ºC, 10ºC/min; 60 min, 90ºC, 10ºC/min		
5.3	SU-8 development	Z3/Developer	15 min FIRST, 15 min FINAL		PGMEA
5.4	Rinse	Z3/Developer	Isopropanol, Air dry		
6	RELEASE				
6.1.	Dry release	manual			
6.2	Release-yield	Optical µscope			
6.3	SEM inspection	SEM-FEI			

Process: **Process B**
Operator: **Stephan Keller**
Last revision: **30.04.2008**
Substrates: **Silicon <100>, 100mm, 525µm, single side**
Description: **Optimized processing of thin SU-8 films**

Step Nº	Description	Equipment	Program/Parameters	Target	Remarks
2	SU-8 FIRST LAYER SPINNING				
2.1a	SU-8 spin-coating	Z3/KS Spinner	1500rpm, 30s, 5000rpm/s	2µm	SU-8 2002
2.2a	SU-8 solvent evap.		30 min		
3	SU-8 FIRST LAYER PHOTOLITHOGRAPHY - PROCESS B				
3.1	SU-8 exposure	Z3/KS Aligner	250-500 mJ/cm2, HC		
3.2	Post-exposure bake	Z3/Hotplate	1h, 50ºC, 2ºC/min		
3.3	SU-8 development	Z3/Developer	2 min FIRST, 2 min FINAL		PGMEA
3.4	Rinse	Z3/Developer	Isopropanol, Air dry		

Process: **Process C**
Operator: **Stephan Keller**
Last revision: **30.04.2008**
Substrates: **Silicon <100>, 100mm, 525µm, single side**
Description: **Optimized fabrication of thin SU-8 cantilevers**

Step Nº	Description	Equipment	Program/Parameters	Target	Remarks
1	RELEASE COATING WITH FLUOROCARBON				
1.1	Stock out				
1.2	C4F8-passivation	Z2/ASE	wettef2 (120sccm, 350W, 0W, 60mTorr, 60s)		
2	SU-8 FIRST LAYER SPINNING				
2.1a	SU-8 spin-coating	Z3/KS Spinner	1500rpm, 30s, 5000rpm/s	2µm	SU-8 2002
2.1b	SU-8 spin-coating	Z3/KS Spinner	2000rpm, 30s, 5000rpm/s	5.5µm	SU-8 2005
2.2a	SU-8 solvent evap.		30 min		
2.2b	SU-8 solvent evap.		2h		
3	SU-8 FIRST LAYER PHOTOLITHOGRAPHY - PROCESS C				
3.1	SU-8 exposure	Z3/KS Aligner	2x250 mJ/cm2, HC		Cantilevers
3.2	Post-exposure bake	Z3/Hotplate	1h, 50ºC, 2ºC/min		
3.3	SU-8 development	Z3/Developer	2 min FIRST, 2 min FINAL		PGMEA
3.4	Rinse	Z3/Developer	Isopropanol, Air dry 1h		
3.5	2nd exposure	Z3/KS Aligner	500mJ/cm2, FE		
3.6	Hard-bake	Z3/Oven	15h, 90ºC		over night
4	SU-8 SECOND LAYER SPINNING - PROCESS C*				
4.1	SU-8 spin-coating	Z3/KS Spinner	400rpm, 30s, 100rpm/s; 800rpm, 60s, 100rpm/s	185µm	SU-8 2075, 8s, 42psi
4.2	SU-8 soft-bake	Z3/Hotplate	10h, 50ºC, 2ºC/min		
5	SU-8 SECOND LAYER PHOTOLITHOGRAPHY				
5.1	SU-8 exposure	Z3/KS Aligner	6x300mJ/cm2, sub 750µm, al 100µm, exp 80µm		GlobalWEC, Prox
5.2	Post-exposure bake	Z3/Hotplate	10h, 50ºC, 2ºC/min		
5.3	SU-8 development	Z3/Developer	15 min FIRST, 15 min FINAL		PGMEA
5.4	Rinse	Z3/Developer	Isopropanol, Air		
6	RELEASE				
6.1	Dry release	manual			
6.2	Release-yield	Optical µscope			
6.3	SEM inspection	SEM-FEI			

Appendix C

Fabrication of
the IBM-chips

Project: **Fabrication of IBM-chips - No metal**
Operator: **Stephan Keller**
Last revision: **30.04.2008**
Substrates: **Silicon <100>, 100mm, 525µm, single side**
Description: **Pure SU-8 cantilevers (Section 6.3)**

Step Nº	Description	Equipment	Program/Parameters	Target	Remarks
1	RELEASE COATING WITH FLUOROCARBON				
1.1	Stock out				
1.2	C4F8-passivation	Z2/ASE	wet_tef2 (120sccm, 350W, 0W, 60mTorr, 60s)		
2	SU-8 FIRST LAYER SPINNING				
2.1	SU-8 spin-coating	Z3/KS Spinner	2000rpm, 30s, 5000rpm/s	5,5 µm	SU-8 2005
2.2	Solvent evaporation		2h		
3	SU-8 FIRST LAYER PHOTOLITHOGRAPHY				
3.1	SU-8 exposure	Z3/KS Aligner	2x250mJ/cm2, SC		mask cantilever
3.2	Post-exposure bake	Z3/Hotplate	1h, 50ºC, 2ºC/min		
3.3	SU-8 development	Z3/Developer	2 min FIRST, 2 min FINAL		PGMEA
3.4	Rinse	Z3/Developer	Isopropanol, Air-drying 1h		
3.5	2nd exposure	Z3/KS Aligner	500mJ/cm2, FE		
3.6	Hard-bake	Z3/Oven	15h, 120ºC		
4	SU-8 SECOND LAYER SPINNING				
4.1	SU-8 spin-coating	Z3/KS Spinner	1000rpm, 30s, 200rpm/s; 3000 rpm, 120s, 400rpm/s	30 µm	SU-8 2075, 6s, 42psi
4.2	SU-8 soft-bake	Z3/Hotplate	2h, 50ºC, 2ºC/min		
5	SU-8 SECOND LAYER PHOTOLITHOGRAPHY				
5.1	SU-8 exposure	Z3/KS Aligner	3x333mJ/cm2, SC		mask body chip extra
5.2	Post-exposure bake	Z3/Hotplate	6h, 50ºC, 2ºC/min		
5.3	SU-8 development	Z3/Developer	5 min FIRST, 5 min FINAL		PGMEA
5.4	Rinse	Z3/Developer			
6	SU-8 THIRD LAYER SPINNING				
6.1	SU-8 spin-coating	Z3/KS Spinner	300rpm, 30s, 100rpm/s; 600 rpm, 60s, 100rpm/s		Gyrset, SU-8 2075
6.2	SU-8 soft-bake	Z3/Hotplate	6h, 50ºC, 2ºC/min		
6.3	SU-8 spin-coating II	Z3/KS Spinner	300rpm, 30s, 100rpm/s; 600 rpm, 60s, 100rpm/s	500 µm	Gyrset, SU-8 2075
6.4	SU-8 soft-bake II	Z3/Hotplate	12h, 50ºC, 2ºC/min		
7	SU-8 THIRD LAYER PHOTOLITHOGRAPHY				
7.1	SU-8 exposure	Z3/KS Aligner	8x338mJ/cm2, sub 1000µm, al 200µm, exp 150µm		GlobalWEC, Prox
7.2	Post-exposure bake	Z3/Hotplate	10h, 50ºC, 2ºC/min		
7.3	SU-8 development	Z3/Developer	20 min FIRST, 20 min FINAL		PGMEA
7.4	Rinse	Z3/Developer	Isopropanol, Air-drying		
8	RELEASE				
8.1	Dry release	manual			
8.2	Optical inspection	Z3/Microscope			
8.3	SEM inspection	SEM-FEI			

Project: **Fabrication of IBM-chips - Metal coating A**
Operator: **Stephan Keller**
Last revision: **30.04.2008**
Substrates: **Silicon <100>, 100mm, 525µm, single side**
Description: **Metal lift-off after processing of the thin SU-8 film (Section 6.4.1)**

Step Nº	Description	Equipment	Program/Parameters	Target	Remarks
1	RELEASE COATING WITH FLUOROCARBON				
1.1	Stock out				
1.2	C4F8-passivation	Z2/ASE	dry_tef2 (120sccm, 300W, 0W, 5mTorr, 60s)		
2	SU-8 FIRST LAYER SPINNING				
2.1	SU-8 spin-coating	Z3/KS Spinner	2000rpm, 30s, 5000rpm/s	5,5 µm	SU-8 2005
2.2	Solvent evaporation		2h		
3	SU-8 FIRST LAYER PHOTOLITHOGRAPHY				
3.1	SU-8 exposure	Z3/KS Aligner	2x250mJ/cm2, SC		mask cantilever
3.2	Post-exposure bake	Z3/Hotplate	1h, 50ºC, 2ºC/min		
3.3	SU-8 development	Z3/Developer	2 min FIRST, 2 min FINAL		PGMEA
3.4	Rinse	Z3/Developer	Isopropanol, Air-drying 1h		
3.5	2nd exposure	Z3/KS Aligner	500mJ/cm2, FE		
3.6	Hard-bake	Z3/Oven	15h, 120ºC		
4	METAL DEPOSITION AND LIFT-OFF				
4.1	AZ spin-coating	Z3/Track1	PR2_2.rcp; AZ5214e; bake at 90ºC	2,2 µm	
4.2	AZ exposure	Z3/KS Aligner	91mJ/cm2, HC	res. 3 µm	mask metallization
4.3	AZ development	Z3/Developer	70s, 3min H2O-rinse		
4.4	Optical inspection	Z3/µscope			
4.5	Metal deposition	Z2/Alcatel	5nm Ti; 50nm Au; deposition rate 5Å/s		
4.6	Lift-off	Z4/Lift-off bench	20 min with U-sound pulses		
4.7	Optical inspection	Z3/µscope			

5	SU-8 SECOND LAYER SPINNING				
5.1	SU-8 spin-coating	Z3/KS Spinner	1000rpm, 30s, 200rpm/s; 3000 rpm, 120s, 400rpm/s	30 µm	SU-8 2075, 6s, 42psi
5.2	SU-8 soft-bake	Z3/Hotplate	2h, 50ºC, 2ºC/min		
6	SU-8 SECOND LAYER PHOTOLITHOGRAPHY				
6.1	SU-8 exposure	Z3/KS Aligner	3x333mJ/cm2, SC		mask body chip extra
6.2	Post-exposure bake	Z3/Hotplate	6h, 50ºC, 2ºC/min		
6.3	SU-8 development	Z3/Developer	5 min FIRST, 5 min FINAL		PGMEA
6.4	Rinse	Z3/Developer			
7	SU-8 THIRD LAYER SPINNING				
7.1	SU-8 spin-coating	Z3/KS Spinner	300rpm, 30s, 100rpm/s; 600 rpm, 60s, 100rpm/s		Gyrset, SU-8 2075
7.2	SU-8 soft-bake	Z3/Hotplate	6h, 50ºC, 2ºC/min		
7.3	SU-8 spin-coating II	Z3/KS Spinner	300rpm, 30s, 100rpm/s; 600 rpm, 60s, 100rpm/s	500 µm	Gyrset, SU-8 2075
7.4	SU-8 soft-bake II	Z3/Hotplate	12h, 50ºC, 2ºC/min		
8	SU-8 THIRD LAYER PHOTOLITHOGRAPHY				
8.1	SU-8 exposure	Z3/KS Aligner	8x338mJ/cm2, sub 1000µm, al 200µm, exp 150µm		GlobalWEC, Prox
8.2	Post-exposure bake	Z3/Hotplate	10h, 50ºC, 2ºC/min		
8.3	SU-8 development	Z3/Developer	20 min FIRST, 20 min FINAL		PGMEA
8.4	Rinse	Z3/Developer	Isopropanol, Air-drying		
9	RELEASE				
9.1	Dry release	manual			
9.2	Optical inspection	Z3/Microscope			
9.2	SEM inspection	SEM-FEI			

Project: **Fabrication of IBM-chips - Metal coating B**
Operator: **Stephan Keller**
Last revision: **30.04.2008**
Substrates: **Silicon <100>, 100mm, 525µm, single side**
Description: **Metal lift-off before processing of the thin SU-8 film (Section 6.4.2)**

Step Nº	Description	Equipment	Program/Parameters	Target	Remarks
1	RELEASE COATING WITH FLUOROCARBON				
1.1	Stock out				
1.2	C4F8-passivation	Z2/ASE	wet_tef2 (120sccm, 350W, 0W, 60mTorr, 60s)		
2	METAL DEPOSITION AND LIFT-OFF				
2.1	AZ spin-coating	Z3/Track1	PR2_2.rcp; AZ5214e; bake at 90ºC	2,2 µm	
2.2	AZ exposure	Z3/KS Aligner	91mJ/cm2, HC	res. 3 µm	mask metallization
2.3	AZ development	Z3/Developer	70s, 3min H2O-rinse		
2.4	Metal deposition	Z2/Alcatel	50nm Au; 5nm Ti; deposition rate 5Å/s		
2.5	Lift-off	Z4/Lift-off bench	20 min with U-sound pulses		
2.6	Optical inspection	Z3/µscope			
3	SU-8 FIRST LAYER SPINNING				
3.1	SU-8 spin-coating	Z3/KS Spinner	2000rpm, 30s, 5000rpm/s	5,5 µm	SU-8 2005
3.2	Solvent evaporation		2h		
4	SU-8 FIRST LAYER PHOTOLITHOGRAPHY				
4.1	SU-8 exposure	Z3/KS Aligner	2x250mJ/cm2, SC		mask cantilever
4.2	Post-exposure bake	Z3/Hotplate	1h, 50ºC, 2ºC/min		
4.3	SU-8 development	Z3/Developer	2 min FIRST, 2 min FINAL		PGMEA
4.4	Rinse	Z3/Developer	Isopropanol, Air-drying 1h		
4.5	2nd exposure	Z3/KS Aligner	500mJ/cm2, FE		
4.6	Hard-bake	Z3/Oven	15h, 120ºC		
4.7	Optical inspection	Z3/µscope			

5	SU-8 SECOND LAYER SPINNING				
5.1	SU-8 spin-coating	Z3/KS Spinner	1000rpm, 30s, 200rpm/s; 3000 rpm, 120s, 400rpm/s	30 µm	SU-8 2075, 6s, 42psi
5.2	SU-8 soft-bake	Z3/Hotplate	2h, 50ºC, 2ºC/min		
6	SU-8 SECOND LAYER PHOTOLITHOGRAPHY				
6.1	SU-8 exposure	Z3/KS Aligner	3x333mJ/cm2, SC		mask body chip extra
6.2	Post-exposure bake	Z3/Hotplate1	6h, 50ºC, 2ºC/min		
6.3	SU-8 development	Z3/Developer	5 min FIRST, 5 min FINAL		PGMEA
6.4	Rinse	Z3/Developer			
7	SU-8 THIRD LAYER SPINNING				
7.1	SU-8 spin-coating	Z3/KS Spinner	300rpm, 30s, 100rpm/s; 600 rpm, 60s, 100rpm/s		Gyrset, SU-8 2075
7.2	SU-8 soft-bake	Z3/Hotplate	6h, 50ºC, 2ºC/min		
7.3	SU-8 spin-coating II	Z3/KS Spinner	300rpm, 30s, 100rpm/s; 600 rpm, 60s, 100rpm/s	500 µm	Gyrset, SU-8 2075
7.4	SU-8 soft-bake II	Z3/Hotplate	12h, 50ºC, 2ºC/min		
8	SU-8 THIRD LAYER PHOTOLITHOGRAPHY				
8.1	SU-8 exposure	Z3/KS Aligner	8x338mJ/cm2, sub 1000µm, al 200µm, exp 150µm		GlobalWEC, Prox
8.2	Post-exposure bake	Z3/Hotplate1	10h, 50ºC, 2ºC/min		
8.3	SU-8 development	Z3/Developer	20 min FIRST, 20 min FINAL		PGMEA
8.4	Rinse	Z3/Developer	Isopropanol, Air-drying		
9	RELEASE				
9.1	Dry release	manual			
9.2	Optical inspection	Z3/Microscope			
9.3	SEM inspection	SEM-FEI			

Appendix D

Fabrication of
the flapperchip

Project: **Fabrication of flapperchips**
Operator: **Stephan Keller**
Last revision: **30.04.2008**
Substrates: **Silicon <100>, 100mm, 525µm, single side**

Step Nº	Description	Equipment	Program/Parameters	Target	Remarks
1	RELEASE COATING WITH FLUOROCARBON				
1.1	Stock out				
1.2	C4F8-passivation	Z2/ASE	wettef2 (120sccm, 350W, 0W, 60mTorr, 60s)		
2	SU-8 FIRST LAYER SPINNING				
2.1a	SU-8 spin-coating	Z3/KS Spinner	1500rpm, 30s, 5000rpm/s	2 µm	SU-8 2002
2.1b	SU-8 spin-coating	Z3/KS Spinner	1500rpm, 30s, 5000rpm/s	5.5 µm	SU-8 2005
2.2a	Solvent evaporation		30min		
2.2b	Solvent evaporation		2h		
3	SU-8 FIRST LAYER PHOTOLITHOGRAPHY - PROCESS C				
3.1	SU-8 exposure	Z3/KS Aligner	250mJ/cm2, HC	res. 3µm	Mask flapper
3.2	Post-exposure bake	Z3/Hotplate2	1h, 50ºC, 2ºC/min		
3.3	SU-8 development	Z3/Developer	2 min FIRST, 2 min FINAL		PGMEA
3.4	Rinse	Z3/Developer	Isopropanol, Air-drying 2h		
3.5	2nd exposure	Z3/KS Aligner	500mJ/cm2, FE		
3.6	Hard-bake	Z3/Oven90C	15h, 90ºC		over night
3.7	Optical inspection	Z3/µscope			
4	SU-8 SECOND LAYER SPINNING				
4.1	SU-8 spin-coating	Z3/KS Spinner	1000rpm, 30s, 100rpm/s; 2000 rpm, 60s, 100rpm/s	65 µm	SU-8 2075
4.2	SU-8 soft-bake	Z3/Hotplate2	4h, 50ºC, 2ºC/min		
5	SU-8 SECOND LAYER PHOTOLITHOGRAPHY				
5.1	SU-8 exposure	Z3/KS Aligner	6x300mJ/cm2, SC		slight stiction to mask
5.2	Post-exposure bake	Z3/Hotplate2	2h, 50ºC, 2ºC/min		

6	SU-8 THIRD LAYER SPINNING				
6.1	SU-8 spin-coating	Z3/KS Spinner	300rpm, 30s, 100rpm/s; 600 rpm, 60s, 100rpm/s	250 µm	Gyrset, SU-8 2075
6.2	SU-8 soft-bake	Z3/Hotplate2	10h, 50ºC, 2ºC/min		over night
7	SU-8 THIRD LAYER PHOTOLITHOGRAPHY				
7.1	SU-8 exposure	Z3/KS Aligner	6x300mJ/cm2, sub 800µm, al 150µm, exp 150µm		GlobalWEC, Prox
7.2	Post-exposure bake	Z3/Hotplate2	10h, 50ºC, 2ºC/min		
7.3	SU-8 development	Z3/Developer	15 min FIRST, 15 min FINAL		PGMEA
7.4	Rinse	Z3/Developer	Isopropanol, Air-drying		
8	SU-8 THIRD LAYER PHOTOLITHOGRAPHY				
8.1	Glass cleaning	Z2/Wet bench	Piranha, 5 min		Borofloat wafers
8.2	SU-8 spin-coating	Z3/KS Spinner	1000rpm, 30s, 300rpm/s	8 µm	SU-8 2005; on Pyrex
6.3	Exposure	Z3/KS Aligner	4x250 mJ/cm2; FE		
6.4	Wafer bonding	Z4/EVG NIL	120ºC, 2000N, 120min, 2ºC/min; first pressure; natural cool-down to 50ºC; small spacer on top of the wafer (centered)		30 min after exposure
9	RELEASE				
9.1	Dry release	manual			
9.2	Optical inspection	Z3/Microscope			
9.3	SEM inspection	SEM-FEI			
10	DICING				
10.1	Wafer dicing	DAD321, Disco	Automatic mode		Pyrex blade